Advanced Illumination Systems for Cardiac Optogenetics

Jin, T.

DOI
10.4233/uuid:a1ec4afc-ae18-4aa1-8ff5-c3b71cd6e717

Publication date
2024

Document Version
Final published version

Citation (APA)
Jin, T. (2024). *Advanced Illumination Systems for Cardiac Optogenetics*. [Dissertation (TU Delft), Delft University of Technology]. https://doi.org/10.4233/uuid:a1ec4afc-ae18-4aa1-8ff5-c3b71cd6e717

ADVANCED ILLUMINATION SYSTEMS FOR CARDIAC OPTOGENETICS

ADVANCED ILLUMINATION SYSTEMS FOR CARDIAC OPTOGENETICS

Proefschrift

ter verkrijging van de graad van doctor
aan de Technische Universiteit Delft,
op gezag van de Rector Magnificus Prof.dr.ir. T.H.J.J. van der Hagen,
voorzitter van het College voor Promoties,
in het openbaar te verdedigen op maandag 16 september 2024 om 12:30 uur

door

Tianyi JIN

Master of Science in Electrical Engineering,
Technische Universiteit Delft, Nederland,
geboren te Zhejiang, China

Dit proefschrift is goedgekeurd door de

Promotor:	Prof. dr. G.Q. Zhang
Promotor:	Prof. dr. D.A. Pijnappels
Copromotor:	Dr. ir. R.H. Poelma

Samenstelling promotiecommissie:

Rector Magnificus,	voorzitter
Prof. dr. G.Q. Zhang,	Technische Universiteit Delft
Prof. dr. D.A. Pijnappels,	Leids Universitair Medisch Centrum
Dr. ir. R.H. Poelma,	Technische Universiteit Delft
Onafhankelijke leden:	
Prof. dr. W.D. van Driel,	Technische Universiteit Delft
Prof. dr. P.J. French,	Technische Universiteit Delft
Dr. M. Palmen,	Leids Universitair Medisch Centrum
Prof. dr. B. Shen,	Peking University
Prof. dr. P.M. Sarro,	Technische Universiteit Delft

Keywords: LED, Optogenetics, System integration, Atrial fibrillation

Printed by: IPSKAMP Printing

An electronic version of this dissertation is available at
http://repository.tudelft.nl/.

"I have noticed that even those who assert that everything is predestined and that we can change nothing about it, still look both ways before they cross the street."

Stephen Hawking, Black Holes and Baby Universes and Other Essays

CONTENTS

SUMMARY

The innovation of health care and biomedical research through the integration of advanced technology plays a significant role in enhancing clinical outcomes and pioneering new frontiers in medical science. This work finds itself at an intersection of advanced optoelectronics technology and the innovative field of cardiac optogenetics.

It presents the journey from the historical significance of light in human evolution to its transformative role in contemporary medical science, particularly in addressing complex cardiac arrhythmic disorders like Ventricular Fibrillation (VF) and Atrial Fibrillation (AF), which are conditions of significant healthcare challenges due to their prevalence and the limitations of current treatment limitations. The dissertation thoroughly examines the intricacies of these arrhythmias, their impact on public health, and the drawbacks of existing therapies. Traditional treatments, while necessary, often fall short due to high failure rates, severe side effects, and patient discomfort. The inadequacy of current treatment methods proposes the need for innovative solutions for cardiac arrhythmia prevention and termination.

In this context, optogenetics emerges as a groundbreaking approach. The dissertation explains the fundamental principles of modern optogenetics technology, which initially is developed for neural applications and later adapted for cardiovascular studies. This technique involves the genetic modification of cells to express light-sensitive ion channels, allowing for the precise control of electrophysiological signals using external lighting. Optogenetics provides medical researchers the possibility to externally, locally, and precisely control cardiac electrophysiological signals, making it a significant tool in transitional cardiovascular research of arrhythmia treatments. It is a great candidate for the solution to the main challenge of finding a novel clinical method for a pain-free and effective treatment of AF or VF without electric shocks. The dissertation highlights the evolution of optogenetics methods, tracing its roots from early gene studies to its current application in neural or cardiac research, with the stressing on the illumination technologies used in the study as it is one of the critical challenges of the state-of-the-art.

A significant part of the dissertation is dedicated to the development of advanced illumination systems for optogenetics in cardiac applications. Employing the V-model system engineering methodology, the work details each phase of the development pro-

cess. The methodology begins with a thorough analysis of system requirements and system architecture design, breaking down the complex system into subsystems with unique functionalities and requirements. The system is implemented and verified by thorough testing and simulations. Finally, the system is validated in optogenetics experiments for arrhythmia study.

The following chapters present the design and development processes of four specialized optoelectronic illumination systems, each uniquely engineered for optogenetic cardiac applications. These chapters illustrate innovative approaches and the systematic methodology behind the technical development.

Firstly the design and development of a custom LED illumination system aimed at treating VF in a rat model is discussed. The comprehensive development cycle of the system, including testing, integration, verification, and validation, both in-vivo and ex-vivo, using rat models is explored. It emphasizes the system's bio-compatible design and its specific optical properties. Additionally, the biological insights of successfully terminating VF with the illumination system from experiments effectively assess the system's functionality and demonstrate its potential impact on future cardiac therapies.

Secondly, the development of an LED matrix illumination system for optogenetic AF termination in the swine model is introduced. Following the same development methodology, the work details the process of designing, testing, and implementing this advanced and implantable system. The system could not be validated in a swine model because of issues regarding the optogenetic modification of the heart, but it still proves the technical potential of integrating an implantable high-power illumination system.

Moreover, the work explores a novel approach to studying arrhythmia behaviors using a human immortalized atrial myocyte (hiAM) model. It focuses on the design and development of a 16x16 LED matrix illumination system, intended for initial proof-of-concept experiments and forming a part of an innovative in-vitro experimental platform. This prototype system lays a solid theoretical and practical foundation for more sophisticated illumination systems in cardiovascular research by successfully validating AF termination in hiAM cultures.

Finally, following the success of the prototype system, the work presents the feasibility of a 16x16 mini-LED matrix illumination system as an advanced proposal. This upgraded system is designed for more precise control in hiAM cell culture experiments, which features mini-LED bare-die chips for refined illumination, enhanced substrate materials for improved performance and flexibility, and an advanced driver and controller system for more effective management of the smaller mini-LED components.

The research not only provides a technical methodology for developing advanced il-

lumination systems but also offers insights into the potential research or clinical applications of optogenetics. The work is positioned to have a significant impact on the related field, offering developing tools for the exploration of novel, shock-free, and therefore pain-free approaches for cardiac arrhythmias.

SAMENVATTING

De innovatie van gezondheidszorg en biomedisch onderzoek door de integratie van geavanceerde technologie speelt een significante rol in het verbeteren van klinische resultaten en het pionieren van nieuwe frontiers in medische wetenschap. Dit werk bevindt zich op het snijpunt van geavanceerde opto-elektronica en het innovatieve veld van cardiale optogenetica.

Het presenteert de reis van de historische betekenis van licht in menselijke evolutie tot zijn transformerende rol in hedendaagse medische wetenschap, met name in het aanpakken van complexe cardiale aritmische stoornissen zoals Ventricular Fibrillation (VF) en Atrial Fibrillation (AF), die aanzienlijke gezondheidszorguitdagingen zijn vanwege hun prevalentie en de beperkingen van huidige behandelmethoden. De dissertatie onderzoekt grondig de complexiteiten van deze aritmieën, hun impact op de volksgezondheid en de tekortkomingen van bestaande therapieën. Traditionele behandelingen, hoewel noodzakelijk, schieten vaak tekort vanwege hoge mislukkingspercentages, ernstige bijwerkingen en ongemak voor de patiënt. De ontoereikendheid van huidige behandelmethoden suggereert de behoefte aan innovatieve oplossingen voor het voorkomen en beëindigen van cardiale aritmie.

In deze context komt optogenetica naar voren als een baanbrekende aanpak. De dissertatie legt de fundamentele principes van moderne optogenetica-technologie uit, die oorspronkelijk is ontwikkeld voor neurale toepassingen en later is aangepast voor cardiovasculaire studies. Deze techniek omvat genetische modificatie van cellen om lichtgevoelige ionkanalen tot expressie te brengen, waardoor nauwkeurige controle van elektrofysiologische signalen mogelijk is met behulp van externe verlichting. Optogenetica biedt medische onderzoekers de mogelijkheid om cardiale elektrofysiologische signalen extern, lokaal en nauwkeurig te regelen, waardoor het een significant hulpmiddel wordt in overgangsonderzoek naar cardiovasculaire behandelingen van aritmie. Het is een uitstekende kandidaat voor de oplossing van de belangrijkste uitdaging om een pijnvrije en effectieve behandeling van AF of VF zonder elektrische schokken te vinden. De dissertatie belicht de evolutie van optogenetische methoden, van vroege genstudies tot de huidige toepassing in neurale of cardiale onderzoek, met nadruk op de verlichtingstechnologieën die in de studie worden gebruikt, aangezien dit een van de

kritieke uitdagingen van de state-of-the-art is.

Een significant deel van de dissertatie is gewijd aan de ontwikkeling van geavanceerde verlichtingssystemen voor optogenetica in cardiale toepassingen. Met behulp van de V-model systeemtechniekmethodologie, worden de fasen van de ontwikkelingsprocessen gedetailleerd beschreven. De methodologie begint met een grondige analyse van systeemvereisten en systeemarchitectuurontwerp, waarbij het complexe systeem wordt opgedeeld in subsystemen met unieke functionaliteiten en vereisten. Het systeem wordt geïmplementeerd en geverifieerd door grondige tests en simulaties. Ten slotte wordt het systeem gevalideerd in optogenetische experimenten voor aritmieonderzoek.

De volgende hoofdstukken presenteren het ontwerp en de ontwikkelingsprocessen van vier gespecialiseerde opto-elektronische verlichtingssystemen, elk uniek ontwikkeld voor optogenetische cardiale toepassingen. Deze hoofdstukken illustreren innovatieve benaderingen en de systematische methodologie achter de technische ontwikkeling.

De volgende hoofdstukken presenteren het ontwerp- en ontwikkelingsproces van vier gespecialiseerde opto-elektronische verlichtingssystemen, elk uniek ontworpen voor optogenetische toepassingen in de cardiologie. Deze hoofdstukken illustreren innovatieve benaderingen en de systematische methodologie achter de technische ontwikkeling.

Ten eerste wordt het ontwerp en de ontwikkeling van een op maat gemaakt LED-verlichtingssysteem besproken, gericht op de behandeling van VF bij een rattenmodel. De uitgebreide ontwikkelingscyclus van het systeem, inclusief testen, integratie, verificatie en validatie, zowel in-vivo als ex-vivo, met rattenmodellen wordt verkend. Het benadrukt het biocompatibele ontwerp van het systeem en de specifieke optische eigenschappen. Bovendien beoordelen de biologische inzichten van het succesvol beëindigen van VF met het verlichtingssysteem effectief de functionaliteit van het systeem en demonstreren ze de potentiële impact op toekomstige harttherapieën.

Ten tweede wordt de ontwikkeling van een LED-matrix verlichtingssysteem voor de beëindiging van AF optogenetica in een varkensmodel geïntroduceerd. Volgens dezelfde ontwikkelingsmethodologie worden het ontwerp, de testen en de implementatie van dit geavanceerde en implanteerbare systeem gedetailleerd beschreven. Het systeem is niet gevalideerd voor zowel in-vivo als ex-vivo experimenten vanwege technische problemen in optogenetische varkensmodellen, maar het toont nog steeds de technische potentie van het integreren van een implanteerbaar high-power verlichtingssysteem aan.

Verder verkent het werk een nieuwe benadering voor het bestuderen van aritmiegedrag met behulp van een menselijk geïmmortaliseerd atrium myocyt (hiAM) model. Er wordt gefocust op het ontwerp en de ontwikkeling van een 16x16 LED-matrix ver-

lichtingssysteem, bedoeld voor initiële proof-of-concept experimenten en als onderdeel van een innovatief in-vitro experimenteel platform. Dit prototype systeem legt een solide theoretische en praktische basis voor meer geavanceerde verlichtingssystemen in cardiovasculair onderzoek door succesvol gevalideerd te zijn in AF-beëindigings experimenten met hiAM-celculturen.

Ten slotte presenteert het werk na het succes van het prototypesysteem de haalbaarheid van een 16x16 mini-LED matrix verlichtingssysteem als een geavanceerd voorstel. Dit geüpgradede systeem is ontworpen voor nauwkeurigere controle in hiAM-celcultuur experimenten, met mini-LED bare-die chips voor verfijnde verlichting, verbeterde substraatmaterialen voor betere prestaties en flexibiliteit, en een geavanceerd stuur- en controlesysteem voor effectiever beheer van de kleinere mini-LED-componenten.

Het onderzoek biedt niet alleen een technische methodologie voor de ontwikkeling van geavanceerde verlichtingssystemen, maar biedt ook inzichten in de potentiële onderzoeks- of klinische toepassingen van optogenetica. Het werk is gepositioneerd om een aanzienlijke impact te hebben op het gerelateerde veld, door ontwikkelingshulpmiddelen aan te bieden voor het verkennen van nieuwe, patiëntvriendelijke benaderingen voor de behandeling van hartaritmieën.

1

INTRODUCTION

1

1.1. LIGHT AND LIFE

Light has been a fundamental element in human life for some time, playing a crucial role as simple as providing illumination. From the beginning of civilization, the sun has symbolized life, growth, energy, and hope. Ancient cultures worldwide worshipped the sun autonomously, recognizing its great importance in sustaining life on earth: Light is the cornerstone of our existence.

The journey of light in human history is not just a tale of natural luminescence but also a story of innovation. From the moment our ancestors learned to harness fire, humanity evolved on a path of creating man-made light, transforming their interaction with the world. The discovery of fire was a great milestone as it provided warmth, protection, nutrition, and a new way to extend the day beyond the setting of the sun. This mastery over a natural element symbolized the beginning of human civilization.

As civilizations advanced, so did the techniques of producing light. The invention of lamps, filled with oil or other combustibles, provided a more controlled and sustainable source of light compared to the open flame of a bonfire. These early innovations were significant, but it was the development of gas lighting that brought the possibility of illuminating streets, homes, and cities more efficiently than ever before.

The true revolution in man-made lighting came with Thomas Edison's invention of the electric light bulb in the 19th century. Edison's breakthrough not only transformed the way people illuminated their homes and streets but also fundamentally changed human lifestyle and productivity. The light bulb became a symbol of human innovation, to manipulate our environment to extend the day and improve the quality of life. It enabled industries to operate beyond daylight hours, accelerated urban development, and played a crucial role in the emergence of modern society. The way we live, work, and interact was forever altered by the availability of reliable, artificial light.

Man-made light is considered one of the most important inventions in human history because it is not just a tool for visibility, but a symbol of mankind's civilization. From the warm glow of a campfire to the bright beam of a streetlight, the evolution of artificial lighting continues to be a key driver of human advancement and a reflection of our intellectual growth. As we stand today, with advanced LED technologies and smart lighting solutions, we continue to push the boundaries of what light can do for us.

As humans continue to explore and understand the exciting ways in which light influences life, it becomes clear that our bond with this essential element is both ancient and enduring. New technology innovations and future opportunities are found in the continuous exploration of the connection between light and human life.

1.2. OPTOGENETICS METHODS IN CARDIOLOGY

1.2.1. CARDIAC ARRHYTHMIA AND TREATMENT

Cardiac arrhythmias, or heart rhythm disorders, are the result of abnormal electrical activity of the heart and represent and huge and growing socioeconomic burden.

Ventricular fibrillation (VF) is a severe cardiac arrhythmia characterized by rapid, irregular pulses that originate in the ventricles of the heart. This abnormal activity seriously impairs the mechanical pump function of the heart, impairing the blood flow and thereby resulting in a life-threatening situation requiring immediate intervention, thus VF is a medical emergency that requires immediate intervention, as it can lead to sudden cardiac arrest and eventually death if not treated in time[1][2]. Out-of-hospital cardiac emergencies account for more than 350,000 unexpected deaths each year in North America, nearly 100,000 of which are attributed to ventricular-related cases[3]. This situation makes VF the most common mechanism of sudden unexpected cardiac death in persons suffering from coronary artery disease[4].

VF is primarily diagnosed through an electrocardiogram (ECG), and immediate Cardiopulmonary resuscitation (CPR) should be initiated as soon as VF is suspected. VF usually requires immediate treatment via external defibrillation methods, such as an automated external defibrillator (AED), which delivers electrical shocks to the heart to restore a regular heart rhythm. Medications and other advanced life support methods may be used alongside defibrillation[5].

Compared to the severe consequences and the emergency in treatment, **Atrial fibrillation (AF)**, also a type of cardiac arrhythmia, is less severe in terms of immediate life-threatening risks since the mortality rate is relatively low. AF is characterized by rapid, irregular pulses that originate in the atrium of the heart and are out of coordination with the ventricles. This activity prevents the atrium from pumping blood effectively to the ventricle, but the whole blood circulation can be still maintained, although inefficiently. Typical AF symptoms are palpitations, fatigue, dizziness, shortness of breath, or chest discomfort, which still affects both the quality of life and overall health as a chronic disease. AF also increases the risk of heart stroke and heart failure, thereby contributing to substantial morbidity and mortality[6].

AF is the most common form of cardiac disorder in the human population, affects 2-3% of people worldwide, spanning various genders and ethnicity's[7][8][9][10], and has a greater impact on elder population. The prevalence of AF increases more than double with increasing each decade of age, from 0.5% at age 50 years to 9% at age 80 years[11]. Therefore, the prevalence of AF is expected to rise significantly in the future due to the aging global population and improved management of chronic diseases. Es-

timates suggest that by 2030, the number of people affected by AF in Europe could reach approximately 15 million, with about 200,000 new cases emerging each year[12]. 1 out of 5 persons with an age higher than 65 years is expected to suffer from AF[7].

Annually over €20 billion of direct healthcare costs are spent on AF related medical treatments in European countries[13]. The general objectives in AF treatment are prevention of thromboemboli, control of the ventricular response, restoration of sinus rhythm, and maintenance of sinus rhythm by preventing recurrences[8]. However, the effectiveness of most treatments is limited due to different reasons. Pharmaceuticals for AF are often ineffective with failure rates as high as 60%, and carry severe side effects such as increasing the risk of severe ventricular arrhythmias[7]. Clinical methods such as catheter ablation can lead to irreversible complications and generally show low long-term efficacy[14]. The pioneering innovation of Cox[15] in developing a series of maze procedures to eliminate atrial fibrillation has led to a very impressive long-term cure, but this invasive procedure is not widely adopted because of its surgical complexity[16][17].

Therefore, many patients with drug-resistant and severely recurrent AF symptoms after multiple ablation operations, need to restore normal rhythm by high-voltage shocks to the heart. This operation must be carried out upon anesthesia due to the severe pain caused by the electric shocks. However, this is still considered a temporary solution because the duration of AF is inversely related to the success of restoration of sinus rhythm, meaning that eventually, the AF recurrence increases after treatment. To avoid this one requires the need for continuous and rapid detection and immediate treatment of AF in a long-term method.

Implantable cardioverter defibrillators (ICD) are developed more than 30 years ago (Figure 1.1). Modern ICD devices (Figure 1.2) are designed for the long-term treatment of AF, delivering automated arrhythmia detection and termination by electrical shocks through embedded electrodes. Some ICD devices are also equipped with pacemaker functions. While these devices are tested effective for AF treatment[18][19][20], their use is often discontinued due to patients intolerance to the repeated painful electric shocks[21], and the depression and anxiety following them[22]. The ICD restoration may also be delivered inappropriately and therefore cause cardiac tissue damage[23][24][25].

Currently, there is no clinical method for a pain-free and effective treatment of cardiac arrhythmia, including VF and AF, that can be applied at any time and any place, which raises a significant challenge and opportunity in cardiovascular research to explore a more sustainable and patient-friendly solution.

The main challenge is the lack of novel techniques to rapidly and precisely control abnormal cardiac electrical activities and restore heart rhythm, preferably without elec-

Figure 1.1: An early ICD device with patch electrodes[26]

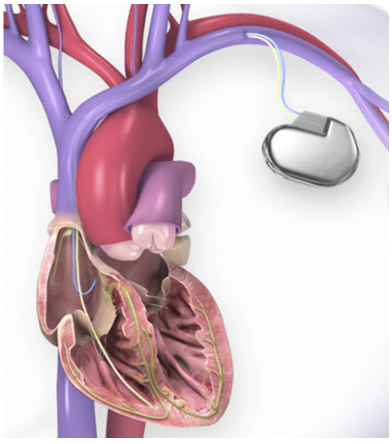

Figure 1.2: Modern ICD with arrhythmia detection and autonomous restoration functions[27]

tric shocks. Pioneering approaches and innovations are created by the combined expertise of cardiovascular and other scientific or engineering competencies such as genetic engineering, applied physics, electrical and mechanical engineering, etc. Promising solutions are proposed as novel gene therapy or optogenetics methods, which are introduced in the following chapters. This significant challenge is further discussed in this work as novel AF treatment strategies based on optogenetics are proposed, with a focus on their technical implementations and realizations.

1

1.2.2. OPTOGENETICS

For a long time in biology and clinical research, there has been a need to control the behavior of electrophysiological signal transmission in various scales, from individual cells to entire live animals. This control is the basis of understanding biological principles or examining clinical treatments. Traditionally, methods like pharmaceutics or physical manipulations have been used. However, these conventional methods come with limitations, especially for advanced biological or clinical studies nowadays.

One significant drawback of traditional electrophysiological control methods is the delay of effects. For instance, pharmaceutical interventions typically do not produce immediate results (in the scale of ms), as it takes time for the drugs to stimulate the subject, and in the meantime, the effects are often long-term with considerable delays. Another challenge with traditional methods is the lack of precision. Controls are often applied over a large area or even the entire body. This broad approach can be particularly challenging in fields like neuroscience or cardiovascular science, where localized effects are critical for understanding specific biological processes. In response to these limitations, researchers in those fields have been in pursuit of new electrophysiological control methods that offer more precise, localized control and rapid, temporary effects.

Optogenetics is a biological technology that generally uses light to control the electrophysiological signal transmission which has been genetically modified to be reactive to light. Optogenetics offers the possibility of rapid, high-temporal, and precise cell-level control of various biological activities[28][29][30]. To date, nearly 8,000 papers have been published on optogenetics making it one of the most popular research topics in translational medical science.

The transmission of neural signals is a complex process in the nervous system, enabling communication within the network of neurons and between neurons and other cell types[31][32]. The process begins with the neurons, the basic units of the nervous system, which are specially structured for electrophysiological signal transmission. In the resting state, a neuron maintains a resting potential, a voltage difference across its membrane, typically around -70 mV (Figure 1.3a). This resting potential is maintained by ion channels and pumps that regulate the concentrations of ions such as sodium (Na+) and potassium (K+) inside and outside the cell.

When a section of neuron membrane is activated by receiving a signal stimulation, ion channels open, allowing Na+ ions to enter the cell, changing the internal electrical charge and causing depolarization (Figure 1.3b). If this depolarization reaches a threshold, it triggers an action potential, a rapid and temporary change in the electrical charge

across the cell membrane. This action potential then travels along the membrane and neuron system through the sequential opening and closing of ion channels along the membrane, creating a wave of electrical activity (Figure 1.3c).

Following the action potential, the membrane resets to its resting state through repolarization, involving the in-flowing of K+ ions and closing of Na+ ion channels (Figure 1.3d). The Na+/K+ pump then actively restores the original ion concentration inside and outside the neuron, making it ready for the next signal transmission.

In a normal neuronal system, the process of electrophysiological signal transmission is typically initiated and sustained by chemical or electrical stimulus within the organ or body itself. However, the development of optogenetics technology introduces a transformative approach to externally interacting and manipulating neuronal systems and signal transmission processes.

In optogenetics, special genes (DNA) are delivered to a certain volume of cells via common gene therapy vectors, such as Adeno-Associated Virus (AAV). The genes are expressed by the subject as light-sensitive ion channels at the cell membrane. Only the cells delivered by the vectors can express the ion channels, thus the genetic modification is highly localized and targeted.

Light-sensitive ion channels are either excitation type (e.g., Channelrhodopsins[33]) or inhibition type (e.g., Halorhodopsin[34]). Excitation ion channels remain closed in the absence of light stimulation or when the light stimulation has low intensity. The neuronal membrane functions as usual, maintaining its resting potential and allowing normal electrophysiological signal transmission (Figure 1.4a). When light stimulation exceeds a certain threshold, light-sensitive ion channels open and allow positive ions, typically sodium ions (Na+) or cation ions (Ca2+), to flow inside the cell (Figure 1.4b). The entry of these ions changes the internal electrical charge of the neuron, and results in potential depolarization. Once the depolarization reaches a threshold, a certain positive action potential level is maintained and the signal is transmitted. The membrane automatically repolarizes by its intrinsic functions, returning to the resting potential.

The inhibitory light-sensitive ion channels function similarly to excitation types but with a different effect. When activated by light of sufficient intensity, these channels open and allow the in-flow of negative ions, usually chloride ions (Cl-) into the cell. This maintains a hyperpolarization, pushing the membrane potential higher than the action potential threshold, thus inhibiting neuronal activity. Once the light stimulation is removed, the light-sensitive channels close, allowing the neuron to return to its resting state.

Optogenetics technology's ability to control neuronal activity with light offers a pow-

1

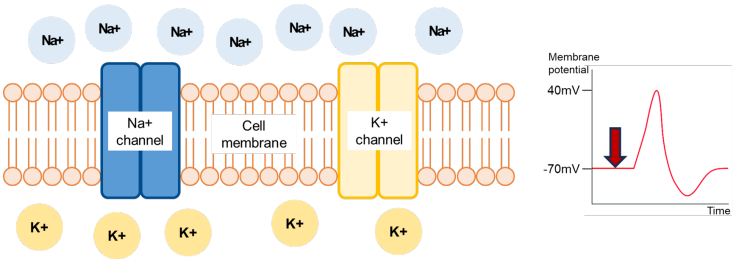

(a) Resting potential: Na+ and K+ ions inside and outside membrane are regulated in stable concentrations

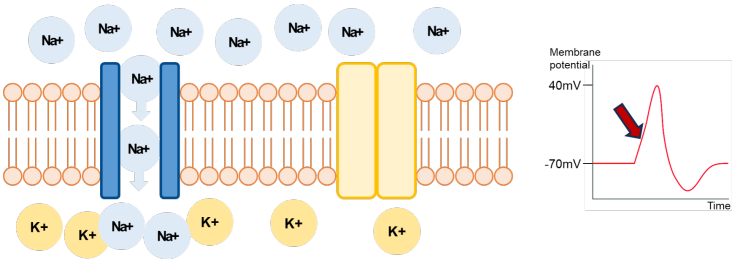

(b) Depolarization: the Na+ ion channels open to allow Na+ ion flowing inside and increase the potential across the membrane

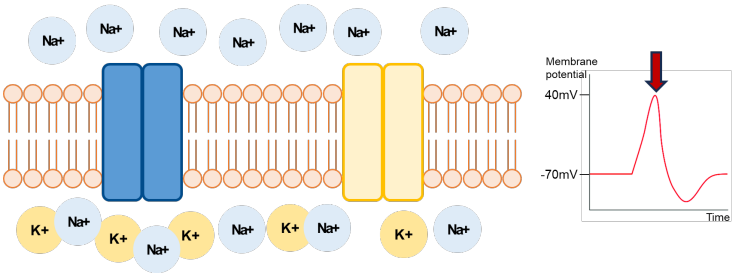

(c) Action potential: the voltage reaches a threshold, Na+ ion channels close and the signal travels

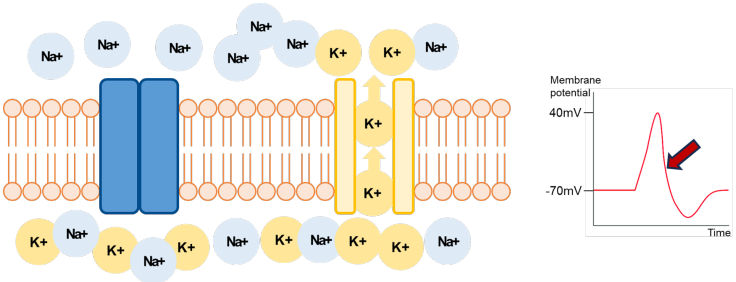

(d) Repolarization: the K+ ion channel open to allow K+ ion flowing outside and decrease the potential across the membrane

Figure 1.3: The electrophysiological signal transmission process in neuronal membranes

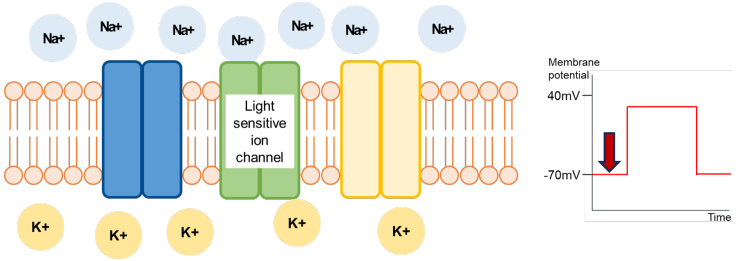

(a) Resting potential: the light-sensitive ion-channels close when no light stimulation or light stimulation is low

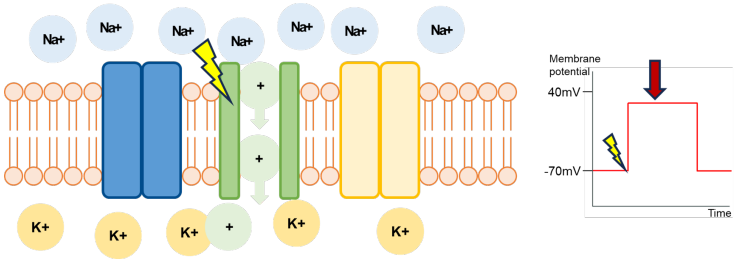

(b) Excited depolarization: the light-sensitive ion-channels open with light stimulation, to allow Na+ or Ca2+ ions to flow inside

Figure 1.4: The optogenetics light-sensitive excitation ion-channels in neuronal membranes

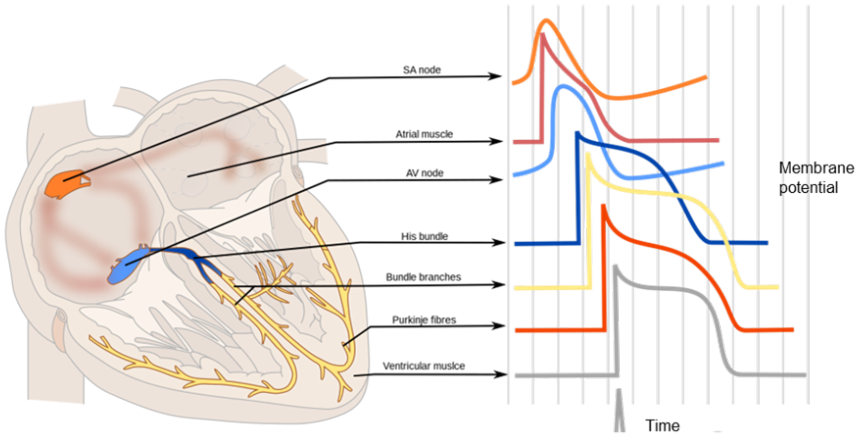

Figure 1.5: Different dynamics of the cardiac action potential in various parts of the heart[35]

erful tool for precise manipulation of neural electrophysiological signals, opening up new possibilities in both research and therapeutic applications. It allows for the initiation, interruption, or termination of neural signal transmission through external light control, opening up possibilities for actively manipulating these signals in highly localized regions with genetic modification applied. By using light to control neurons that have been genetically modified to express light-sensitive ion channels, researchers can now precisely modulate neuronal activity in ways that were previously unattainable.

Optogenetics is a recent technology that has foundations of traced back to the early 2000s, where various genes with light-sensitive expressions were found and studied[36][37], such as rhodopsins and arrestins[38], ion-gate channels[39][40][41][42][43][44]. Following the development of the first genetically targeted method to excite rhodopsin-sensitized neurons[33], optogenetics has primarily been used to manipulate neurons[45][46][47]. Comprehensive optogenetic tools were then introduced for neuronal excitation [48][49][50] as well neuronal inhibition[34][51][52]. The tools were used for precise and rapid control of neural activities and eventually control the bio-activities by genetically modifying a part of the body (e.g. brain cortex) of an animal. The optogenetics application on neuronal research has continuously been popular until now. In more recent years, new applications of optogenetics have been found. For example, it was proven as a promising approach for vision restoration as the light-sensitive microbial opsins can replace or restore the function of the vision retina without invasive surgery[53][54].

Optogenetics technology was soon proved possible to be introduced to cardiac cells[55], offering novel approaches for fundamental understanding of cardiovascular principles and proposing potential treatments for cardiac deceases. Various related cardiac researches followed and explored with the optogenetics[56][57][58].

Cardiac signals, similar to neural signals, are also transmitted through changes in membrane potential across the cell membranes of heart cells. This activity is driven and sustained by the movement of charged ions across the membrane.

Still, the cardiac action potential differs from the neural action potential in signal dynamics. The resting membrane potential and the peak voltage reached during an action potential in cardiac cells vary compared to usually a constant value in neurons. Also, cardiac action potentials are generally longer in duration compared to neuronal action potentials. This is due to a prolonged influx of Ca2+ ions, which is critical for the heart's muscle contraction[59]. The heart comprises different types of cells, each with its own set of ion channels (Figure 1.5). This leads to variations in action potential dynamics across different parts of the heart, ensuring coordinated and efficient pumping function of the heart.

Light-sensitive ion channels were successfully transferred and expressed in cardiac tissues[56][58][60]. Early feasibility studies demonstrated that whole-heart arrhythmias can be terminated through local epicardial illumination[61] in rat models. This technique evolved by using customized stimulation tailored to the specific mechanisms of arrhythmias[62], which can significantly reduce the energy required for defibrillation illumination. The potential of this method as an alternative to traditional, painful electric cardioversion treatments is particularly valuable. Optogenetics, by providing a means to externally, locally, and precisely control cardiac signals, makes it a significant advancement in transitional cardiovascular research. It is a great candidate for the solution to the main challenge of finding a novel clinical method for a pain-free and effective treatment of arrhythmia without electric shocks.

Laboratory of Experimental Cardiology in Leiden University Medical Center (LUMC) has a rich history and extensive experience in the research field of cardiac optogenetics. Over the years, they have developed and refined techniques in genetic engineering to create rat-based cardiac arrhythmia models, as well as preliminary studies for using optogenetics method for arrhythmia treatments[60][61][63][64][65][66][67][68][69]. This expertise is critical in advancing the understanding of arrhythmia mechanisms and innovating new therapy methods. The experience in their specialized area illustrates the team's commitment to cardiovascular research and its leading role in exploring novel interventions for arrhythmia treatment and prevention by optogenetics.

1.2.3. DEVELOPMENT METHODOLOGY OF ILLUMINATION SYSTEM FOR OPTOGENETICS

Optogenetics technology provides the possibility of a revolutionary method for arrhythmia study by offering precise cardiac signal control. The success of this approach requires a few technical components, each playing a crucial role in its overall effectiveness.

Selecting the most suitable arrhythmia model is critical. This could be a rat, swine, or another novel model, but it must accurately represent the characteristics of human arrhythmias. The chosen model should mimic the physiology of arrhythmias, ensuring the relevance and applicability of the research findings. As gene therapy is the central aspect of optogenetics, the technology involves identifying the right genes of light-sensitive ion channels, along with developing efficient systems for gene delivery, and ensuring the expression of these genes in the model is both consistent and efficient. Another important aspect is the ability to characterize and potentially visualize arrhythmias in the model. This requires sophisticated techniques, such as the optical voltage mapping technique, that can accurately monitor the heart's electrical activity and assess the im-

pacts of optogenetic manipulation.

However, equally important, if not more important, is the development of an advanced illumination system. This system needs to precisely control local light stimulation to actively manipulate the light-sensitive ion channels. The ability to accurately target these channels is fundamental to the effectiveness of optogenetic interventions in studying and treating arrhythmias.

In this context, the cardiac study acts as the 'customer' for the illumination system, determining its specifications and functionality. Therefore, a customer-oriented approach emphasizes that the design of such an illumination device must be tailored to meet the specific needs and objectives of the biomedical experiments. Such customization ensures that the device provides the precise optical triggering conditions required for the optogenetics methods, such as specific wavelength for ion channel activation, intensity levels for tissue penetration, optical distribution for targeted illumination, etc. The experiment's requirements steer the basis of the illumination device's design, ensuring that the device effectively supports the experiments for generating reliable, accurate results, and maintaining the integrity and safety of the biological subjects involved.

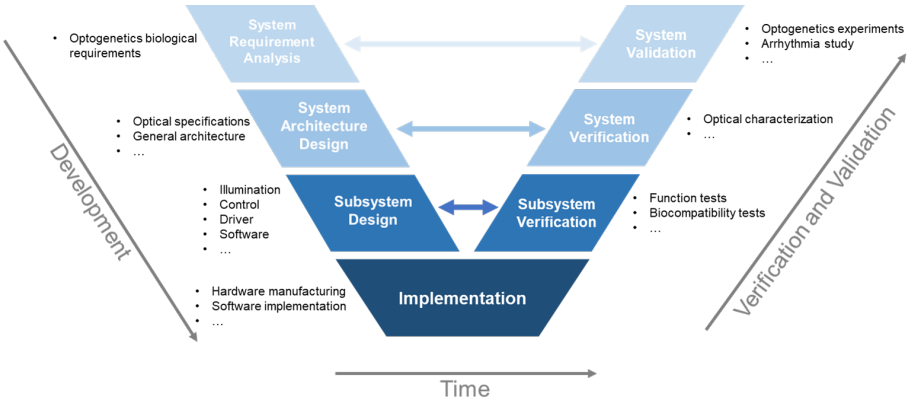

Figure 1.6: V-model methodology for the illumination system development

The V-model methodology is important as a design guideline for the development of illumination systems for optogenetics cardiac applications. The V-model is a highly structured system engineering approach often employed in the development of complex technical systems. It's particularly suited for projects where errors or mistakes in design can be costly if not identified early in the development process. The V-model methodology is structured in a V-shape, representing a systematic and disciplined development approach (Figure 1.6).

- **System Requirement Analysis**
  In the initial step of the V-model development phase, requirement analysis is conducted to understand the specific needs of the illumination system in the context of optogenetics cardiac research. This includes clear communication with the biomedical researchers to concretely define the overall application requirements of the system such as intensity, wavelength, control precision, as well as its compatibility with the intended biological applications.

- **System Architecture Design**
  Following the requirement analysis, the system design phase outlines the overall architecture of the illumination system. It includes planning the overall structure of subsystems with hardware and software components that will form the system. This step breaks down the system into smaller, manageable modules, each with its specific design parameters, such as light sources, control circuits, software, and user interfaces. The application requirements are decomposed, translated, and extended into technical requirements with specifications of each subsystem.

- **Subsystem Design**
  The next stage involves the detailed design of subsystems and components. Each subsystem is defined in detail, considering specific functionalities and requirements. This approach allows for a focused and in-depth development of each part of the system, ensuring that all aspects are thoroughly addressed and integrated effectively in later stages.

- **Implementation**
  Once the designs are in place, the implementation step begins. This involves building and assembling the components as per the subsystem design specifications. Components are either fabricated or outsourced, and integrated into functional subsystems. Practical expertise is needed such as printed circuit board (PCB) design and assembly or bio-compatible encapsulation processes.

- **Subsystem Verification**
  After implementation, each component and subsystem is verified by individual tests. This is a critical aspect of the V-model, where testing is done in parallel with each stage of development to ensure that each element functions as intended and meets the criteria, for example, the light source illumination function is qualitatively tested so that all elements should be working without defects, and the electrical circuits are functional without interruptions.

- **System Verification**
  All subsystems are integrated into a fully functional system. The integrated system is then subjected to comprehensive testing to verify its overall functionality and performance to align with the initially defined system specifications. Important parameters such as optical characteristics are tested, to ensure that the complete illumination system operates effectively and reliably under the conditions it is expected in the applications.

- **System Validation**
  Finally, the system is delivered to application validation, which is the optogenetics experiments for the arrhythmia study. It should support intensive biomedical experiments with sufficient technical performance as well as long-term consistency and reliability. The system is continuously monitored for performance and will be updated as necessary.

Using the V-model system engineering methodology in the development of the illumination system ensures that each phase of development is thoroughly tested and validated, significantly reducing the risk of errors and ensuring a high-quality final product.

1.3. RESEARCH OBJECTIVES

1. Identifying the challenges in the design and development of optoelectronics illumination systems for cardiac optogenetics studies. Filling the research gap between the realization of these systems and currently available optoelectronics products and technologies.

2. Demonstrating various technical system developments that follow an efficient design methodology. Illustrating the system engineering approaches and highlighting key stages in the development including requirement analysis, design, development, verification, and validation, ensuring each phase is conducted effectively and efficiently.

3. Contributing to the original and translational cardiac optogenetics studies that explore insights into novel biomedical methods of treating cardiac arrhythmias, which have not been thoroughly explored before.

4. Building a technical foundation for further research, offering insights, technology expertise, development methodologies, or questions that others can build upon for future advanced systems for cardiac optogenetics studies.

5. Developing and demonstrating professional research skills including critical thinking, analytical writing, and presenting complex ideas. Supporting the unique multi-discipline collaboration between technical competencies.

1.4. LAYOUT OF THIS DISSERTATION

The layout of this dissertation is as follows.

Chapter 2 of this dissertation presents a thorough background introduction to LED technology, tracing its evolution from inception to its diverse applications, and focusing particularly on the characteristics that make it an important tool in optogenetics. This chapter also provides a comprehensive review of state-of-the-art optoelectronic illumination systems used in neural and cardiac optogenetics research and summarizes the challenges associated with their development and practical design.

Following Chapters 3 to 6, are dedicated to exploring various design and development processes of individual optoelectronic illumination systems specifically tailored for optogenetic cardiac applications, showcasing the innovative approaches and technical development methodology.

Chapter 3 presents the design and development of a novel, custom-developed LED illumination system for treating ventricular fibrillation (VF), a serious cardiac arrhythmia. It discusses the system's development cycle including testing, integration, verification, and validation for both in-vivo and ex-vivo experiments in rat models, highlighting its unique bio-compatibility design and optical characteristics. The chapter also presents biological findings from these experiments, assessing the system's effectiveness in treating VF and exploring its implications for future cardiac therapies.

Chapter 4 presents an innovative optogenetics approach for Atrial fibrillation (AF) termination, focusing on the development of a high-power LED matrix illumination system. It details the design, testing, and implementation of this specialized, implantable system for use in both in-vivo and ex-vivo optogenetics experiments for swine models.

Chapter 5 presents an innovative method of studying arrhythmia behaviors using a

human immortalized atrial myocyte (hiAM) model with a focus on the design and development of the 16x16 LED matrix illumination system for proof-of-concept purposes. This involves the designing, testing, and implementation of the specialized, modular LED matrix and its controlling system as part of the novel in-vitro experimental platform. This demonstrative system set a good theoretical and practical basis for the more advanced illumination system for cardiovascular research.

Chapter 6 follows the successful practice in the proof-of-concept system from the last chapter and presents the development of a 16x16 mini-LED matrix illumination system as an enhanced version. This upgraded system focuses on achieving finer control in hiAM cell culture experiments. It features mini-LED bare-die chips for more precise illumination, improved substrate materials for enhanced performance and flexibility, and a refined driver and controller system for better management of the smaller mini-LED elements. This system supports the intersection of fundamental cardiovascular research and electronics technology, offering new insights into cardiac arrhythmia control.

Chapter 7 summarizes the overall conclusion of this dissertation and discusses some limitations and suggestions for future work.

In conclusion, this dissertation begins with a discussion of design methodology with relevant backgrounds. This foundational knowledge sets the basis for the following examples of illumination systems. Each example facilitates the background information and follows the outlined methodology as part of its development cycle. This approach not only illustrates the practical application of the theoretical framework but also demonstrates the versatility and effectiveness of the methodology in real-world scenarios.

BIBLIOGRAPHY

[1] Roy M John et al. “Ventricular arrhythmias and sudden cardiac death”. In: *The Lancet* 380.9852 (2012), pp. 1520–1529.

[2] Carl J Wiggers. “The mechanism and nature of ventricular fibrillation”. In: *American Heart Journal* 20.4 (1940), pp. 399–412.

[3] Alan S Go et al. “Heart disease and stroke statistics—2014 update: a report from the American Heart Association”. In: *circulation* 129.3 (2014), e28–e292.

[4] Borys Surawicz. “Ventricular fibrillation”. In: *The American Journal of Cardiology* 28.3 (1971), pp. 268–287.

[5] Sheldon Cheskes et al. “Defibrillation strategies for refractory ventricular fibrillation”. In: *New England Journal of Medicine* 387.21 (2022), pp. 1947–1956.

[6] William G Stevenson Gregory F Michaud 1. “Atrial Fibrillation”. In: *The New England Journal of Medicine* 28.384 (2021), pp. 353–361.

[7] Juqian Zhang et al. “Epidemiology of atrial fibrillation: geographic/ecological risk factors, age, sex, genetics”. In: *Cardiac electrophysiology clinics* 13.1 (2021), pp. 1–23.

[8] Christopher RC Wyndham. “Atrial fibrillation: the most common arrhythmia”. In: *Texas Heart Institute Journal* 27.3 (2000), p. 257.

[9] Yong-Mei Cha et al. “Atrial fibrillation and ventricular dysfunction: a vicious electromechanical cycle”. In: *Circulation* 109.23 (2004), pp. 2839–2843.

[10] Deirdre A Lane Gregory Y H Lip 1 Hung Fat Tse. “Atrial fibrillation”. In: *Lancet* 379.648-61 (2012).

[11] Emelia J Benjamin et al. “Independent risk factors for atrial fibrillation in a population-based cohort: the Framingham Heart Study”. In: *Jama* 271.11 (1994), pp. 840–844.

[12] Gerhard Hindricks et al. “2020 ESC Guidelines for the diagnosis and management of atrial fibrillation developed in collaboration with the European Association for Cardio-Thoracic Surgery (EACTS) The Task Force for the diagnosis and management of atrial fibrillation of the European Society of Cardiology (ESC) Developed with the special contribution of the European Heart Rhythm Association (EHRA) of the ESC”. In: *European heart journal* 42.5 (2021), pp. 373–498.

[13] Maria Velleca et al. “A review of the burden of atrial fibrillation: understanding the impact of the new millennium epidemic across Europe”. In: *Cardiology* (2019).

[14] Alvaro Alonso, Zakaria Almuwaqqat, and Alanna Chamberlain. “Mortality in atrial fibrillation. Is it changing?” In: *Trends in cardiovascular medicine* 31.8 (2021), pp. 469–473.

[15] James L Cox et al. “An 8 1/2-year clinical experience with surgery for atrial fibrillation.” In: *Annals of surgery* 224.3 (1996), p. 267.

[16] Timo Weimar et al. “The Cox-maze IV procedure for lone atrial fibrillation: a single center experience in 100 consecutive patients”. In: *Journal of Interventional Cardiac Electrophysiology* 31 (2011), pp. 47–54.

[17] Timo Weimar et al. “The cox-maze procedure for lone atrial fibrillation: a single-center experience over 2 decades”. In: *Circulation: Arrhythmia and Electrophysiology* 5.1 (2012), pp. 8–14.

[18] Steven L Higgins et al. “Cardiac resynchronization therapy for the treatment of heart failure in patients with intraventricular conduction delay and malignant ventricular tachyarrhythmias”. In: *Journal of the American College of Cardiology* 42.8 (2003), pp. 1454–1459.

[19] James B Young et al. “Combined cardiac resynchronization and implantable cardioversion defibrillation in advanced chronic heart failure: the MIRACLE ICD Trial”. In: *Jama* 289.20 (2003), pp. 2685–2694.

[20] TV Salukhe, DP Francis, and R Sutton. *Comparison of medical therapy, pacing and defibrillation in heart failure (COMPANION) trial terminated early; combined biventricular pacemaker-defibrillators reduce all-cause mortality and hospitalization*. 2003.

[21] J Christoph Geller et al. “Treatment of atrial fibrillation with an implantable atrial defibrillator—long term results”. In: *European heart journal* 24.23 (2003), pp. 2083–2089.

[22] Takashi Ashihara and Natalia A Trayanova. “Cell and tissue responses to electric shocks”. In: *EP Europace* 7.s2 (2005), S155–S165.

[23] Giuseppe Boriani et al. “Evaluation of myocardial injury following repeated internal atrial shocks by monitoring serum cardiac troponin I levels”. In: *Chest* 118.2 (2000), pp. 342–347.

[24] Mark Josephson and Hein JJ Wellens. “Implantable defibrillators and sudden cardiac death”. In: *Circulation* 109.22 (2004), pp. 2685–2691.

[25] Jason S Bradfield et al. “Mechanisms and management of refractory ventricular arrhythmias in the age of autonomic modulation”. In: *Heart Rhythm* 15.8 (2018), pp. 1252–1260.

[26] MPLMM Mirowski et al. “Clinical treatment of life-threatening ventricular tachyarrhythmias with the automatic implantable defibrillator”. In: *American heart journal* 102.2 (1981), pp. 265–270.

[27] Cardionetoworks Foundation and the Health[e]Foundation. *Textbook of Cardiology*. https://www.textbookofcardiology.org. 2022.

[28] Lief Fenno, Ofer Yizhar, and Karl Deisseroth. “The development and application of optogenetics”. In: *Annual review of neuroscience* 34 (2011), pp. 389–412.

[29] Jens Duebel, Katia Marazova, and José-Alain Sahel. “Optogenetics”. In: *Current opinion in ophthalmology* 26.3 (2015), p. 226.

[30] Brian Y Chow and Edward S Boyden. “Optogenetics and translational medicine”. In: *Science translational medicine* 5.177 (2013), 177ps5–177ps5.

[31] Lung National Heart and Blood Institute. *HOW THE HEART WORKS: How the Heart Beats*. https://www.nhlbi.nih.gov/health/heart/heart-beats. 2022.

[32] Frederic H Martini and Frederic Martini. *Anatomy & physiology*. Rex Bookstore, Inc., 2005.

[33] Edward S Boyden et al. “Millisecond-timescale, genetically targeted optical control of neural activity”. In: *Nature neuroscience* 8.9 (2005), pp. 1263–1268.

[34] Viviana Gradinaru, Kimberly R Thompson, and Karl Deisseroth. “eNpHR: a Natronomonas halorhodopsin enhanced for optogenetic applications”. In: *Brain cell biology* 36 (2008), pp. 129–139.

[35] American Heart Association. *Implantable Cardioverter Defibrillator (ICD)*. https://www.heart.org/en/health-topics/arrhythmia/prevention--treatment-of-arrhythmia/implantable-cardioverter-defibrillator-icd. 2022.

[36] Gero Miesenböck and Ioannis G Kevrekidis. “Optical imaging and control of genetically designated neurons in functioning circuits”. In: *Annu. Rev. Neurosci.* 28 (2005), pp. 533–563.

[37] Pau Gorostiza and Ehud Y Isacoff. “Optical switches for remote and noninvasive control of cell signaling”. In: *Science* 322.5900 (2008), pp. 395–399.

[38] Boris V Zemelman et al. “Selective photostimulation of genetically chARGed neurons”. In: *Neuron* 33.1 (2002), pp. 15–22.

[39] Boris V Zemelman et al. “Photochemical gating of heterologous ion channels: remote control over genetically designated populations of neurons”. In: *Proceedings of the National Academy of Sciences* 100.3 (2003), pp. 1352–1357.

[40] Susana Q Lima and Gero Miesenböck. “Remote control of behavior through genetically targeted photostimulation of neurons”. In: *Cell* 121.1 (2005), pp. 141–152.

[41] Matthew Banghart et al. “Light-activated ion channels for remote control of neuronal firing”. In: *Nature neuroscience* 7.12 (2004), pp. 1381–1386.

[42] Matthew R Banghart, Matthew Volgraf, and Dirk Trauner. “Engineering light-gated ion channels”. In: *Biochemistry* 45.51 (2006), pp. 15129–15141.

[43] Stephanie Szobota et al. “Remote control of neuronal activity with a light-gated glutamate receptor”. In: *Neuron* 54.4 (2007), pp. 535–545.

[44] Matthew Volgraf et al. “Allosteric control of an ionotropic glutamate receptor with an optical switch”. In: *Nature chemical biology* 2.1 (2006), pp. 47–52.

[45] Brian Y Chow et al. “High-performance genetically targetable optical neural silencing by light-driven proton pumps”. In: *Nature* 463.7277 (2010), pp. 98–102.

[46] Xue Han and Edward S Boyden. “Multiple-color optical activation, silencing, and desynchronization of neural activity, with single-spike temporal resolution”. In: *PloS one* 2.3 (2007), e299.

[47] Karl Deisseroth et al. “Next-generation optical technologies for illuminating genetically targeted brain circuits”. In: *Journal of Neuroscience* 26.41 (2006), pp. 10380–10386.

[48] Doug Tischer and Orion D Weiner. “Illuminating cell signalling with optogenetic tools”. In: *Nature reviews Molecular cell biology* 15.8 (2014), pp. 551–558.

[49] Linda Madisen et al. “A toolbox of Cre-dependent optogenetic transgenic mice for light-induced activation and silencing”. In: *Nature neuroscience* 15.5 (2012), pp. 793–802.

[50] Guolin Ma et al. “Optogenetic toolkit for precise control of calcium signaling”. In: *Cell calcium* 64 (2017), pp. 36–46.

[51] Viviana Gradinaru et al. “Molecular and cellular approaches for diversifying and extending optogenetics”. In: *Cell* 141.1 (2010), pp. 154–165.

[52] Feng Zhang et al. “Multimodal fast optical interrogation of neural circuitry”. In: *Nature* 446.7136 (2007), pp. 633–639.

[53] Anding Bi et al. “Ectopic expression of a microbial-type rhodopsin restores visual responses in mice with photoreceptor degeneration”. In: *Neuron* 50.1 (2006), pp. 23–33.

[54] Kenneth P Greenberg, Aaron Pham, and Frank S Werblin. “Differential targeting of optical neuromodulators to ganglion cell soma and dendrites allows dynamic control of center-surround antagonism”. In: *Neuron* 69.4 (2011), pp. 713–720.

[55] Aristides B Arrenberg et al. “Optogenetic control of cardiac function”. In: *Science* 330.6006 (2010), pp. 971–974.

[56] Karl Deisseroth. “Optogenetics”. In: *Nature methods* 8.1 (2011), pp. 26–29.

[57] Seppo Ylä-Herttuala and Andrew H Baker. “Cardiovascular gene therapy: past, present, and future”. In: *Molecular Therapy* 25.5 (2017), pp. 1095–1106.

[58] Patrick M Boyle, Thomas V Karathanos, and Natalia A Trayanova. “Cardiac optogenetics: 2018”. In: *JACC: Clinical Electrophysiology* 4.2 (2018), pp. 155–167.

[59] Oscar J Abilez. “Optogenetic LED array for perturbing cardiac electrophysiology”. In: *2013 35th Annual International Conference of the IEEE Engineering in Medicine and Biology Society (EMBC)*. IEEE. 2013, pp. 1619–1622.

[60] Brian O Bingen et al. “Light-induced termination of spiral wave arrhythmias by optogenetic engineering of atrial cardiomyocytes”. In: *Cardiovascular research* 104.1 (2014), pp. 194–205.

[61] Emile CA Nyns et al. “Optogenetic termination of ventricular arrhythmias in the whole heart: towards biological cardiac rhythm management”. In: *European heart journal* 38.27 (2017), pp. 2132–2136.

[62] Claudia Crocini et al. “Optogenetics design of mechanistically-based stimulation patterns for cardiac defibrillation”. In: *Scientific reports* 6.1 (2016), p. 35628.

[63] Emile CA Nyns et al. “An automated hybrid bioelectronic system for autogenous restoration of sinus rhythm in atrial fibrillation”. In: *Science translational medicine* 11.481 (2019), eaau6447.

[64] Emile CA Nyns et al. “Optical ventricular cardioversion by local optogenetic targeting and LED implantation in a cardiomyopathic rat model”. In: *Cardiovascular research* 118.10 (2022), pp. 2293–2303.

[65] Masaya Watanabe et al. “Optogenetic manipulation of anatomical re-entry by light-guided generation of a reversible local conduction block”. In: *Cardiovascular research* 113.3 (2017), pp. 354–366.

[66] Iolanda Feola et al. “Optogenetic engineering of atrial cardiomyocytes”. In: *Optogenetics: Methods and Protocols* (2016), pp. 319–331.

[67] Iolanda Feola et al. “Localized optogenetic targeting of rotors in atrial cardiomyocyte monolayers”. In: *Circulation: Arrhythmia and Electrophysiology* 10.11 (2017), e005591.

[68] Rupamanjari Majumder et al. “Optogenetics enables real-time spatiotemporal control over spiral wave dynamics in an excitable cardiac system”. In: *Elife* 7 (2018), e41076.

[69] ECA Nyns et al. “2160 Continuous shock-free termination of atrial fibrillation by local optogenetic therapy and arrhythmia-triggered activation of an implanted light source”. In: *European Heart Journal* 40.Supplement_1 (2019), ehz748–0090.

2

Optoelectronics Illumination System for Optogenetics Applications: State-of-the-art

2.1. INTRODUCTION

This chapter explores the illumination technology and technical solutions of optoelectronic systems in the field of optogenetics. It explores various aspects, including the background of LEDs, optical systems with advanced LED technology, and their roles in medical and biomedical applications. The chapter provides a comprehensive overview of the state-of-the-art solutions for integrating illumination systems for neural optogenetics and cardiac optogenetics studies. It offers insights into the design challenges of integration of the LED illumination system for cardiac optogenetics study, highlighting the challenge of balancing biomedical requirements and technical implementation.

2.2. LIGHT EMITTING DIODE (LED)

Light Emitting Diode (LED) is a kind of semiconductor light source that emits light when current flows through it. This name directly describes the fundamental function and construction of the device: Light Emitting and Diode.

Unlike incandescent bulbs, which produce light by heating a filament, or fluorescent lamps, which use a gas discharge, LEDs generate light through electroluminescence: a phenomenon where a material **emits light** in response to an electric current or a strong electric field. A **diode** is a type of semiconductor device that allows current to flow in one direction only. A diode is the key component of an LED, giving the basic structure that allows for the electroluminescence effect.

The phenomenon of electroluminescence was discovered in the early 20th century. In 1907, H.J. Round, a British experimenter, reported light emission from semiconductor diodes using a crystal of silicon carbide and a cat's-whisker detector[1]. In the 1920s, Russian scientist Oleg Losev conducted several experiments on diodes in radio sets and observed light emission from zinc oxide (ZnO) and silicon carbide (SiC) point-contact junctions. Throughout the early to mid-20th century, theoretical and experimental work on semiconductors laid the foundation for the development of the LED.

The first practical LED was created in 1962 by Nick Holonyak Jr.[2], an engineer working at General Electric. Holonyak's LED emitted visible red light and was based on gallium arsenide phosphide (GaAsP) as the semiconductor material. Holonyak's invention was the first LED that could emit light in the visible spectrum, making it suitable for practical use in indicators. He is often referred to as the "father of the LED".

Early LEDs were limited in terms of efficiency and brightness. A significant breakthrough came in the early 1990s with the collaborative invention of the blue LED by Isamu Akasaki, Hiroshi Amano, and Shuji Nakamura. This development was particularly

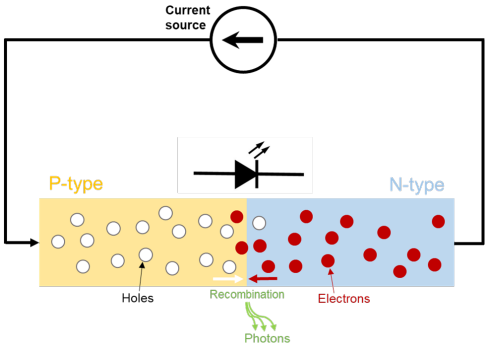

Figure 2.1: Electroluminescence of a P-N junction under forward current

important as it eventually led to the creation of white LEDs by combining blue LEDs with phosphor coatings, and opened up a wide range of applications in lighting and displays. The invention of the blue LED was so significant that Akasaki, Amano, and Nakamura were awarded the Nobel Prize in Physics in 2014 for their work[3].

LEDs are often referred to as Solid-State Lighting (SSL) for are made of semiconductor materials, which are often referred to as Solid-State Devices. LEDs are made from typically group III and group V of the periodic table, such as gallium arsenide (GaAs), gallium nitride (GaN), or indium gallium nitride (InGaN). Those materials are doped by the introduction of impurities to change their electrical properties. In one part of the semiconductor, an element with more valence electrons than the base material is added. This creates excess free electrons and forms an n-type (negative-type) semiconductor, where electrons are the majority of charge carriers. In another part of the semiconductor, an element with fewer valence electrons than the base material is introduced. This creates "holes" (places where an electron is missing), forming a p-type (positive-type) semiconductor, where holes are the majority of charge carriers.

The p-type and n-type materials are brought together into one device and it creates a P-N junction at the interface, which becomes the core structure of a diode. When a suitable voltage is applied to each side of the P-N junction, electrons can recombine with electron holes within the device, releasing energy in the form of photons. This effect is called electroluminescence (Figure 2.1), which is the fundamental principle of LED's illumination[4].

The color of the light, corresponding to the energy of the photons the LED emits, is determined by the energy band gap of the semiconductor material. This band gap defines the energy difference between the highest occupied electronic state (in the valence band) and the lowest unoccupied electronic state (in the conduction band). When an

electron falls from the conduction band to the valence band, it releases energy in the form of a photon. Higher energy photons correspond to shorter wavelengths (towards the blue/violet end of the spectrum), while lower energy photons correspond to longer wavelengths (towards the red end of the spectrum)[5].

Because the band gap represents a fixed energy difference, the photons emitted when electrons transition back to the valence band have a specific energy, and thus a specific wavelength. This means the light emitted is not a continuous spectrum but rather a narrow range of wavelengths corresponding to the band gap energy. Though tuning of semiconductor doping can also change the band gap, it is challenging to create a continuous spectrum of LED products due to efficiency and manufacturing complexity. Phosphor conversion is another way to change the wavelength an LED emits. A blue or ultraviolet LED is coated with a phosphor material that absorbs some of the blue or UV light and re-emits photons at longer wavelengths. By tuning the phosphor's chemical compositions, the combination of the original electroluminescence light and the longer wavelength light can result in white light.

LEDs have become increasingly popular due to their advantages over traditional light source solutions like incandescent and fluorescent bulbs, such as

1. **Energy Efficiency:** LEDs are significantly more energy-efficient than traditional light sources by typically 75% less energy[6]. This efficiency also translates to overall lower heat generated, making it safer and economical in many applications.

2. **Reliability:** LEDs have a much longer lifespan compared to traditional light sources. An average LED can last up to 25,000 to 50,000 hours, whereas an incandescent bulb typically lasts about 1,000 hours and a fluorescent tube around 8,000 hours[7]. Also, LEDs are more resistant to shock, vibrations, or external impacts.

3. **Wide Color Range:** LEDs can be designed to emit light at very specific wavelengths, allowing for precise control over the color of the light. This is particularly useful in applications like displays. By varying the semiconductor materials and the manufacturing process, LEDs can cover a broad spectrum of colors, from deep ultraviolet through the visible spectrum to far infrared.

4. **Design Flexibility:** Due to their small size, LEDs offer great design flexibility. They can be used in applications ranging from slim displays and delicate lighting of large architectural installations.

5. **Fast lighting and Frequent Switching:** LED lights start up immediately when the current is powered on, which is a significant advantage over fluorescent lamps that

take time to warm up. Additionally, LEDs can be switched off and on frequently and rapidly by a programmable control signal to achieve efficient dimming functions.

6. **Ecologically Friendly:** LEDs are free from toxic chemicals and do not contain mercury or rare gases, unlike fluorescent lights. This makes them environmentally safer and easier to dispose of or recycle.

Other advantages such as high color purity, directional lighting, etc. are not further discussed here. However, there are also some disadvantages and challenges associated, such as

1. **Cost:** The cost of LED lighting is typically higher than that of traditional incandescent and fluorescent lights. However, this is often reduced over time by energy savings and longer lifespan.

2. **Temperature Sensitivity:** LEDs can be sensitive to high temperatures by overheating, which can affect their lifetime and efficiency. Proper heat dissipation and management are needed especially in high-power LED applications.

3. **Lumen Depreciation:** The light flux output (unit: lumen) of an LED will gradually decay over time, due to the increase of non-radiant recombination which reduces the total number of emitted photons. Lumen depreciation is physically inevitable but can be predicted and reduced by proper maintenance and using conditions[8][9].

4. **Blue Light Content:** Some LEDs emit a high level of blue light, which can be a concern for eye health and circadian rhythm disruption, especially in high-intensity or high-exposure environments[10].

5. **Color Shift:** Over time, the light output of LEDs can shift in color, especially if the LEDs are of lower quality or are operating in high-temperature environments, usually due to the depreciation of phosphor coatings in the chip.

6. **Electronic Complexity:** LEDs require drivers and other electronics to operate, which adds complexity and potential points of failure compared to simpler lighting technologies like incandescent bulbs.

7. **Disposal and Recycling:** While LEDs don't contain toxic chemicals such as mercury, they do have electronic components that can make disposal and recycling more complex compared to traditional incandescent bulbs.

The global LED market has been growing steadily over the past decade. The global LED lighting market size was valued at USD 78.24 billion in 2022. The market is projected to grow from USD 87.10 billion in 2023 to USD 298.38 billion by 2030, exhibiting a CAGR of 19.2% during the forecast period[11]. This growth is attributed to the widespread adoption of LED technology in various sectors including residential, commercial, industrial, and outdoor applications. Companies like Philips (Signify), Osram, Cree, and GE Lighting are among the leading players in the global LED market.

2.3. OPTICAL SYSTEM WITH LED

LEDs are current-driven devices, meaning their brightness or optical power is proportional to the current flowing through them at most working range (Figure 2.2) before power saturation due to reduced quantum efficiency. A constant current source ensures uniform optical output and prevents fluctuations that can occur with voltage variations. The current and voltage of a typical LED can be described by the P-N junction current function:

$$i_D = i_s(e^{\frac{V_D}{nKT}} - 1) \tag{2.1}$$

Where i_D is the current flow through the LED device, i_s is a constant value of reverse saturation current, V_D is the voltage across the LED, n and K are constants and T is the temperature in Kelvins. An LED only starts to illuminate when the applied voltage exceeds a certain limit, which is determined as the threshold voltage.

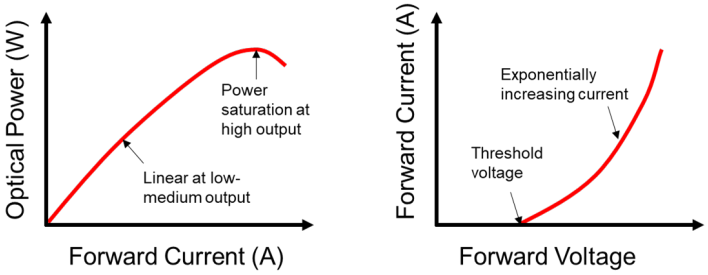

Figure 2.2: Optical power-current and current-voltage characteristics of a typical LED chip

The reason why it is important to drive LEDs with current control is that LEDs can experience thermal runaway if driven by a voltage source. Unlike resistive devices, their resistance can change dramatically with temperature. As an LED heats up due to Joule

heating from the flowing through current, its internal resistance decreases, which can lead to more current flowing through it if the voltage is constant. This increased current can generate more heat, further lowering resistance, and creating a positive feedback cycle that can eventually damage the LED by excess heat. Accurate current control prevents this by ensuring that the current remains at a safe level regardless of temperature changes.

A current limiting resistor is a common practice for the safe and efficient operation of the LED. This resistor is connected in series with the LED chip to prevent the LED from being exposed to the full supply voltage and serves as a regulator of the current to the LED to prevent excessive current from damaging the device or reducing performance. The physical value of this resistor is determined using Ohm's Law, taking into account the voltage drop across the resistor and the desired current flowing through the LED. The calculation typically used is:

$$R_{limit} = \frac{V_{source} - V_{LED}}{I_{max}} \tag{2.2}$$

Where R_{limit} is the value for the current limiting resistor Resistor, V_{source} is the power supply's maximum voltage, V_{LED} is the specific voltage drop of the LED and I_{max} is the specific maximum current of the LED. The power rating of the resistor, usually measured in watts, is also an important consideration for the system design. It must be capable of handling the power dissipated, calculated using the equation:

$$P_{limit} = I_{max}^2 \times R_{limit} \tag{2.3}$$

As it dissipates excess energy as heat, thermal management becomes a crucial aspect of circuit design, especially in high-power applications. Usually, a high-power rating resistor has a large footprint and needs additional volume and air convection in the system.

When driving multiple LEDs, connecting them in series is often preferred over a parallel arrangement. In a series configuration, the same current flows through each LED, ensuring that each one has a consistent optical output level as it is proportional to the input current. This uniformity is crucial for applications that require consistent light output across all LEDs. Additionally, managing the current in a series circuit is simpler as it requires only one current-limiting resistor and current source for the entire string, making the circuit design more straightforward.

Series connections also have drawbacks. Because each LED has a specific voltage drop determined by its intrinsic manufacturing process, in a series circuit, these drops

add up. The total voltage required is the sum of all the individual drops in a string of LEDs. When more LED elements are connected in one series string, the total voltage needed for the circuit becomes higher. This gives additional considerations for a high-voltage-output current source, which is in practice more costly, and bulky. For applications that have limited allowed voltage for safety requirements, for example, bio-medical systems, series connection gives a limitation of the amount of LED elements in a string. Moreover, if one LED fails, particularly in an open-circuit failure, it can cause the entire string of LEDs to stop working. Therefore a common practice is to split the full amount of LED elements into a few strings of LED in series and connect them separately with their current sources. The output of those current sources should be equally calibrated to ensure uniformity and protect against variations in LED performance.

2.4. OPTICAL SYSTEM WITH ADVANCED LED TECHNOLOGY

Advanced LED technology refers to the latest developments and innovations in the field of LED lighting that go beyond basic domestic illumination. These advancements have significantly broadened the applications and capabilities of LED technology, making LEDs not just sources of light, but also tools for communication, health, and environmental sustainability. A few major advanced LED applications are listed as follows.

Advanced LED Displays LED technology plays a crucial role in modern display technologies. Since the 1990s, Liquid Crystal Display (LCD) screens started to use LEDs for back-lighting instead of cold cathode fluorescent (CCFL) lighting. Currently days LCD screens with LED as back-lighting are used almost everywhere in life, including televisions, computer monitors, and smart devices. With the help of advanced LED development, quantum dot LEDs (QLEDs) and Micro-LED displays represent two advanced technologies in the field of display.

QLEDs use quantum dots, which are tiny semiconductor particles only a few nanometers in size in the display, to enhance the light from the LED back-light before it passes through the LCD layer to form an image[12][13]. A QLED display uses a traditional LED backlight, which emits white light. The light then passes through a layer of quantum dots, which absorb some of the back-light and re-emit it at different wavelengths based on their sizes. This process enhances the color purity and brightness of the LED-emitted light. QLED technology is popularly used in high-end televisions and monitors nowadays.

The micro-LED display is made of micro-LED chips, which are very small LED units, typically less than 100um in size, commonly about 1-10um[14] large. The manufacturing processes place thousands or millions of micro-LEDs onto a planar substrate. This

process is technically challenging, especially for smaller, high-resolution displays. Each Micro-LED acts as an individual pixel in a display, and has very high brightness levels to allow for high contrast ratios, while maintaining good energy efficiency[15]. Micro-LED display is deal for high-end televisions, smartwatches, and smartphones where high brightness and high contrast ratio are desired. With innovations in substrate technologies, micro-LED displays can be flexible or even stretchable for special applications. However, due to manufacturing complexity and high cost, the micro-LED displays are limited currently in research concepts and technical demonstrators.

Extend LED wavelength to UV(C) and IR The development of LEDs with extended wavelengths other than the visible spectrum is a significant result of the semiconductor material and process advancements, opening new possibilities for advanced applications.

Aluminum gallium nitride (AlGaN) is a semiconductor material commonly used for LED manufacturing. By varying the aluminum content, the band gap can be adjusted, which is crucial for tuning the wavelength of the emitted light. AlGaN LEDs are particularly noted for their ability to produce ultraviolet (UV) light[16]. AlGaN LEDs that emit wavelengths ranging from about 200 to 280 um (UV-C band) are called UVC LEDs and are already used for disinfecting water, air, and surfaces in various settings, including medical facilities, laboratories, and consumer products[17]. Unlike conventional UVC lamps that contain mercury, UVC LEDs are favored for being environmentally friendly and safe, as well as more energy-efficient and more reliable. Also, the small size of UVC LEDs, usually in mm dimensions compared to a few tens of cm of traditional mercury lamps, allows for innovative designs in portable disinfection devices and minimized integrated systems. Challenges still exist, however, such as the high cost of UVC LED chips due to manufacturing complexity and low power output per chip due to material limitations. Though prices have been decreasing with advancements in semiconductor technology and high performance, high-power UVC LEDs are seen in the markets.

Photo-catalysis material like titanium dioxide (TiO2), becomes active when exposed to light at certain wavelengths (usually UV). UV LEDs are commonly used as a light source to activate a photo-catalyst[18], leading to a highly efficient chemical reaction. This method is widely used in air purification devices or water treatment systems for sterilization or disinfection purposes.

Infrared (IR) LEDs typically emit light in the wavelength range of 700nm to 1000nm. Common materials used for IR LEDs include GaAs and AlGaAs[19]. They have various applications in consumer electronics, communication, security, and medical devices. IR LEDs are commonly used to transmit data via optical fibers by modulating light rapidly

to represent digital information. IR photo-diodes are used to detect the modulated IR light and convert it back into electrical signals to transmit the original data. This well-established communication technology is widely used due to its cost-effective and robust characteristics. IR LEDs are also commonly used in sensing applications in industrial, automotive, or home security.

High-power LED Lighting High-power LEDs are designed to deliver high optical flux and high irradiance, usually for industrial lighting applications, such as outdoor displays, such as LED billboards. They are large, bright screens used for displaying images, videos, or texts in outdoor environments. They are widely used for advertising, information broadcasting, and entertainment purposes. These LED displays usually consist of numerous LED modules, which contain arrays of LED pixels. Each pixel contains one or multiple high-power LED chips and an optical lens to regulate light direction. The modules can be configured to various sizes and resolutions depending on the application, and each pixel can be programmed by a center controller for image or video display. Outdoor displays are designed with high brightness levels to be visible even in direct sunlight, and they are built to withstand various weather conditions, including rain, wind, and extreme temperatures. Weatherproof packages and thermal solutions are the key design aspects for these LED applications.

Laser-Enhanced LED Lighting Laser-enhanced LED lighting is an innovative technology that combines the principles of laser diodes and LEDs to produce highly efficient and high-power light. Instead of traditional electroluminescence diodes, it uses laser diodes to generate coherent and highly focused light beams. Similar to conventional LEDs, phosphor material converts the laser intensity into a bright, broad-spectrum, and diffused light. In this way, the total efficiency is increased while maintaining high power output. It is especially favored in high brightness and intensity light sources in very limited sizes. One of the most prominent applications of laser-enhanced LED lighting is in the automotive[20][21], particularly for car headlights. These Laser-enhanced LED headlights provide superior illumination, extending the light range and intensity of the beam compared to standard LED headlights.

Special LED applications LED lighting has become increasingly important in agriculture, particularly in controlled-environment agriculture like commercial greenhouses and vertical farming. The ability of LEDs to produce specific light wavelengths efficiently makes them favorable for plant growth and development while maintaining lower energy consumption.

Modern LED lighting systems have excellent color rendering capabilities with the ability to adjust wavelength or color temperature, which means they can accurately re-

produce the colors of artworks without distortion. With limited UV or IR components and minimal heat emission, LEDs are used in galleries or museums to avoid damaging delicate artworks or historical relics.

2.5. LED LIGHTING IN MEDICAL OR BIOMEDICAL APPLICATIONS

LED lighting technology is seen in clinical research and biomedical applications, offering significant advantages due to its unique characteristics such as flexibility, energy efficiency, and ability to provide controlled, specific illuminations. Its continued development promises even more innovative uses in medical or biomedical applications.

2.5.1. LED LIGHTING IN GENERAL MEDICAL OR BIOMEDICAL APPLICATIONS

Intense Pulsed Light (IPL) for skincare is a non-invasive cosmetic treatment for skin conditioning purposes[22]. The concept is based on selective photothermolysis: skin-penetrating light energy is absorbed by specific target cells in the skin at different depths with different light wavelengths, such as melanin in hair or pigmented lesions and hemoglobin in blood vessels. The absorbed light then converts energy to heat at local spots, which selectively damages the target cells. It is widely used in hair removal treatment, and photo-rejuvenation to improve skin texture, wrinkles or sunspots removals, etc. With LED-based IPL systems, this is achieved through multiple LEDs customized to emit light at different wavelengths with specified light dose[23]. They emit less heat and therefore discomfort compared to traditional flashlamp-based IPL systems and provide higher precision and safety due to the ability of narrow band wavelength and better dose control. While IPL skincare treatments are generally considered safe when performed by qualified professionals, there are potential risks and side effects associated such as allergy or irritation, skin pigment darkening, and burns.

Phototherapy is a medical treatment method that involves exposing the skin or body to specific types of light, to treat skin diseases or skin conditions[24]. It exposes the patient's skin under controlled illumination, usually Ultraviolet A (UVA) or Ultraviolet B (UVB) with a wavelength between 280 to 400nm. The dose of the illumination must be strictly controlled as the extra UV causes damage to human cells, even skin cancer. Phototherapy is the most frequently used treatment for different skin diseases, including parapsoriasis, psoriasis, pityriasis lichenoides chronica, eczema, and many others. Newborns with jaundice are treated with blue light therapy. The blue light helps break down bilirubin in the skin, which the newborn liver can't process effectively. LED lighting technology has become increasingly important in phototherapy due to its efficiency, safety, and ability to produce specific narrow-band wavelengths of light with well-controlled

doses.

2.5.2. ILLUMINATION SYSTEM IN NEURAL OPTOGENETICS

LEDs have become a crucial tool in optogenetics for both biomedical research and clinical applications, largely due to their small size and the precision with which they can achieve localized illumination. This precision is particularly significant in the fields of neural and cardiac optogenetics.

In neural optogenetics, LEDs are used to manipulate specific neural activities with high controlling resolution both in location and time. This is critical for understanding complex functions such as brain activities and for exploring the fundamental neural principles of behavior and neurological disorders. The ability of LEDs to provide targeted illumination allows researchers to activate or inhibit specific neurons or groups of neurons, leading to insights into brain function that were previously unattainable with broader stimulation techniques.

Optogenetics technology enables the activation or inhibition of specific neurons that have been genetically modified to express light-sensitive ion channels in vitro and in vivo settings. Customized light delivery technologies have significantly refined spatial and temporal control over biological research (Table 2.1).

The majority of studies usually focus on the stimulation of the cortex in a controlled environment in animal models. Early studies use high-power xenon lamps as the illumination light source, and guide the illumination to the targeted cortex area via light guides or optical fibers through color filters[25][26][27]. The large-scaled and powerful xenon lamps provide more than 300W power, offering more than enough irradiance at the target end of the optical cable, but also limiting the whole system from mobile due to the size of the light source and its large power supply. Moreover, the high power of the xenon light source creates challenges in the thermal management of the source, optical fibers, and fiber coupling components to avoid heat damage or measurement artificial due to thermal drifting. The broad spectrum of xenon lamp light source however offers great freedom in manipulating irradiance wavelength by using color filters although sacrificing the overall efficiency. This is particularly beneficial for early research pioneers to discover the light-sensitive ion channel spectrum sensitivity based on cultured neurons.

Once the spectrum sensitivity of popular light-sensitive ion channels is determined, Laser light sources are adopted by multiple researchers in neural optogenetics with in-vivo models[28][29][33] for their coherent and very narrow frequency spectrum, to concentrate the optical power at desired wavelength and bandwidth. The laser light sources have higher efficiency than gas lamps and the dimension of the hardware is greatly re-

Table 2.1: Illumination solutions in neural optogenetics research
*values are calculated or estimated based on the statement from the article

Author	Year	Illumination solution	Irradiance (mW/mm2)	Wavelength (nm)	Application
Boyden et.al[25]	2005	300W Xenon lamp through color filter with 20x objective lens	8–12	490-510	Cultured neurons
Berndt et.al[26]	2009	75W Xenon lamp through color filters with 2mm light guides	1	450-600	Cultured neurons
Gunaydin et.al[27]	2010	300W xenon lamp through color filter with optical fibers	1.4	470	Cultured neurons
Cardin et.al[28]	2010	Laser source with 0.2mm optical fibers	46	473	Mouse cortex, small spots at surface
Zorzos et.al[29]	2010	Laser source with waveguides probe by micro-fabrication	>50*	473/632	Not tested
Grossman et.al[30]	2010	64 × 64 micro-LED matrix fabricated by monolithic microfabrication	250	470	Mouse retina, square area at surface
Wentz et.al[31]	2011	2 LED chips with direct illumination	60*	470	Mouse cortex, small spots at surface
Iwai et.al[32]	2011	1 LED chip with optical fiber, powered wirelessly by IR	4*	470*	Mouse cortex, small spots at surface
Cruikshank et.al[33]	2012	Laser source with 40x optical lens	> 30000*	447	Mouse cortex, small spots at surface
Sakai et.al[34]	2013	LED with DMD mirror and optics	> 1.2*	380/505	Cell culture, small spots at surface
Clements et.al[35]	2013	1 LED chip with 200um fiber	150*	450-850	Mouse striatum, small spots at surface
Park et.al[36]	2015	1 LED encapsulated in flexible polymer patch	10	470	Mouse spine, small spots at surface
Scharf et.al[37]	2016	16 micro-LED in line with 6 probes	400	450	Mouse cortex, deep probing
Shin et.al[38]	2017	1 micro-LED at the tip of a probe	50	390-650	Mouse cortex, deep probing
Keppeler et.al[39]	2020	10 LED chips in a line with deformable polymer encapsulation	236	453.8	Rat auditory pathway, long and narrow area at surface
Rajalingham et.al[40]	2021	5x5 LED matrix with silicone encapsulation	0.4–0.6*	530	Monkey lunate sulcus, square area at surface

duced. The laser light sources are better compatible with optical fibers or waveguides, which makes them practical in in-vivo tests where the overall system is expected to be minimized and mobile. The major challenge exists in the very limited wavelength choices for laser sources as it is highly dependent on the source materials. Blue color laser light sources commonly come with a wavelength of 473nm which lands precisely at the high sensitive range of ChR2 ion channels. However, the further exploration of red-shift ion channels can be difficult with laser light sources if a continuous spectrum is needed in the illumination system to characterize the spectrum sensitivity, as well as the potential of using other wavelengths for better transmission in the tissue.

LEDs present a preferable alternative to lamps or laser as a light source for the neural optogenetics research recently[30][31][32][35][38][39][40], offering advantages in cost-effectiveness, compactness, reliability, switching speed, and more freedom of control over light intensity and wavelength. However, LEDs emit light in a non-collimated, Lambertian pattern, which poses challenges in effectively coupling this light into an optical fiber. Due to the requirements of high-intensity light required for neural optogenetics stimulation, LED devices are therefore usually integrated without optical fibers but directly illuminate the stimulation area.

LED illumination system without optical fibers offers researchers the flexibility to freely design illumination patterns that are customized specifically to the target area. This adaptability in creating various illumination patterns is achieved by manipulating the number and arrangement of LED elements. For instance, in deep brain optogenetic stimulation, where pinpoint illumination is required at a depth of a few millimeters, the illumination device can be designed like a probe, with a small LED chip at its tip (Figure 2.3a). This design ensures focused light delivery to deeper regions. In studies requiring stimulation of a narrow area on the cortex, the device might be configured with a series of LED elements arranged linearly (Figure 2.3d). This layout creates a narrow yet concentrated pattern of light, ideal for targeting specific areas with strip shapes. For other experiments that need to illuminate a square area, for example on the cortex surface, LED elements can be aligned in a matrix layout (Figure 2.3e and Figure 2.3f). This arrangement offers uniform illumination across the desired area, ensuring an even distribution of light with high irradiance.

It is worth noting that LED driving signals can cause measurement artifacts by stimulation-induced noise [35][41], therefore the electrical isolation and encapsulation are critical for LED devices with direct contact to tissues, especially in an in-vivo case with implanted devices.

The versatility of LED design allows for precise control over the area and intensity of

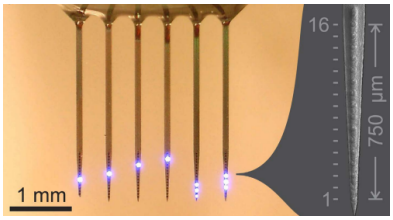

(a) Micro-LEDs at the tip of probes[37]

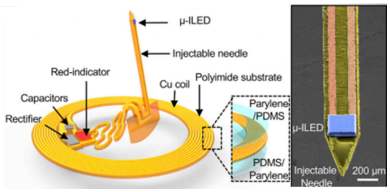

(b) Micro-LED at the tip of the probe with wireless power[38]

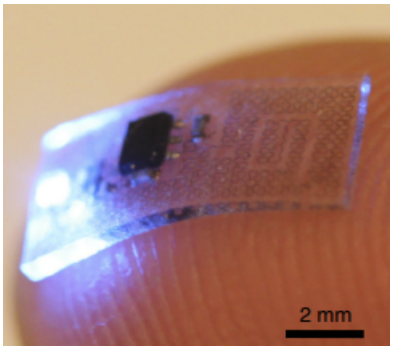

(c) Mini-LED encapsulated in a flexible patch

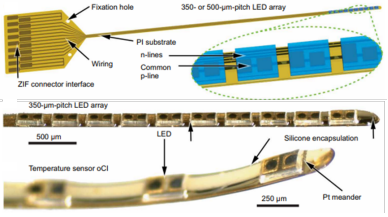

(d) Mini-LED chips at the tip of a deformable strip[39]

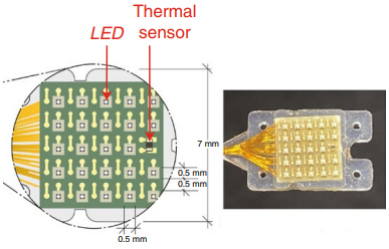

(e) Mini-LED chips in a matrix[40]

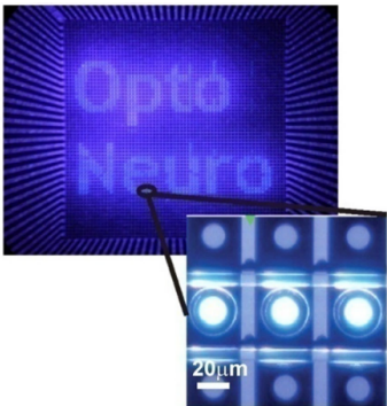

(f) Micro-LED matrix monolithic fabricated [30]

Figure 2.3: Some examples of LED element layouts in illumination systems for neural optogenetics research

illumination, making LEDs a highly valuable tool in various types of neural optogenetic studies. It allows researchers to conduct more sophisticated experiments, leading to deeper insights into the workings of the nervous system.

2.5.3. ILLUMINATION SYSTEM IN CARDIAC OPTOGENETICS

In cardiac optogenetics studies, there's a notable preference for using LED light sources over traditional xenon lamps or laser sources. One of the reasons is that cardiac optogenetics was developed around the 2010s, years after the initial development of neural optogenetics in the 2000s. During this period, semiconductor technology, particularly solid-state-lighting technology had rapid advancements. Modern LEDs became smaller, brighter, and available in a wider range of wavelengths. This evolution means that researchers in cardiac optogenetics do not have to rely on the more complex systems such as xenon lamps with color filters, which require precise setup, and positioning, and are often challenging in rapid control.

Additionally, the requirements of cardiac optogenetics differ significantly from those of neural optogenetics. Neural optogenetics often targets small, specific areas like individual neurons or localized regions of the cortex, where high-concentration illumination is required. Cardiac optogenetics typically involves larger target areas such as the atrial wall or ventricular epicardium. The goal is to achieve uniform illumination over these larger areas or multiple spots but with relatively lower irradiance compared to neural applications. LEDs are particularly well-suited for this purpose. They can be easily constructed into arrays or matrices, enabling the distribution of light over a broader surface area with uniformity. This flexibility and ease of customization make LEDs an ideal choice for cardiac optogenetics (Table 2.2).

In cardiac optogenetics, LEDs offer benefits such as precisely controlling the electrical activity of heart cells, which is vital for studying cardiac principles or cardiac disorders such as arrhythmias including atrial fibrillation and ventricular fibrillation. By illuminating specific areas of the heart, researchers can pace the heartbeats, and suppress or terminate arrhythmias, allowing them to understand the mechanisms underlying these activities better and to explore new clinical treatments.

In the early stages of cardiac optogenetics, the illumination systems typically featured a low number of LED elements, often just a single element integrated into a metal heat-sink from commercial products[45][46][47][48]. This LED product projects light onto the target area through optical system, optical fibers or objectives. These setups have several advantages, particularly in terms of their simplicity and the availability of commercially mature solutions. It guarantees certain optical specifications and ensures

Table 2.2: Illumination solutions in cardiac optogenetics research

Author	Year	Illumination solution	LED size	Irradiance (mW/mm2)	Wavelength (nm)	Application
Abilez et al.[42]	2013	6 LEDs with lens under 6-well plate	4.61 x 3.17 x 2.10	5	470	Cell cultures, large spot
Bingen et al.[43]	2014	1 LED under a cell well	4.61 x 3.17 x 2.10	5	470	Cell cultures, small spot
Xu et al.[44]	2014	mini-LED array integrated at a stretchable matrix	0.3x0.3x0.003 ultra-thin	Unknown	670	Rat ventricular epicardium, large area pattern, in-vitro
Nussinovitch et al.[45]	2015	1 LED with 2mm optical fiber	Unknown	5.13	450	Rat ventricular epicardium, 5mm spot, in-vivo
Vogt et al.[46]	2015	1 LED with optical fiber and optics	Unknown	5	470	Mouse ventricular epicardium, small spot, in-vivo
Klimas et al.[47]	2016	1 LED lamp with collimated optics and color filters	Unknown	0.4-7	470-700	Cell cultures, large spot
Bruegmann et al.[48]	2016	1 LED lamp with an objective	Unknown	1.5	470	Mouse ventricular epicardium, large spot, in-vitro
Crocini et al.[49]	2016	Laser source with a dichroic beam splitter and optics	Unknown	40	473	Mouse ventricular epicardium, small spot, in-vivo
Diaz-made et al.[50]	2018	1 LED with reflective DMD to generate patterns	Unknown	2	460	Mouse ventricular epicardium, small area pattern, in-vitro
Nyns et al.[51]	2019	1 LED integrated with PDMS light guide	1.7 x 1.3 x 0.5mm	3.5	470	Rat right atrial wall, in-vivo
Zgierski et al.[52]	2019	mini-LED chips integrated at the tip of a probe	0.270 x 0.220 x 0.05, pitch 0.3mm	12.4	456	Rat ventricular epicardium, deep probing, in-vitro
Lemme et al.[53]	2020	24 LED with lens under a 24-well plate	5mm x 5mm x 8.3mm, through-hole	0.3	470/700	Cell cultures, small spot
Izadi et al.[54]	2021	2x2 mini-LED array with aspheric lenses	0.93 x 0.93 x 0.17	1.5	470	Mouse ventricular epicardium, large spots, in-vitro
Obaid et al.[55]	2022	4 micro-LEDs integrated in transparent and flexible electrode film	30um x 30um*	25.3	462/531	Mouse left atrial wall and left ventricular epicardium, in-vivo
Diaz-made et al.[56]	2022	3x3 mini-LED array integrated at flexible PCB and encapsulated with PDMS	0.65 x 0.35 x 0.2 mm, pitch 1.14mm	1	470	Mouse ventricular epicardium, large area, in-vitro
Junge et al.[57]	2023	16x16 micro-LED array with a dichroic mirror and optics	50um x 50um, pitch 140um	52.3	455	Cell cultures, large area with pattern

good reliability in long-term usage. Researchers could thus concentrate more on the biomedical aspects of their studies without needing to dive into the complexities of optoelectronics. However, these commercial illumination solutions have their drawbacks, primarily due to their size. The LED modules in these systems are often big and are usually significantly larger than the experimental subjects themselves, typically mouse or rat heart models. This big product size makes precise control of the light pattern challenging, as commercial optics tend to produce a large light spot that is not ideal for focused illumination. Therefore, the bulkiness of these systems limits their use primarily to in-vitro experiments or in-vivo experiments involving only open-chest procedures. The size and design of these early illumination systems make them unsuitable for implantation in closed-chest tests, which are crucial for more advanced, clinically relevant cardiac optogenetics research.

In the study of cardiac optogenetics, optical mapping is a crucial technique where a camera captures the light emitted by a fluorescence dye applied to the test subject, such as cell cultures or rat hearts, and translates the optical signals to electrical activities of the test subject. A challenge in this technique is the need to de-couple the low-intensity fluorescent light emitted by the dye from the high-intensity light used for stimulation. Direct imaging from the test subject often leads to difficulties in separating these two light sources due to the too-low dynamic range of the camera. Many researchers employ a dichroic optical element, which could be either a mirror[57] or a beam splitter[49]. This element is designed to have different transmission or reflection properties for different wavelengths. Since the wavelengths of the fluorescent light and the stimulation light are designed to be different, the dichroic element effectively splits these two into separate light paths. The camera is positioned in the path of the fluorescent light, where it can capture the necessary fluorescence intensity without interference from the stimulation light. Conversely, the LED light source used for stimulation is placed in the other light path (Figure 2.4a). This setup allows for efficient separation of the fluorescence signal from the stimulation light, enabling accurate optical mapping. This optical mapping setup shares a common limitation in its size. The considerable size of the optical components, including the dichroic element, makes them too bulky for implantable devices. Consequently, their application is seen in in-vitro experiments with cell cultures or ex-vivo experiments.

The use of micro-fabrication technology is seen in the development of illumination systems for optogenetics, especially for implantable devices in closed-chest in-vivo experiments. This technology allows the creation of extremely small structures, incorporating mini-LED or micro-LED dies, suitable for fabricating miniature devices directly

attaching to the heart tissues. The design of these illumination systems is highly dependent on the specific requirements of the cardiac area being investigated and the type of illumination required. For example, a design approach involves a long probe structure with an array of mini-LED chips integrated at the tip[52]. This design is particularly designed for stimulating deep within the epicardium, facilitating better light penetration through blood-filled tissue, which is crucial for effective optogenetic activation (Figure 2.4b).

Some system designs are tailored to provide more uniform illumination over larger heart surfaces, such as the atrial wall or ventricular epicardium. Since a small number of LEDs are insufficient for covering extensive areas, these devices typically feature multiple LEDs arranged in a matrix or array configuration. By using very small mini-LED or micro-LED chips, these designs are integrated into a substrate patch, which is then attached directly to the heart tissue[55][56]. The patches are constructed from flexible and stretchable polymer materials. This flexibility is important to ensure that the LED matrix conforms to the heart's curved surface, allowing for even and consistent illumination across the targeted area. The stretchable substrate is also crucial as it reduces interference that the implanted device might have on the contraction and movement of the heart.

Further advancements in micro-fabrication lead to the integration of micro-LED chips and electrodes into a single stretchable matrix[44], which is made of bendable metal wires, allowing for a perfect attachment to the heart's surface. Such innovative designs not only provide uniform light distribution for effective optogenetic stimulation but also ensure that the device moves synchronously with the heart, reducing the risk of physical disturbance or damage to the cardiac tissue.

Micro-fabrication technology in designing LED illumination systems for optogenetics offers significant customization and precision but comes with drawbacks like complexity in fabrication, higher costs, and increased risk. The complex processes and specialized equipment required for micro-scale device fabrication require significant technical expertise, contributing to the overall expense and time. While these advanced systems are highly beneficial for optogenetic research, the potential for fabrication errors and technical challenges adds a layer of risk, making it crucial for research teams to weigh these factors carefully in their project planning.

The use of LEDs in optogenetics represents a significant advancement over traditional stimulation methods, which often lack the same level of precision and control. LEDs can be easily integrated into a variety of experimental setups, from in vitro cell

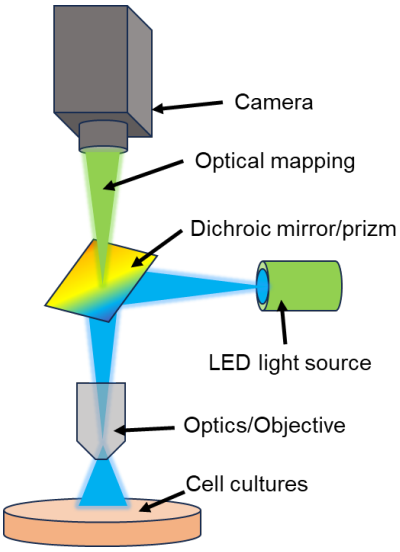

(a) Illustration of a typical setup for combining optical stimulation and optical mapping with a dichroic mirror/prizm[49][57]

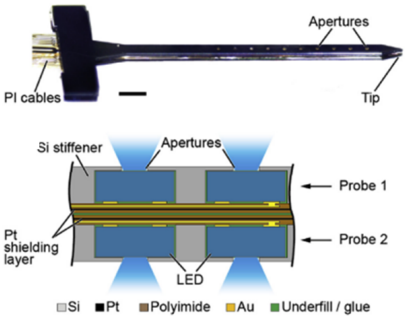

(b) Mini-LED chips integrated at the tip of a probe[52]

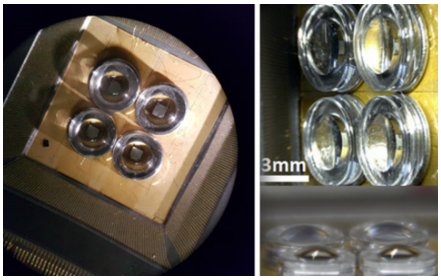

(c) Mini-LED array with lenses[54]

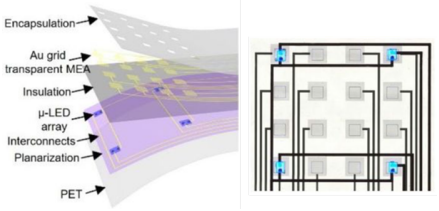

(d) Micro-LEDs integrated in transparent and flexible electrode film[55]

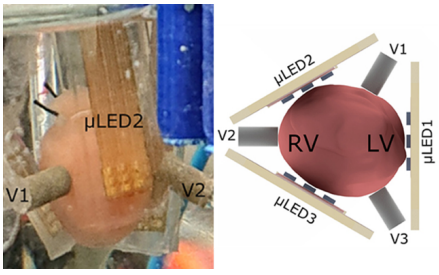

(e) Mini-LED array integrated at flexible substrates[56]

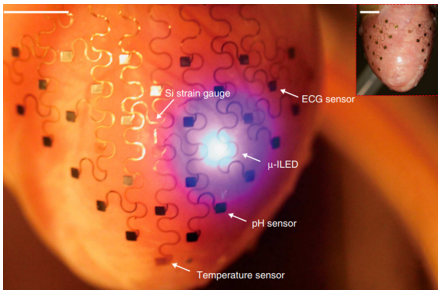

(f) Micro-LED array integrated at a stretchable matrix[44]

Figure 2.4: Examples of LED illumination systems for cardiac optogenetics research

cultures to in vivo studies in animal models, making them valuable tools for a wide range of optogenetic applications. This adaptability, combined with the development of new optogenetic techniques and improvements in LED technology, is likely to continue driving progress in both neural and cardiac optogenetics.

2.6. CHALLENGES IN OPTOELECTRONIC SYSTEMS FOR OPTOGENETICS APPLICATIONS

The integration of optoelectronic systems in cardiac optogenetics applications presents several challenges, reflecting the intricate nature of combining biomedical requirements and technical implementation. These challenges include:

- **Miniaturization and Bio-compatibility**
  Developing small-scale optoelectronic devices that can be safely and effectively used in biological environments is a major challenge. These devices must be bio-compatible and small enough to minimize implanting interference. Commercially illumination solutions are not able to fulfill both requirements, therefore the system must be customized for certain applications. Advanced products such as mini-LED or micro-LED chips are considered preferred candidates, which however increase the complexity and risk for the assembly and integration process.

- **Precise Illumination Control**
  Optoelectronic systems for cardiac optogenetics require precise control over light intensity, wavelength, duration, and pattern. This creates challenges in designing and integrating while balancing technical trade-offs from various requirements. Calibrating these parameters accurately is also essential for ensuring effective and targeted stimulation of cardiac tissues. This requires a structured characterization process and advanced control electronics, both in hardware and software.

- **High-power and Thermal solutions**
  Providing stable and safe power to optoelectronic devices, especially in in-vivo applications can be challenging. Additionally, managing heat dissipation from these devices is crucial to prevent damage to biological tissues.

- **Integration with Biological Systems**
  Seamlessly integrating optoelectronic devices with biological systems, ensuring they work functionally without interfering with natural biological processes such as heart contraction or movement, creates significant challenges, especially for in-vivo applications.

- **Reliability and Durability**
  Ensuring the long-term reliability and durability of optoelectronic devices, especially those used in prolonged or repeated experiments is important. These systems need to withstand various physiological conditions without degradation or failure.

- **Practicality**
  Efficiently capturing and analyzing data for real-time monitoring, requires sophisticated data acquisition systems, data communication, and analysis software. The system should apply to ethical and safety considerations.

2.7. CONCLUSION

This chapter presents a thorough background introduction to LED technology, tracing its evolution from inception to its diverse applications, and focusing particularly on the characteristics that make it an important tool in optogenetics. This chapter also provides a comprehensive review of state-of-the-art optoelectronic illumination systems used in neural and cardiac optogenetics research and summarizes the challenges associated with their development and practical design. The following Chapters 3 to 6, are dedicated to exploring various design and development processes of individual optoelectronic illumination systems specifically tailored for optogenetic cardiac applications, showcasing the innovative approaches and technical development methodology.

BIBLIOGRAPHY

[1] Nikolay Zheludev. “The life and times of the LED—a 100-year history”. In: *Nature photonics* 1.4 (2007), pp. 189–192.

[2] Nick Holonyak Jr and S Fo Bevacqua. “Coherent (visible) light emission from Ga (As1- x P x) junctions”. In: *Applied Physics Letters* 1.4 (1962), pp. 82–83.

[3] Isamu Akasaki et al. “The nobel prize in physics 2014”. In: *The Royal Swedish Academy of Science* (2014).

[4] Govind B Nair and Sanjay J Dhoble. *The fundamentals and applications of light-emitting diodes: the revolution in the lighting industry*. Woodhead Publishing, 2020.

[5] Patrick Mottier. *LED for lighting applications*. Vol. 134. John Wiley & Sons, 2010.

[6] U.S. Department of Energy. *LED Lighting*. https://www.energy.gov/energysaver/led-lighting. 2022.

[7] MM Aman et al. “Analysis of the performance of domestic lighting lamps”. In: *Energy policy* 52 (2013), pp. 482–500.

[8] Jianfei Dong et al. “Diagnosing lumen depreciation in LED lighting systems: an estimation approach”. In: *IEEE transactions on signal processing* 60.7 (2012), pp. 3796–3808.

[9] Cheng Qian et al. “Prediction of lumen depreciation and color shift for phosphor-converted white light-emitting diodes based on a spectral power distribution analysis method”. In: *IEEE Access* 5 (2017), pp. 24054–24061.

[10] John D Bullough, Andrew Bierman, and Mark S Rea. “Evaluating the blue-light hazard from solid state lighting”. In: *International Journal of Occupational Safety and Ergonomics* 25.2 (2019), pp. 311–320.

[11] Fortune Business Insights. *LED Lighting Market Size, Growth Share | Forecast [2030]*. https://www.fortunebusinessinsights.com/led-lighting-market-106832. 2022.

[12] Benjamin S Mashford et al. “High-efficiency quantum-dot light-emitting devices with enhanced charge injection”. In: *Nature photonics* 7.5 (2013), pp. 407–412.

[13] Geoffrey J Supran et al. “QLEDs for displays and solid-state lighting”. In: *MRS bulletin* 38.9 (2013), pp. 703–711.

[14] Tingzhu Wu et al. “Mini-LED and micro-LED: promising candidates for the next generation display technology”. In: *Applied Sciences* 8.9 (2018), p. 1557.

[15] Yuge Huang et al. “Mini-LED, Micro-LED and OLED displays: present status and future perspectives”. In: *Light: Science & Applications* 9.1 (2020), p. 105.

[16] Burhan SaifAddin et al. “Developments in AlGaN and UV-C LEDs grown on SiC”. In: *Light-Emitting Diodes: Materials, Devices, and Applications for Solid State Lighting XXII*. Vol. 10554. SPIE. 2018, pp. 67–76.

[17] Sara E Beck et al. “Evaluating UV-C LED disinfection performance and investigating potential dual-wavelength synergy”. In: *Water research* 109 (2017), pp. 207–216.

[18] Wan-Kuen Jo and Rajesh J Tayade. “New generation energy-efficient light source for photocatalysis: LEDs for environmental applications”. In: *Industrial & Engineering Chemistry Research* 53.6 (2014), pp. 2073–2084.

[19] Hiroyuki Kitabayashi et al. “Development of high power infrared LED”. In: *Sei Tech. Rev.* 70 (2010), p. 71.

[20] Xiangbing Zhu et al. “Optical design of LED-based automotive headlamps”. In: *Optics & Laser Technology* 45 (2013), pp. 262–266.

[21] Ceren Altingöz. “Laser technology in automotive lighting”. In: *High-Power Diode Laser Technology and Applications XII*. Vol. 8965. Spie. 2014, pp. 227–237.

[22] Philipp Babilas et al. “Intense pulsed light (IPL): a review”. In: *Lasers in Surgery and Medicine: The Official Journal of the American Society for Laser Medicine and Surgery* 42.2 (2010), pp. 93–104.

[23] Jane G Khoury and Mitchel P Goldman. “Use of light-emitting diode photomodulation to reduce erythema and discomfort after intense pulsed light treatment of photodamage”. In: *Journal of cosmetic dermatology* 7.1 (2008), pp. 30–34.

[24] Dipali G Rathod, Hira Muneer, and Sadia Masood. “Phototherapy”. In: (2020).

[25] Edward S Boyden et al. “Millisecond-timescale, genetically targeted optical control of neural activity”. In: *Nature neuroscience* 8.9 (2005), pp. 1263–1268.

[26] André Berndt et al. “Bi-stable neural state switches”. In: *Nature neuroscience* 12.2 (2009), pp. 229–234.

[27] Lisa A Gunaydin et al. “Ultrafast optogenetic control”. In: *Nature neuroscience* 13.3 (2010), pp. 387–392.

[28] Jessica A Cardin et al. “Targeted optogenetic stimulation and recording of neurons in vivo using cell-type-specific expression of Channelrhodopsin-2”. In: *Nature protocols* 5.2 (2010), pp. 247–254.

[29] Anthony N Zorzos, Edward S Boyden, and Clifton G Fonstad. “Multiwaveguide implantable probe for light delivery to sets of distributed brain targets”. In: *Optics letters* 35.24 (2010), pp. 4133–4135.

[30] Nir Grossman et al. “Multi-site optical excitation using ChR2 and micro-LED array”. In: *Journal of neural engineering* 7.1 (2010), p. 016004.

[31] Christian T Wentz et al. “A wirelessly powered and controlled device for optical neural control of freely-behaving animals”. In: *Journal of neural engineering* 8.4 (2011), p. 046021.

[32] Youichi Iwai et al. “A simple head-mountable LED device for chronic stimulation of optogenetic molecules in freely moving mice”. In: *Neuroscience research* 70.1 (2011), pp. 124–127.

[33] Scott J Cruikshank et al. “Thalamic control of layer 1 circuits in prefrontal cortex”. In: *Journal of Neuroscience* 32.49 (2012), pp. 17813–17823.

[34] Seiichiro Sakai et al. “Parallel and patterned optogenetic manipulation of neurons in the brain slice using a DMD-based projector”. In: *Neuroscience research* 75.1 (2013), pp. 59–64.

[35] Isaac P Clements et al. “Miniaturized LED sources for in vivo optogenetic experimentation”. In: *Optogenetics: Optical Methods for Cellular Control*. Vol. 8586. SPIE. 2013, pp. 94–102.

[36] Sung Il Park et al. “Soft, stretchable, fully implantable miniaturized optoelectronic systems for wireless optogenetics”. In: *Nature biotechnology* 33.12 (2015), pp. 1280–1286.

[37] Robert Scharf et al. “Depth-specific optogenetic control in vivo with a scalable, high-density μLED neural probe”. In: *Scientific reports* 6.1 (2016), p. 28381.

[38] Gunchul Shin et al. “Flexible near-field wireless optoelectronics as subdermal implants for broad applications in optogenetics”. In: *Neuron* 93.3 (2017), pp. 509–521.

[39] Daniel Keppeler et al. “Multichannel optogenetic stimulation of the auditory pathway using microfabricated LED cochlear implants in rodents”. In: *Science Translational Medicine* 12.553 (2020), eabb8086.

[40] Rishi Rajalingham et al. “Chronically implantable LED arrays for behavioral optogenetics in primates”. In: *Nature Methods* 18.9 (2021), pp. 1112–1116.

[41] Jacob G Bernstein and Edward S Boyden. “Optogenetic tools for analyzing the neural circuits of behavior”. In: *Trends in cognitive sciences* 15.12 (2011), pp. 592–600.

[42] Oscar J Abilez. “Optogenetic LED array for perturbing cardiac electrophysiology”. In: *2013 35th Annual International Conference of the IEEE Engineering in Medicine and Biology Society (EMBC)*. IEEE. 2013, pp. 1619–1622.

[43] Brian O Bingen et al. “Light-induced termination of spiral wave arrhythmias by optogenetic engineering of atrial cardiomyocytes”. In: *Cardiovascular research* 104.1 (2014), pp. 194–205.

[44] Lizhi Xu et al. “3D multifunctional integumentary membranes for spatiotemporal cardiac measurements and stimulation across the entire epicardium”. In: *Nature communications* 5.1 (2014), p. 3329.

[45] Udi Nussinovitch and Lior Gepstein. “Optogenetics for in vivo cardiac pacing and resynchronization therapies”. In: *Nature biotechnology* 33.7 (2015), pp. 750–754.

[46] Christoph C Vogt et al. “Systemic gene transfer enables optogenetic pacing of mouse hearts”. In: *Cardiovascular research* 106.2 (2015), pp. 338–343.

[47] Aleksandra Klimas et al. “OptoDyCE as an automated system for high-throughput all-optical dynamic cardiac electrophysiology”. In: *Nature communications* 7.1 (2016), p. 11542.

[48] Tobias Bruegmann et al. “Optogenetic defibrillation terminates ventricular arrhythmia in mouse hearts and human simulations”. In: *The Journal of clinical investigation* 126.10 (2016), pp. 3894–3904.

[49] Claudia Crocini et al. “Optogenetics design of mechanistically-based stimulation patterns for cardiac defibrillation”. In: *Scientific reports* 6.1 (2016), p. 35628.

[50] Laura Diaz-Maue et al. “Follow the light-from low-energy defibrillation to multisite photostimulation”. In: *2018 40th Annual International Conference of the IEEE Engineering in Medicine and Biology Society (EMBC)*. IEEE. 2018, pp. 4832–4835.

[51] Emile CA Nyns et al. “An automated hybrid bioelectronic system for autogenous restoration of sinus rhythm in atrial fibrillation”. In: *Science translational medicine* 11.481 (2019), eaau6447.

[52] Callum M Zgierski-Johnston et al. “Cardiac pacing using transmural multi-LED probes in channelrhodopsin-expressing mouse hearts”. In: *Progress in Biophysics and Molecular Biology* 154 (2020), pp. 51–61.

[53] Marta Lemme et al. “Chronic intermittent tachypacing by an optogenetic approach induces arrhythmia vulnerability in human engineered heart tissue”. In: *Cardiovascular research* 116.8 (2020), pp. 1487–1499.

[54] Ida Izadi et al. “Wide Area Uniform Illumination Scheme Using LED Matrix for Optogenetic Cardiac Pacing”. In: *Photonics*. Vol. 8. 11. MDPI. 2021, p. 499.

[55] Sofian N Obaid et al. “Multifunctional flexible electro-optical arrays for simultaneous spatiotemporal cardiac mapping and modulation”. In: *bioRxiv* (2022), pp. 2022–05.

[56] Laura Diaz-Maue, Janna Steinebach, and Claudia Richter. “Patterned illumination techniques in optogenetics: An insight into decelerating murine hearts”. In: *Frontiers in Physiology* 12 (2022), p. 750535.

[57] Sebastian Junge et al. “A micro-LED array based platform for spatio-temporal optogenetic control of various cardiac models”. In: *Scientific Reports* 13.1 (2023), p. 19490.

3

IMPLANTABLE LED ILLUMINATION SYSTEMS FOR IN-VIVO AND EX-VIVO VF TERMINATION IN RAT MODELS

The work in this chapter is a result of collaborative research between TU Delft and the Laboratory of Experimental Cardiology, LUMC. The content relates directly to findings and methodologies presented in the following collaborative publications:

1. *Nyns, E. C., Jin, T., Bart, C. I., Bax, W. H., Zhang, G., Poelma, R. H., ... & Pijnappels, D. A. (2022). Ultrasound-Guided Optogenetic Gene Delivery for Shock-Free Ventricular Rhythm Restoration. Circulation: Arrhythmia and Electrophysiology, 15(1), e009886.*
2. *Nyns, E. C., Jin, T., Fontes, M. S., van den Heuvel, T., Portero, V., Ramsey, C., ... & Pijnappels, D. A. (2022). Optical ventricular cardioversion by local optogenetic targeting and LED implantation in a cardiomyopathic rat model. Cardiovascular research, 118(10), 2293-2303.*
3. *Nyns, E. C., Portero, V., Deng, S., Jin, T., Harlaar, N., Bart, C. I., ... & Pijnappels, D. A. (2023). Light transmittance in human atrial tissue and transthoracic illumination in rats support the translatability of optogenetic cardioversion of atrial fibrillation. Journal of Internal Medicine.*

3.1. INTRODUCTION

As introduced in the previous chapter, ventricular fibrillation (VF) is a life-threatening cardiac arrhythmia characterized by rapid, erratic electrical impulses that cause the ventricles of the heart to function ineffectively. This condition leads to a critical reduction in cardiac output and, if left untreated, can result in sudden cardiac death. The exploration of innovative methods for VF termination is thus of high importance in the field of cardiac electrophysiology.

This chapter introduces a critical contributing part of a novel approach to the potential treatment and termination of VF by optogenetics, focusing on the fully customized, implantable, high-power LED light source system for both in-vivo and ex-vivo VF treatment experiments in rats. The utilization of the LED light source system in this treatment presents a unique intersection of optogenetics and cardiac electrophysiology, offering a new insight for understanding and possibly controlling VF.

Firstly, the development, testing, and integration of the LED light source system are discussed following the V-model development cycle, starting from requirement analysis, emphasizing its bio-compatibility and optical characteristics it affords. The design and fabrication process of the system is therefore explained in detail. Secondly, the system is verified and validated through the results of in-vivo and ex-vivo experiments, analyzing its effectiveness in cardiac electrophysiology treatments, including terminating VF and its potential implications for future applications.

This chapter aims to contribute a novel tool for cardiac electrophysiologists to understand VF and its treatment, offering insights into the potential of optogenetics in future cardiac therapy. This work stands at the intersection of advanced electronics system integration technology and medical science, proposing a new era in the treatment of cardiac arrhythmias.

3.1.1. REQUIREMENTS ANALYSIS

The high-power LED light source system is a critical contributing part of the novel approach to the potential treatment and termination of VF by optogenetics. In this context, the biomedical study and experiment act as the °Customer' for the LED device system, dictating its specifications and functionality. Therefore, a customer-oriented approach emphasizes that the design of such LED devices must be tailored to meet the specific needs and objectives of the biomedical experiments. Such customization ensures that the device provides the precise optical triggering conditions required for the optogenetics methods, such as specific wavelength for optogenetic channel activation, intensity levels for tissue penetration, or optical distribution for targeted illumination.

The experiment's requirements shape the basis of the LED device's design, ensuring that the device effectively supports the experiments for generating reliable, accurate results, and for maintaining the integrity and safety of the biological subjects involved. Without a thorough understanding of these requirements, there's a risk of designing a system that is either ineffective or potentially harmful, compromising the experiment's success and ethical standards in biomedical research.

Rat models are selected for the work in this chapter. The choice is motivated by the physiological similarities their cardiac systems share with humans, alongside practical (economical) considerations of size and the feasibility of genetic modification. This makes them an ideal model for pioneering studies in cardiac arrhythmia. Furthermore, the Laboratory of Experimental Cardiology, LUMC has a rich history and extensive experience in the genetic modification of rat models for arrhythmia studies.

The LED device used in the experiments is therefore requested to be custom-made, designed for direct in-vivo experiments, as well as in-direct ex-vivo experiments arrhythmia studies on rat models, with the following key requirements based on the model:

- **Wavelength:** Capable of producing light at specific wavelengths, chosen based on good effectiveness in penetrating blood-perfused ventricular myocardium as well as good ability to generate strong reaction by light-gated ion channel red-activatable channelrhodopsin (ReaChR[1] or Citrine) in cardiomyocytes. Also, the selected wavelength should be delivered by commercially available LEDs with reasonable economic resources. Four wavelengths are initially proposed: 470nm (Blue), 530um (Green), 567nm (Lime), and 617nm (Red-Orange).

- **Irradiance:** Capable of producing light with sufficient irradiance at the target surface, chosen based on good effectiveness in penetrating blood-perfused ventricular myocardium as well as good ability to generate strong reaction by light-gated ion channel red-activatable channelrhodopsin (ReaChR or Citrine) in cardiomyocytes. This is further discussed in the following section.

- **Physical dimensions:** Compact and miniaturized, suitable for implantation in the rat model used in the study, both in-vivo and ex-vivo experiments. Designed for attachment to the cardiac apex of the rat model, considering its favorable position to both ventricles and the septum and also due to the apex's potential role in attracting re-entrant activity sustaining arrhythmias

- **Physical compatibility:** Robust enough to withstand the physiological conditions during the experiment, including temperatures, moisture levels, possible chemi-

cal or biological reactions, and potential mechanical stress from the beating heart or movements of the rat model

- **Bio-compatibility:** functions within a living system without inducing excess strain or tension that interferes with normal biological behaviors (e.g. normal heart beating), or creates measurement artifacts (e.g. leaking current or voltage). The device should have reasonable surgical accessibility and the potential for recovery post-implantation.

- **Consistency:** The device's design and functionality are integral to the success of the optogenetic VF termination experiments conducted in the study. constant light distribution and intensity with a central LED surrounded by three equally spaced LEDs with the same specifications, while characteristics keep consistency over experimental reproductions over time.

These requirements are analyzed separately in the following sections, to provide a clear view of the system development procedure.

3.1.2. PHYSICAL LAYOUT

The experiments require circular light illumination at the end tip of the ventricle of the rat model. This requires an assessment of the rat's heart and ventricle. The average adult rat heart is relatively small, typically measuring around 1 cm in length and 0.8 cm in width (cross-section diameter) (Figure 3.1).

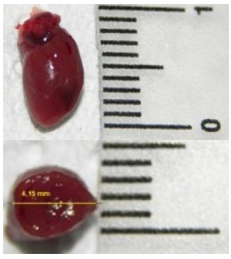

Figure 3.1: Dimension of a similar rat heart used in this work[2]

The rat ventricles, being a major component of the heart, offer a relatively larger area for device placement compared to other parts of the heart: a 'cone' shape with an 'apex' diameter and height of 1cm, similar to the end tip of adult's little finger. This compact size requires a corresponding miniaturization of the LED device to ensure it can be placed without causing excessive physical disruption or damage. The device

should also compromise in a 3-dimensional shape to conform to the 'apex' shape of the ventricle, including the side of the apex point because of its larger epicardial surface to ventricular mass ratio, as well as central apex location about both ventricles and septum. The placement of the LED device should take into account the intricate anatomy of the rat heart, including the location of major blood vessels, the thickness of the ventricular epicardium, and the overall shape and movement of the heart during the cardiac cycle. Therefore, three LED device physical layouts (Figure 3.2) are proposed:

- 'Cylinder' around the ventricle
- 'Apex-cup' with arms attached to the ventricle
- 'Discrete LEDs' attached to the ventricular epicardium

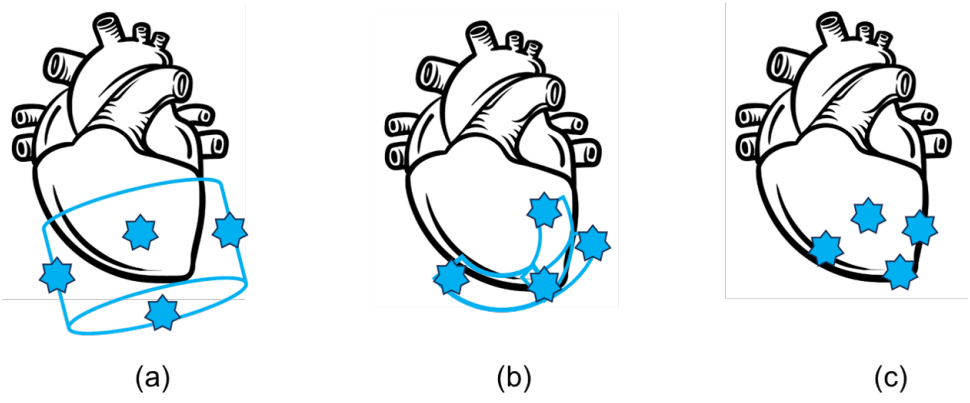

Figure 3.2: Three proposals of layout, blue stars are LED chips: (a)'Cylinder' (b)'Apex-cup' (c)'Discrete LEDs'

Table 3.1: Trade table for proposed layouts of the device

Proposals	**'Cylinder'**	**'Apex-cup'**	**'Discrete LEDs'**
Overall fitting for in-vivo test	-	+	+
Overall fitting for ex-vivo test	-	+	+
Conformity to Ventricle	-	+	+
Light Distribution	++	-	-
Impact on Heart Function	++	-	+
Irradiance/power	-	++	++
Manufacturing/Implementation Complexity and Flexibility	++	+	-

The proposals are evaluated by a trade-off matrix of overall fitting for the in-vivo test, overall fitting for the ex-vivo test, conformity to Ventricle, light distribution, impact on heart function, and manufacturing/implementation complexity and flexibility, as listed in Table3.1.

'Cylinder'

The shape of the cylinder geometry does not conform as naturally to the ventricle's shape, but rather 'floats' over at the ventricle surface with a certain distance of a few mm. This geometry gives a big problem when an in-vivo test requires minimum invasion inside a rat's chest while the bulky shape will greatly occupy the limited area of other organs such as the lung. Also, the floating device might face consistency issues in ex-vivo tests where the positioning of the device is supported by external structures and must be adjusted perfectly every time.

The light emission from a cylinder wall and cap is more spread due to the distance between the almost-point light sources and the target ventricle area. The consequence is that the illumination is spread more uniformly at the ventricular surface with fewer irradiance peaks at certain hot spots. This might change the overall response of the ion channels over the surface due to different irradiance distributions. The wall and base of the cylinder can be manufactured with reflective material or surface coating to increase illumination efficiency by re-directing all possible photons to the target area. The large surface of the wall and cap also ensures good thermal dissipation to avoid the concentration of heat.

The non-detached cylinder will not interfere with the heart's normal movement, no matter whether the material of the device is rigid or not. Additional lubrication liquid or coating is considered to be placed on the inner surface to reduce interference if there is any contact.

The manufacturing of the cylinder device is rather simple with two pieces of components as a wall and a base, both can be manufactured from 2-dimensional sheets of material and glued together. The LED chips and wiring are directly attached/glued to the flat surface without additional process. The device can be re-used for multiple experiments with the exchanging of rat hearts, as long as the physical geometry remains integral.

'Apex-cup'

A cup-shaped design can potentially conform better to the ventricle, especially if it's designed to match the ventricle's outer curvature 'apex'. The cup device can be mini-

mized in dimension and very thin in thickness to avoid other organs in the in-vivo experiments. The cup device will be directly bonded to the ventricle apex by bio-compatible glue to avoid relative movement against the ventricle surface, where the consistency of the reproduction is protected.

The cup geometry allows for a more focused distribution of light at the location of the LED chips than spread over the ventricular epicardium surface, which could be beneficial for local ion channels that request high irradiance to activate. However, this focused illumination could also lead to a concentration of heat and cause thermal damage to the LED chip itself (including irradiance thermal drift), glue attachment, wiring, or tissue. This can be estimated via thermal simulations.

Designed with flexibility, and placed according to the biological movement direction, an apex-cup-shaped device might move more naturally with the heart, reducing the risk of interference with normal cardiac function.

The manufacturing of the cup shape device is also simple while the frame part of the cup can be cut from 2-dimensional sheet material via high precision laser cut and then attached with LED chips by glue. The wiring can follow the arms of the cup frame with sufficient flexibility. The device cannot be re-used due to being directly glued to the test subject.

'Discrete LEDs'

Individual LEDs directly bonded to the ventricle surface offer the highest degree of flexibility in terms of placement and can be arranged in a pattern that best fits the ventricular epicardium surface, no matter for in-vivo or ex-vivo tests. The minimal dimension, only the LED chips and wiring, avoids interference with other organs or tissues.

Similar to the cup design, the discrete LED proposal also provides focused irradiance while ensuring uniform illumination might be more challenging. It also has thermal concentration risks. Discrete LED chips should be only constrained by their connecting (flexible) wires, should move naturally with the heart moving, and are likely to have the least impact on normal cardiac function.

The manufacturing and implementation are however challenging for discrete LED design where each LED chip is expected to be manually and precisely bonded to the ventricle surface at desired locations. This should be difficult in practice for in-vivo experiments where the operational windows, both experimental time and workspace, are very limited. The device cannot be re-used due to being directly glued to the test subject.

In conclusion, each design has its advantages and drawbacks among three design proposals. The choice between them would depend on the trade-off among specific requirements of the experiments. Careful design and precise surgical techniques are essential to achieve this balance.

In this work, the 'apex-cup' proposal is selected for its flexibility of well-fitting the rat model ventricle apex, and good consistency in manufacturing and implementation practice.

3.1.3. IRRADIANCE AND WAVELENGTH

In this study, a key focus was on understanding the optimal irradiance and wavelength requirements for optogenetic ventricular fibrillation (VF) termination. Recognizing that the penetration depth of visible light into biological tissues increases with wavelength[3], and given that ReaChR[1], the light-activated protein used in this work to genetically modify the rat's cardiomyocyte, has a broad active spectrum extending into the red (higher wavelength) spectrum, research was carried out for evaluating the efficacy of different wavelengths, specifically 470nm, 567nm, and 617nm, which are the peak wavelengths of the most common and commercially available high-power LEDs. A series of analyses were conducted to determine which of these tested wavelengths were most suited for optogenetic applications in this work.

Patch clamp experiments reveal that the peak photocurrent amplitudes (Figure 3.3), from activated genetically modified ion-channels, at a normalized irradiance of 1 mW/mm^2, excited by 567nm and 617nm light pulses were significantly higher, by an average of 54.6 ± 8.3% and 40 ± 31% respectively, compared to 470nm wavelength. This is observed in a sample of six cardiomyocytes from three different hearts, yielding statistically significant results (P = 0.0006 and P = 0.0054, respectively). Interestingly, the plateau photocurrent amplitudes across these wavelengths do not show a significant difference, suggesting a degree of uniformity in sustained photocurrent response irrespective of the wavelength used.

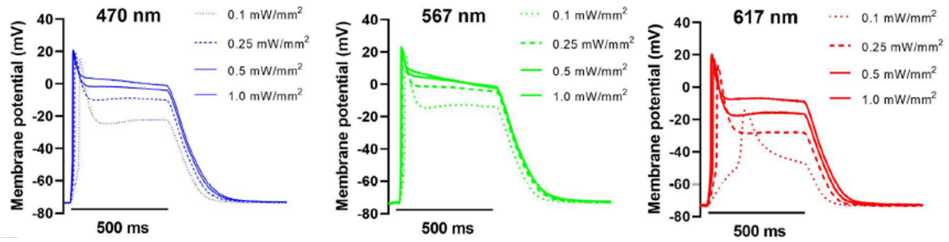

Figure 3.3: Patch clamp experiments, sharp electrode measurements and analysis[4]

With sharp electrode measurements on ReaChR-expressing apical tissue samples, membrane plateau potentials measured upon illumination with 500ms light pulses at an irradiance of 1 mW/mm^2 across the three wavelengths show no significant differences, which demonstrates strong and sustained membrane depolarization when illuminated with light pulses of either 470, 567, or 617nm for 500 ms at intensities greater than or equal to 0.25 mW/mm^2.

A crucial observation from these experiments is the 'un-excitability' induced in tissue samples during illumination. This was evidenced by a loss of capture in response to electrical pacing during illumination, starting from an irradiance of 0.1 mW/mm^2 for 470 and 567nm light, and from 0.25 mW/mm^2 for 617nm light. These findings suggest a significant role of light intensity in modulating cardiac excitability.

Furthermore, computational simulations provide insights into the tissue penetration capabilities of these wavelengths. The simulation subject is defined in a 2-dimensional model of 50x40mm area, where the top 20mm is considered as lumen tissue and the bottom 30mm is considered as myocardial wall tissue (Figure 3.4).

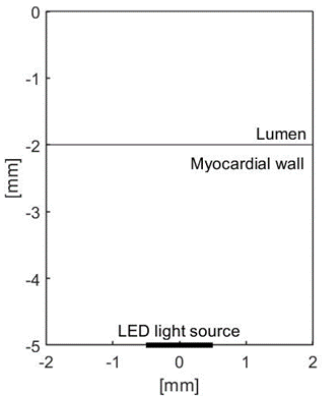

Figure 3.4: computational simulations for tissue penetration capability against wavelength

The simulation is conducted via MATLAB 2019a (MathWorks, USA) with a 3rd-party toolbox used: ValoMC v1.0rc[5]. ValoMC is an open-source Monte Carlo toolbox designed to simulate the travel of photons in the visible and near-infrared spectrum through various media. Based on the photon packet approach, this tool effectively calculates photon distribution within a defined computational domain and determines the photon's existence at the boundaries of this domain. This toolbox provides the ability to accurately model the behavior of light with specified parameters: wavelength, and irra-

diance, in different media with specified parameters: reflective index, absorption index, scattering index, and anisotropy index, making it a valuable resource in optical simulations for this work.

Optical parameters of the media: Lumen and Myocardium are found from existing references (Table 3.2). Note that some data (*) are derived from available figures by interpolating the data curves.

Table 3.2: Tissue optical data from references and used in the simulation

	Property/Lambda	470 nm	530 nm	565 nm	617 nm	Source
Lumen	Absorption (1/mm)	2.28	1.83	1.15	0.79	[3]
	Scattering (1/mm)	2.29	2.12	2.03	1.92	[6]
	Anisotropy	0.9	0.9	0.9	0.9	[6]
	Refractive index	1.4	1.4	1.4	1.4	[7]
Myocardium	Absorption (1/mm)	1.28	1.83	1.15	0.79	[3]
	Scattering (1/mm)	2.15	1.85	1.56	1.39	[3]
	Anisotropy	0.9	0.9	0.9	0.9	[7]
	Refractive index	1.4	1.4	1.4	1.4	[7]

The LED light source is considered as a 1mm wide 2D line providing light irradiance of 10mW/mm^2 at the tissue boundary. The LED light emits light along the normal direction to the tissue boundary and in a cosine light distribution. Four wavelengths are simulated: 470 nm, 530 nm, 567 nm, and 617 nm. Threshold irradiance from previous experiments (patch clamp experiments, sharp electrode measurements) is used as the reference for evaluating whether the light irradiance is sufficient to trigger membrane polarization/depolarization.

Table 3.3: Simulation results of maximum penetration depth of activation against wavelength of LED

Wavelength	**Threshold irradiance**	**Maximum penetration depth**
470nm	0.1 mW/mm2	1.96mm
530nm	0.1 mW/mm2	1.51mm
567nm	0.1 mW/mm2	2.17mm
617nm	0.25 mW/mm2	2.10mm

Based on the simulation result of maximum penetration depth of activation against wavelength of LED(Table 3.3), it is predicted that 567 and 617 nm wavelengths were more effective in penetrating blood-perfused ventricular myocardium compared to 470 nm and 530 nm light, even though the red-shit wavelength 617 nm requires 2.5x higher threshold irradiance compared to others (Figure 3.5). This implies that these longer

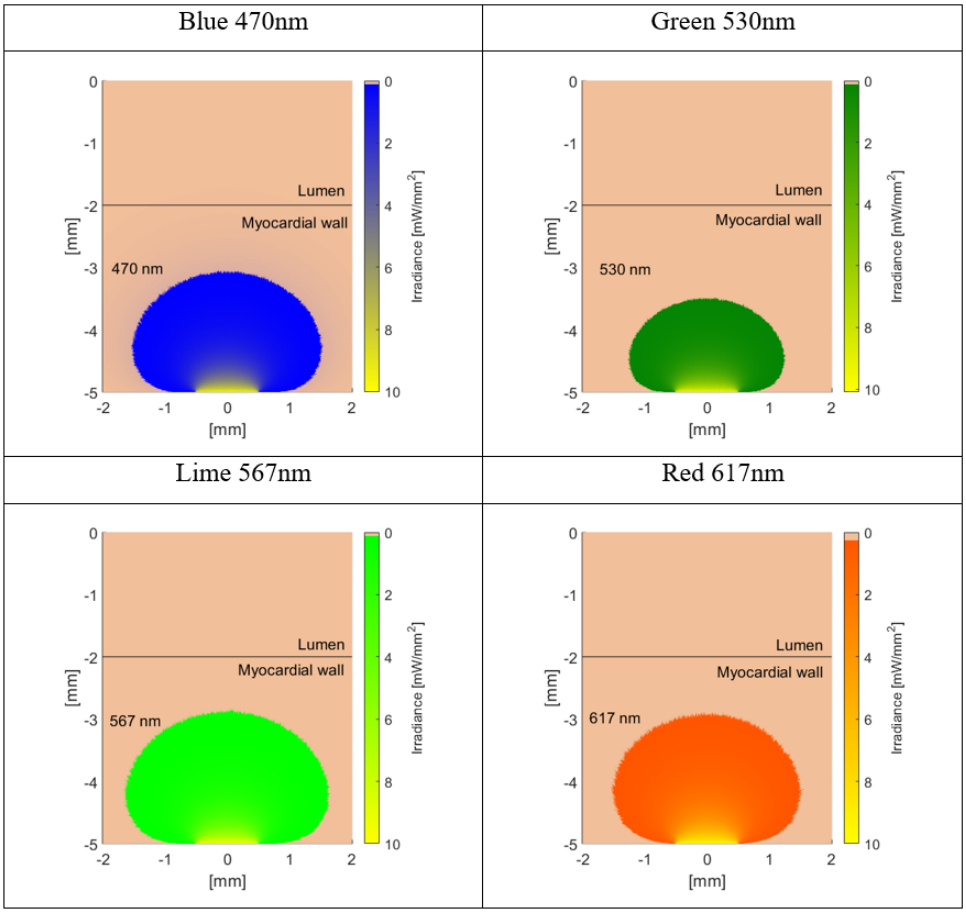

Figure 3.5: Maximum penetration depth of activation against wavelength of LED

wavelengths could potentially excite a substantially larger mass of the ventricular epicardium tissue.

Given these findings, the study concluded that for intensities greater than or equal to 0.25 mW/mm^2, 567 and 617 nm light not only produced similar membrane potential responses but also offered larger peak photocurrents and superior tissue penetration than 470 nm light. Consequently, the 567 nm and 617 nm wavelengths were selected for subsequent whole-heart experiments, underscoring their suitability in terms of both irradiance and wavelength for effective optogenetic modulation in cardiac research. 470 nm light device is still manufactured and tested as a reference.

It is important to mention that the estimated irradiance for optogenetic AF termination in rats might be higher than necessary for potential human applications. The threshold of 0.25 mW/mm^2 used in calculations also includes a safety margin, as lower intensities have already proved effective. Moderating irradiance could also reduce risks like phototoxicity, improving safety and aiding in developing efficient, compact light delivery systems for large animal tests or clinical use.

3.2. SYSTEM DESIGN, FABRICATION AND IMPLEMENTATION

3.2.1. LED CHARACTERIZATION

LED model LZX1 series (LUXEON Z COLOR LINE, LUMILEDS, the Netherlands) chips are selected from various candidates after comparing requirements with multiple advantages:

- High radiant power to provide sufficient irradiance
- Broad selection of light wavelength from 440 to 670nm, including unique lime color 567nm
- Minimized footprint (approximately 2.2mm^2) for size-constrained design
- Relatively wide viewing angle
- Good in availability

As well as disadvantages:

- Non-standard footprint that requires customized pad design
- Bare terminal contacts without solder preparation

- Different packaging depending on wavelengths. Chips in some wavelengths come with ceramic packaging, but some come with epoxy packaging, which is worse against thermal concentration and physical handling during integration
- Relatively expensive, especially in small amounts of acquirement

The technical datasheet for the LZX1 series offers a detailed overview of all essential electrical and optical characteristics. However, it's important to note that many of these key specifications are largely influenced by the intrinsic properties of the LED chips and their microfabrication processes. Due to the natural variability in material properties and manufacturing process variations, there can be minor deviations from the specified values in these specifications. To address this, the manufacturer categorizes the LED chips into various 'bins'. This binning process is based on factors such as variations in radiant power, shifts in color, deviations in dominant peak wavelength, and differences in forward threshold voltage. In the context of large-scale industrial applications, this system allows customers to select the specific bin that best aligns with their specific requirements, ensuring they receive components that precisely meet their needs.

In this work, the LED chips are acquired in small sample quantities from several distributors, where specific binning options are not offered. Given this situation, it becomes essential to conduct in-house characterization of the LED chips to ensure the integrity of the final design. Characterization tests are performed on four variants within the LZX1 LED series: LZX1-pb01 (blue, 470 nm), LZX1-pm01 (green, 530nm), LZX1-px01 (lime, 567 nm), and LZX1-ph01 (red-orange, 617 nm). These models span a range of wavelengths from blue to orange-red, covering the necessary spectrum as requested.

The key specifications to focus on include 1) the forward electrical characteristics, namely the forward current-voltage (I-V) characteristics, and 2) the radiant output characteristics, specifically the radiant power-forward current (P-I) characteristics. Although valuable for some other applications, the secondary specifications, like reverse electrical characteristics, are not relevant to the particular use case in this work, and will not be discussed. Therefore, a selection of test samples is prepared and a specialized setup for these characteristics is assembled.

Four individual test samples are built (Figure 3.6), each incorporating a single LZX1 LED chip. These chips are surface-mounted at the center of custom-designed 50x20mm metal printed circuit boards (PCBs) made of aluminum core. This substrate is composed of layers of laminated copper, dielectric, and aluminum, offering significantly improved thermal conductivity compared to normal fiberglass core PCBs (FR4), without sacrificing design and manufacturing availability. During testing, an additional heat sink is attached to the substrate's backside to enhance thermal dissipation, as temperature is a

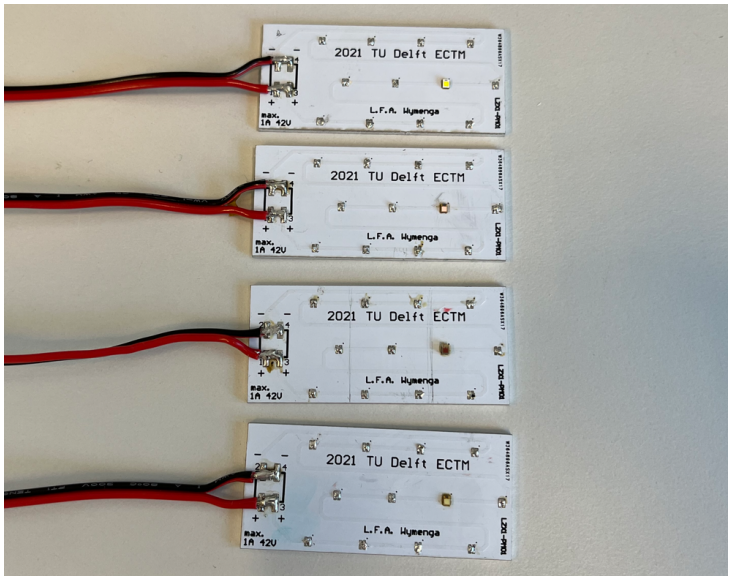

Figure 3.6: LED chips integrated to aluminum PCBs for characterization

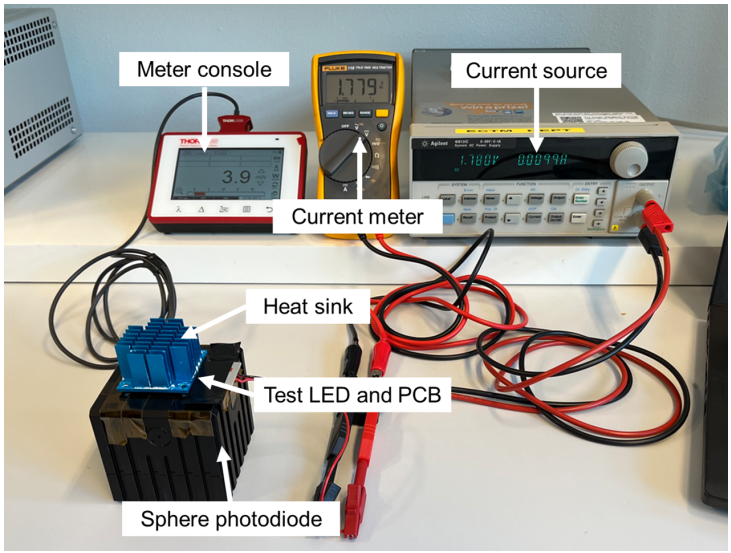

Figure 3.7: Characterization setup

critical factor in high-power LED illumination applications. Poor heat management can lead to dimmed light output and reduced system long-term reliability. Such decreased radiant power due to heat accumulation could cause immediate component damage in extreme cases. Note that detailed thermal characteristic modeling and measurements will be discussed later in this work.

The front top of the substrate is coated with a white solder mask, which serves as a reflecting layer for any light that might leak from the sides or back of the chip. The LED chip was manually assembled, first by attaching it to stencil-printed Sn42/Bi57.6/Ag0.4 (SAC) solder paste with additional rosin flux, and then secured in place through a 250°C hot air reflow process. Any residual rosin flux was subsequently cleaned off with an ethanol flush. The assembly process of all test samples follows the standard procedure of a computer-controlled soldering tool, to ensure consistency in sample preparation.

The characterization setup is shown in Figure 3.7. Two cables extend from the substrate to facilitate the delivery of forward current. The design of the sample allows for easy insertion into the input aperture of an integrating sphere sensor, ensuring accurate measurement and analysis of the LED's optical performance characteristics.

An integrating sphere photodiode power sensor (S142C, Thorlabs Inc., USA) is employed to characterize the test samples' optical performance. This sensor features a 12mm diameter aperture for capturing external light power, which is directed onto the inner surface of a 2-inch sphere coated with reflective PTFE. Inside the sphere, light rays are subjected to multiple diffuse reflections before being uniformly dispersed onto a side-mounted InGaAs photodiode. The radiant power is then converted into an electrical current and sent to a meter console (PM400, Thorlabs Inc., USA), where it undergoes data processing and is then displayed to the operator. This sensor is pre-calibrated by the manufacturer, with sensitivity data for various input wavelengths already stored in the console's built-in memory. The console displays real-time measurements of the radiant power at the peak wavelength of the LED sample placed inside the integrating sphere, and these values are recorded by the operator.

To power the LED sample and precisely record its forward current and voltage, a DC power supply system (Agilent 6613C, Keysight Technologies, USA) is used. The power supply is set to constant current (CC) mode and adjusted through incremental steps of DC current. The DC voltage output is monitored and recorded by the operator. It's important to note that forward voltage is measured using a 2-point connection. This means that voltage drops across the measuring unit, connecting cables, solder joints, and PCB traces all contribute to the readout. To accurately capture the actual forward voltage, a separate multimeter (Fluke 115, Fluke Corporation, USA) is connected parallel to the

solder pads on the PCB. Comparisons of the results show that the values are sufficiently close (less than a 2% difference) to be considered negligible in subsequent analyses.

The entire characterization process is conducted in a darkroom to eliminate interference from environmental light, ensuring the accuracy and reliability of the measurements.

The characterization result of four LED models is plotted (Figure 3.8). Here the radiant power, also called radiant flux in radiometry studies, is measured by the integrating sphere. It represents the total optical emitting power of the LED sample in watts. The electrical power is calculated by multiplying the forward current and forward voltage at the LED sample. The radiant efficiency, or wall-plug efficiency in domestic applications, is defined as the energy conversion efficiency in the percentage that the system converts electrical power in watts, to optical radiant power in watts.

$$\eta = \frac{P_{output}}{P_{input}} = \frac{P_{radiant}}{P_{electrical}} = \frac{P_{radiant}}{V_F \times I_F} \tag{3.1}$$

It can be concluded that all tested LED samples show typical non-linear forward current-voltage (I-V) characteristics as expected. There is minimal current flow through the LEDs until they reach the forward threshold voltage (Vth). Once this threshold is surpassed, the forward current begins to rise exponentially with an increase in forward voltage. It's important to note that these measurements are conducted below the LEDs' maximum rated forward current to prevent the forward voltage from reaching the breakdown value.

Variations in the threshold voltage among the four samples are primarily attributed to the bandgap of the semiconductor material of its core chip, which is a key determinant in wavelength tuning. LEDs with smaller wavelengths (470 nm, 530 nm, and 567 nm), which utilize wider bandgap materials like AlGaN, InGaN, or GaP, typically have a higher threshold voltage of around 2.5V. On the other hand, the larger wavelength LED (617 nm), made with narrower bandgap materials such as AlGaInP or AlGaAs, exhibits a lower threshold voltage, approximately near 1.6V. However above statements are assumptions based on the measured value of threshold voltage, as the actual chip material of the tested chips remains unknown from the supplier's datasheet. Under ideal conditions, these LEDs display near linear radiant power-forward current characteristics under low current conditions (lower than half of the maximum current). This linearity is a result of the emitting physics of the LEDs, where the energy emitted is proportional to the number of recombined free electrons. This behavior underscores the fundamental principles governing the operation of these semiconductor devices.

As the forward current amplitude increases, the junction temperature of the LEDs

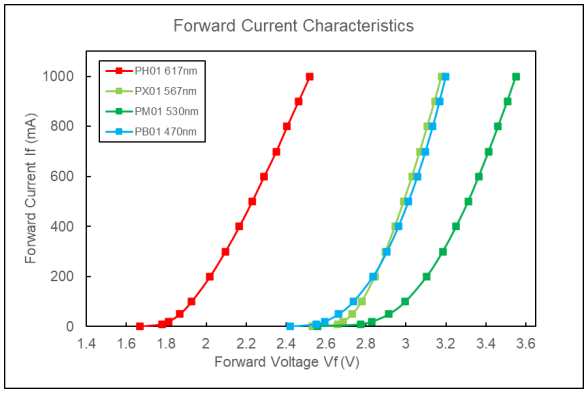

(a) Forward current-voltage characteristics

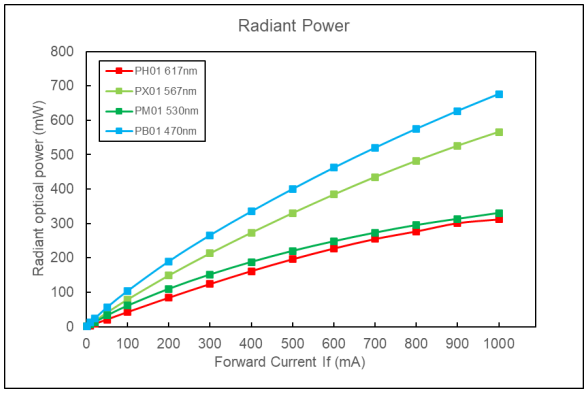

(b) Forward current - radiant power characteristics

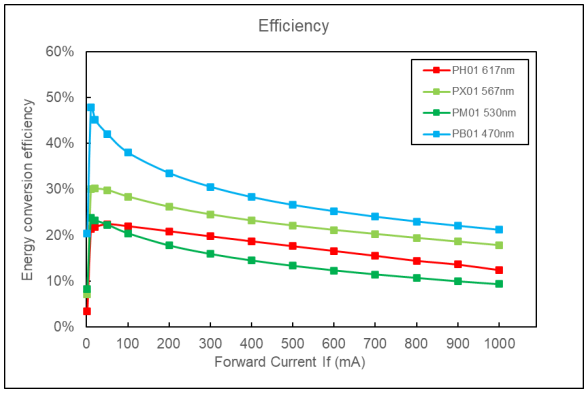

(c) Forward current - energy conversion efficiency characteristics

Figure 3.8: Characterization results of the four LED models

also rises, leading to a decrease in electroluminescence efficiency. This phenomenon is consistent with the measurement results observed that as the current rises close to its maximum allowed value, the radiant power linearity reduces. Also, the decrease in radiant efficiency with increasing forward current can be attributed to the same thermal effect, where the excess electrical power is transformed into Joule heat. Consequently, it is important to maintain the forward current at the lowest possible level to achieve higher efficiency. However, this approach involves a trade-off with the need for higher radiant power. The peak radiant power is observed at the maximum rated current, a factor that is crucial for the subsequent system design considerations. This balance between efficiency and power output is a key aspect in optimizing the performance of these LED systems.

3.2.2. FABRICATION OF 3D "APEX-CUP" DEVICES

In line with the previously outlined requirements, a collection of miniaturized "apex cup" devices, each incorporating integrated LEDs with designated wavelengths, has been designed and fabricated for rat ventricular fibrillation (VF) treatment experiments. The design process includes detailed physical measurements of the three-dimensional geometry of the rat heart, with a particular focus on the ventricular apex. These measurements are conducted on a heart excised and cannulated from a male Wistar rat (Charles River Laboratories, Germany). The 'apex' region of the rat heart ventricle resembles a cone shape, featuring a radius of 4mm at its base (Figure 3.9). Additionally, the edges of this cone-like structure symmetrically extend outward by 4mm along its sides. This three-dimensional structure is the area targeted for illumination by the 'apex-cup' shape device.

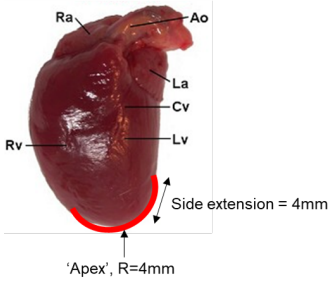

Figure 3.9: Measurement of the rat ventricle 'apex'[8]

To achieve optimal illumination, the four high-power LEDs must be positioned tangentially to the surface of this cone-like structure. A cup-shaped support structure with

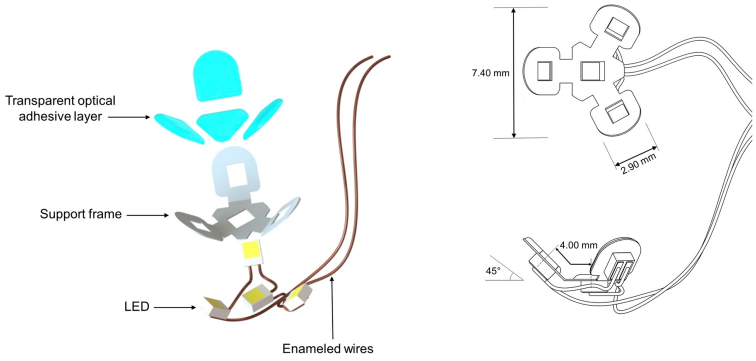

(a) 3D exploding view (b) Schematic view with dimensions

Figure 3.10: The illustrations of apex-cup illumination device

three arms does not only hold the LEDs in the correct orientation but also facilitates the electrical interconnections necessary for power delivery and control. This design ensures that the LEDs are precisely aligned with the apex surface, maximizing the efficacy of the illumination.

The cup's main structure is designed as a three-point star-shaped support frame. This frame consists of a central area, three arms, and four window openings, each measuring 1.2mm by 1.6mm, to accommodate the placement of the LEDs. The LEDs are arranged so that the center LED is 4mm from the outer LEDs, ensuring the illuminating surface of all four LEDs is tangentially aligned with the designated apex area. A computer-aided design (CAD) diagram of this setup is illustrated in Figure 3.10.

The frame needs to be lightweight and have a design that minimally interferes with the natural expansion and contraction of the ventricle. To achieve this, a 0.15mm thick film of white polyethylene terephthalate (PET) is precisely cut using a programmable laser cutter. The thin PET film's high flexibility permits the arms to bend freely up to 45 degrees, allowing the cup device to conform to the 3D geometry of the rat ventricular apex and minimizing stress on the apex during installation and use. The white film also enhances light reflection, reducing potential light energy loss.

Four identical high-power LXZ1 LEDs are affixed to the support frame using transparent UV-curable optical adhesive (NOA63, Norland Products Inc. USA). A thin, transparent layer of the UV-curable optical adhesive, with a thickness of 0.5mm at the illumination side of the LED, and 0.1mm at the side and back side of the LED, is then applied

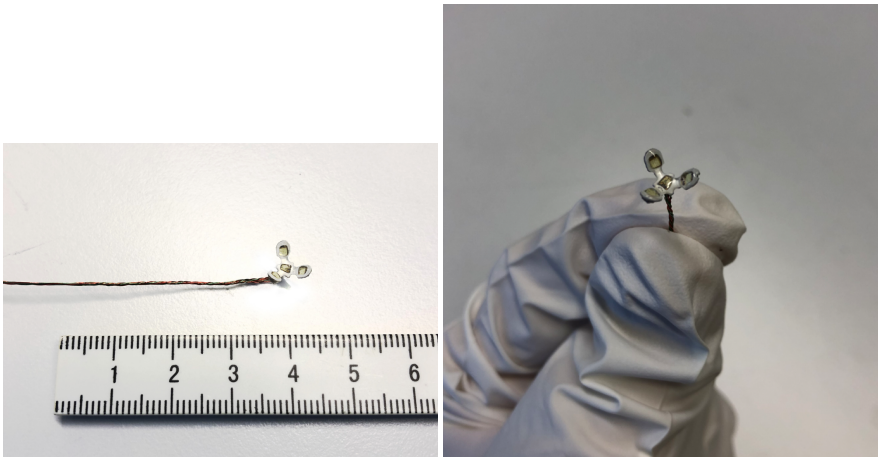

Figure 3.11: Fabricated Apex-cup device with four 567nm LEDs

together with the support frame. This layer serves to both physically secure the LEDs in place and provide electrical insulation. The adhesive is cured at room temperature under four 15W ultraviolet lamps (CLEO Compact, Philips, the Netherlands) for 10 minutes. A fabricated apex-cup device is shown in Figure 3.10.

The wiring of the LEDs is designed to allow independent control of the central LED and the outer LEDs. This design enables selective illumination of the apex myocardium, both from the tip of the apex and from three side spots. The anodes and cathodes of the high-power LEDs are connected to enameled copper wires, each with a diameter of 150µm. These wires are chosen for their exceptional softness and flexibility, which helps prevent any additional strain on the apex's movements. Also, the enamel layer of the wires protects the electrical power against bio-chemical reactions during the experiments and prevents short circuits even with tight and twisted cabling. The enameled copper wires extend to a length of approximately 30cm to facilitate ease of handling during in-vivo open-chest operations. They are connected to thicker multi-core cables via a removable socket on an external LED driver (LEDd1b, Thorlabs, USA).

This LED driver functions as a constant current source with adjustable output current levels. Additionally, the LED driver is equipped with trigger control through an external 5V Transistor-Transistor Logic (TTL) signal. This setup allows synchronization with an STG4002 stimulus generator and MC Stimulus software (Multi Channel Systems, Germany) for coordinating electrical rhythm pacing, VF induction, and optical termination. The illumination pulse duration, interval, and cycle amount can be precisely programmed via a computer user interface.

Four distinct LED apex-cup devices have been constructed to offer illumination at different wavelengths: blue (470nm, LXZ1-pb01), green (530nm, LXZ1-pm01), lime (567nm, LXZ1-px01), and red (617nm, LXZ1-ph01). The current for each LED can be continuously adjusted from zero up to their maximum rated values, corresponding to: blue: 1000mA/3.35W, green: 1000mA/3.25W, lime: 700mA/2.85W, red-orange: 700mA/2.25W. During the in-vivo and ex-vivo experiments, the apex-cup device is securely attached to the rat heart's apex using two drops of Histoacryl tissue glue (Braun, Germany), as shown in the Figure 3.12. The details and results of the experiments are explained in the following validation sections.

Figure 3.12: The apex-cup device is glued to the rat's ventricular apex

The radiant characteristics of all four LED apex-cup devices are evaluated using an optical calibration setup. This setup includes an S130C wide-spectrum photodiode and a PM100D readout head unit (both Thorlabs Inc., USA). The setup is used to measure the maximum radiant intensity at the illumination surface of each device across different wavelengths, with the results presented in the table below. The measurements indicate that the irradiance of all devices comfortably exceeds the initial light intensity requirements. This efficiency means that the devices can achieve the minimum necessary stimulus at a lower forward current, translating to reduced input power. Consequently, this leads to a decrease in operating temperature and an increase in electrical-optical efficiency, enhancing the overall performance and reliability of the devices.

3.2.3. TEMPERATURE PROBING MEASUREMENTS

To comprehensively evaluate the thermal responses of the 567 nm and 617 nm LED devices, a detailed study is conducted, based on temperature probing measurements and computational simulation. The focus is on the temperature changes when these

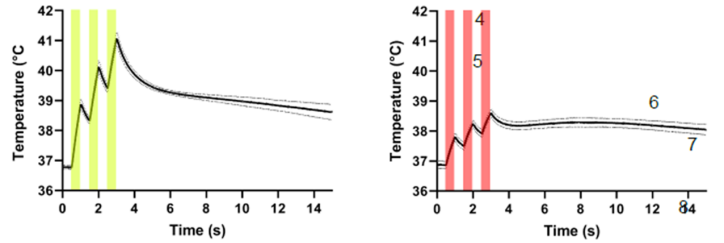

(a) LED 567nm (b) LED 617nm

Figure 3.13: Temperature probing measurements of LEDs

devices are activated for three consecutive 500ms light pulses, each separated by a 500ms interval. Temperature measurements are performed ex-vivo within an incubator set at a constant 37°C, which is the same as the physiological temperature conditions of the body.

Before illumination, the maximum temperature recorded on the ventricle surface, directly above the polymer-insulated LED chip, is 36.8°C(ranging between 36.7–37.0°C). However, upon activation of the LED device, a notable temperature increase is observed. For the 567 nm LED device (operating at 15 mW/mm^2, 500mA), the average maximum temperature briefly peaks to 41.1 ± 0.2°C after the third light pulse. Similarly, for the 617 nm LED device (at 10 mW/mm^2, 500mA), it peaks at 38.1 ± 0.1°C (Figure 3.13).

Specifically, for the 567 nm LED device, the duration for which the temperature remained between 40.0 and 41.1°C was less than 2 seconds, indicating a rapid thermal response and cooling. The variance in thermal response observed between the two wavelengths may be attributed to differences in their packaging (Figure 3.14). The 567 nm LED (LXZ1-PX01) has ceramic packaging which has better thermal conductivity, compared with the epoxy packaging for the 617 nm LED (LXZ1-PH01). The higher the thermal conductivity of the packaging material, the more rapidly heat generated by the core semiconductor chip is dissipated to the exterior. This results in a quicker thermal response and elevated short-term thermal peaks. Thermal equilibrium is eventually achieved after 12 seconds and the system temperature is stabilized at a similar value. Such detailed thermal measurements are crucial for understanding the transient thermal effects of LED activation, particularly in the context of their safe application in biomedical settings.

3.2.4. THERMAL MODELLING

Finite Element Method (FEM) is used to simulate and estimate the thermal characters of the apex-cup LED device during the in-vivo experiments. FEM is a cornerstone in com-

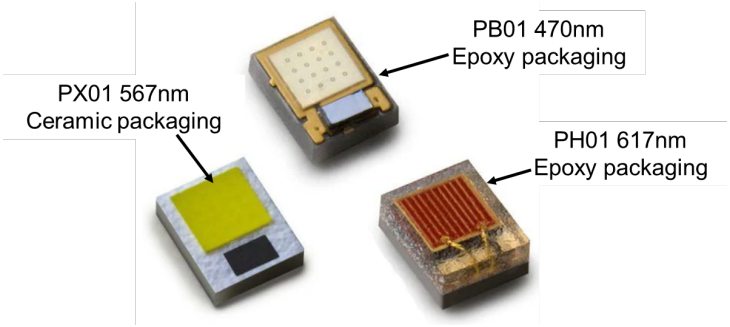

Figure 3.14: Packaging materials for LEDs with different wavelengths

putational simulation, especially in modeling complex systems like electrical-thermal interactions in the context of this work. FEM divides a large problem into smaller, simpler parts called finite elements, enabling detailed analysis of various physical phenomena. This integration is crucial in accurately predicting how electrical devices, such as LED chips, interact with and affect their surrounding bio-environment, leading to more precise estimation and safer designs.

Simulation Environment

COMSOL Multiphysics 5.1 (COMSOL Inc., Sweden) is the preferred choice for this simulation due to its advanced capabilities in handling multi-physics problems. Its user-friendly interface allows for easy modeling of complex systems, integrating various physical phenomena including thermal interactions. COMSOL's extensive library of material properties enhances the efficiency of simulations. Additionally, it offers simplicity and flexibility in customizing models and is well-suited for simulating the dynamic interactions in biomedical devices, making it an ideal tool for detailed and reliable analysis for this work.

Model

A 2-dimensional model is created to accurately represent the real-world scenario, focusing on the rat's cardiac region. The model is designed based on the cross-sectional anatomy of a rat (12cm in length, 5cm in width), specifically focusing on the heart's typical location when the rat is positioned as it would be during experimental procedures. This approach ensures that the simulation closely replicates the actual experimental conditions, allowing for more accurate and relevant results. For simplicity, the limbs are not included in the model as they are distant from the area of interest.

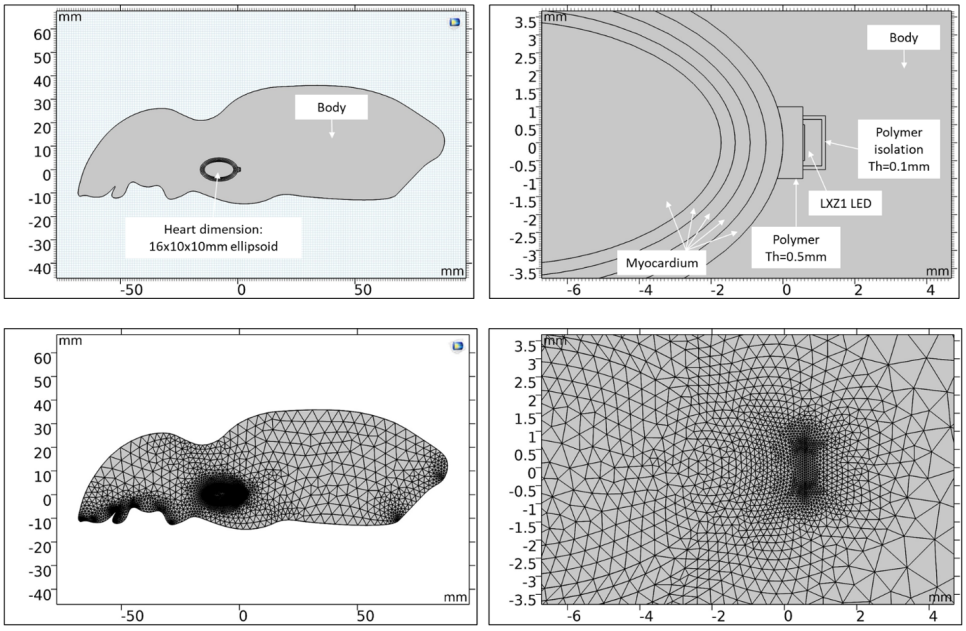

Figure 3.15: Simulation model dimensions (a) Overview of a cross-section of rat, (b) Region of interest with heart and LED chip (c) Model meshing with 7797 triangle domain elements (d) Region of interest with finer meshing near the interface between LED chip and tissue surface

The dimensions of the heart in the model are represented as an ellipsoid measuring 16mm in length, 10mm in height, and 10mm in width. The region of interest has five ellipsoidal layers representing the myocardium of the heart to increase the meshing fineness, surrounded by a larger uniform area representing the body. One LXZ1 LED chip, instead of four due to reduction in complexity, is defined from the dimensions of the datasheet, including a 0.05mm thick core chip (a semiconductor die) area as well as the ceramic packaging. A layer of polymer, directly surrounding the LED, has a thickness (Th) of 0.5mm, representing the glue to bond the LED to the myocardium, and the second layer of polymer has a thickness of 0.1mm, representing the isolation polymer around the LED chip. This setup is presumably to simulate the geometry of the LED device when implanted near the heart within the body.

Model meshing in FEM is a process where the geometric space of the model is divided into discrete elements. The quality of the mesh directly affects the accuracy, convergence, and computational efficiency of the simulation. An adaptive finer mesh near the region of interest, the interface between the LED chip and myocardium surface, can capture more details in areas with high-temperature gradients being analyzed. But it requires more computational resources. Therefore a coarser mesh is used in other areas far away from the region of interest. The model meshing consists of 7797 triangle domain elements in total.

Material properties

Material properties are fundamental to model accuracy. They determine how different elements within the model will react to physics, such as heat or force. For thermal simulations, key properties include thermal conductivity, heat capacity, and density. These properties are inputted into the FEM solver, allowing it to calculate temperature distribution and changes within the modeled materials under specific conditions. Accurate material properties are essential for reliable simulation outcomes and are sourced from reference experimental data and built-in material databases.

Boundary conditions

Boundary conditions that define the initial state and how the model interacts with each other. Setting correct boundary conditions is vital for simulating accurately, ensuring that the computational results are meaningful and can predict physical behavior only under various conditions.

They are the constraints that guide the simulation to a correct solution. In this simulation, the LED chip is specified with a power output of 2W, powered by a 750mA current

Table 3.4: The material properties used in the simulation.

Domain(s)	Material	Thermal conductivity, k [W/(m·K)]	Heat capacity, Cp [J/(kg·K)]	Density, $\rho[kg/m3]$	Source
Rat body	Rat muscle	0.49	3421	1090	[9]
Rat heart	Rat myocardium	0.56	3686	1081	[9]
LED body	Al2O3	35	730	3965	COMSOL built-in
LED die chip	GaN	130	490	6070	COMSOL built-in
Polymer (Optical adhesive & tissue adhesive)	Polyurethane	0.197+3.349E-4*T	1460	1250	COMSOL built-in

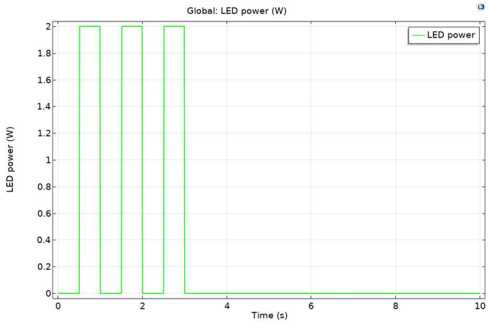

Figure 3.16: Input electrical (light) signal to the LED chip

at 2.8V with a wavelength of 567nm. The device is driven by three 500ms light pulses with 500ms intervals in between, the same as the pulses used in the in-vivo experiments for VF termination (Figure 3.16). The assumption is that all electricity input to the LED is eventually transferred to thermal energy since no light escapes from the body of the rat. The physical model includes only heat transfer without considering material expansion, applying a biological heat transfer model for both the myocardium and the body. Thermal expansion is not considered in this simulation to further reduce complexity.

The initial and ambient temperatures are set at a constant 37°C to mimic physiological conditions. The study is time-dependent with fine temporal resolution, using a step size of 0.01 seconds.

Simulation result and analysis

The simulation results show a dynamic thermal profile of the LED device and the surrounding biological tissue.

1. Maximum temperature

The maximum temperature in the myocardium reached 44.1°C at T=3.29s at the interface to the polymer bonded to the LED chip (Figure 3.17 and Figure 3.18). Spatially, different parts of the model—namely the LED, myocardium, and body—show varied temperature responses due to their distinct material properties, with the LED naturally exhibiting the highest temperatures. The maximum temperature in the body area surrounding the region of interest reached 47.5°C at the interface to the side of LED packaging (Figure 3.19). The maximum temperature in the LED device reached 151°C at the center of the LED semiconductor die (Figure 3.20). Although the maximum temperature seems extreme, it should be analyzed together with the relatively short peak duration.

2. Temperature distribution

   The simulated temperature distribution indicates a localized thermal increase at the LED die, with a quick gradient extending into the polymer and then the myocardium. The temperature distribution is more uniform and flatter throughout the LED device and polymer due to the greater thermal conductivity of the ceramic package.

3. Temperature over time with pulses

   The system's thermal dynamics reveal a prompt thermal response, with temperatures rapidly escalating to a peak during the LED's active phases. Over time, the temperature fluctuates by the pulsed nature of the LED, showcasing a rise with each pulse and a subsequent fall during intervals. These peaks, although brief, represent crucial moments of thermal 'hit'. Following these short-lived spikes, the system efficiently dissipates heat, gradually restoring itself to thermal equilibrium to the ambient temperature of 37°C in approximately 12 seconds.

   This cyclical pattern of sharp temperature increases followed by cooling suggests that the LED device and tissue interface manage heat effectively, minimizing the duration of any potential thermal damage. Although the maximum temperature seems extreme, it is still decided to be safe for the in-vivo experiments due to very short duration as well as limited light pulses. However the risks still exist and operators should be alerted not to use light pulses longer than 1 second, where the peak temperature might cause damage to the tissue, body (protein denaturation and cell damage, etc.), or the LED chip itself (burn out).

4. Compare simulation with probing measurements

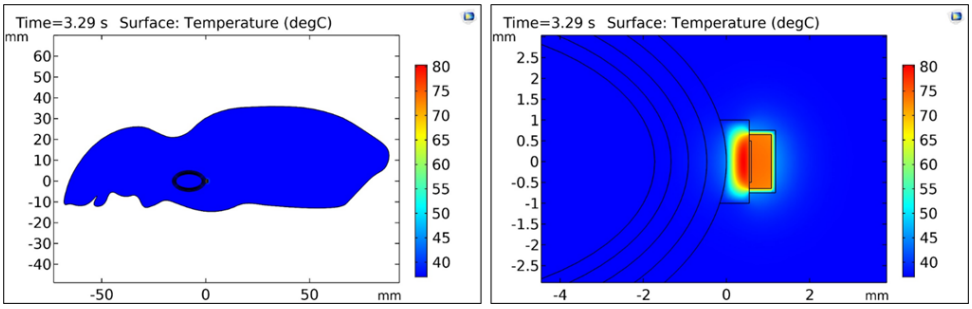

Figure 3.17: Transient temperature distribution where the highest myocardium temperature is reached (44.1°C)

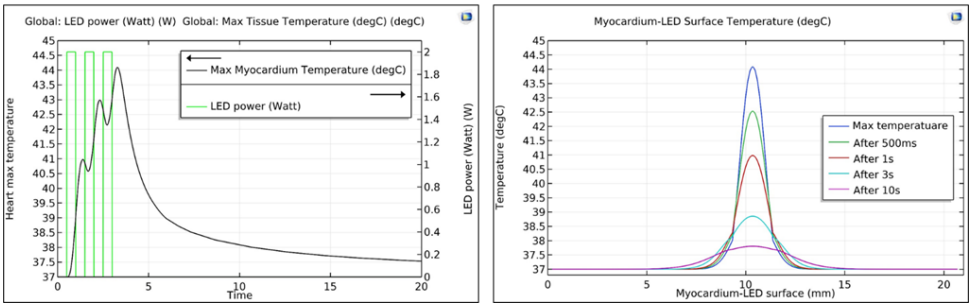

Figure 3.18: Thermal response and distribution at the out surface of myocardium

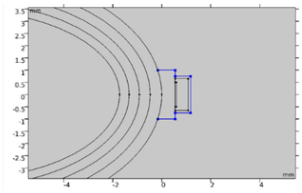

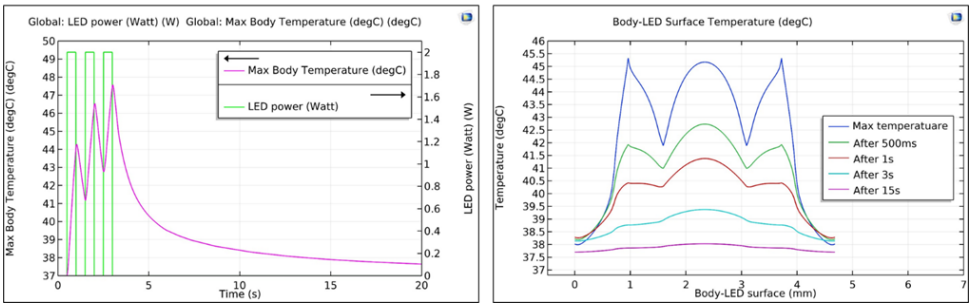

Figure 3.19: Thermal response and distribution at the out surface of LED device (insulation polymer)

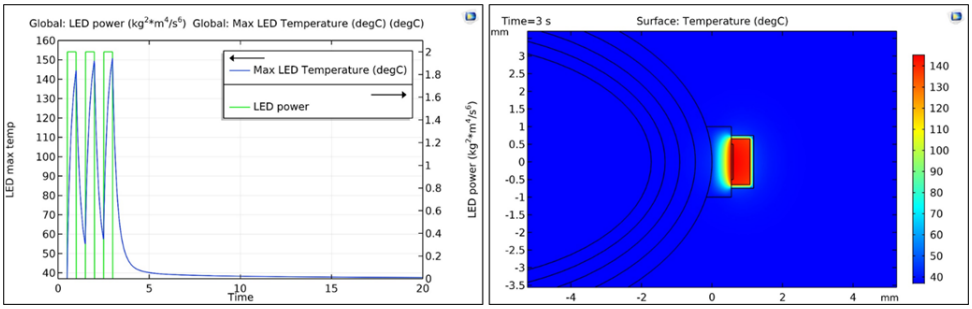

Figure 3.20: Thermal response and distribution inside LED device

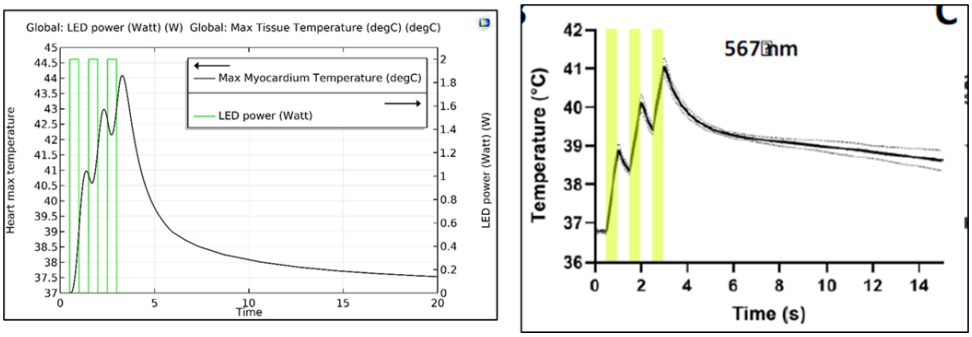

Figure 3.21: Comparing (a) simulated thermal response with (b) probing measurements

It needs to be clearly stated that FEM simulations are powerful tools that can approximate real-life conditions but with many limitations. The accuracy of FEM simulations depends on the quality of the boundary conditions, the precision of material property definitions, and the assumptions made during model setup. Simplifications necessary for computational feasibility, such as neglecting certain physical interactions (physical movement, thermal boundaries, thermal expansions, etc.) or dimensions (corner effect, inhomogeneous in density, etc.), can affect the results even with large variations. Hence, while FEM can provide valuable insights, its predictions should always be validated against experimental data and understood within the scope of its defined parameters. The simulated maximum temperatures at the myocardium surface are approximately 3°C higher than those measured by probing temperature measurements (Figure 3.21). This discrepancy can be explained by the thermal capacity of the LED device being small in comparison to the thermocouple used for measurement, leading to rapid temperature changes that could surpass the measurement resolution of the equipment. In other words, the probing measurements cannot accurately capture the sharp peak of maximum temperature in a very short duration, but instead a 'flattened' peak by thermal capacity. However, the cyclical pattern of sharp temperature increases followed by cooling down along with the LED light pulses match well between simulation and real-life measurements.

The thermal simulation concludes with a discussion that the LED device design is safe for the in-vivo experiments, in the context of the tissue damage and hardware damage by thermal effects will be minimal.

3.3. SYSTEM VALIDATION: EXPERIMENTS OF VENTRICULAR FIBRILLATION TREATMENT

The apex-cup LED device is then sent through a series of comprehensive in-vivo and ex-vivo experiments. These experiments were meticulously structured to assess the functionality, reliability, and efficacy of the system under varying conditions that closely mimic the physiological environments encountered in real-world scenarios. In-vivo tests provided critical insights into the system's performance in a living organism, examining its bio-compatibility, operational stability, and overall impact on physiological processes. Ex-vivo experiments allowed for a more controlled analysis of the system's mechanisms, enabling detailed investigation into its operational parameters and interactions with biological subjects outside of a living organism. Together, these experimental approaches have been instrumental in validating the system's design, ensuring its readiness for potential clinical application and further research possibilities.

3.3.1. PREPARING THE RAT MODEL FOR IN-VIVO AND EX-VIVO EXPERIMENTS

Weeks before the experiments, rats, aged 9-10 weeks, are anesthetized with isoflurane and oxygen for ECG data collection before undergoing Transverse Aortic Constriction (TAC) to prepare for inducing (with genetic treatments) or sham surgery (as a control group). The absence of pedal reflexes confirms adequate anesthesia, and anesthesia is maintained post-operatively. TAC is a surgical technique commonly used in research to model heart disease in animals. It involves narrowing the aorta, the main artery leading from the heart, which overpressures the heart and can lead to hypertrophy, similar to certain conditions in humans. This is achieved by tying to suture the aorta with a spacer, which is then removed to maintain a consistent level of constriction. Animals that are part of the control group for the study received a sham operation, which mirrors the procedure of the TAC surgery but without the actual constriction of the aorta, and no suture is secured around it.

Weeks later, they receive a tail vein injection of a viral vector for one of the two types of gene delivery: ReaChR light-sensitive ion channels[1] or Citrine as a control reference. Baseline ECG data is then collected using an 8-channel PowerLab data acquisition device and recorded and analyzed using LabChart Pro software version 7 (both from AD Instruments, UK). After 8 weeks of the surgery, the rats are ready for in-vivo experiments for VF treatments. Then the rats were euthanized, and their hearts were extracted for further ex-vivo analysis.

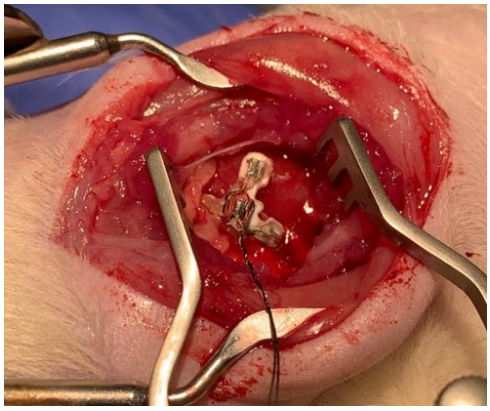

Figure 3.22: The apex-cup device is attached to rat's ventricular apex during in-vivo experiments

3.3.2. IN-VIVO VF INDUCING AND TERMINATION EXPERIMENTS

In vivo experiments are carried out to test the feasibility and efficacy of optogenetic VF termination by the LED apex-cup implanted. Between weeks 8 and 10 post-preparation operations, the rats are anesthetized, and their hearts are exposed for VF induction and later treatments. VF is induced using programmed electrical stimulation, a burst pacing of 20 to 30ms, and 5V signals using an STG4002 stimulus generator with MC Stimulus II software (Multichannel Systems, Germany). Only persistent, non-self-limited VFs exceeding 5 seconds are considered valid inducing and then proceeded with optical termination experiments.

The LED apex-cup device is bonded to the ventricle apex using two drops of tissue glue (Braun, Germany) to the anesthetized and mechanically ventilated TAC rats (Figure 3.22). The enameled wires that supply power and signal to the device are arranged in such a way that they do not hinder the movement of the heart or other organs, ensuring they remain unobstructed and function normally. While it is possible to fully close the thoracic wall with the LED apex-cup device functioning inside, the optogenetic VF termination experiments are conducted with an open chest.

VF is expected to be optically terminated using a programmed electrical signal to control the LED illumination. The VF termination protocol consists of up to three 500ms pulses with a 500ms interval. Success is defined by arrhythmia termination within 1 second after the final light pulse. ECGs are recorded and analyzed in line with previous methods in baseline collection.

Sustained VFs are effectively terminated using one pulse, two pulses, and three pulses

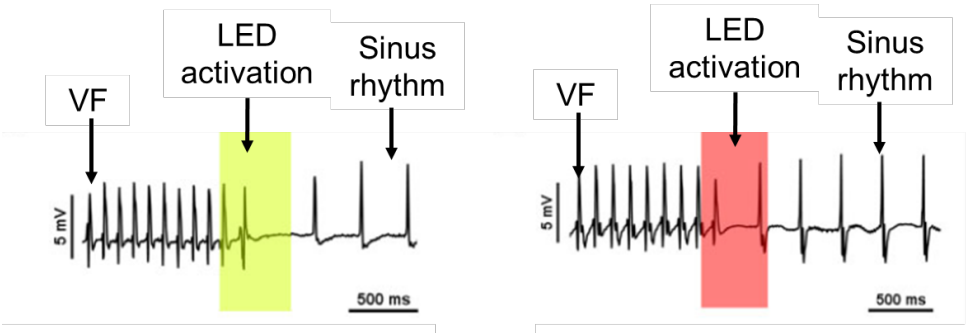

(a) LED 567nm (b) LED 617nm

Figure 3.23: ECG recordings of terminating VF by light stimulus

500 ms light pulses with ReaChR-expressing rats (Figure 3.23). The success rate of optogenetic VF termination with three consecutive pulses is high, with 95% for 567 nm light at 15 mW/mm2 irradiance and 86.7% for 617 nm light at 10 mW/mm2 irradiance. These rates contrasted with lower termination rates in controlling Citrine-expressing rats under the same conditions, with 15.0% for 567 nm light and 13.3% for 617 nm light. Post-termination measurements show an immediate return to normal rhythm after optical cardioversion and no significant differences in average heart rhythm between the two wavelengths.

Beyond the primary measurements, the experiments also include an analysis of optical voltage recordings from the apex after repeated LED light activation, in both living organisms and lab settings. This was crucial to evaluate if the LED apex-cup device might cause any long-term electrophysiological issues in the test subjects. The results show no significant disturbances in electrical conduction across the apex, indicating that the use of LED apex-cup devices does not lead to any persistent electrophysiological changes. These findings also correlate with the CEM43 concept, which is a standard for assessing thermal exposure's impact on cell viability and is well below the critical threshold for myocardium, suggesting minimal thermal effect from the LED device.

3.3.3. EX-VIVO EXPERIMENTS

Ex-vivo experiments allowed for a more controlled analysis of the system's mechanisms, enabling detailed investigation into its operational parameters and interactions with biological subjects outside of a living organism. The rats were euthanized, and their hearts were extracted and moved to a Langendorff setup. An apex-cup device is attached to the ventricular apex with the same gluing techniques (Figure 3.24).

Figure 3.24: Fitting of the apex-cup device to the ex-vivo setup of rat heart ventricular epicardium

Sustained VFs are induced by electrical burst pacing using the same methods as in-vivo setups. Then the VF is treated with one pulse, two pulses, or three pulses 500ms LED activation. The effectiveness of VF termination varied depending on the LED location configuration and wavelength. For ReaChR expressing hearts, using the central LED alone resulted in a lower termination rate, with 76.7% for 567nm light and 60% for 617 nm light (n = 6), than when all four LEDs were activated, with 100% for 567nm light and 93.3% for 617 nm light (n = 6). The results are notably different in hearts expressing the controlling Citrine gene, where the termination rates are significantly lower, with 5% for 567 nm light and 5% for 617 nm light (n = 4).

Supported by electrode measurements, data show that the apex of ReaChR-expressing hearts becomes unresponsive to electrical pacing during illumination with 567 or 617 nm light, indicating effective light-induced signal blockage. This response is not observed in Citrine-expressing hearts under similar conditions, aligning with the expected outcomes.

3.3.4. CONCLUSIONS OF THE EXPERIMENTS

The in-vivo and ex-vivo experiments successfully demonstrate optogenetic VF termination in rat hearts, with structural and electrical remodeling, using an implanted LED apex-cup light source for apex illumination. These findings prove a significant advance-

ment in applying cardiac optogenetics for managing ventricular arrhythmias, especially relevant for the majority of VF patients with structural heart conditions. However, due to differences between rat and human hearts and potential variability in gene expression, further research with larger animals is still essential.

In addition to demonstrating successful optogenetic VF termination for clinical purposes, the experiments also extensively test the implanted LED apex-cup devices in various aspects: functionality, optical performance, reliability, and compatibility. This comprehensive testing ensures the devices' efficacy and safety in real-world clinical applications, particularly for patients with structural heart diseases requiring immediate termination delivery. This holistic approach significantly enhances the clinical viability of cardiac optogenetics in ventricular arrhythmia treatment with LED technology.

3.4. AN LED LIGHT ILLUMINATION SYSTEM FOR IN-VIVO TRANS-THORACIC AF TREATMENT

3.4.1. TRANS-THORACIC AF TREATMENT

Trans-thoracic AF treatment is a proposal, following the success of in-vivo and ex-vivo VF termination experiments described in previous sections, that explores the potential of trans-thoracic illumination for optogenetic AF termination, a non-invasive alternative to open chest operations as demonstrated in previous sections. In previous experiments, it has been proven successful VF termination with localized illumination at the apex area of the heart. With the same concept, by focusing light on the genetically modified heart's atrial externally, a similar optogenetics method could revolutionize a highly successful rate of AF treatment, while reducing surgical risks and recovery times for the subject.

This work includes assessing optogenetic excitation illumination to effectively penetrate the human heart tissue for arrhythmia termination. Then the first-ever evaluation of close-chest optogenetic AF termination in rats, aiming to understand its feasibility and effectiveness.

3.4.2. OPTICAL TRANSMITTANCE MODELLING

The study of light transmittance and attenuation in human atrial myocardium is the basis for advancing optogenetic trans-thoracic AF treatment because it determines how well light can penetrate heart tissue and deliver the irradiance to trigger light-sensitive ion channels. This knowledge allows for the design of the LED light source and precise calibration of light intensity, ensuring that it reaches target areas effectively.

Left atrial appendages from AF patients are collected during cardiac surgery after the

heart is stabilized with cardioplegia, according to ethical guidelines and anonymized collection protocols. These samples, still containing blood, are carefully sectioned into varying thicknesses (0.5 to 2.0mm) using vibratome and ceramic injector blades, and then preserved in cold phosphate-buffered saline (PBS). The tissues are embedded in a low-melting-point agarose. These processes are critical for maintaining the integrity of the samples while allowing for detailed analysis.

Tissue slices are then placed on a glass coverslip on top of an optical power sensor (S130C, Thorlabs, USA) connecting to a read-out interface (PM100D, Thorlabs, USA) for light transmittance measurements. Using a collimated 565nm LED light source (M565L3, Thorlabs, USA) with adjustable intensity, transmittance through human atrial tissue is then characterized. Relative light attenuation is calculated by comparing the light passing through just the coverslip, with the light passing through the tissue sample and coverslip.

$$T = \frac{I}{I_0} \tag{3.2}$$

Where T is the light transmittance, I_0 is the light irradiance of light passing through just the coverslip, and I is the light irradiance of light passing through the tissue sample and coverslip, with the same light source input power. The process was repeated across various tissue thicknesses from different patients, a total of 12 individual measurements.

The light attenuation equation commonly used in optical material physics, including studies of light transmission through materials like tissues, is based on the Beer-Lambert Law[6][10][11][12][13]. This law states that the transmittance of light through a medium is exponentially related to the product of the medium's absorption coefficient and the path length of the light through the medium. Mathematically, it is often expressed as

$$T(D) = e^{-\mu D} \tag{3.3}$$

or

$$I(D) = I_0 e^{-\mu D} \tag{3.4}$$

Where μ is the attenuation coefficient, and D is the depth or thickness of the medium. This equation is fundamental in determining how much light is absorbed as it passes through a substance with a certain thickness, in this case, the tissue samples. Data points of T and D pairs are fitted to the Beer-Lambert law via Curve Fitting Toolbox (MATLAB R2019a, MathWorks, United States) and yield a coefficient of determination R2 > 0.73 (Figure 3.25). This allowed the determination of the light attenuation coefficient

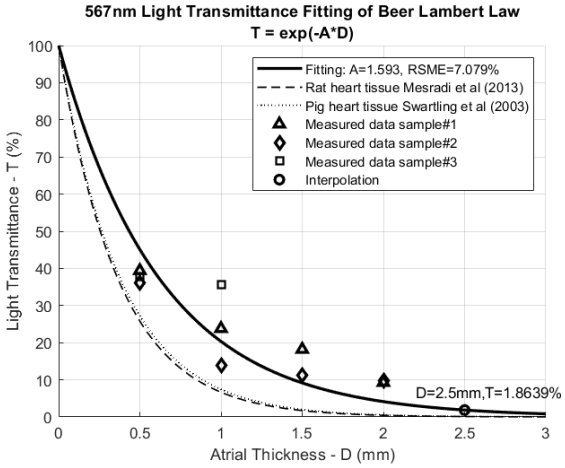

Figure 3.25: 567nm Light Transmittance Fitting of Beer-Lambert Law[3][12]

μ = 1.679 mm-1 of human atrial myocardium. By extrapolating the model to greater sample thickness, one can estimate that the transmittance of 565-nm light of 2.0mm- and 2.5mm-thick atrial myocardium are correspondingly 3.48% and 1.50%.

So far, this analysis represents a preliminary investigation with a limited number of samples (n=3) and data points (n=12). As the research progresses after this investigation, more comprehensive data is collected from new samples (n = 80 individual measurements on 20 samples derived from 5 patients), which enhances the accuracy of the light attenuation model. Improved fitting results determine an attenuation depth of 0.70mm for human atrial tissue, equivalent to an attenuation coefficient of 1.42mm^{-}1, with a higher coefficient of determination (R2 > 0.87). This finding, along with the ReaChR activation threshold, suggests that 565-nm light pulses at 25mW/mm^2 should effectively penetrate the typical human atrial wall thickness of 2–2.5mm.

3.4.3. DEVICE DESIGN, FABRICATION AND IMPLEMENTATION

It's important to understand that the above section mentioned irradiance threshold is meant for the heart tissue's surface. However, to reach this surface, the light must first penetrate through the chest thoracic, requiring much higher irradiance at the chest's outside skin. Therefore, the light source used for thoracic treatments must have a significantly higher power density to ensure effective penetration and reach the heart tissue effectively.

To provide transthoracic illumination of the rat heart, an integrated high-power LED

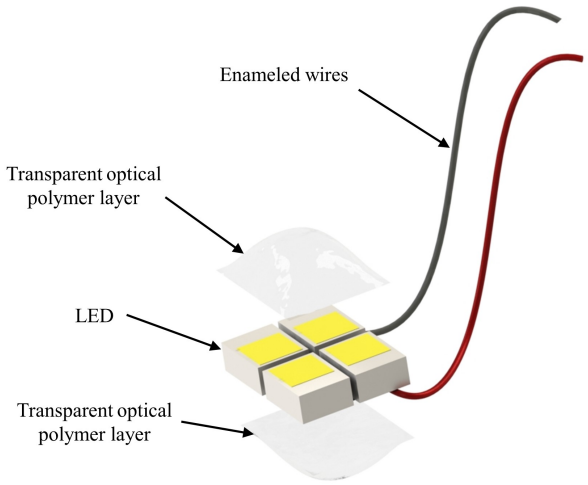

Figure 3.26: Illustration of the integrated high-power LED device for transthoracic illumination of the rat heart

device is designed and fabricated (Figure 3.26 and Figure 3.27).

Four identical high-power LEDs (LUXEON Z LXZ1-PX01, Lumileds, USA) are placed side-by-side and bonded together with UV-curable optical polymer (NOA63, Norland Products, USA). The anodes and cathodes of nearby LEDs are soldered by lead-free solder. The distance between the center of every LED is 1.3mm to achieve a 2x2 square arrangement. A transparent layer (center thickness 1.0mm) of UV-curable optical polymer is applied on the front side of the LED arrangement to physically fix and electrically insulate the high-power LEDs. The input anode and input cathode are soldered to enameled copper wires with a diameter of 150um. The solder joints and exposed copper wires on the back side of the LED arrangement are then covered by the same transparent layer of optical polymer with the same thickness and curing procedures to ensure electrical insulation and mechanical robustness of the interconnects. The curing of all UV curable optical polymer layers was performed at room temperature under four UV lamps (Cleo Compact 15W, Philips, The Netherlands) for 10 minutes.

The four LEDs provide a constant color spectrum with a peak wavelength of 567nm (lime), and all LEDs are simultaneously controlled by an external LED driver (LEDD1B, Thorlabs, USA), and the current can be continuously adjusted from zero to the maximum rated values of the LEDs at 700mA (2.85W for each LED).

The optical simulation of the 2x2 LED device, based on datasheet specifications and

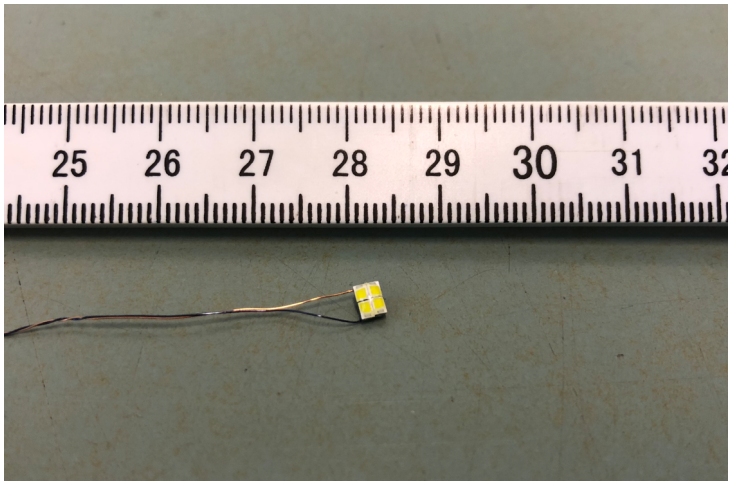

Figure 3.27: The fabricated integrated high-power LED device for transthoracic illumination of the rat heart

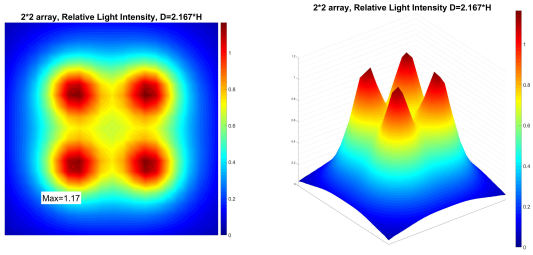

(a) 2D plot (b) 3D plot

Figure 3.28: Optical simulation of the transthoracic LED device

conducted through MATLAB 2019b numerical calculations, indicates a notable aspect of its performance. The maximum peak irradiance of this LED arrangement can reach approximately 1.17 times that of a single LED (Figure 3.28). This implies that the light emitted is not only intense but also narrowly focused and concentrated.

The maximum irradiance at the surface of the LED device is measured with the same setup as previous sections by optical sensors. However, the irradiance is larger than 500mW/mm2 and the maximum measurement range is reached. Such characteristic suggests that the light from this device has the potential to penetrate deeply into tissue and activate the genetically modified heart tissue by overreaching the irradiance threshold.

3.4.4. DEVICE VALIDATION: TRANSTHORACIC OPTOGENETIC AF TERMINATION EXPERIMENTS

The experiment to explore transthoracic optogenetic AF termination in rats is carried out to assess the potential of delivering therapy through chest illumination, without open chest operations. The test rats are treated the same way as described in previous sections of VF treatments, with a different gene delivery target of the atrium instead of the ventricle. The 2x2 LED device is placed on the shaved skin of the adult rat near the fourth intercostal space and delivers illumination to the heart through the thoracic, penetrating the thoracic wall and other tissues such as the lung (Figure 3.29).

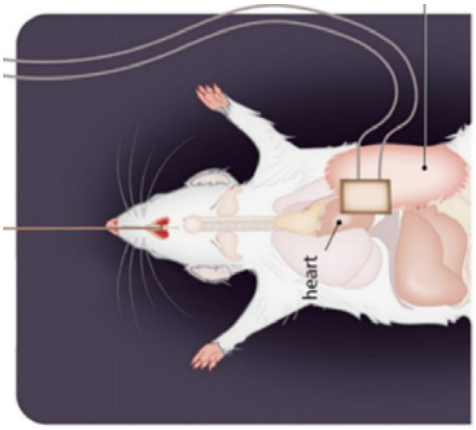

Figure 3.29: Illustration of placing the LED device on the chest of rat with transthoracic illumination to the heart atrium

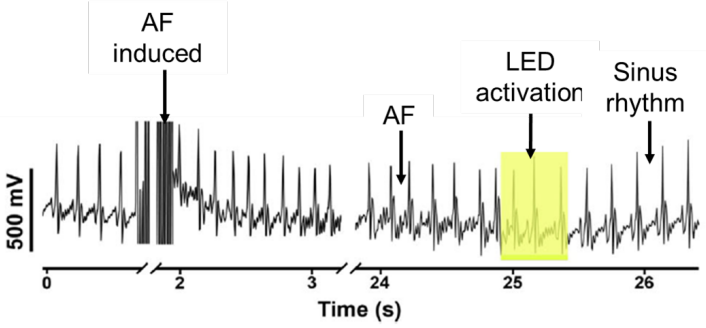

Figure 3.30: ECG recordings of terminating AF by transthoracic light stimulus

By controlling the LED device with 10ms light pulses with an irradiance of 25mW/mm^2, transthoracic optical atrium pacing of 10Hz is successfully tested in all test rats (n = 4),

demonstrating the capability of 565nm light to stimulate the ReaChR expressing heart through the chest wall.

This is followed by an experiment to test optogenetic AF termination with the same protocol. Sustained AFs are effectively terminated using 500ms light pulses at 500ms intervals, with an irradiance of 25 mW/mm^2, on ReaChR-expressing rat hearts (Figure 3.30). The success rate of optogenetic AF termination efficiency with ReaChR-expressing rats is as high as 95% (n=4), however, the termination efficacy in Citrine-expressing control rats was 0%(n=4).

In addition to demonstrating successful optogenetic trans-thoracic AF termination, the experiments also extensively tested the high-power LED devices in various aspects: functionality, optical performance, reliability, and compatibility. This comprehensive testing ensures the devices' efficacy and safety in real-world clinical applications. This holistic approach significantly enhances the clinical viability of cardiac optogenetics in ventricular arrhythmia treatment with LED technology.

3.5. CONCLUSIONS AND LIMITATIONS

This chapter introduces technical advancements in the field of cardiac electrophysiology with specific discussions on the development of an innovative LED device for the treatment of ventricular fibrillation. A novel treatment is proposed for this life-threatening arrhythmia with the help of the integration of optogenetics with high-power LED light source systems.

The research first includes a detailed design, testing, and refinement of a specialized, implantable LED apex-cup system designed for use in both in-vivo and ex-vivo experiments on rat VF models. Particular attention is paid to the system's effective biocompatibility and its unique optical characteristics. Exploration is carried out to determine optimal wavelengths for the LED illumination. Through comprehensive experiments and simulations, the research identified longer wavelengths (567 nm and 617 nm) as more effective for penetrating the ventricular myocardium, compared to shorter wavelengths, while still maintaining good response in optogenetics ion-channels. In both in-vivo and ex-vivo experiments, the custom-developed LED apex-cup devices demonstrated successful termination of optogenetic VF in rat hearts, which presents the potential the possibility of this advanced technology in the treatment of ventricular arrhythmias.

Secondly, the trans-thoracic experiments explore the clinical feasibility of optogenetic AF termination by investigating light penetration through the chest. This approach, building on previous implant-based, open-chest apex-cup successes, discovers safer, more accessible treatments for cardiac arrhythmias, broadening the applicability of op-

togenetic therapies in clinics. The potential benefits of this non-invasive technique include enhanced patient comfort, lowered safety risks, and expanded treatment options for those unable to undergo open chest surgery.

Apart from technical advancements, however, some limitations need to be addressed. A primary limitation is that the current research has only tested the implant-based apex-cup device and the transthoracic device under anesthetized rat models. In real-world clinical expectations, an ideal solution would be a fully implantable system that allows patients to live their normal lives without being aware of the device's presence or its activation during treatment.

Another critical limitation is the manual operation for both arrhythmia identification and the triggering of termination in current systems. In the clinical context, the system should ideally be equipped with an algorithm capable of autonomously detecting abnormal arrhythmia events and automatically initiating the appropriate optogenetics response with the implant illumination devices. This level of automation is important for ensuring timely and effective treatment, particularly in first-response emergency scenarios where manual intervention may not be immediately available for critical VF treatment.

Furthermore, practical considerations are presented in the power supply for the implantable system. The development of a wearable or minimally invasive power supply system, possibly using wireless power delivery, is essential for the system's practicality in future clinical applications. Such a power supply must be reliable, safe, and capable of sustaining the device's operational needs without frequent recharging or maintenance.

As future research suggestions, it will be important to focus on improvements in these aspects, aiming to develop an integrated system that combines arrhythmia detection algorithms with effective, automated treatment protocols. The system should be tested closer to real-world patient experiences with advanced power solutions to support the long-term, continuous operation of these devices.

BIBLIOGRAPHY

[1] John Y Lin et al. “ReaChR: a red-shifted variant of channelrhodopsin enables deep transcranial optogenetic excitation”. In: *Nature neuroscience* 16.10 (2013), pp. 1499–1508.

[2] Sara Gargiulo et al. “PET/CT imaging in mouse models of myocardial ischemia”. In: *BioMed Research International* 2012 (2012).

[3] Mohammed Mesradi et al. “Experimental and analytical comparative study of optical coefficient of fresh and frozen rat tissues”. In: *Journal of biomedical optics* 18.11 (2013), pp. 117010–117010.

[4] Emile CA Nyns et al. “Optical ventricular cardioversion by local optogenetic targeting and LED implantation in a cardiomyopathic rat model”. In: *Cardiovascular research* 118.10 (2022), pp. 2293–2303.

[5] Aleksi A Leino, Aki Pulkkinen, and Tanja Tarvainen. “ValoMC: a Monte Carlo software and MATLAB toolbox for simulating light transport in biological tissue”. In: *Osa Continuum* 2.3 (2019), pp. 957–972.

[6] Steven L Jacques. “Optical properties of biological tissues: a review”. In: *Physics in Medicine & Biology* 58.11 (2013), R37.

[7] Frank P Bolin et al. “Refractive index of some mammalian tissues using a fiber optic cladding method”. In: *Applied optics* 28.12 (1989), pp. 2297–2303.

[8] John F Van Vleet, Victor J Ferrans, and Eugene Herman. “Cardiovascular and skeletal muscle systems”. In: *Handbook of toxicologic pathology* (1991), pp. 539–624.

[9] Manuel Murbach et al. “Heating and safety concerns of the radio-frequency field in MRI”. In: *Current Radiology Reports* 3 (2015), pp. 1–9.

[10] Donald F Swinehart. “The beer-lambert law”. In: *Journal of chemical education* 39.7 (1962), p. 333.

[11] Wai-Fung Cheong, Scott A Prahl, and Ashley J Welch. “A review of the optical properties of biological tissues”. In: *IEEE journal of quantum electronics* 26.12 (1990), pp. 2166–2185.

[12] Johannes Swartling et al. “Changes in tissue optical properties due to radio-frequency ablation of myocardium”. In: *Medical and Biological Engineering and Computing* 41 (2003), pp. 403–409.

[13] Patrick M Boyle et al. “A comprehensive multiscale framework for simulating optogenetics in the heart”. In: *Nature communications* 4.1 (2013), p. 2370.

4

AN IMPLANTABLE LED ILLUMINATION SYSTEM FOR IN-VIVO AND EX-VIVO EXPERIMENTS OF SWINE ATRIAL FIBRILLATION TREATMENT

4.1. INTRODUCTION

As previously mentioned in the introduction chapter, Atrial fibrillation (AF) is a common type of heart arrhythmia, characterized by rapid and irregular movement of the atrium. AF results from abnormal electrical impulses in the heart, leading to an irregular and often rapid heart rate. Unlike ventricular fibrillation (VF), which is life-threatening and requires immediate medical attention, AF is often a chronic condition that can lead to long-term heart complications if not properly managed. Terminating AF as soon as possible is important for reducing the risk of heart stroke and improving overall heart health and quality of life. Terminating AF involves strategies aimed at restoring normal heart rhythm or controlling the heart rate. Treatment approaches vary depending on the duration and severity of the AF, as well as the patient's overall health. Consequently, finding new ways to terminate AF is a crucial aspect of cardiac electrophysiology research.

In this chapter, an innovative approach for AF termination using optogenetics is presented stressing the development of the high-power LED matrix illumination system following the V-model development methodology. This involves the designing, implementation, and verification of the specialized, implantable, high-power LED light system for use in both in-vivo and ex-vivo experiments based on the swine model. This device contributes to a novel intersection of optogenetics and cardiac electrophysiology and opens a new path for understanding and potentially controlling AF.

Similar to the previous chapter, this chapter consists of two main sections. The first part details the development, testing, and integration of the high-power LED matrix system. It covers the initial requirements analysis, focusing on bio-compatibility and the system's optical properties, and describes the fabrication process as follows. The second part presents the outcomes of in-vivo and ex-vivo experiments, evaluating the system's efficacy in cardiac electrophysiology research, particularly in terminating AF and its possible future applications.

The objective of this work is to introduce a hardware tool for cardiac electrophysiologists to be possible to comprehend AF and its treatment based on swine models. It promises the potential of optogenetics in future cardiac therapies for clinic implementations. This research represents a fusion of advanced electronic system integration technology and bio-medical science.

4.2. REQUIREMENTS ANALYSIS

The high-power LED light source system plays a vital role in the innovative optogenetic approach for potentially treating and terminating AF. The biomedical research and ex-

periments serve as the °Customer' for this LED system, setting its specifications and functionality, as the LED system must be specifically made to fulfill the unique requirements and goals of the biomedical experiments.

Swine models are selected for the work in this chapter. Swine have cardiovascular systems that are more similar to humans in terms of size, structure, and function compared to rats. This similarity makes them particularly valuable for cardiovascular studies[1]. The larger size of swine hearts allows for easier surgical manipulation and the application of medical procedures, technical requirements and the design of the light source device are more comparable to those expected to be used in human clinic implementations in the proposed future. Therefore, research findings from swine models are often more directly translatable to human conditions.

The design of the light source should provide the exact optical conditions needed for optogenetic techniques on swine models, including the precise wavelength for activating optogenetic channels, the intensity levels necessary for penetrating thick tissue, and the optical distribution required for targeted lighting. A lack of deep understanding of requirements could result in a system that is either ineffective or potentially harmful, blocking the success of the experiment and the ethical standards in biomedical research.

However, when initiating the work in this chapter, a unique challenge was found: there was no sufficient existing information on applying optogenetic AF termination methods to swine models, as this exact work was the pioneer in this area of research.

The approach is to adapt the successful techniques and mature methods that were previously validated on rat models multiple times and apply them to swine models. This adaptation involves collaboration with experts in swine models to make necessary adjustments. Consequently, there are no specific guidelines tailored for swine models; instead, requirements are made with hypotheses and assumptions.

- **Wavelength:** Capable of producing light at specific wavelengths, chosen based on good effectiveness in penetrating blood-perfused atrial myocardium as well as good ability to generate strong reaction by light-gated ion channel red-activatable channelrhodopsin ReaChR[2], same as used in rat models, in swine atrial cardiomyocytes. Also, the selected wavelength should be delivered by commercially available LEDs with reasonable economic resources. Three wavelengths are initially proposed: 470nm (Blue), 530um (Green), and 567nm (Lime). The wavelength of 617nm (Red-Orange) is not considered due to too low power output to penetrate larger scale of tissue in swine models.
- **Irradiance:** Capable of producing light with sufficient and uniform irradiance at the target surface, chosen based on good effectiveness in penetrating blood-perfused

atrial myocardium as well as good ability to generate strong reaction by light-sensitive ion channel ReaChR in cardiomyocytes. The myocardium wall of swine hearts is thicker than rat hearts, therefore the required irradiance is expected to be much higher. The proposal is to use exaggerated irradiance when designing the LED (>10mW/mm2) with the same LED chips and modify the LED driver to be able to dim the irradiance during experiments. The total electrical input energy of the panel is then estimated to reach 200W, which is a considerably high value due to its potential thermal effect.

- **Multiple light zones:** Capable to independently activate and deactivate different 'zones', allowing for selective illumination of various areas of the atrial wall. Each zone's irradiance operates independently and can be adjusted to create controlled lighting patterns. This feature significantly enhances the experiment's flexibility, enabling researchers to determine the most effective illumination locations for successful termination. 10 zones are proposed for the design.

- **Physical dimensions:** Compact and miniaturized, suitable for implantation in the swine model used in the study, both in-vivo and ex-vivo experiments. Designed for full irradiance coverage of the right atrial wall of the swine heart.

- **Physical compatibility:** Robust enough to withstand the physiological conditions during the experiment, including temperatures, moisture levels, possible chemical or biological reactions, and potential mechanical stress from the beating heart or movements. Also, easily removable and movable to swap between different devices or test subjects, or simply move to different locations of the atrium.

- **Bio-compatibility:** functions within a living system without inducing excess strain or tension that interferes with normal biological behaviors (e.g. normal heart beating), or creates measurement artifacts (e.g. leaking current or voltage). The device should have reasonable surgical accessibility and the potential for recovery post-implantation.

- **Consistency:** The device's design and functionality are integral to the success of the experiments. Constant light distribution and intensity with all high-power LEDs with the same specifications, while characteristics keep consistency over experimental reproductions over time.

These requirements are analyzed separately in the following sections, to provide a clear view of the system development procedure.

It is important to note that the approach for this research is largely based on a trial-and-error methodology. This means that the research proceeded by experimenting with various techniques, learning from each attempt, and iteratively refining the methods. Through this exploratory and adaptive approach, the most effective strategies are expected to be identified by gradually building upon each experience to optimize the methods and outcomes.

4.3. LED ARRAY SUBSYSTEM DESIGN AND IMPLEMENTATION

4.3.1. DEVICE PHYSICAL LAYOUT

The experimental proposal involves a surface light illumination at the right atrial wall of swine hearts. Evaluation of the swine's heart and atrial structure is then carried out. The heart of an average lab swine is similar in size to a human heart, with typical dimensions of about 15cm in length. The right atrial wall is visible from the outlook of the heart due to its trabeculated surface, close to a disk shape with a dimension of about 50mm and thickness of about 3mm (Figure 4.1). When placing the LED device, it's critical to

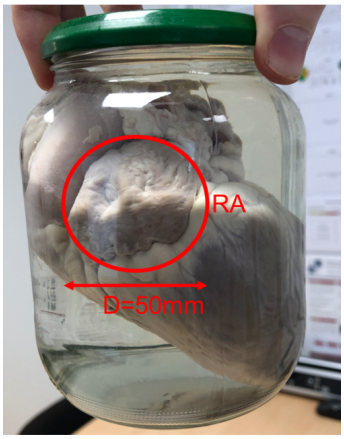

Figure 4.1: Photo of a swine heart sample with typical right atrial wall dimension of 50mm

consider the complex anatomy of the swine heart. This includes the positions of major blood vessels, the thickness of the ventricular walls, and the overall shape and dynamics of the heart throughout the cardiac cycle. During in-vivo experiments when the heart is operating normally, the right atrial wall is partially enveloped by lung tissue, which exerts pressure on it through movement. The gap between the right atrial wall and the adjacent lung tissue is quite small, typically less than 5mm. Thus, the LED device must be suitably

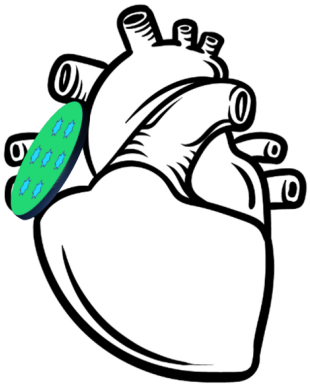

Figure 4.2: Proposed 'disk shape' high-power LED device for right atrial wall in swine models.

miniaturized to fit appropriately into this gap space without causing significant physical interference or harm. The device needs to be designed in a 'disk shape' (Figure 4.2) with a diameter similar to the right atrial wall dimension, and with a thickness of less than 5mm to to the gap.

4.3.2. LED LAYOUT OF THE DEVICE

To deliver the requested high irradiance and uniform illumination on the targeted atrial wall surface, the total amount of LED chips is estimated to be increased to 100 pieces and spread out evenly on the panel. Five LED device physical layouts are proposed (Figure 4.3):

- 'Checkerboard' panel
- 'Clock zones' panel
- Projecting optical mirror or lens
- Diffusion panel with side LEDs
- Discrete LED matrix directly bonds to tissue

The proposals are evaluated by a requirement matrix of Overall fitting for in-vivo or ex-vivo experiments test, Irradiance, Illumination homogeneity, Zone control, Impact on Heart Function, and Manufacturing and Implementation Complexity and Flexibility (Table 4.1).

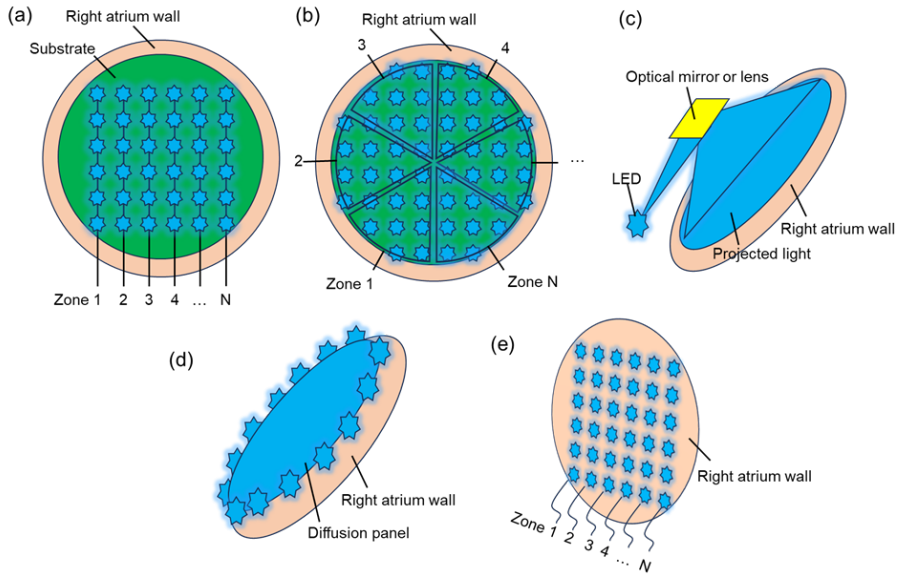

Figure 4.3: Five proposals of layout, blue stars are LED chips: (a) 'Checkerboard' panel (b) 'Clock zones' panel (c) Projecting optical mirror or lens and (d) Discrete LED matrix directly bond to tissue

'Checkerboard' panel

In this proposed design, a panel-shaped device is composed of an array of LEDs arranged on a substrate that follows a structured matrix layout of rows and columns (like a Checkerboard). This substrate serves as the intermediate support for the LED chips, providing a stable (solid or flexible) platform while also accommodating the necessary electrical interconnections between individual LEDs.

The panel is then precisely positioned over the target right atrial wall area, with the intent that the light from the LEDs uniformly illuminates this space by the matrix layout of the point sources. To achieve optimal light delivery and uniformity, the substrate is designed to match the dimensions of the target area exactly (diameter = 50mm). This correspondence distance between the substrate and the target ensures that the illumination from the LEDs is well-distributed over the entire area of interest. All LED chips are facing directly to the target area to maximize the efficiency of the light delivery and the substrate can be coated or painted with a reflective surface to minimize any loss of light beyond the intended target.

However, this focused illumination could also lead to a concentration of heat and cause thermal damage to the LED chips, encapsulation materials, wiring, or targeting

Table 4.1: Trade table for proposed layouts of the device

	'Checkerboard' panel	**'Clock zones' panel**	**Projecting optical mirror or lens**	**Diffusion panel with side LEDs**	**Discrete LED matrix directly bond to tissue**
Overall fitting for in-vivo test	++	++	-	++	++
Overall fitting for ex-vivo test	++	++	++	++	++
Irradiance (power)	++	++	-	-	++
Illumination homogeneity	+	+	++	++	+
Zone control	-	+	-	-	+
Impact on Heart Function	+	+	++	+	-
Manufacturing or Implementation Complexity and Flexibility	++	++	-	+	-

tissues. This can be roughly estimated via thermal simulations.

Local zone controls are achieved by each LED being part of a series of connected groups, where they are either organized in rows or columns, allowing for systematic activation and control of the light emitted across the panel.

The panel-shaped, or disk-shaped geometry of the proposed device allows a tight fit to the thin gap between the right atrial wall and the lung. If designed with smoothness and flexibility, and placed according to the biological movement direction, the panel device might move or slide naturally with the heart, reducing the risk of interference with normal cardiac function.

The manufacturing of the panel device is rather simple while the substrate part of the panel can be made from planar technologies such as printed circuit board (PCB) and cut out the shape via machining. LED chips are then placed and bonded by either manual or automatic placing and soldering, and later protected by encapsulation or isolation materials. These techniques can be found commonly in electronics with water or weatherproof applications, or commercial implantation medical devices. The device can be re-used without directly gluing to the test subject, as fixation structures such as holes or hooks can be designed on the substrate to be fixed to the heart tissue by threads.

'Clock zones' panel

This proposal shares most of the design with the 'Checkerboard' panel layout, with the difference in the zone area layout. As the Checkerboard layout has independently controlled rows or columns of LEDs, the 'Clock zones' panel controls a group or groups of LEDs at a corner of the panel. This gives a better zone controlling for the AF treatment experiments as the illuminated location on the atrial wall is precise and more localized to a concentrated area or considered as 'points'. The challenge remains at the interconnects and wiring between the LEDs within each group as the delivered power (therefore current) is relatively high and space is limited. This can be evaluated by designing electric rules and computer-aided wiring programs.

Projecting optical mirror or lens

The proposal requests a standalone light source by single or multiple LED chips to emit high-power illumination, and an optical system with mirror(s) or lens to redirect and diffuse the light to the targeted atrial wall surface. These method is similar to some setups with dichroic mirrors[3][4] or with focusing objectives[5][6].

The light source part of the system does not need to fit snugly against the heart's shape, as it can be either placed next to the atrial wall or at other locations, even outside the chest, and the light should be guided into the target area through optical elements. However, the optical guiding part of the system should fit within the limited space between the atrial wall and the lung where minimal intrusion is requested. The possible simplest optical solutions, such as single-lens systems or single-concave-mirror systems, request bulkiness in space that is almost impossible for the physical requirement of dimensions. Additionally, maintaining consistent placement of this non-fixed device can be problematic during tests, where these optical systems need to adjust their focus to maintain stable and consistent illumination. Zone control can be achieved by either mechanically moving the optical elements, or selectively switching the pattern of the input light source if a waveguide is used, but a very precise and challenging optical system design is needed. The distribution of light from the lens or mirrors can be designed as homogeneous at the targeted distance, should the focus of the systems be well adjusted. The light covering the atrial wall is uniform without illumination hot spots, or thermal hot spots thanks to the detachment of the hot high-power light sources.

The projecting lens or mirrors can be designed in such a way that it has a flat and smooth interface to the target and does not disrupt the heart's natural movements. To minimize any potential interference, a lubricating coating or fluid may be applied to the interface should contact occur.

The manufacturing and implementation of this proposal can be very challenging.

Designing an optical system to transmit light at the required power levels (200W) is challenging, particularly when it involves channeling high-energy density from an external source to an internal panel. Common light guide solutions such as waveguides or optical cables cannot hold this power density within the limited dimension. This proposal is designed to be reusable across multiple experiments, with the interchange of test subjects, provided its structural integrity is maintained.

Diffusion panel with side LEDs

In this proposed design, LEDs are positioned along the sides of a diffuser panel. This panel is capable of redirecting the light emitted from the LEDs, guiding it from the sides to the front surface. Additionally, the diffuser panel serves to evenly distribute, or diffuse, the light, creating a uniform illumination across the targeted area. A similar design is proven to be effective in optogenetics AF termination on rat models[7].

This configuration allows for a compact and slim form factor, making the panel device smaller and thinner, to be able to fit the space-constrained area between the right atrial wall and the lung. Such a structure is commonly utilized in the manufacturing of thin computer monitors.

Due to the LEDs being placed only at the edges of the diffuse panel, the total amount of LEDs, therefore total light power output, is limited. Moreover, this design makes it difficult to support local zone control. Since the LEDs are positioned at the edges, it is not feasible to control or adjust the illumination in specific areas or zones of the panel independently because the light will be diffused and redirected to cover the full panel (as the diffuser is designed to do). This contrasts with direct-lit LED arrangements proposed in previous designs, where individual LEDs or groups of LEDs can be controlled separately. This proposal is designed to be reusable across multiple experiments, with the interchange of test subjects,

Discrete LED matrix directly bonds to tissue

Individual LEDs directly bonded to the right atrial wall surface offer the highest degree of flexibility in terms of placement and can be arranged in a pattern that best fits the target surface, no matter for in-vivo or ex-vivo tests. The minimal dimension, only the LED chips and wiring, avoids interference with other organs (lungs) or tissues. Similar approaches have been tested on rat hearts[8][9].

The discrete LEDs provide focused irradiance however ensuring uniform illumination might be more challenging, where additional diffusing solution is needed. It also has thermal concentration risks.

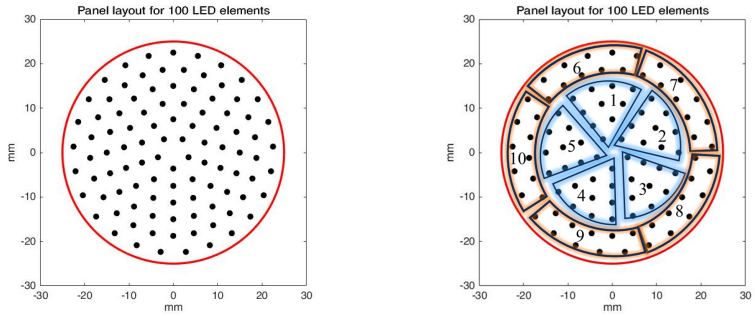

(a) LED layout with 100 LED elements (b) 10 illumination zones

Figure 4.4: The LED layout of the LED panel device. Black points indicate the location of LED elements. The red circle indicates the 50mm diameter panel edge

Zone controlling can be achieved by similar methods as the previous two-panel proposals with additional control and driving electronics. Discrete LED chips should be only constrained by their connecting (flexible) wires, should move naturally with the heart moving, and are likely to have the least impact on normal cardiac function.

The manufacturing and implementation are however challenging for discrete LED design where each LED chip is expected to be manually and precisely bonded to the tissue surface at desired locations. This should be difficult in practice for in-vivo experiments where the operational windows, both experimental time and workspace, are very limited. The device cannot be re-used due to being directly glued to the test subject.

In summary, each of the five proposed designs presents its unique set of strengths and weaknesses. Deciding which one to use will hinge on how they align with the specific demands of the experiments, balancing various factors. For this project, we have chosen the 'Clock zones' panel design due to its good manufacturability using commercially available processes, slim and tight geometry to fit the area, and promised high light output.

The LED panel layout (Figure 4.4a) in the final design setup consists of 100 LED chips mounted on a circular substrate with a diameter of 50mm. These LEDs are arranged with an equal spacing of 4 mm between them to ensure uniform light distribution, which is simulated and discussed in the following section.

The LEDs are organized into 10 distinct zone groups, with each group containing 10 LEDs (Figure 4.4b). Each LED group is connected in a series configuration, with routings predetermined to ensure optimal electrical flow and organization. These groups are

further categorized into two types: inside zones and outside zones. Five of these zone groups are positioned in the inner ring of the circular substrate. Each group in the inner ring is placed at intervals of 60 degrees. This precise arrangement allows for an even spread of the LEDs in the inner zone. Similarly, the remaining five groups are located in the outer ring of the substrate. These groups are also spaced out every 60 degrees, mirroring the layout of the inner zone. Each group covers approximately 1/10th of this target area. This design allows for versatile and precise lighting control, which meets the requirement of specific patterns or intensities of light over a defined atrial wall area.

Each of these ten groups can be controlled independently, allowing for on-and-off switching of the LEDs within each group. This level of control enables the user to selectively illuminate specific portions of the target area. The wiring and controlling of the zones are discussed in the following sections.

4.3.3. OPTICAL MODELLING

As the LED matrix layout on the panel device is determined, optical simulations follow to estimate the optical characteristics of the design. The optical simulation of the 100 LED panel device, based on datasheet specifications and conducted through MATLAB 2019b numerical calculations. The simulation is carried out with arbitrary units, focusing on understanding how uniformly the light from the LEDs would cover the targeted area.

The layout used in the simulation transferred the layout design previously determined for the actual LED panel. Each LED in the simulation is predefined with a viewing angle of 125 degrees, as specified in the LED's datasheet. To accurately model the light emission characteristics of the LEDs, the illumination profile for each LED is fitted using a cosine curve by the fitting box of Matlab from the LED datasheet. The profile represents the variation in light intensity as a function of the angle from the LED's central illumination axis.

Each LED is assigned an arbitrary peak irradiance value of 1 unit. This value represents the maximum light intensity emitted by an LED along its central illumination axis, also represented as the pea value of the cosine profiles. Normalizing is used to simplify the modeling and calculation as the simulation focuses on the relative distribution and uniformity of light at the panel, rather than the absolute light irradiance. The actual irradiance is expected to largely exceed the required value and will be characterized in later sections in the integration phase.

The results of the optical simulation show insights into the light distribution characteristics of the LED panel device. A high-intensity plateau over the targeted area matching the 50mm diameter of the LED panel is observed from the simulation. This plateau

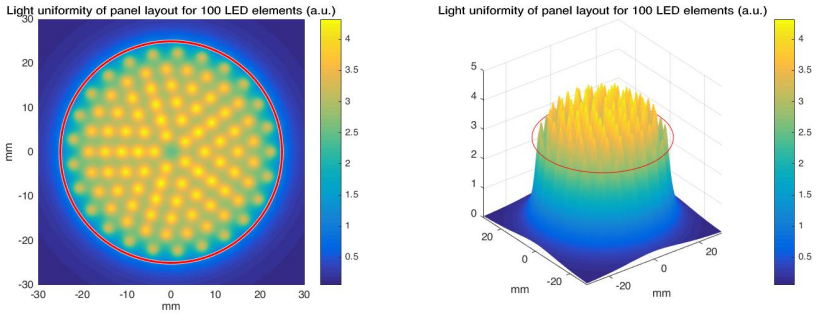

(a) 2d plot (b) 3d plot

Figure 4.5: Simulated illumination pattern of the LED panel device at the target surface. The red circle indicates the 50mm diameter target area

suggests a relatively uniform illumination pattern, which is critical for effectively activating ion channels in optogenetic experiments with irradiance above the threshold value. Very sharp edges around the high-intensity plateau with intensity dropping rapidly outside the panel area are also observed. This sharp edge between illuminated and non-illuminated areas indicates that the LED panel is efficient in focusing its light energy precisely on the target area. In the context of the swine model experiments, this means that the illumination is concentrated on the atrial wall.

Light 'hot spots' are observed in the illumination pattern. These 'hot spots' are identified directly above each LED element in the simulation. The peak intensity values of each hot spot, represented in the simulation figure as yellow areas, which have approximately twice as intensity as the plateau values, represented in the simulation figure as green areas. The diameter of these 'hot spots' is measured around 2mm. The presence of these 'hot spots' and their specific dimensions indicates the limitation of uniform distribution of light intensity across the target area.

The overall irradiance of the LED panel can be simply estimated by the total radiant power of all 100 LED elements divided by the area of the 50-diameter panel. When the 470nm LED is driven at its maximum allowed current of 1000mA, the maximum average irradiance of the LED panel is:

$$I_{max} = \frac{676mW \times 100}{\pi \times (25mm)^2} = 34.4mW/mm^2 \tag{4.1}$$

The maximum average irradiance for a 567nm LED panel at a maximum current of 700mA is:

$$I_{max} = \frac{435mW \times 100}{\pi \times (25mm)^2} = 22.2mW/mm^2 \tag{4.2}$$

The irradiance produced by the panel is significantly higher than the required threshold to activate the ion channels in the atrial wall cells, meaning that even the lower-intensity areas such as the plateau surrounding the 'hot spots' are adequate for effective stimulation. Additionally, the light from the panel will have diffusion and scattering as it passes through the encapsulation material and the myocardium tissue of the atrial wall. This process is expected to further spread out the light distribution, reducing the impact of 'hot spots' and leading to a more uniform illumination pattern on the target tissue. Consequently, the overall effectiveness of the LED panel is likely to not be affected by these 'hot spots'.

4.3.4. LED PANEL FABRICATION, INTEGRATION AND ASSEMBLY

Layout design (Figure 4.6) is based on previously discussed coordinates of LEDs and implemented to the PCB design on computer-assisted software. Then the design files are sent to the manufacturer and suppliers for fabrication, following the fabricating classifications of the manufacturer which represent the capabilities and limitations.

The device used in this work is outsourced to a supplier (EuroCircuits, Belgium) with their Standard PCB Pool classification. Main fabrication specifications include:

- Dielectric core material: 1.8mm High Tg FR-4 board
- Copper layer: 2 layers (top and bottom only) with 2oz (70um) thickness
- Minimum trace width: 8 mil (0.2 mm)
- Minimum trace clearance: 8 mil (0.2 mm)
- Minimum clearances between features: 8 mil (0.2 mm)
- Minimum via hole size: 2 mils (0.5 mm)
- Silkscreen color: Green

Other specifications are considered not important in the design of this work and thus not listed. The panel is composed of a high Tg FR-4 board. The glass transition temperature (Tg) is the temperature at which the material transitions from a glassy, rigid state to a more pliable, rubbery state. Standard FR-4 materials usually have a Tg of around 130°C, but high Tg FR-4 materials have a Tg typically around 170°C - 180°C, or

even higher. It offers better stability at high temperatures. This is critical for applications that experience high operating temperatures or heat cycling, as it reduces the risk of PCB deformation or failure. Each LED group is connected in a series configuration, with

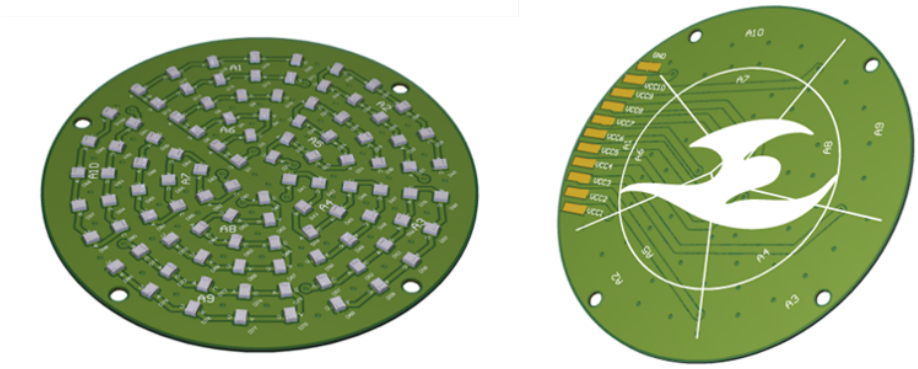

Figure 4.6: Front and back of the PCB design illustration for the LED panel device

routings predetermined to ensure optimal electrical flow and organization. The width of the routings is determined based on the maximum current load (2A), the thickness of the copper (2oz), and the allowable temperature rise (10°C). Based on the supplier's calculation tool[10] the minimum trace width of the LED wiring on the PCB is 40mil (1.0mm) per layer. This value is then adopted in the panel design. The wire layout for the device is configured by computer assistance using the design software by its automatic routing feature.

For each LED chip, interconnects of the cathode and anode are placed with the provided coordinates defined by the previous section. The footprint is converted from the chip manufacturer's recommended design. A group of 11 large connection pads are placed next to each other at the bottom side of the PCB design as the interface for the wiring to the control subsystem of the system. The control subsystem design is discussed separately in the following sections. All exposed interconnect pads are finished with flash gold treatment for better electrical connections. The remaining area without interconnect pads is finished with a green solder mask, to reflect the green/lime light from the LEDs. White silkscreen text is placed at the top side of the panel indicating the numbers of the components for easy diagnostics. A university's flame logo is placed on the back side of the panel.

All LED groups share the same ground electrically to simplify the wiring by reducing the total number of wires and routes needed, thereby minimizing potential clutter and complexity in the circuit design. The remaining areas without interconnects or routes

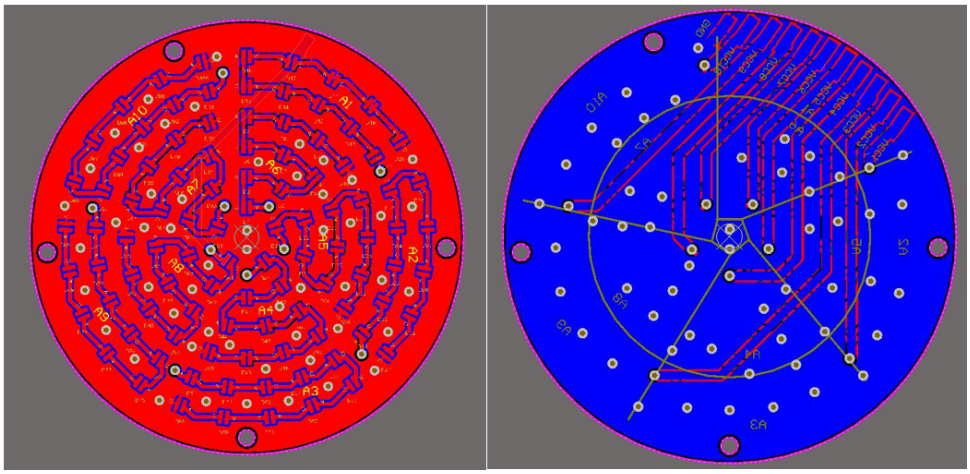

Figure 4.7: Front (red) and back (blue) wire routing and interconnects of the PCB design for the LED panel device

of the PCB design are finally plated with grounding copper structures on both sides, enhancing the electrical interference stability of the device (Figure 4.7).

Four through holes with a diameter of 2mm are placed near the edge of the LED panel providing the possibility of mechanically fixature of the panel. These holes can be used as connection points for surgical threads to fix the panel to the atrial wall during the in-vivo experiments. The fixation holes and the geometry of the substrate are mechanically cut with high-accuracy milling.

After the PCB is fabricated, LED chips are assembled using surface-mount technology (SMT). Lead-free solder paste (SAC305) is applied to the board where components will be placed. This is typically done using a stencil that ensures paste is applied only to the intended interconnect pads. LED chips are placed on the PCB by automated pick-and-place machines that accurately place the chips on their designated pads with programmed coordinates. The PCB with all LEDs placed is then passed through a reflow oven. The solder paste melts (reflows), solidifying to form solder joints that electrically connect the LED chips to the board. The assembled PCB with LEDs is inspected for any soldering defects, misplaced components, or other issues. This can be done through manual checks, Automated Optical Inspection (AOI), or X-ray inspection by the manufacturer. Two types of panels are made respectively with two types of LED chips: LXZ1-PB01 (blue 470nm), and LXZ1-px01 (lime 567nm).

The large connection pads at the bottom side of the PCB are then connected to ten enameled copper wires, each with a diameter of 150µm. The wiring is designed to allow

independent control of each of the ten groups (channels) of LEDs. These wires are chosen for their exceptional softness and flexibility, which helps prevent any additional strain on the heart movements. Also, the enamel layer of the wires protects the electrical power against bio-chemical reactions during the experiments and prevents short circuits even with tight and twisted cabling. The enameled copper wires extend to a length of approximately 30cm to facilitate ease of handling during in-vivo open-chest operations.

4.3.5. BIO-COMPATIBLE ENCAPSULATION PROCESS

The assembled LED panel device is not yet ready for in-vivo or ex-vivo experiments with swine models. The device must be processed bio-compatible, as the standard materials used in the PCBs do not meet this requirement, and they can potentially leak chemicals or degrade in a way that could be harmful to tissues. For applications involving any kind of implantation or direct contact with biological tissues, alternative materials that have been certified as bio-compatible must be used, or the whole device must be adequately encapsulated with a bio-compatible material. These bio-compatible materials or coatings are designed to be inert and stable within the body and include options like medical-grade silicone, perylene, or specific polymers that have passed bio-compatibility tests according to standards such as ISO 10993 or USP Class VI. In the context of the LED panel device in this work, the encapsulation materials should meet the requirements:

- **Optical Transparent:** The encapsulating material must be transparent to allow required wavelength light to pass through without significant attenuation or scattering.
- **Electrical Insulation:** The encapsulation must provide an effective electrical barrier to protect the tissue from any potential electrical hazards and to prevent measurement artifacts, short circuits, or corrosion on the PCB. The electrical isolation should not only be applied at the top (front) side of the panel, but it should wrap the whole device including the bottom (back) side, sides, and extension of the connecting wires.
- **Thermal Barrier:** The material should also act as a thermal barrier, preventing heat generated by the LEDs from causing thermal damage to biological tissues.
- **Bio-compatibility:** Above all, the encapsulating material must be bio-compatible. This means it should not elicit an adverse biological response and should be non-toxic, non-carcinogenic, and not cause an immune reaction. It should also be stable and not degrade or leak harmful substances into the tissue over time.

The encapsulation process is a critical step in the preparation of electronic medical devices for implantation, ensuring that they can safely interact with biological systems for the required duration of their use.

Polydimethylsiloxane (PDMS) (SYLGARD 184, Dow Chemical Company, USA) is used in this work as the encapsulation of the device. PDMS is commonly known as a kind of silicone rubber and is a versatile silicon-based organic polymer that is widely used in various applications. PDMS is well-tolerated by the human body and does not produce a significant immune response, which makes it suitable for use in long-term implants, medical tubing, and other devices that come into contact with bodily tissues and fluids. PDMS is used in similar illumination systems as encapsulation material[7][9][11][12].

PDMS is optically relatively transparent to visible wavelength with an almost transmission ratio of 70% to 80% for wavelength 400 to 600nm. PDMS is naturally hydrophobic, chemically inert, and thermally stable with melting point Tm higher than 200°C. It has a very low thermal conductivity of 0.15W/mK^{-1}, which makes it a great and stable thermal barrier layer. PDMS has electrically high resistance with a high resistivity of 1E14 ohm-cm and high impedance with a very low dielectric constant of 2.7 in the range of 0.1 to 10 kHz. This makes it also a good layer of electrical isolation for the device[13].

PDMS can be synthesized by polyaddition curing with simple processes and equipment. It starts with a mix of elastomer and curing agents with a predefined ratio based on the manufacturer's instructions. Then the mixture is poured or injected into the mold which keeps the polymer geometry of the final product. After mixing, the PDMS mixture often contains air bubbles. To remove these, the mixture is degassed under vacuum. This step is crucial to ensure a homogeneous and clear final product. It is then cured, which can be done at room temperature or accelerated with heat (e.g., 60-150°C) to accelerate the curing speed. Sometimes a post-curing step is applied, where the cured PDMS is heated to a higher temperature for an extended period. This step can improve the material's mechanical properties and stability, and remove any remaining unreacted components.

Figure 4.8 shows the encapsulation process: (1) Mold preparation, (2) Mixing and de-gassing, (3) Placement of the PCB panel and further de-gassing, and (4) Curing and mold release The encapsulation process using PDMS for the LED panel device is carried out through several steps to ensure consistent and quality outcomes:

1. Preparation of the Mold-Release Layer:

   The process begins with the spray coating of a thin layer of Polymethyl Methacrylate (PMMA)(Plastik 70, Kontakt Chemie, the Netherlands) onto the glass disk as a mold. This coating serves as a hydrophobic mold-release layer, which ensures that

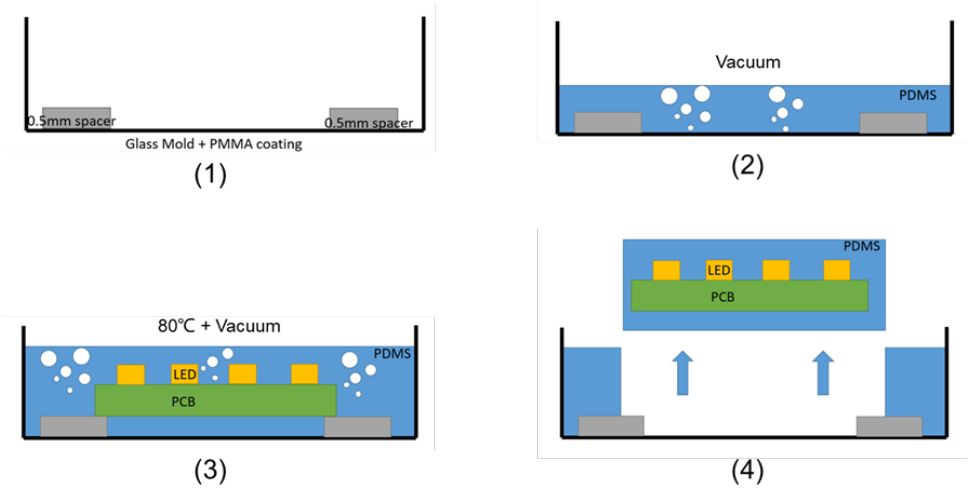

Figure 4.8: Illustration of the LED panel encapsulation process

the PDMS can be easily separated from the mold once cured. Spacers with 0.5mm thickness are set up to define the thickness of the PDMS layer, ensuring uniformity across the entire panel.

2. Mixing and De-gassing of PDMS:

   PDMS elastomer and curing agent liquid are then mixed 10 to 1, the recommended ratio by the supplier to ensure the best curing quality. The amount of the polymer is accurately weighted and calculated by the volume needed to achieve the desired thickness of 2.2mm at the front side of the product. The determination of the PDMS front side thickness is based on thermal simulation and is discussed in the following section. The viscous mixture is carefully poured over the prepared mold. This liquid covers the mold uniformly due to the hydrophobic layer of PMMA.

   The mold is then placed in a vacuum oven for 10 minutes without heating to degas the PDMS to remove any air bubbles.

3. Placement of the PCB Panel and Further De-gassing:

   Once the initial de-gassing is complete, the LED PCB panel is placed onto the liquid PDMS layer. The panel slides into the polymer mixture sideways and gently to avoid introducing air bubbles.

   The entire assembly is then subjected to a second vacuum de-gassing for 15 minutes without heating. This further ensures that any air trapped during the place-

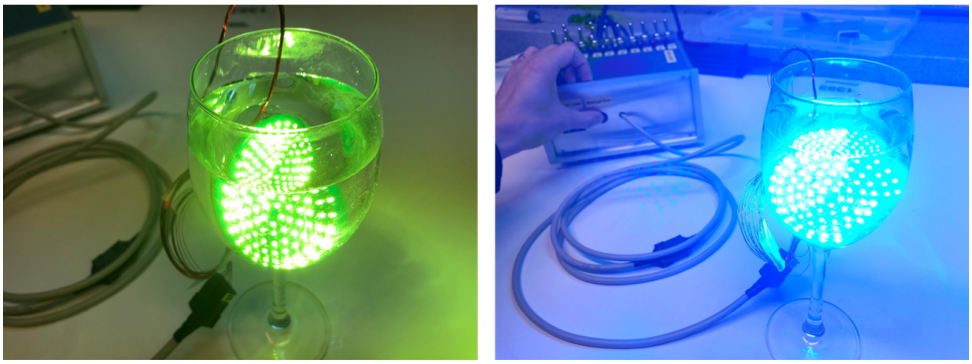

Figure 4.9: Encapusulation tests with saline solution

ment of the PCB panel is removed, preventing defects in the final encapsulated product.

4. Curing and Mold Release:

   After de-gassing, the PDMS starts to cure. The oven is set to 80°C for 1 hour with the vacuum remaining in the chamber. The temperature drops naturally and the assembly is left to cool down to room temperature after the oven set time in about 2 hours with the vacuum disconnected.

   Excess PDMS at the edge of the LED panel device is cut out with 2 mm clearance to the PCB by a sharp razor. The device is then carefully released from the mold with the help of the hydrophobic layer as a release agent.

The LED panels after the encapsulation process are tested by operating at full power while immersed in saline solution (0.9% NaCl) for 1 minute (Figure 4.9. The duration of the test is short due to the extremely high power (300W) of total energy of the device will heat the water quickly even to boiling, which might damage the device. The panels are then disconnected and placed in the same saline solution overnight (> 12 hours) and remain fully functional.

This encapsulation process not only secures the LED PCB panel within a bio-compatible package but also maintains the necessary optical properties for the LEDs to function effectively. The hydrophobic mold-release layer and the meticulous de-gassing ensure a high-quality encapsulation free from defects such as air bubbles or tear-offs.

4.3.6. THERMAL MODELLING

Finite Element Method (FEM) is used to simulate and estimate the thermal characters of the LED panel device during the in-vivo and ex-vivo experiments. In this case, thermal interactions among LED chips, PCB substrate, encapsulation polymers, and atrial wall tissue are predicted, leading to more precise estimation and safer designs.

Simulation Environment

COMSOL Multiphysics 4.1 (COMSOL, Inc.) is the preferred choice for this simulation due to its advanced capabilities in handling multi-physics problems. Its user-friendly interface allows for easy modeling of complex systems, integrating various physical phenomena including thermal interactions. COMSOL's extensive library of material properties enhances the efficiency of simulations. Additionally, it offers simplicity and flexibility in customizing models and is well-suited for simulating the dynamic interactions in biomedical devices, making it an ideal tool for detailed and reliable analysis for this work.

Model

A 2-dimensional model is created for computational simplicity instead of a 3-dimensional model (Figure 4.10), yet still be able to accurately represent the real world. The model is designed based on a focused area of the proposed positions of the LED panel device on the swine's right atrial wall. This approach ensures that the simulation closely replicates the actual experimental conditions, allowing for more accurate and relevant results.

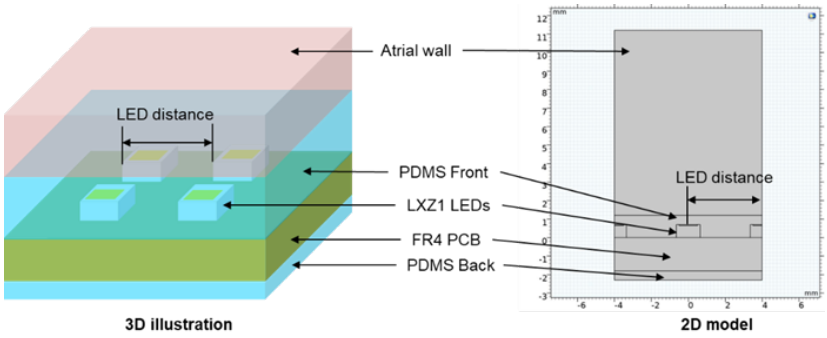

Figure 4.10: Adapting real-life parameters into a 2D model for simulation

The simulation model is created to represent a 2D cross-section of the interface where the LED device contacts the right atrial wall, covering an area of 8mm width by 13mm length. This focused area is constructed to accurately depict the layered cross-sectional

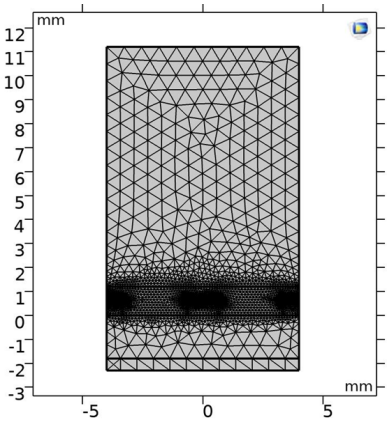

Figure 4.11: Simulation model meshing with 9254 triangle domain elements

structure in the actual setup, which includes from top to bottom: atrial wall tissue, the front encapsulating polymer layer, the individual LED chips, the LED panel's PCB, and the back side of the encapsulating polymer layer (Figure 4.10). The dimension of each component in the model is listed in Table 4.2.

A considerable thickness (10mm) of the atrial wall is also modeled to ensure a realistic representation of the biological interface. The thickness values (1.2, 1.7, and 2.2mm) of the top layer of encapsulating PDMS polymer are respectively simulated to evaluate the thermal barrier performance of different thickness profiles.

To reduce the computational complexity of the thermal simulation, a symmetrical design approach is adopted. This method assumes that the behavior of the components within the model will be repetitive across the periodic structure of the LED matrix. Hence, only two LEDs (1 full LED and 2 half LEDs) are modeled, working under the premise that these will provide a reliable approximation of the performance of the entire array. The distance (4mm) between each LED is the same as the device design.

Material properties Model meshing in FEM is a process where the geometric space of the model is divided into discrete (triangular) elements (Figure 4.11). The quality of the mesh directly affects the accuracy, convergence, and computational efficiency of the simulation. An adaptive finer mesh near the region of interest, the interface between the LED chip and the atrial wall surface, can capture more details in areas with high-temperature gradients being analyzed. However, a finer meshing requires more computational resources. Therefore, a coarser mesh is used in other areas far away from the region of interest. The model meshing consists of 9254 triangle domain elements in

total.

Table 4.2: The material properties used in the simulation

Domain from top to bottom	Dimension [mm]	Material	Thermal conductivity, k [W/(m·K)]	Heat capacity, Cp [J/(kg·K)]	Density, ρ [kg/m3]	Reference
Atrial wall	Thickness: 10.0	Human atrial wall tissue	0.56	3689	1041	[14]
Encapsulation layers, front	Thickness: 1.2 / 1.7 / 2.2	PDMS	0.2	367.2	970	COMSOL built-in
LED package	Thickness x width: 0.7 x 1.7	Al2O3 ceramic	35	730	3965	COMSOL built-in
LED chip	Thickness x width: 1.0 x 0.05	GaN	130	490	6070	COMSOL built-in
LED panel PCB	Thickness: 1.8	FR-4	0.3	600	1369	COMSOL built-in
Encapsulation layers, back	Thickness: 0.5	PDMS	0.2	367.2	970	COMSOL built-in

The accuracy of the FEM simulation relies greatly on the material properties in the model, which determines how various components in the model respond to physics inputs. In the context of these thermal simulations, critical properties such as thermal conductivity, heat capacity, and density play major roles. These characteristics are fed into the FEM solver, enabling it to precisely compute how temperature varies and evolves within and between the materials under defined conditions. Material properties are typically obtained from experimental data from external references and/or integrated material databases. Table 4.2 lists the simulated dimensions and important material properties used in the simulation.

Boundary conditions

Boundary conditions that define the initial state and how the model interacts with each other. Setting correct boundary conditions is vital for simulating accurately, ensuring that the computational results are meaningful and can predict physical behavior only under various conditions.

In this simulation, the only input source is the LED chips, which are specified with a power output (3.35 / 2 / 1.58 / 0.56 W, each representing power of blue LED driving at 1000mA / lime LED at 700mA / blue LED at 500mA / blue LED at 200mA). The LEDs are driven by three 500ms light pulses with 1000ms intervals in between (Figure 4.12), the same as the pulses used in the in-vivo experiments for AF termination. The assumption is that all electricity input to the LED is eventually transferred to thermal energy since no light escapes from the other side of the atrial wall. The physical model includes only

heat transfer without considering material expansion to further reduce computation complexity.

The initial temperature of the system is set at 37°C to mimic physiological conditions. The top edge of the atrial wall is defined as an ideal heat sink with a constant temperature of 37°C and an infinite heat transfer coefficient (k). The bottom edge of the encapsulating PDMS bottom layer is considered to contact air during the experiments, therefore the interface is defined as isothermal since the heat transfer to air from PDMS is minimal. All physics properties and behavior of the two side edges are defined as symmetric to represent the periodic structure of the LED matrix. The study is time-dependent with fine temporal resolution, using a step size of 0.01 seconds.

Simulation result and analysis

The simulation results show a dynamic thermal profile of the LED device and the interfacing biological tissue. The results are presented and discussed from the following simulation aspects.

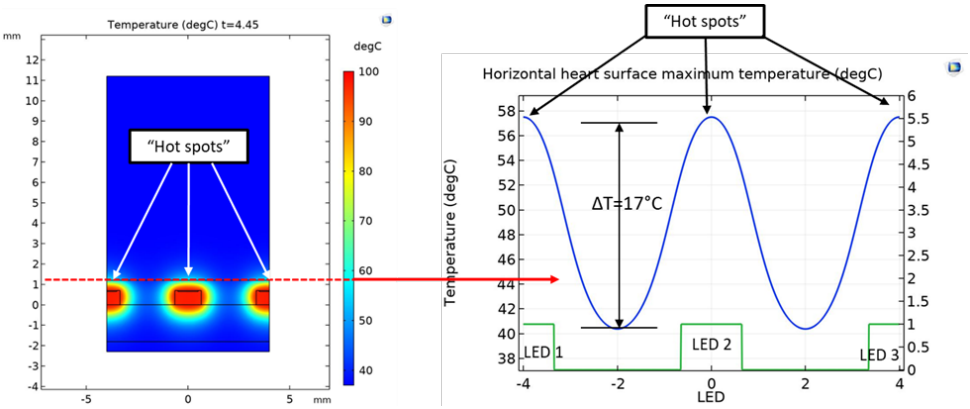

Figure 4.12: Temperature distribution at the interface of the device and atrial wall at the time point T=4.45 seconds (when the maximum temperature at the tissue interface is reached)

1. Temperature distribution and hot spots

   The analysis first focuses on the temperature distribution within the simulated structure. When the LED is in active pulse, both the LED chip and its ceramic packaging reach very high temperatures. This heat is then conducted to the surrounding materials and ultimately to the tissue through the PDMS polymer layer. 'Hot spots' near the LED chips are clearly shown (Figure 4.12), where temperatures

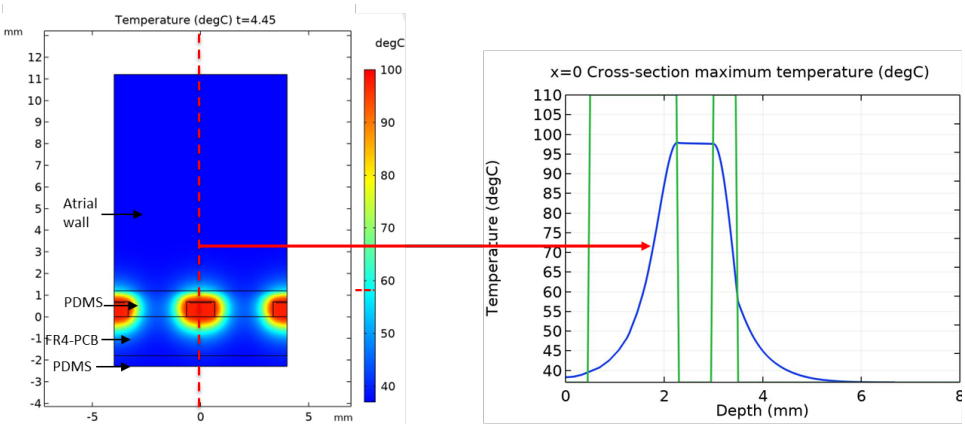

Figure 4.13: Temperature distribution at the cross-section of the device and atrial wall at the time point T=4.45 seconds (when the maximum temperature at the tissue interface is reached)

are significantly elevated locally. In contrast, the areas between the two hot spots remain cool during the 3-cycles of light pulses, with a maximum temperature difference of 17°C.

A temperature plot is created (Figure 4.13), capturing the temperature profile along a vertical cross-section through the center of the LED chip at the time point T=4.45 seconds (when the maximum temperature at the tissue interface is reached). The plot shows very sharp temperature gradients on both the front and back sides of the LED.

On the bottom side of the LED, the temperature starts high and then gradually decreases as the thermal energy diffuses away from the LED, towards the backside of the panel PDMS layer. Notably, the bottom part of the PDMS encapsulation maintains a cool temperature, close to ambient conditions. This effect can be attributed to the thickness of the PCB board combined with the relatively low thermal conductivity of the FR-4 material, which together act as effective barriers to heat transfer.

The temperature curve on the front (right) side of the LED, where it interfaces with the atrial wall tissue is even steeper. The thin layer of PDMS in this area effectively blocks the high temperatures generated by the LED chips from reaching the tissue surface. This indicates that despite the significant heat generated by the LEDs, the design with the thin PDMS layer at the front successfully prevents excessive thermal transfer to the tissue as a medium for thermal transfer, and plays a crucial

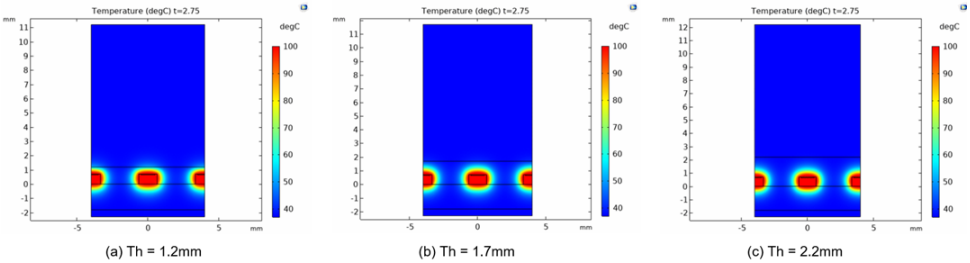

Figure 4.14: Temperature distribution at the LED panel and atrial tissue interface at T = 2.75s with different thicknesses of front PDMS layers: 1.2mm, 1.7mm, and 2.2mm. A clear 'thermal barrier' of the low-temperature zone is observed in thicker PDMS polymer simulations.

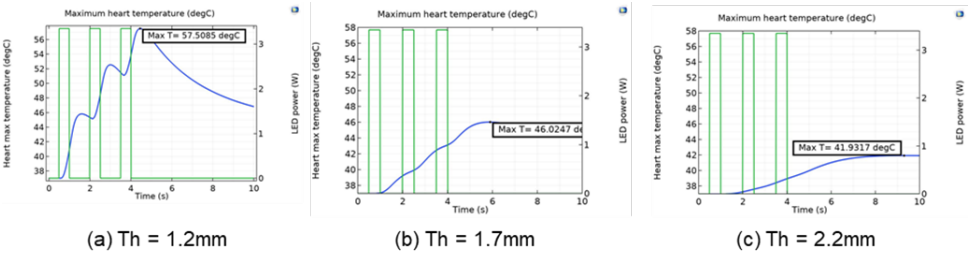

Figure 4.15: Maximum temperature at the LED panel and atrial tissue interface with different thicknesses of front PDMS layers: 1.2mm, 1.7mm, and 2.2mm

role in how this heat is distributed.

2. Thickness of front PDMS layer

   With LED power input fixed at 3.35W (1000mA / lime LED), the thermal responses, sampled by the maximum temperature at the interface of LED and tissue observed in the simulated model vary depending on the thickness of the PDMS layer. Specifically, with a PDMS thickness of 1.2mm, there are rapid increases in temperature reaching a peak during every active period of the LED device, followed by a rapid cooling down when the LED is switched off. This pattern is repeated over three cycles, corresponding to the LED's pulsed power input, as depicted in Figure 4.15a. These temperature spikes, although short, are observed at the thermal impact of the tissue with the maximum peak temperature of 57°C. After these brief periods of elevated temperature, the model shows effective heat dissipation after the LED power cycle is finished, allowing the system to return to a thermal balance at the ambient temperature of 37°C around 30 seconds (not plotted in the figure).

With an increased PDMS layer thickness of 1.7 mm, the thermal behavior within the model shows a significant change. Compared to the thinner PDMS layer, the temperature rise in this condition is more gradual, and thermal peaks are not observed between the short pulse intervals (Figure 4.15b). Instead of reaching a peak temperature within each pulse and then quickly cooling down, the process of thermal heating extends over time, leading to an almost continuous temperature increase throughout three cycles. The lower peak temperature of 46°C is achieved after 1.5 seconds of the last active phase of the LED, indicating a delay in thermal response. The system returns to a thermal balance at the ambient temperature of 37°C around 35 seconds.

With a further increase in the PDMS layer thickness to 2.2mm, the model's temperature profile becomes even lower and more uniform (Figure 4.15c). The three-cycle pulsing pattern of the LED is no longer evident in the temperature profile. Instead, what is observed is a smooth and gradual increase in temperature to the maximum peak of 42°C after 4 seconds of the last active phase of the LED. The system returns to a thermal balance at the ambient temperature of 37°C around 40 seconds.

This observed phenomenon can be attributed to the low thermal conductivity of the increased thickness of PDMS. The heat generated by the LED requires more time to transfer through the thicker PDMS layer to the adjacent tissue to increase temperature and equally more time to transfer back to PDMS during the cooling down phase. The increased thickness of PDMS acts as a more effective thermal barrier, enhancing its thermal capacity. This results in slower heat dissipation and a delayed response in reaching peak temperatures, illustrating the impact of tiny changes in the PDMS thickness on heat transfer dynamics in the model.

The decision from these observations is that a PDMS layer thickness of 2.2mm is the optimal choice for the device design. This decision is based on balancing the need for effective thermal insulation without an excess increase in thickness. A thickness of 2.2mm provides sufficient insulation to prevent rapid temperature spikes to risky temperatures higher than 42°C, while still allowing for close distance between LED light sources to the targeted tissue to maintain concentrated high irradiance of light, as simulated in the previous section.

3. Input LED power

The simulation then fixes the front encapsulating PDMS layer thickness at 1.2mm and varies the input power of the LEDs to examine the correlation between the

maximum temperature at the interface and the LEDs' input power. As the input power for each LED increases from 0.56W to 1.58W, then to 2W, and finally to the maximum of 3.35W, there is a corresponding rise in the maximum temperature at the interface between panel device and tissue (Figure 4.16). Specifically, at the highest input power of 3.35W, the peak temperature reaches 57.5°C, whereas, at the lowest power, the temperature experiences only a slight increase from the ambient 37°C. A similar trend is noted in the core chip temperature (junction temperature) of the LED, where the peak temperature can surge to as high as 167.5°C but only for an extremely brief duration. This rapid temperature escalation and subsequent fall is characterized as a 'thermal hit.' Such findings are particularly useful in assessing the reliability and durability of the solder joints under varying thermal conditions, providing valuable insights for the design and testing of the LED device.

When plotting the maximum temperature observed during three cycles of light pulses against the input power of each LED, a linear relationship is found (Figure 4.17). This relationship can be beneficial for both the design phase and the execution of biomedical experiments. It allows testers to predict and estimate the thermal impact or potential thermal damage to the tissue based on the input power of the LEDs. By understanding this linear trend, experimenters can adjust the LED input power to control the maximum temperature or 'thermal hits' at the tissue interface, thereby minimizing the risk of thermal damage while optimizing the effectiveness of the experiment or treatment.

4. Conclusion and limitations of the simulation

The simulation shows important information about how temperature is distributed across the device, horizontally and vertically, particularly in identifying hot spots near the LED chips. It also proves the significant thermal barrier effect from the encapsulating PDMS polymer layer. The simulation shows that the chosen optimal thickness effectively prevents excessive heat transfer to the tissue, maintaining a safe temperature profile. The simulation demonstrates a clear relationship between the input power of the LEDs and the temperature profile of the device. Higher input power leads to higher temperatures, both in the LEDs and in the surrounding areas.

These observations and discussion are essential in understanding and estimating the thermal dynamics in the biomedical experiments of AF termination where controlling temperature rise and preventing thermal damage to tissues is of im-

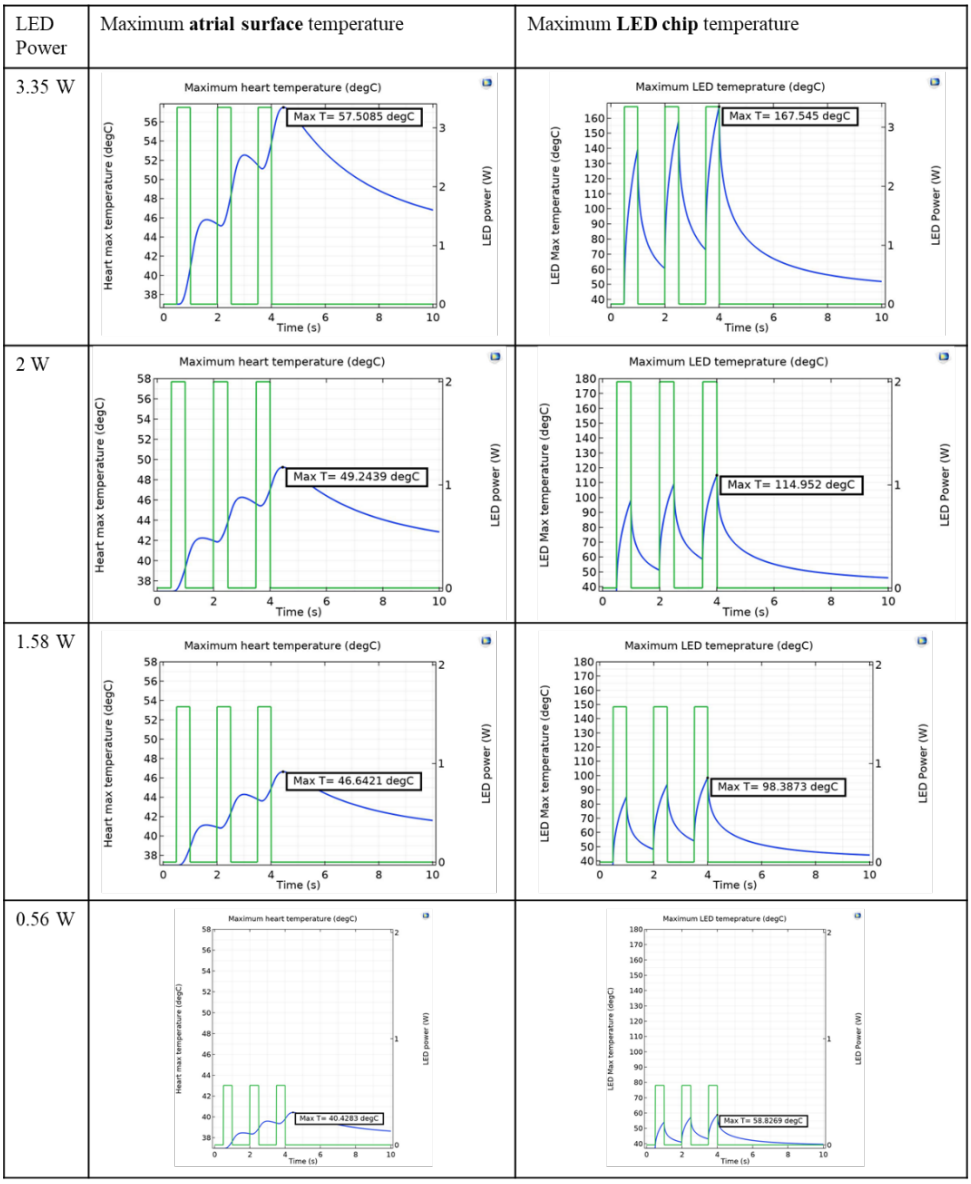

Figure 4.16: Transient behavior of the maximum temperatures in the atrial wall and in the LED chips with different LED power input

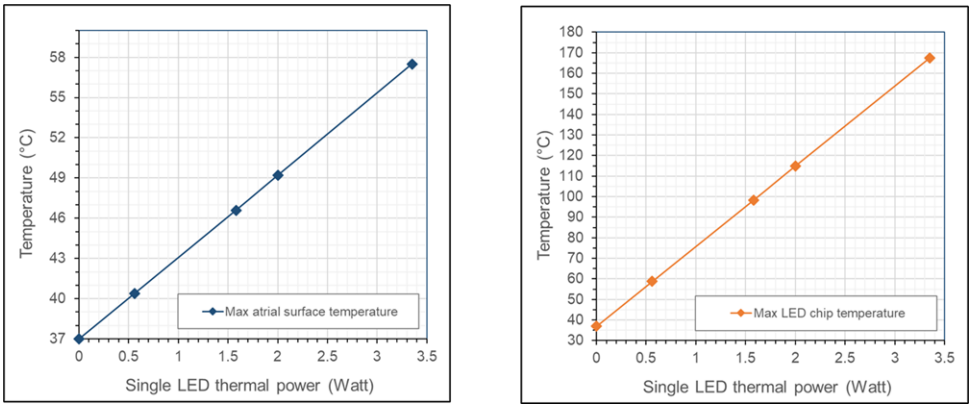

Figure 4.17: Maximum temperature during 3-cycles of light pulses versus input power of each LED at (a) atrial wall tissue surface and (b) inside LED chip

portance. The thermal simulation concludes with a discussion that the LED device design is safe for the in-vivo and ex-vivo experiments, in the context of the tissue damage and hardware damage by thermal effects is design to be minimal.

Though the thermal simulations conducted provide valuable insights into the thermal behavior of the LED device, some limitations must be acknowledged.

One of the primary limitations is the absence of real-life measured data to validate the simulated values. Without real-world measurements to compare against, the accuracy of the simulation's outcomes remains unverified. This lack of validation means that while the simulation can offer theoretical insights, its practical accuracy may vary.

Secondly, the boundary conditions in the simulation are based on several simplifications and assumptions that may not fully capture the complexities of real-world scenarios, followed by a few main examples. It is assumed that all interfaces within the device have an ideal heat transfer interface, which might not be the case in a real application where liquid (blood), air gap, or other imperfections can largely affect heat transfer between materials. Another assumption is given that all electrical input is converted into thermal heat within the simulated scope, however, in reality, some light emitted by the LEDs might leak outside the intended area. No consideration is given to the physics of thermal expansion, which can play a significant role in how materials behave under temperature changes.

Finally, the materials in the simulation are treated as thermally homogeneous,

which oversimplifies their actual behavior. The model does not account for blood vessels and other biological structures in the atrial wall tissue, which can significantly affect thermal properties and heat dissipation as the blood circulation acts like an active cooling system. The PCB is considered as being made of homogeneous FR-4 while ignoring the inhomogeneity of the composite material and other components like solder, copper, or thermal vias that can impact thermal conductivity and heat distribution.

4.4. DRIVER AND CONTROL SUBSYSTEM DESIGN AND IMPLEMENTATION

4.4.1. SYSTEM ARCHITECTURE

The high-power LED panel requires external driver electronics to function and be controlled as desired. With 10 illuminating zones, a driver should be capable of individually managing the on and off switching for each of these 10 channels. The driver must offer precise dimming capabilities to accurately adjust the light power (therefore irradiance) emitted by the LED panel during experiments. This fine control is essential for ensuring consistent and reliable experimental conditions. The LED panel should be operable in various programmed pulse patterns, which can be initiated based on trigger signals received from a signal generator or a computer. This feature allows for the customization of lighting patterns to suit specific experimental needs, such as pacing, inducing, or terminating AF.

To safeguard the LED panel and ensure its durability, the driver electronics must incorporate protective measures. These could include over-current protection, thermal shutdown, and voltage regulation to prevent any potential damage due to electrical malfunctions or other operational incidents.

A simplified system architecture is proposed in Figure 4.18. The driver system for the LED panel is integrated into a control subsystem, with each of the 10 channels on the panel receiving independent power and operational controlling by individually managed by channel LED driver modules, ensuring targeted and precise control over the light output.

Each channel LED driver subsystem comes equipped with a built-in high-power current source, designed to provide a stable and sufficient power supply to the 10 LEDs in each channel with a series connection. The current flowing to each LED series can be adjusted and programmed using the external switch signal port supported by the channel LED driver subsystem. These signals offer the flexibility of being connected

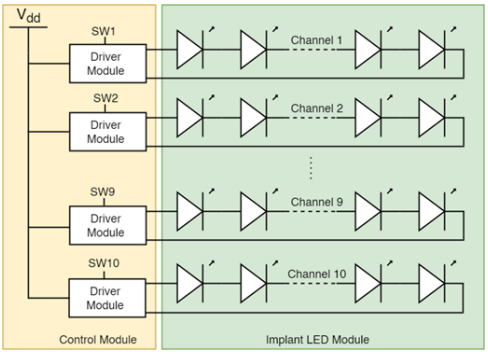

Figure 4.18: A simplified driver system architecture illustration

to a manual override for instant control or an external input from devices like a signal generator or computer output. A standalone DC power source supplies all 10-channel LED driver modules.

The control subsystem is connected to the LED panel subsystem through extended wiring. Positioned externally to the test subject's body, the control subsystem is designed with an interface that includes switches and buttons, to allow testers to manually adjust the operational parameters during experiments to the specific needs of each experimental setup

4.4.2. ELECTRICAL CIRCUIT DESIGN

Detailed electrical circuit design is made to implement the proposed architecture of the control and driver system.

To reduce the complexity of wiring, the LED panels have been engineered to share a common ground signal across all 10 zones. This is also a necessary solution to extremely limited space for connecting pads on the LED panel. This shared grounding approach, while effective in meeting the requirements of the implanting LED panel, gives certain restrictions on the design of the LED driver subsystem. Combined with the high power requirements of the LEDs, it's not feasible to employ commercially available integrated LED current sources (modules) that support the shared grounding layout among channels, which are typically designed for lower-power applications such as decorative lights. This determines that the LED driver subsystem uses discrete electronic components.

The core of the custom-built driver subsystem is a high-power, high-current PMOS transistor (PCP1302-TD-H, Onsemi, USA) operating in the linear region, which plays a critical role in regulating the output current to the LEDs. The design of the surrounding circuit, including feedback resistors and isolating capacitors, is aligned with the man-

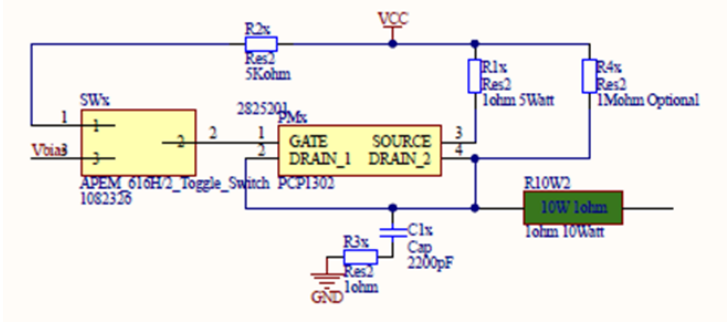

Figure 4.19: Schematic drawing of the driver electronics per LED channel using a transistor to regulate current

4

ufacturer's recommended layout (Figure 4.19). This ensures that the electronic components function optimally, providing stable and precise control over the high-power LEDs.

A high-power current limiting resistor is used per channel to ensure the safe and efficient operation of the LED. This resistor serves to regulate the current to the LED, to prevent excessive current from damaging the LED or the driving transistor. The value of this resistor is determined using Ohm's Law, taking into account the voltage drop across the resistor and the desired current through the LEDs as discussed in the previous section. A 1ohm resistor (MCKNP0ASF100KB00, MULTICOMP PRO, USA) with a 10W specific power rating is selected per channel. The larger size of these high-power resistors is due to their need to dissipate more heat generated by the higher currents. This requirement for a larger physical footprint on the PCB must be taken into account during the design process. A series of toggle switches are added to individually switch on and off every LED channel out of a total of 10. This allows individual control of the local illumination of the 10 zones on the panel.

External triggering signal is fed to the control subsystem via a BNC type connector (Figure 4.20). A logic level enhancement transistor (NDT3055L, Onsemi, USA) is used to translate the nominal 5V TTL triggering signal to the on and off state of the switching circuits. A digital adjustable resistor (potentiometer) is placed in the switching circuits to allow the user to change the gate voltage of current-controlling transistors for all drive modules. The two-digit potentiometer serves as a user interface to freely adjust the LED driving current from 0% to 100% with 1% increments.

The design for the control and driver subsystem is translated into PCB layout design (Figure 4.21), the same software previously employed. This ensures consistency in design methodology and allows for the use of established workflows and component libraries. Following the design phase, the PCB layout is sent off for fabrication, using

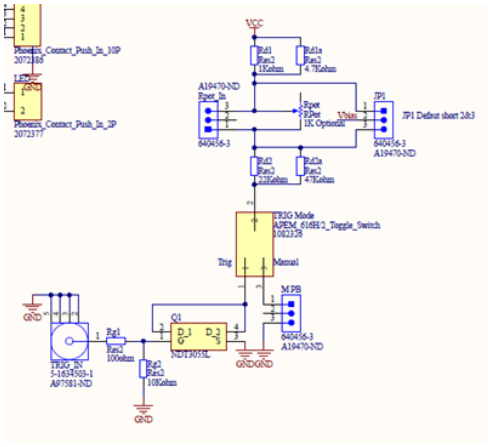

Figure 4.20: Schematic drawing of the electronics for trigger and dimming functions

the same classification of manufacturing standards (PCB proto pool) and tolerances as discussed in previous chapters. After successful testing, the PCBs move on to the assembly service by the manufacturer. The components are mounted onto the PCBs through an automated PCBA process to precisely place components onto the board, followed by soldering processes such as reflow (for surface mount components such as IC and transistors) or wave soldering (for through-hole components such as connectors and resistors) to secure the components in place.

Once the PCB assembly is completed, covering all electronic components, the entire assembly is treated with conformal coating. This is achieved through the application of a spray coating (URETHAN 71, Kontakt Chemie, the Netherlands), which is designed to uniformly cover and protect the PCB and its components against potential moisture or liquid during future experiments.

This approach, while more complex than using integrated solutions, allows for greater flexibility and customization in meeting the specific high-power requirements of the LED panels.

4.4.3. SYSTEM INTEGRATION AND ASSEMBLY

The control and driver subsystem is powered by a standalone AC-DC power supply (Figure 4.22c-A) (RPS-400, Mean Well, USA). The power supply is selected by its high power density (maximum 400W, 48V) and high energy efficiency (94%) with minimum footprint. It conforms to international medical regulations and EMC standards, perfectly fitting for various medical system equipment.

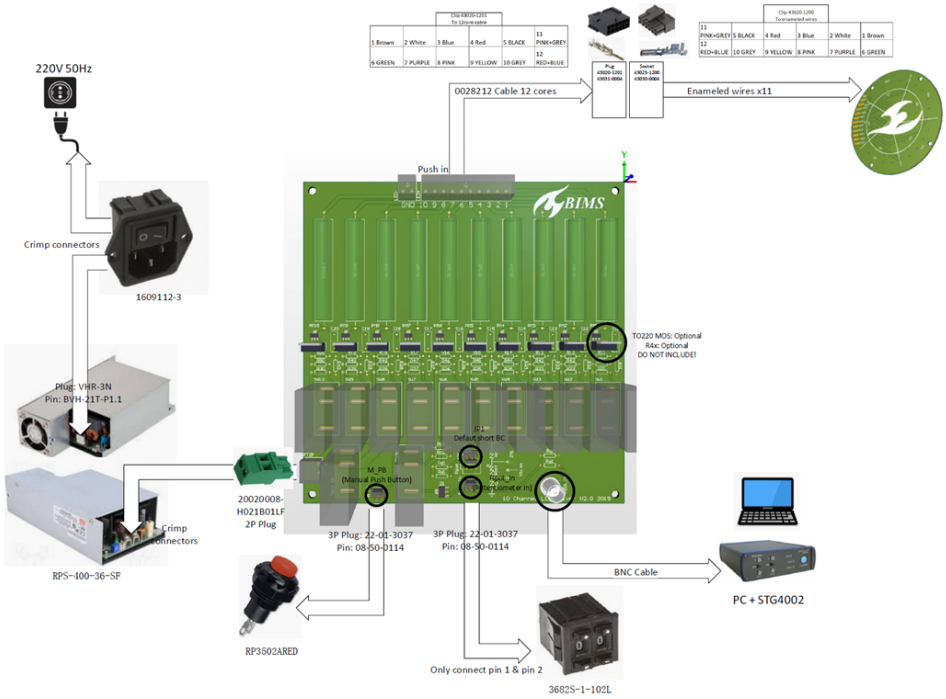

Figure 4.21: Layout for the LED driver and control subsystem

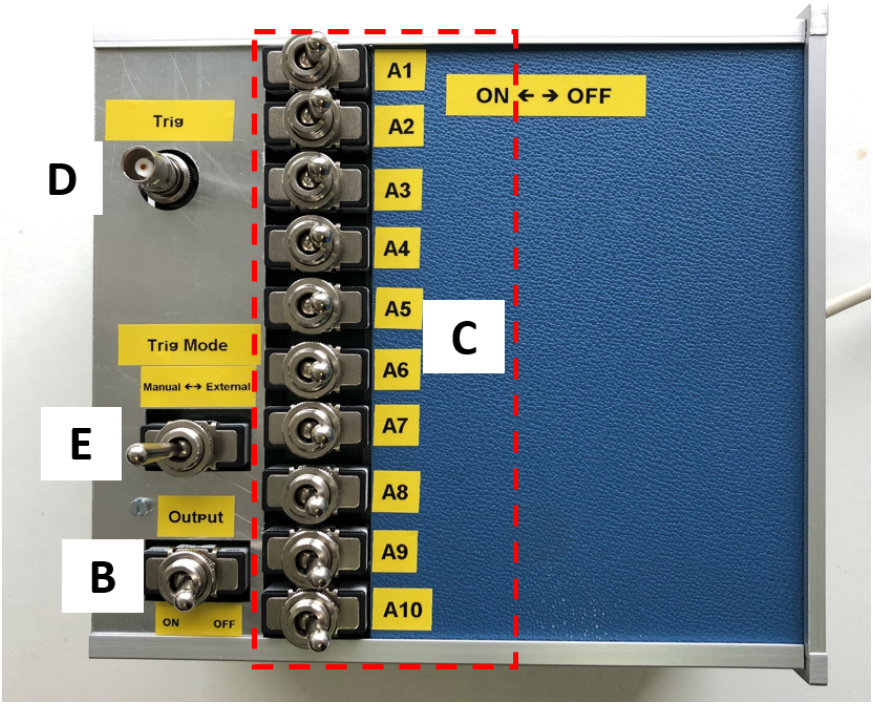

(a) Top view

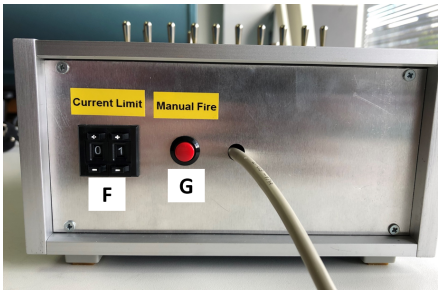

(b) Front view

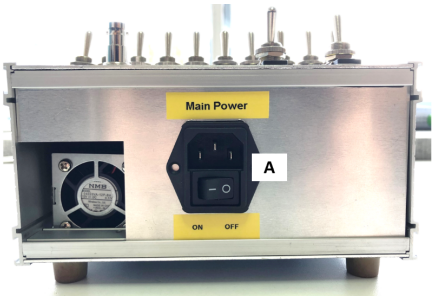

(c) Back view

Figure 4.22: The control and driver subsystem integrated in the metal case

The PCB board with driver electronics and power supply is carefully assembled into a custom-made metal case, designed to accommodate the components with a compact and efficient layout. The metal case not only provides robust physical protection for transferring and storage but also offers shielding from electromagnetic interference, which is critical for maintaining the integrity of the signals and operations.

On the top panel and front panel of the case, switches for selecting channels (Figure 4.22a-C), a BMC type connector (Figure 4.22a-D) for input triggering signal, a push-button for manual overrides (Figure 4.22b-G), and the potentiometer (Figure 4.22b-F) for power percentage controlling are mounted for easy access. Particular attention has been paid to the user interface, especially considering the operational context where the device will be used during biomedical experiments. The buttons and switches are deliberately chosen to be large. This design consideration is made to accommodate users who typically wear gloves during experiments, ensuring that the controls can be easily and accurately manipulated.

The connection between the driver subsystem and the LED panel is established using a multicore power cable, which is designed to handle the necessary power and signal requirements with a shielding feature. One end of this cable is connected to the front panel of the driver case, and the other end interfaces with the enameled wires of the LED panel, as described in the previous sections detailing the panel's fabrication. A modular connector joins the multicore power cable to the enameled wires. This connector is specifically chosen for its ease of use, allowing for quick and simple connection and disconnection to swiftly swap out LED panels with different colors.

At the bottom panel of the box, the power outlet and the main power switch are located. The power cable is connected to a common 230V AC power socket. This not only serves ergonomic considerations but also adheres to safety standards, as it keeps high-voltage connections isolated from the user interaction points and away from accidental contact.

Following the assembly of the driver subsystem and LED panel, a series of tests and calibrations are conducted to ensure the system is functioning optimally.

The first step involves calibrating the output current against the potentiometer digital number input. This calibration is crucial to verify that the transistors within the driver subsystem are operating correctly within their linear region. Transistors must function within this region to provide precise control over the current supplied to the LEDs, which directly affects the performance of the lighting system.

A current meter is introduced into the circuit, placed in series between the driver subsystem and the LED panel. During the calibration process, the potentiometer is

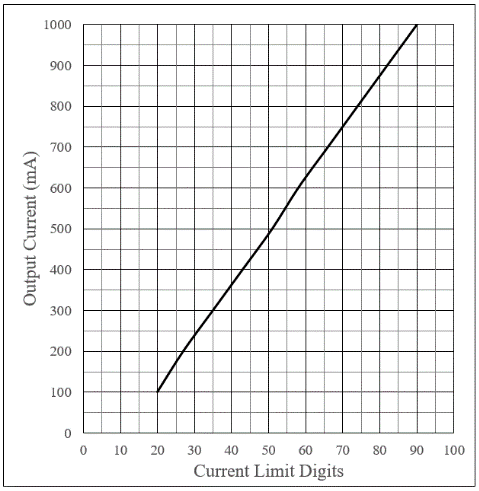

Figure 4.23: Calibration of output current with potentiometer digital numbers

adjusted incrementally from 0 to 99, and at each step, the digital value displayed on the potentiometer is recorded, alongside the corresponding current reading on the current meter. By systematically recording these values, a calibration curve or table can be established, mapping the potentiometer's digital numbers to the actual current delivered to the LED panel in a linear manner (Figure 4.23). Because the potentiometer linearly alters the voltage applied to the gate of the transistors, the linearity observed in the calibration results indicates that the transistors are indeed functioning within their linear region across the full range of input. This expected behavior is critical for the accurate and predictable modulation of current through the transistors, which, in turn, allows for precise control over the intensity of the LEDs.

Once the current calibration is confirmed, the test focuses on the calibration of the potentiometer digital numbers with the irradiance at the LED panel's front surface for various wavelengths. An optical sensor (S130C, Thorlabs, USA) is positioned against the front side of the LED panel at three distinct locations: the center, the middle, and the side. By doing so, variations in light intensity across the surface of the panel can be assessed, ensuring a comprehensive understanding of the panel's performance.

The sensor is connected to a readout console (PM100D, Thorlabs, USA), which is designed to display the irradiance value for the specified wavelength. With this setup in place, the potentiometer is adjusted incrementally (from 0 to 99) to increase the driving current gradually. At each increment, the irradiance reading is taken from the console and recorded. To ensure accuracy and account for any possible fluctuations, each irradi-

ance measurement is conducted three times at each location and for each potentiometer setting. The three readings are then averaged to produce a final value that is representative of the irradiance at that specific setting and location on the panel, as the results show in Table 4.3.

It is noticed that the characterized irradiance for 470nm LED is higher than estimated, while the 567nm LED is lower. This could be explained in two aspects. Firstly, similar to the observation in the previous chapter, the 567nm LED chip has ceramic packaging which has better thermal conductivity, compared with the epoxy packaging for the 470nm LED. The higher the thermal conductivity of the packaging material, the more rapidly heat generated by the core semiconductor chip is dissipated to the exterior and therefore to the thermal barrier. This results in a quicker thermal response and elevated short-term thermal peaks in 671nm LEDs, especially when the matrix has a dense layout. Therefore the 617nm LED might suffer from the irradiance degradation of lower efficiency due to high junction temperature. Secondly, the optical sensor used has a relatively smaller detection window of 8mm, and measuring artifacts are introduced with 4mm intervals of LED elements since 4 to 6 LEDs are measured every time. However, the optical characterization results still show that the device can deliver sufficient irradiance as required in the specifications.

Table 4.3: Calibration of the potentiometer digital numbers with the irradiance at the LED panel. The lime LED panel is measured up to its maximum allowed current of 700mA.

Limit Digits	**Current** (mA)	**Irradiance(mW/mm^2)**	
		Blue 470nm	Lime 617nm
20	100	7.8	3.43
27	200	12.47	5.76
35	300	20.27	8.91
43	400	26.51	11.24
51	500	31.18	13.71
58	600	35.86	15.76
66	**700**	40.54	17.82
74	800	45.22	
82	900	48.02	
90	**1000**	53.01	

This calibration is critical for ensuring that the user can reliably control the LED irradiance based on the digital input of the potentiometer. It provides a clear reference for what current, and thus what level of irradiance, can be expected for given potentiometer

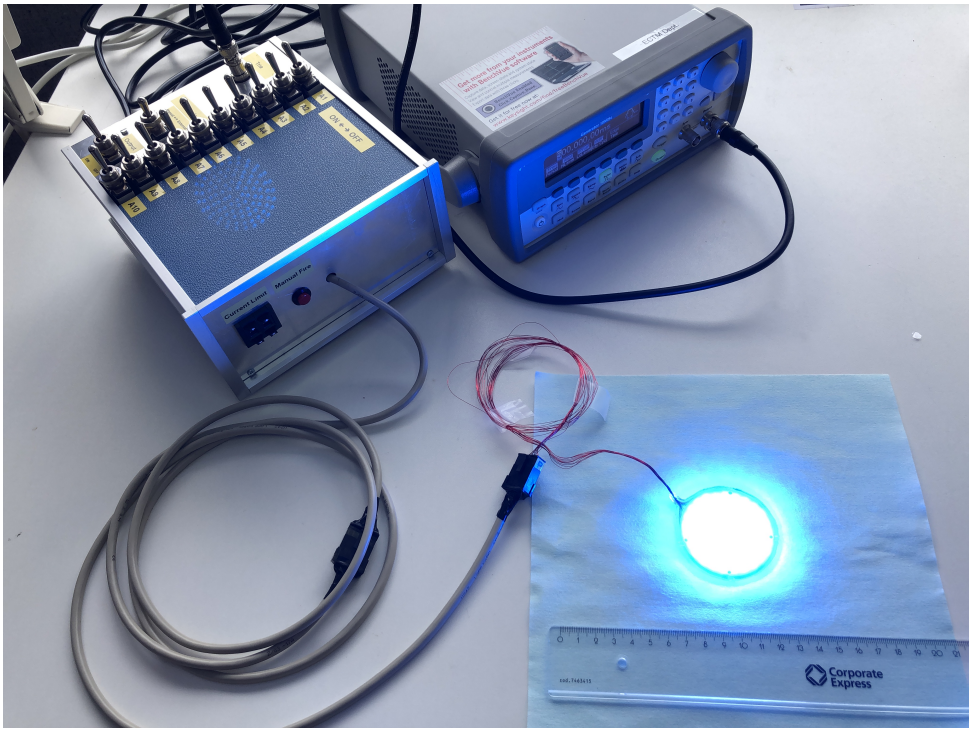

Figure 4.24: Assembly of the control and driver subsystem, signal generator, connecting cablings, and the blue LED panel in operation

settings. It also demonstrates the device's capabilities and that the panel device can deliver the sufficient levels of irradiance necessary for the intended experiments. Also, the irradiance range is found to be sufficient across the panel's surface, including the center, middle, and sides, affirming the uniformity and consistency of the LED panel's performance as predicted in the optical simulation.

The following tests focus on evaluating the system functionality of local illumination across its 10 zones which is a key feature of the panel that allows for targeted illumination in specific areas on the atrial wall. Different zones are activated individually by manipulating the toggle switches located on the top of the case. The results of these tests are shown in figures, each illustrating the panel with different zones in operation.

It's important to note that the variations in brightness observed in these photos are not indicative of changes in the LED irradiance. Instead, they are a result of the camera settings used during the tests due to the extreme dynamic range of the illumination. The LED irradiance remains consistent across all zones and is not influenced by the selective activation of different zones.

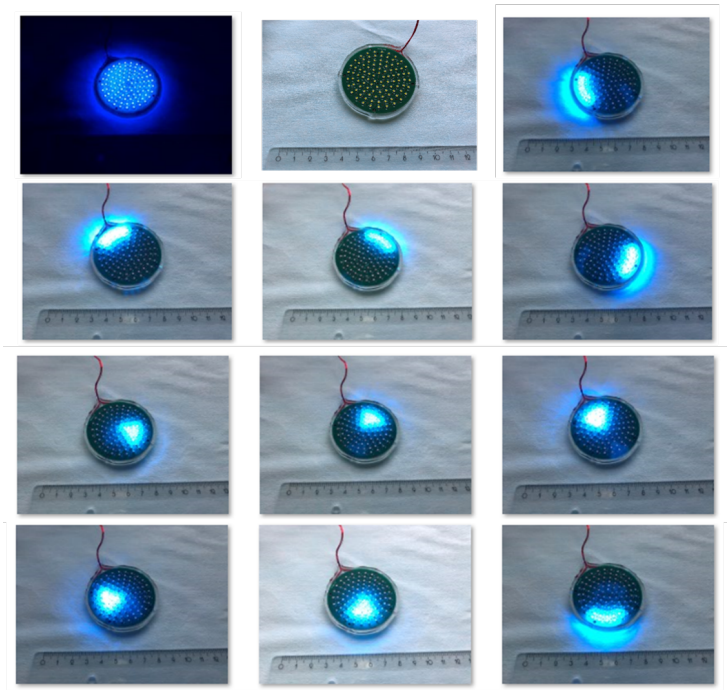

(a) $\lambda = 470nm$ Blue

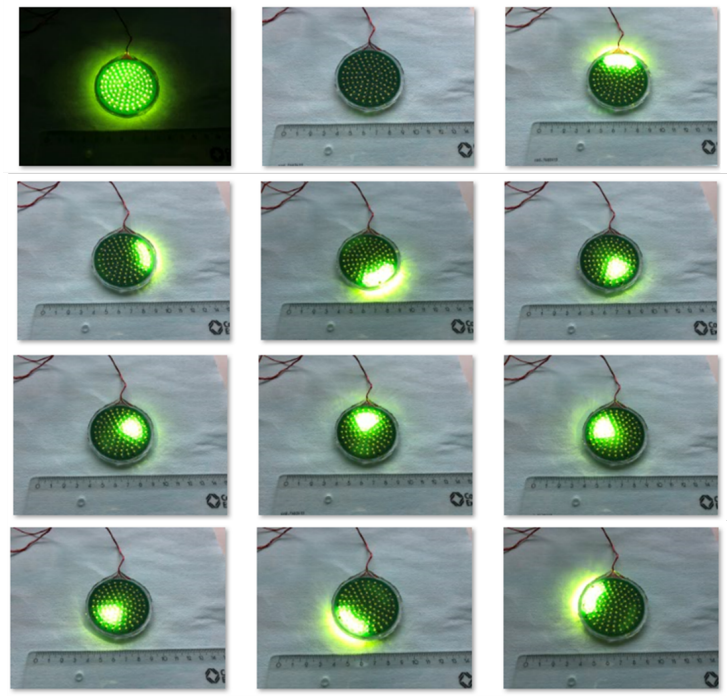

(b) $\lambda = 567nm$ Lime

Figure 4.25: Illumination zone controlling of the LED panels

From the above calibrations and tests, this system is verified as functional, professional, and user-friendly, and the LED illuminating system is ready for functional validation in the in-vivo and ex-vivo experiments of optogenetics AF termination.

4.5. SYSTEM VALIDATION: OPTOGENETICS AF TERMINATION EXPERIMENTS IN SWINE MODEL

In the preparation of experiments, the swine hearts are genetically modified using the same methods and gene (ReaChR) as those employed in the previously discussed rat models. The experiments are a collaborative effort between LUMC and Heidelberg University in Germany. During the experimental procedure, the swine is anesthetized, and a surgical procedure is performed to open the chest and expose the heart's right atrial wall. This preparation is essential for conducting atrial fibrillation (AF) treatment experiments using optogenetic methods with the LED illumination system.

However, despite these preparations, the experiments involving the optogenetics methods do not yield successful results. It is observed that regardless of the wavelength or the intensity of the light used, the LED panels fail to pace the atrial activity in the swine models (n = 9), with various trigger patterns or intervals tried, given that self-sustained AF can be successfully induced using electric probes, suggesting that the swine hearts are indeed capable of being paced and entering an AF state. Subsequent attempts to terminate the AF using the LED device are also not successful (n = 9), regardless of the wavelength or the intensity of the light used or with various trigger patterns or intervals.

The post-experimental autopsy of the heart used in the experiments found the absence of the transferred gene's expression in the atrial cells. This crucial observation indicates a fundamental problem in the genetic modification process that is intended to make the atrial cells responsive to light stimulation. This explains why these cells do not respond to the light stimulation from the LED panels.

The absence of gene expression could be due to a variety of factors in the genetic modification process, such as issues with the gene delivery method, the vector used, the integration of the gene into the host, or the expression mechanisms within the cells. This failure indicates a significant gap in the understanding or application of optogenetic techniques in these swine models, as compared to the earlier successes in rat models. Such outcomes, while disappointing, are not uncommon in the progression of experimental medical research, especially when scaling up from smaller to larger animal models or when applying techniques to different physiological systems.

These results highlight the complexities and challenges in translational cardiology

research, particularly when dealing with advanced techniques like optogenetics. The disparity in the outcomes between the rat and swine models underscores the need for further research and perhaps modifications to the approach, technique, or equipment used in these optogenetic experiments.

4.6. CONCLUSIONS AND LIMITATIONS

Work in this chapter combines advanced electronic system integration with biomedical science to another level, aiming to provide cardiac electrophysiologists with new tools for understanding and treating AF. The chapter outlines an innovative approach to terminate Atrial Fibrillation (AF) using optogenetics, with a focus on developing a high-power LED matrix illumination system through the V-model methodology. The full development cycle from requirement analysis, system design, implementation, and verification phases for the implantable LED system is presented. A few layout proposals for the LED panel are considered, leading to the selection of an optimal layout design that meets system requirements, followed by the design phase includes simulations for thermal and optical modeling. Two key subsystems, the illumination panel, and the control and driver system, are developed and tested. Special attention is given to ensuring the bio-compatibility of the LED illumination subsystem, aligning with the system requirements of biomedical applications.

While the developed LED illumination system functioned as intended and met its design specifications, the validation of the system for AF treatment in an in-vivo swine model did not yield the expected biomedical breakthroughs. The primary issue was the failure of gene expression, despite the illumination system's operational success. The LED illumination system, originally designed for effective AF treatment as an implant device, thus remains unvalidated in this specific application, leaving room for further research and development in the future.

The research methodology adopted in this study predominantly involves a trial-and-error approach due to the lack of concrete and specified requirements of the pioneering research. This involves experimenting with a variety of techniques, learning from each trial, and iteratively improving the methods. The LED illumination system presented in this chapter is the first iteration of the proof-of-concept design. Through this process of exploration and adjustment, the research aims to gradually uncover the most effective strategies of optogenetics study with swine models, building upon each step to refine the methods and enhance the outcomes in the future. For future development of illumination systems, the design requirements and specifications will be defined clearly and concretely which will make the design process smoother with lower risks.

In the currently discussed LED illumination system, while the illumination irradiance exceeded the requirements, the uniformity of the light distribution is still not optimal where hot spots exist in the light pattern. For future system improvements, it is considered to use more LED elements with a finer interval layout. This approach might achieve more uniform illumination, eliminating hot spots, while ensuring that the entire area maintains the required irradiance levels.

In the current design, individual light zones in the LED subsystem cannot adjust intensity independently, a limitation because of the simplification of the driving units. This limitation reduces the flexibility in creating varied illumination patterns. Additionally, the use of a common grounding electrical layout restricts the integration of commercially available, convenient integrated current source modules, and therefore requires the additional calibration of all transistors. For future iterations, it's recommended to revise the electrical layout to incorporate high-power LED control modules, enhancing the system's functionality and versatility in pattern creation and control.

BIBLIOGRAPHY

[1] Eric M Walters and Randall S Prather. "Advancing swine models for human health and diseases". In: *Missouri Medicine* 110.3 (2013), p. 212.

[2] John Y Lin et al. "ReaChR: a red-shifted variant of channelrhodopsin enables deep transcranial optogenetic excitation". In: *Nature neuroscience* 16.10 (2013), pp. 1499–1508.

[3] Claudia Crocini et al. "Optogenetics design of mechanistically-based stimulation patterns for cardiac defibrillation". In: *Scientific reports* 6.1 (2016), p. 35628.

[4] Sebastian Junge et al. "A micro-LED array based platform for spatio-temporal optogenetic control of various cardiac models". In: *Scientific Reports* 13.1 (2023), p. 19490.

[5] Aleksandra Klimas et al. "OptoDyCE as an automated system for high-throughput all-optical dynamic cardiac electrophysiology". In: *Nature communications* 7.1 (2016), p. 11542.

[6] Tobias Bruegmann et al. "Optogenetic defibrillation terminates ventricular arrhythmia in mouse hearts and human simulations". In: *The Journal of clinical investigation* 126.10 (2016), pp. 3894–3904.

[7] Emile CA Nyns et al. "Optogenetic termination of ventricular arrhythmias in the whole heart: towards biological cardiac rhythm management". In: *European heart journal* 38.27 (2017), pp. 2132–2136.

[8] Lizhi Xu et al. "3D multifunctional integumentary membranes for spatiotemporal cardiac measurements and stimulation across the entire epicardium". In: *Nature communications* 5.1 (2014), p. 3329.

[9] Laura Diaz-Maue, Janna Steinebach, and Claudia Richter. "Patterned illumination techniques in optogenetics: An insight into decelerating murine hearts". In: *Frontiers in Physiology* 12 (2022), p. 750535.

[10] Digikey.nl. *Conversion calculator PCB tracewidth*. https://www.digikey.nl/en/resources/conversion-calculators/conversion-calculator-pcb-trace-width. 2022.

[11] Daniel Keppeler et al. “Multichannel optogenetic stimulation of the auditory pathway using microfabricated LED cochlear implants in rodents”. In: *Science Translational Medicine* 12.553 (2020), eabb8086.

[12] Rishi Rajalingham et al. “Chronically implantable LED arrays for behavioral optogenetics in primates”. In: *Nature Methods* 18.9 (2021), pp. 1112–1116.

[13] Giovanni Camino, SM Lomakin, and Massimo Lazzari. “Polydimethylsiloxane thermal degradation Part 1. Kinetic aspects”. In: *Polymer* 42.6 (2001), pp. 2395–2402.

[14] Christian Rossmann and Dieter Haemmerich. “Review of temperature dependence of thermal properties, dielectric properties, and perfusion of biological tissues at hyperthermic and ablation temperatures”. In: *Critical Reviews™ in Biomedical Engineering* 42.6 (2014).

5

A LED MATRIX ILLUMINATION SYSTEM FOR HIAM OPTOGENETICS RESEARCH

5.1. INTRODUCTION

In this chapter, an innovative method of studying arrhythmia behaviors using the human immortalized atrial myocyte (hiAM) model is presented stressing the design and development of the LED matrix illumination system for proof-of-concept purposes. This involves the designing, testing, and implementation of the specialized, modular LED matrix and its controlling system as part of the novel in-vitro experimental platform. This demonstrative system set a good theoretical and practical basis for the more advanced illumination system for cardiovascular research in the following chapter.

5.1.1. HIAM CELL CULTURES

One of the challenges of effectively studying and treating human cardiac arrhythmia is the absence of precise human models that accurately represent the condition in terms of tissue size and electrical characteristics. Modern experimental cardiology research depended on animal experiments and cardiomyocyte samples derived from animals[1]. The reason for this is that human heart tissue has not only limited availability but also low mitotic activity after being derived from donors. However, growing ethical concerns over animal use in biomedical research push the urgency of the search for alternative human cardiac disease models. Advancements in tissue engineering, such as immortalized cell culturing[2][3] could lead to more accurate human tissue-based models, offering enhanced test platforms for drug tests or other novel methods. Additionally, computational modeling based on human cardiac physiology could serve as a valuable tool, to simulate various electrical patterns and responses, providing a virtual platform for in-depth theoretical research.

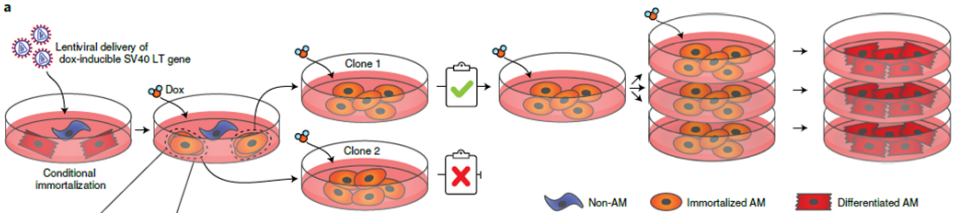

Figure 5.1: The growing process of hiAM cell cultures [3]

The human immortalized atrial myocyte (hiAM) model is one of the promising candidates for alternative human cardiac disease in-vitro models. It is a novel method of the selective and conditional immortalization of human cardiomyocytes, and transfer them into cell cultures as a platform for cardiological studies and analysis. hiAM has an active

acetylcholine-dependent potassium which makes it preferred in cardiovascular research of atrial fibrillation (AF), the most common cardiac rhythm disorder.

The hiAM cell cultures provide similar cardiac ion channel response in terms of their electrophysiological properties and it is suitable for most common and necessary in-vitro analysis methods of cardiovascular studies, such as microscopy, optical voltage mapping, and patch-clamp. Atrial arrhythmia activity with multiple degrees of complexity could be induced by high-frequency electrical stimulation to the edge of the cell cultures, which creates opportunities for researchers to design, test, and evaluate novel theories or methods of AF treatment on the hiAM atrial arrhythmia model. Gene expression analysis also proves that genetically modifying the hiAM cell cultures with similar methods of in-vivo models such as a rat or swine is possible.

By far the findings suggest the good feasibility of transitioning from animal models to hiAM models in optogenetics research for AF treatments. This transition to using human cells is exceptionally critical for the field of study as human cell models offer a more direct correlation to human cardiac physiology, potentially leading to more accurate and relevant insights into AF fundamentals and its treatment methods. Results obtained from hiAM models are likely to be more readily translatable to clinical settings. With advancements in hiAM models, there is the potential to tailor optogenetic treatments to individual patient needs, enhancing the efficacy and safety of cardiac arrhythmia therapies.

5.1.2. FULLY AUTOMATED OPTOGENETICS AF TERMINATION ON HIAM MODEL

An experimental cardiovascular research concept of fully automated optogenetics AF termination on the hiAM model is proposed, representing a novel approach to the treatment of AF using a combination of optogenetics, optoelectronics, and artificial intelligence (AI). This innovative experiment is demonstrative of advanced technology that can collaborate to develop novel treatments for cardiac arrhythmia. The setup consists of three primary components:

Optical Mapping System: This sub-system is designed to constantly monitor the electrical activities of the hiAM cell culture monolayer, which is prepared with a special dye to translate the electronic activities to optical signals. It includes optical magnifying lenses, high-gain cameras, and image-processing electronics. The system continuously captures and transmits optical mapping images of the cell culture to a PC, providing real-time monitoring of the electrical activities of the cell culture.

Optoelectronic Illumination System: This sub-system consists of an illumination matrix device and its control electronics. It is responsible for displaying dynamically

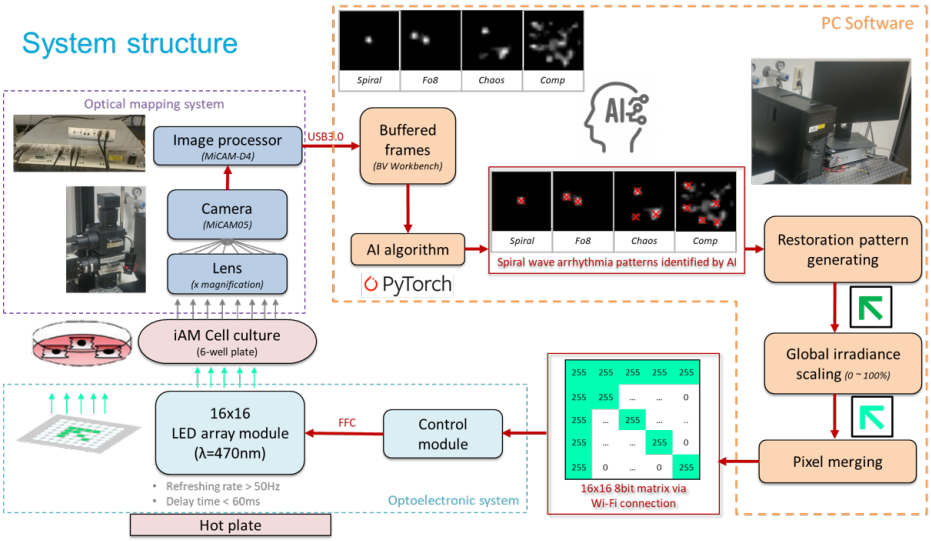

Figure 5.2: Architectural illustration of the concept of fully automatic optogenetics AF termination on hiAM model

programmed restoration patterns with specific irradiance levels onto the hiAM cell culture. The matrix is designed to respond rapidly to the input from the PC, adjusting the pattern and intensity of the light to terminate AF effectively in the cell culture.

Embedded Software with AI on a PC: The embedded software incorporates an AI algorithm, trained through machine learning, to identify abnormal AF patterns captured by the optical mapping system. The AI algorithm analyzes the dynamic movements of the AF rotational pattern and generates a corresponding restoration pattern. This pattern is processed and translated into input settings for the optoelectronic illumination system, guiding the system to deliver precise light stimulation to terminate AF.

The experimental setup is designed to create a closed-loop, fully automated treatment process. The hiAM cell culture monolayer is maintained in an environment with controlled temperature, liquid solutions, and nutrients. AF is initially induced using external high-frequency electrical stimuli, and the system's AI algorithm then works to identify and respond to the induced AF. The seamless integration of optical mapping, AI-driven analysis, and responsive optoelectronic illumination showcases a novel approach in AF treatment for the hiAM model, demonstrating the potential of combining optogenetics with AI in medical research and therapy.

5.2. REQUIREMENTS ANALYSIS

With the establishment of the hiAM model as a novel test platform for automated optogenetic AF termination setup, the next crucial step is to develop the customized illumination system. This illumination system needs to meet the specific requirements of the optogenetics experiments and be adaptable enough to serve as a versatile platform for a wide range of in-vitro optogenetic research applications with the hiAM model, considering the rapid evolution of the hiAM model. System requirements analysis is separated into two parts, the illumination source (LED matrix) requirements, and the control system requirements.

In designing an illumination system, particularly for applications like optogenetics, it's a practically to divide the system into two parts: the illumination part and the controlling or driver part. This division allows for specialized focus on each component's unique requirements and functionalities. The illumination part generates light, and the design of this part focuses on the optical specifications of the light sources, such as wavelength, intensity, uniformity, and the ability to create specific illumination patterns. Requirements also include the size and shape of the light-emitting elements, their arrangement (such as in a matrix of LEDs or a projector setup), and the materials used, which should be compatible with the experimental environment. The requirement also includes the interface between the light source and the test subject for the proposed in-vitro experiments. For potential future exploitations to in-vivo or ex-vivo applications, the design must account for factors such as biocompatibility, flexibility, and the minimization of invasiveness. These requirements are analyzed separately in the following section, to provide a clear view of the system development procedure.

Wavelength

Capable of producing light at specific wavelengths, chosen based on good effectiveness to generate strong reaction by light-gated ion channel activatable channelrhodopsin in hiAM cell cultures. In the initial trial experiments involving the hiAM model for optogenetic AF treatment, the gene used probably is the same as or similar to the one employed in the rat and swine models (ReaChR[4]). Therefore, 470nm (Blue) is selected as it has an excellent and stable response for pacing, blocking, and AF termination on the light-gated ion channel, while the light sources (LEDs) with this wavelength are commercially available with high energy efficiency and minimized dimensions.

Irradiance and illumination homogeneity

Capable of producing light with sufficient irradiance to generate strong reactions by

light-gated ion channel activatable channelrhodopsin in hiAM cell cultures. In the rat or swine models, the genetically modified cells are densely packed and enveloped by various tissue layers. In these models, light must penetrate these thick tissue structures to reach and stimulate the target cells, therefore requires high-irradiance light to ensure adequate penetration and effective stimulation. However, in the hiAM model, the cells are typically cultured in a monolayer. This single-layer culture means that the light efficiency is expected to be significantly higher, as the light doesn't need to penetrate through multiple layers of tissue.

Growing the hiAM directly on the light sources is not likely feasible due to biocompatibility concerns. Therefore, a barrier layer is necessary between the cell cultures and the light sources. This barrier could be air or a transparent medium, such as the plastic of a Petri dish. The light sources must therefore provide a high enough irradiance to penetrate this media layer effectively and still deliver sufficient irradiance to the cells. A reference value of 0.3mW/mm^2 at the hiAM monolayer surface is proposed based on preliminary experiments on the hiAM AF models. The genetically modified, light-sensitive hiAM monolayer's responsiveness to optical stimuli makes uniform light distribution a critical factor in the design of the illumination system. Any significant variation in light intensity, particularly when high irradiance levels are involved, can lead to uneven stimulation across the targeted area of the cell culture. This non-uniformity in light exposure can induce artifact responses, deviating from the intended behavior of the cells. In cases where the light distribution is uneven, with areas of high contrast in irradiance, the cells in different parts of the monolayer might react differently. For instance, areas receiving higher irradiance ('bright spot') might react to an exaggerated response, while areas with lower irradiance ('dark spot') might not respond adequately. Therefore, ensuring a consistent and uniform light distribution is required. This uniformity is especially crucial in studies aiming to block or restore arrhythmia activities, where precise control over the cells' response is necessary for the success of the experiment.

Interface

Well plates are fundamentally used for growing, transporting, and analyzing hiAM cell cultures. These plates consist of multiple small wells, each serving as separate rooms. Well plates come standard in various formats, with different numbers of well cells, such as 6, 12, 24, 48, 96, or more wells per plate. In the study of hiAM optogenetics research the 6-well plate is commonly used for small-scale cell cultures. Petri dishes are frequently used for larger cell cultures. Both well plates or Petri dishes are typically made from transparent materials like glass or plastic, which is essential for allowing researchers to

observe and monitor the cell cultures without any interference.

hiAM atrial arrhythmia models are successfully presented in different scales of cell cultures up to 10cm2 size (in 6-well plates), but a much larger hiAM monolayer model is expected to reach up to 100cm2 size (in 145mm Petri dish). Therefore, the proposed illumination system must be flexible in test dimensions to fulfill different sizes of hiAM cell culture samples in both types of platforms.

The hiAM models are only active in biological temperatures, or 37°C environment, during culturing, storage, and analysis. Therefore, the illumination system should keep the temperature environment stable at body temperature without creating extra heat or cold sources.

The progression of the research from initial in-vitro experiments using well plates to potential in-vivo or ex-vivo applications is expected. Therefore, forward-thinking and preparation in the illumination system physical layout design should include the possibility of transferability of implanting the setup inside the body of large test subjects such as swine or humans.

Light pattern and local illumination

The hiAM optogenetics AF treatment experiments require illumination techniques that can target specific areas of the cell culture with precision. The illumination patterns are programmed to be highly adaptable, for the diverse needs of these experiments. For instance, point illumination is needed at selected locations within the cell culture to generate pacing signals and to initiate and analyze the propagation of electrical signal waves across the cell culture. Another use case is line-shaped illumination between selected points, which serves to create a depolarized barrier to block the propagation of arrhythmic activities or rotating signals of the cell culture. Additionally, a global illumination that covers the entire cell culture provides efficient global termination of any cellular activity. This proposes that the light source should be capable of producing a matrix of point light pixels, or it could be a type of projector that can cast a pixelized image onto the target cell culture.

Pixel dimensions

hiAM atrial arrhythmia models are successfully presented in different scales of cell cultures, but the minimum element of the cell culture shares similar dimensions. A sarcomere, the smallest functional unit of muscle tissue in hiAM cell cultures, has an approximate length of 1.8 um. Theoretically, for the most precise ontogenetically control over the hiAM cell culture, the pixel size of the illumination system should ideally match

the size of a single sarcomere. However, this level of precision is not necessary for the initial demonstrator version of the system due to several practical considerations.

Firstly, stimulating a single sarcomere is unlikely to be effective for pacing or terminating arrhythmia signals, which typically requires the cooperation of multiple sarcomeres, often in the hundreds, suggesting that a minimum control pixel size in the level of 500 micrometers would be more appropriate and practical. Moreover, creating an illumination system with such minute pixel sizes has high technical challenges. It would involve complex, high-precision technology that could escalate the costs and risks associated.

For the initial proof-of-concept system discussed in this chapter, it is more practical to start with a simpler, available, and lower-risk solution to test the concept. The pixel size has been set at 2 mm, which is much larger than the sarcomere size. However, it still provides the capability for testing optogenetics features such as pacing, blocking, and global termination of AF in the hiAM model in 6-well plates and Petri dish conditions. This decision is to compromise a balance between the need for experimental functionality and the feasibility of the system's design, especially for the system for initial proof-of-concept purposes.

Consistency and safety

Each session of the experiment is expected to last for at least 30 minutes. The illumination system's design and functionality are integral to the success of the experiments. Constant light distribution and intensity with all high-power LEDs with the same specifications, while characteristics keep consistency over experimental reproductions over time.

While the illumination system is not in direct contact with biological tissues or implanted within the body, it's still crucial to incorporate basic safety functions into its design. Given the laboratory environment and the nature of cell culture work, the system might occasionally be exposed to water droplets, especially during the exchange of well plates or the handling of liquid samples. Therefore, the system should be designed to be resistant to such water exposure. This could involve waterproof coatings or protective layers to prevent water ingress that could damage the electronics system or affect its performance.

The illumination system must be designed to avoid any electrical leakage. Electrical leakage can not only pose a safety hazard but also interfere with the experimental measurements, leading to artifacts or inaccurate results. This prevention can be achieved through proper insulation of electrical components, careful circuit design, and the use

of materials that provide good electrical isolation.

Control and driver interface

The transition from the simpler illumination systems used in rat or swine models to the system for the hiAM AF model increases greatly in technical complexity and operational demands. Unlike the previous devices where the illumination could be simply controlled on or off using pulse signals, the new system needs to handle patterns consisting of several hundred pixels. Moreover, these patterns must be capable of rapidly changing in response to an algorithm running on a PC. The system requires the integration of fast operational electronics for rapid signal processing, and a high-speed and reliable communication link between the illumination system and the PC user interface to transfer the pattern information. The performance can be measured by refresh rate, which indicates how quickly the illumination pattern can be changed or updated. The total refresh rate specification can be determined by communication speed, control logic operation speed, and light element switching dynamics. By analyzing the biological dynamics of the hiAM AF models, a reference value of 60ms refresh rate of each light pattern is proposed. This rapid refresh rate is determined by the biological characteristics of the light-sensitive ion-channel switching time.

The software interface must be equally powerful for processing and user-friendly for ease of operation by the experiment operators. For future in-vivo or ex-vivo applications, the driver part would also need to be designed for implantation, focusing on miniaturization, (wireless) power management, and ensuring stable operation within a biological environment.

Scalability and flexibility

A modular design of both hardware and software of the illumination system is statically important for the proof-of-concept demonstrating purpose, particularly when considering future developments that might require a larger matrix with more pixels, higher light power, or faster communication speed. A modular design offers flexibility and scalability, that independent functions or units can be easily added, removed, or replaced without interference or replacement of other parts. The system should allow the expansion of the pixel matrix without the need for completely redesigning. As research demands grow or change, additional modules can be integrated to increase the number of pixels or to enhance other capabilities like resolution or pattern complexity.

5.3. SYSTEM ARCHITECTURE DESIGN

5.3.1. PROPOSALS OF THE ILLUMINATION SYSTEM DESIGN

Following above discussed requirements for the optogenetics hiAM AF model research, two design proposals are given: the Top Projector and the Bottom Illuminating Matrix (Figure 5.3). The primary difference between these two approaches is the orientation of the light source relative to the cell culture. In the Top Projector design, the light is directed downwards, emanating from above the cell culture. In the Bottom Illuminating Matrix design, the light source is positioned underneath the cell culture, illuminating upwards.

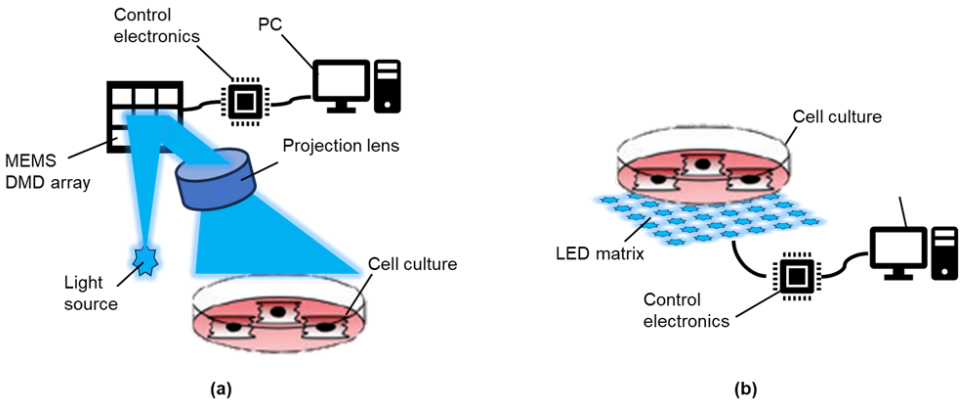

Figure 5.3: Proposed illumination system designs: (a) Top Projector setup and (b) Bottom Illuminating Matrix setup

This difference in light source orientation significantly influences the physical layout and implementation strategy of each design. The Top Projector setup would develop a system that can effectively project light onto the cell culture from above, which involves considerations for positioning, angling, and ensuring even light distribution across the cell culture surface. It might also require mechanisms to avoid obstructions and shadows that could interfere with uniform illumination.

On the other hand, the Bottom Illuminating Matrix design would involve embedding an array of LEDs beneath the cell culture. This arrangement demands careful planning to ensure that the light can penetrate through the bottom of the culture container (well plate or Petri dish). Additionally, this setup would need to account for heat dissipation, as the heat of the high-power LEDs to the cell culture could potentially impact the temperature of the environment.

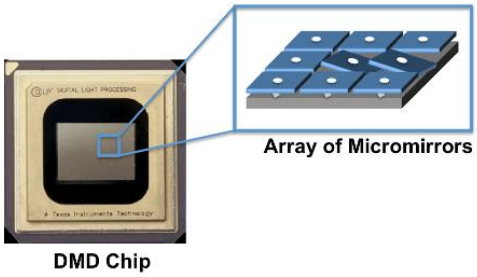

Figure 5.4: A commercial Digital Micromirror Device chip[8]

Top Projector

The Top Projector setup, designed for illuminating the cell culture from above, is proposed to use a Micro-Electro-Mechanical Systems (MEMS) Digital Micromirror Device (DMD) array to achieve dynamic patterning in the projected light (Figure 5.4). This technology is key in allowing precise control over the light patterns cast onto the cell culture, which is seen in other researches[5][6][7]. A MEMS DMD array consists of thousands of tiny mirrors, each capable of tilting independently. By controlling the orientation of these mirrors, the DMD can create complex light patterns with high spatial resolution. This technology has found its significant application in modern projector systems. In these systems, the MEMS DMD acts as a sophisticated light modulator to control the intensity of each pixel to create dynamic images or videos. MEMS DMD projectors are capable of producing images with very high resolution (HD) and excellent image quality.

In the Top Projector setup, similar to a projector system, the DMD array receives the high-power light from a single light source and manipulates the light direction per pixel to generate the desired illumination patterns over the targeted cell culture. This approach offers the flexibility to quickly and accurately change projected patterns with extremely high resolutions.

The Top Projector setup comes with challenges and considerations from the complexity and precision required between its components. A DMD requires specialized control and driver electronics to manage the rapid and precise movements of its numerous micro-mirrors. Developing or integrating these control systems can be complex and costly. In addition to the DMD, projecting optics are necessary to magnify and focus the light onto the surface of the cell culture. Designing and integrating the appropriate optics system adds another layer of complexity. The accurate alignment of the light source, the DMD device, the projecting optics, and the target is also critical. Accurate optical design, in the scale of mm, is required to ensure that the light is in focus and that the patterns projected are free from distortion. Any misalignment can lead to unfocused

light and distorted patterns, which gives the experimental setup additional practical challenges.

Moreover, in the setup for hiAM experiments, an optical mapping setup is positioned above the cell culture for continuous monitoring of the optical-electrical signal. The placement of the projecting optics can be very challenging as it can potentially interfere with the optical mapping system, leading to shadows or reflections.

Bottom Illuminating Matrix

The Bottom Illuminating Matrix design presents a structurally simpler alternative for the optogenetics hiAM experiment setup compared to the Top Projector design. This design consists of a light source matrix, which is typically made up of an array of LED chips. This approach is seen in other optogenetics research[9][10][11]. The complexity and capability of this matrix can vary greatly, ranging from a few hundred to thousands or even millions of LEDs, depending on the technological capabilities and the requirements of the experiment.

The matrix is positioned directly under the container holding the hiAM cell culture. This placement ensures that the light from the LEDs effectively reaches the cell culture. For the light from the LED matrix to penetrate the cell culture, the bottom of the container must be transparent to the wavelength of light being projected. With its direct emission of the light source towards the cell cultures, this proposal also promises relatively higher light irradiance compared to setups where the light source is more distant or indirect.

The matrix can dynamically change the light patterns with the controlling electronics, allowing for the modulation of light patterns in response. The pattern resolution and the refresh rate depend on the illumination technology used for the matrix.

The implementation of the Bottom Illuminating Matrix design can be supported by existing technologies commonly used in high-brightness displays and billboards. This similarity in principle between the LED matrix needed for the Bottom Illuminating Matrix design and the technology used in modern displays offers several advantages for simple and effective implementation, including available hardware solutions or software packages. Similar components can be found in general mass production, making them more accessible and potentially more cost-effective.

Both designs offer unique advantages and challenges, yet The Bottom Illuminating Matrix proposal is selected for the illumination system design in hiAM optogenetics experiments.

The Top Projector with MEMS DMD device projection system offers advanced capabilities for controlling light patterns, but the complexities involved in its design, cost, and implementation present substantial challenges that need to be carefully considered. The Bottom Illuminating Matrix could potentially provide more direct and uniform illumination with more simplicity, ease of implementation, and enhanced control over light patterns making it an ideal fit for the requirements.

Another reason for choosing the Bottom Illuminating Matrix design over the Top Projector design is its similarity in hardware and software design methodology to the LED devices previously used in rat and swine model experiments. This helps fast development of the new system in the experiments.

5.3.2. LED MATRIX INTERCONNECT LAYOUT

Controlling an LED matrix to produce dynamic patterns comes with challenges, which require a trade-off balance among various factors. These include for example the complexity of interconnects and routing, the scale of the driver electronics, overall efficiency in terms of the matrix's light intensity, and power consumption, etc. For the Bottom Illuminating Matrix device as discussed in the previous section for use in the proof-of-concept demonstrator for hiAM optogenetics research, three different control options have been proposed (Figure 5.5).

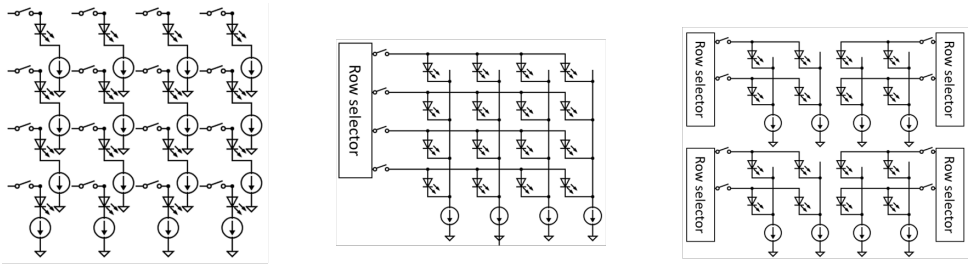

(a) Option 1 (b) Option 2 (c) Option 3

Figure 5.5: Three LED matrix interconnect layout proposals

The first option involves the most complex approach, offering individual control over each LED element. This method allows for the highest flexibility and precision in pattern creation but also involves the most intricate wiring and control mechanisms. The second option largely simplifies the control mechanism by employing a row-column scanning approach to reduce wiring and control complexity. An intermediate, hybrid zone scanning solution combines the concepts of both the individual control and row-

column scanning options by splitting the matrix into a few zones, with scanning control over the LEDs within each zone.

The key parameters and considerations for these three proposals are estimated in a trade Table 5.1. This table provides a clear comparison of the complexities, efficiencies, and power consumption characteristics of each control option, aiding in the decision-making process.

Table 5.1: Key parameters trade table of three proposed matrix interconnect layout options

	Option 1	Option 2	Option 3
	N*N LED array Individual control	N*N LED array Row-column scanning	N*N LED array Scanning in M*M zones
No. of interconnects	2*N*N (or N*N+1 for common ground)	2N	2N*M
No. of current sources (column)	N*N	N	N*M
No. of scanning channels (row)	N*N	N	N*M
Total irradiance	1	1/N	M/N
Power & heat	1	1/N	M/N
Complexity in layout	High	Low	Medium

Option 1: Individual control of each LED element

Individual control over each LED element in an LED matrix is theoretically the optimal solution for precision and flexibility in pattern generation. This approach allows for the finest control over the light pattern, as each LED can be independently managed in intensity. There's no risk of flickering the pattern due to scanning, and all elements can be simultaneously switched on if required. This allows the highest possible maximum irradiance, given that the duty time of each LED element is theoretically as high as 100%.

However, this method comes with significant drawbacks due to its extremely high complexity. The matrix requires a very complex control system, with a separate current source for each LED element. This means that if the matrix consists of at least a couple of hundreds of LEDs, the control system must be able to individually manage the same amount of current sources, which is also practically difficult in the physical layout of the control electronics. Furthermore, each LED requires two wires, one for the anode and one for the cathode, all directly connecting to the corresponding current source. This significantly increases the complexity of wiring and routing of the matrix panel, espe-

cially when dealing with a matrix where the LEDs are spaced closely together. In such a scenario, managing and organizing these wires without causing short circuits or signal interference becomes a great challenge to the design and manufacturing techniques.

Option 2: Raw-column scanning control through LED matrix

The Row-column scanning method for an LED matrix is commonly used in the control logic of display technology. This approach offers a more simplified solution compared to individual LED element control. The scanning electronics scans through the entire matrix, activating only one row at a time. A set of current sources, corresponding in number to the columns of the matrix, controls the LEDs in the currently scanned row. After one row is illuminated, the scan progresses to the next row in sequence.

The scanning speed in this method can be fast, typically reaching a few thousand times per second (kHz scanning). This speed is critical to determine that the LED pattern remains perceptible to both human observation and the target ion channels, where the response times for opening and closing, and the scanning speed must be compatible to avoid the flickering effect. This is because even though the illumination might appear uniform to the human eye over time, there are transient moments during the scanning process when the light distribution is not uniform due to only 1 row being active at any moment. This flickering can impact the consistency of the stimulation provided to the ion channels, particularly in scenarios where uniform and continuous light exposure is necessary.

This row-column scanning approach also comes with another disadvantage the maximum irradiance achievable by the matrix is only a fraction of the total number of rows. This is because at any given moment only the LEDs in a single row are active, reducing the overall light output compared to a scenario where all LEDs could be on simultaneously such as in an individual controlled matrix.

Option 3: Scanning through multiple zones (intermediate solution)

In the intermediate solution for controlling the LED matrix, the design merges concepts of both the individual control and row-column scanning methods. The full LED matrix is split into several symmetrical and identical zones. Within these zones, a scanning method similar to row-column scanning is used, but unlike full matrix scanning, each zone is independently controlled by its own set of electronics. This hybrid approach reduces the complexity of wiring and electronics compared to controlling each LED individually across the entire matrix. While the scanning within each zone may still produce some degree of flickering, the independent control of smaller zones can reduce

this effect and increase the averaged irradiance. This intermediate solution thus offers a more balanced approach, combining the advantages of both individual LED control and row-column scanning, making it a practical option for managing complex light patterns of an LED matrix, especially when the scale of the matrix becomes larger.

The second option, Row-column scanning control proposal is determined for the demonstrator for hiAM optogenetics research, to balance the complexity of the system with the functional needs of the research. This method offers a practical and efficient way to control the light patterns, which is important for the proof-of-concept demonstrator (16x16 matrix) to implement and manage the system simply and reliably. While it may not offer the same level of precision as individual LED control, the Row-column scanning method provides sufficient irradiance for the activation. The detailed estimation of optical irradiance is discussed in the following section. This method also tends to be more energy-efficient and cost-effective.

Following a successful proof-of-concept with the row-column scanning method, there are plans to enhance the matrix for more precise control for further applications and research on the hiAM optogenetics. This will involve reducing the LED element size, increasing the number of LED elements, and potentially expanding the total matrix size. As these enhancements make the Row-column method insufficient for lower irradiance and worse flickering effects, the focus will shift to the hybrid zone control design. This method, which can be introduced by the experiences of the initial demonstrator, offers a better balanced and practical solution, marking a natural progression in the project's evolution.

5.4. LED IRRADIANCE PATTERN ANALYSIS

In the proposed optogenetic experimental setup, achieving a uniform light distribution is essential, especially when activating polarization or depolarization ion channels for blocking or termination of arrhythmia signals. This uniformity requires a certain level of light energy, with irradiance larger than 0.3mW/mm^2, a reference design specification from a preliminary study. Ideally, the LED matrix design should function similarly to a panel light source, ensuring that the light intensity is evenly spread across the target exposure surface.

The LED matrix is composed of multiple (a couple of hundred) LED chips, each contributing to the overall light pattern. Given that the illuminated area created by the LEDs is significantly smaller than the scale at which it is measured, a single LED chip can effectively be treated as a point light source with a specific viewing angle.

However, achieving a perfectly uniform exposure, similar to what a panel light source would provide, is challenging due to the nature of point light sources. Despite this, through the optimized layout design of the point light matrix, a solution that closely approximates this ideal uniformity is achieved. This involves light intensity pattern analysis from a single LED chip, and a layout analysis of the matrix elements to maximize the homogeneity of light distribution across the target area, ensuring effective and consistent

5.4.1. SINGLE LED CHIP

This section analyzes the intensity pattern of a single LED chip. The selected LED chip from the LUMILEDS LXZ1 series has typical illumination pattern specifications to represent the most common high-power, surface-mount LEDs with phosphor conversion (Figure 5.6). The intensity pattern is defined as the relative light intensity (radiant energy per area) in percentage, against the angle of viewing at an imaginary sphere with a fixed distance (R) to the light source (Figure 5.7). The significant parameter in LED specification, viewing angle, is defined as the maximal angle of viewing to obtain more than 50% relative light intensity.

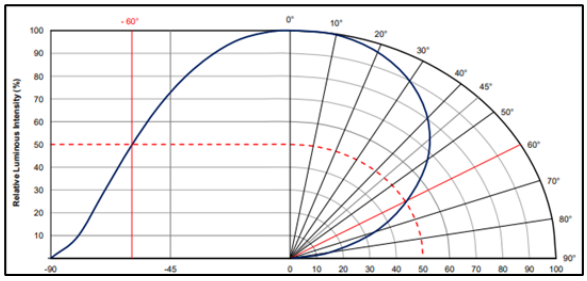

Figure 5.6: Light distribution of a high-power LED from the datasheet. The viewing angle $2\theta = 120\,\text{deg}$

Mathematically, the intensity pattern of an LED chip is described as a sum of Gaussian or cosine-power functions for the major portion of the full viewing angle. The numerical model can be fitted from the radiation patterns from the manufacturer's datasheet. Here a cosine-power model (Figure 5.8) is used to analyze the theoretical intensity distribution since the model has sufficiently good fits with the provided data from the specification document:

$$I_{norm}(\theta) = cos^n(\theta) \tag{5.1}$$

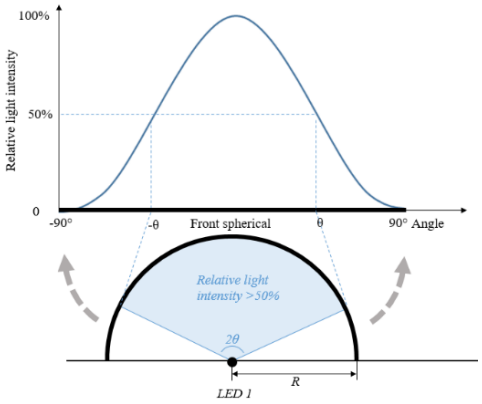

Figure 5.7: Intensity pattern measured at an imaginary sphere with a fixed distance

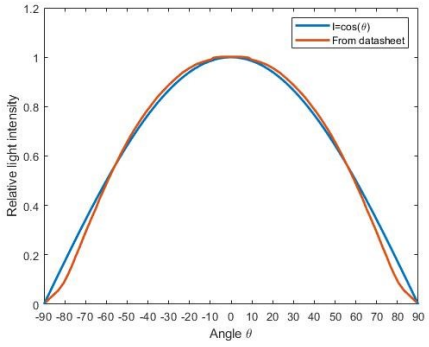

Figure 5.8: Fitting the light distribution pattern with a cosine model

Defining I_R as the relative light intensity which normalized the maximum intensity I_{max} at the fixed radius of R, and θ is the angle of viewing, the power coefficient n is determined from curve fitting of the measured result or factory datasheet. In this case, n=1 can well fit the curve from the datasheet for simplification. Therefore, the actual light intensity pattern $I_R(\theta)$ at the fixed radius of R is:

$$I_R(\theta) = I_{max} I_{norm}(\theta) = I_{max} cos(\theta) \tag{5.2}$$

The intensity pattern is measured at the front half of the illumination sphere with a certain distance R. The intensity of light radiating from the LED light point source is inversely proportional to the square of the distance from the source, also called inverse-square law. Thus, the intensity I at any point, whose direct distance to the light source is

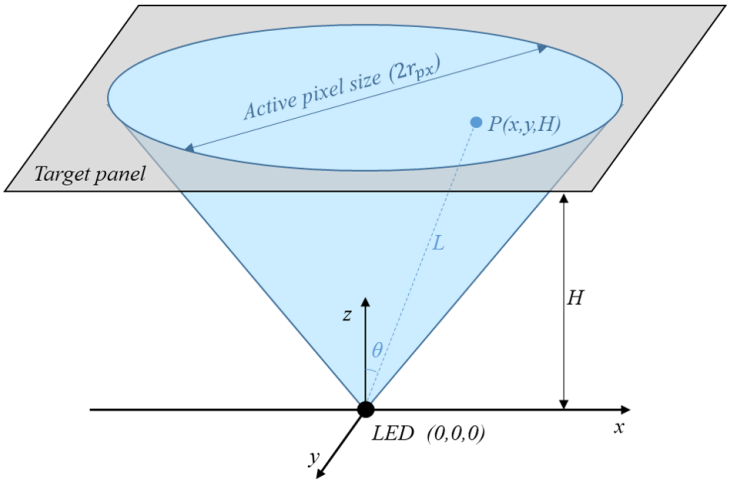

Figure 5.9: Light projecting distribution on the plane in front of the LED source

L, can be described as the equation:

$$I(\theta) = I_R(\theta)(\frac{R}{L})^2 \tag{5.3}$$

For any point $P(x, y, H)$ at a fixed infinitive flat plane (Figure 5.9) with the vertical distance H, and establish an x-y coordinate where the light source is placed at the origin point, the light intensity at the panel can be described as the functions:

$$cos^2\theta = \frac{H^2}{x^2 + y^2 + H^2} \tag{5.4}$$

$$I(x, y) = I_R(x, y)\frac{H^2}{x^2 + y^2 + H^2} = I_{max}cos(\theta)\frac{H^2}{x^2 + y^2 + H^2} = I_{max}\frac{H^3}{(x^2 + y^2 + H^2)^{\frac{3}{2}}} \tag{5.5}$$

PL is the total light power emitted from the LED, which is the surface integral volume below the intensity curve, and is described as equations:

$$P_L = \iint_{-\infty}^{+\infty} I(x, y)dxdy = I_{max}H^3 \iint_{-\infty}^{+\infty} \frac{1}{(x^2 + y^2 + H^2)^{\frac{3}{2}}}dxdy = I_{max} \cdot 2\pi H^2 \tag{5.6}$$

Finally, the light intensity pattern at the flat panel with distance H to the LED light source can be described as below function:

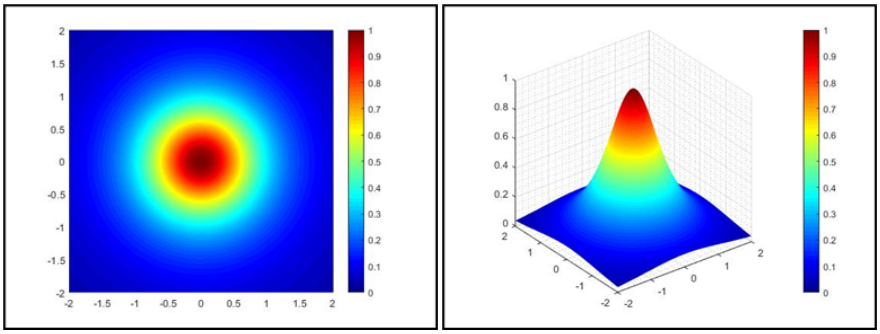

(a) 2D plotting of a 'hot-spot' (b) 3D plotting of a 'cone'

Figure 5.10: Simulated maps of single LED light intensity pattern at a target panel with distance to the light source H=1

$$I(x,y) = \frac{P_L H}{2\pi(x^2+y^2+H^2)^{\frac{3}{2}}} \tag{5.7}$$

The above function has a "cone" shape if plotted in the 3D coordinates (Figure 5.10b. If defining an "active pixel" as the circular area where the light intensity is more than 50% of the maximum value, the radius of the active pixel r_{px} is calculated via the equation:

$$I(r_{px},0) = 0.5 \times I(0,0) \rightarrow \frac{4}{(r_{px}^2+H^2)^3} = \frac{1}{H^6} \tag{5.8}$$

$$r_{px} = \sqrt{\sqrt[3]{4}-1} \times H = 0.7664H \tag{5.9}$$

or

$$H = 1.3048 r_{px} \tag{5.10}$$

5.4.2. LEDS IN A LINE LAYOUT

The light intensity model derived from the previous section is fundamental in predicting the distribution of light intensity when the number of LED chips is increased to form a line layout. In configurations where multiple LED chips are arranged in a single line with uniform intervals (D), the resulting light intensity pattern can be visualized as the sum effect of several overlapping 'cone' shaped patterns from single chip distribution. As illustrated in Figure 5.11, the pattern of light intensity at a certain height (H) above the LEDs is a function of spacing (D) between each LED chip.

In a simulated scenario with 16 LED chips arranged linearly, each separated by a

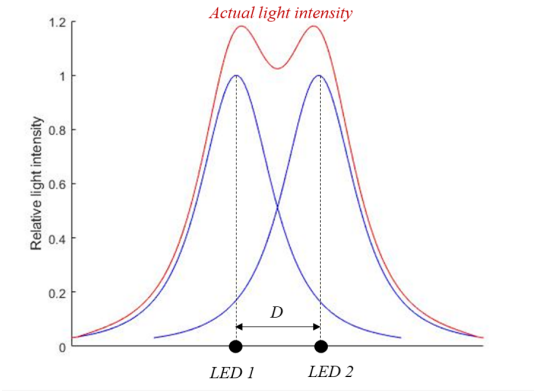

(a) 2D plotting

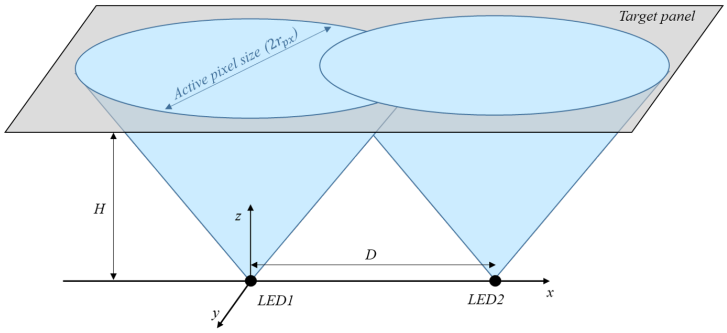

(b) 3D plotting

Figure 5.11: The light intensity pattern is the sum of two “cone” curves by two LED light sources with a distance of D.

distance D is described as a function of H, the height of the measuring panel above the light sources, D=n*H. To remove edge effects resulting from the finite number of LEDs, the area of the outside three LED chips at both ends is excluded from calculations of average intensity and standard deviation.

The multiplier n serves to normalize the distance D about the projecting height H. When n is close to zero, the LED chips’ light patterns overlap significantly and behave as a one-point light source. Whereas at higher values of n (e.g., n=3), the overlap decreases, reducing the interference between adjacent LEDs, and behaving as multiple individual light systems. The simulation results demonstrate that the uniformity of the actual light intensity pattern is highly dependent on the spacing between each LED chip. Figure 5.12 shows the accumulated light pattern distribution with the 16 LED simulation.

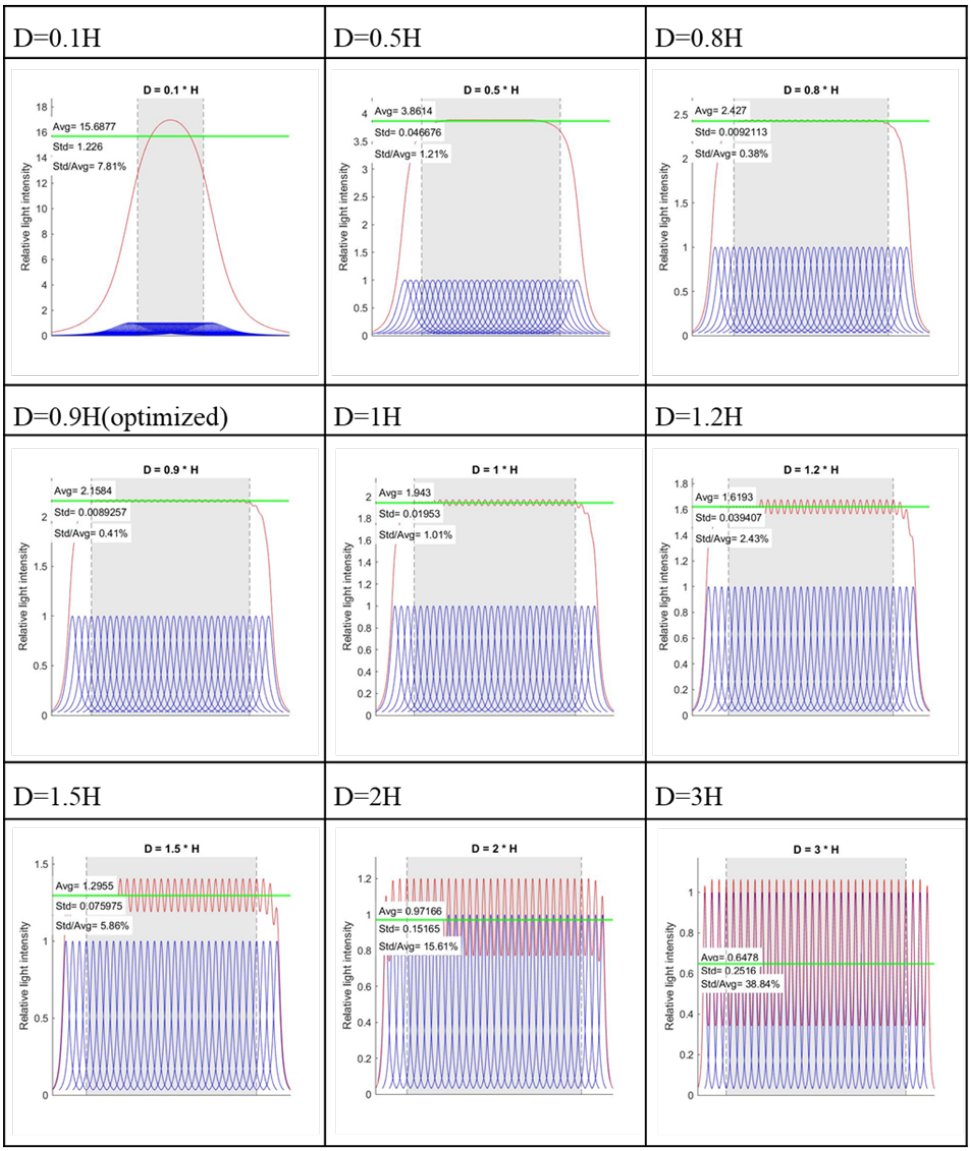

Figure 5.12: 2D-Simulation of the actual light intensity pattern of 16 LED chips lining up in a line with a fixed interval of D=n*H, where H is the measuring panel above the light sources. The average intensity and standard deviation are calculated from the data in the gray range to eliminate the edge effects of limited LED amount

The intensity standard deviation (Std), relative standard deviation (Std/Avg), and relative light intensity variation (Max-Min/Avg) are calculated for the overall light intensity,

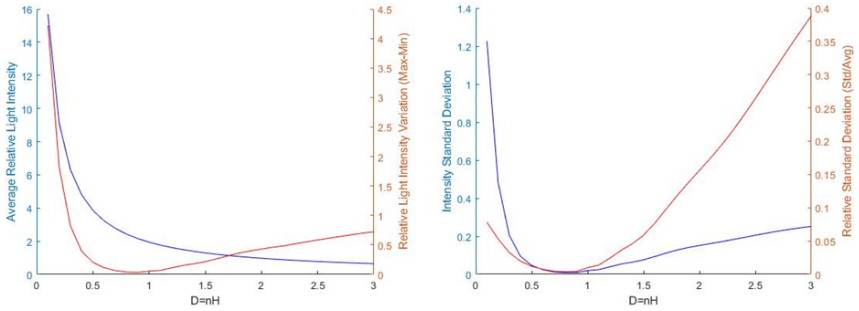

(a) Average intensity (A.U.) and intensity delta (A.U.)

(b) intensity standard deviation and relative standard deviation

Figure 5.13: The parameters to evaluate the light uniformity in simulated 16 LEDs with interval distance of D=nH. The most uniform intensity distribution is found near D=0.9H

to evaluate the uniformity of the light pattern. The calculated parameters first drop before n=0.9, indicating a more uniform pattern, and increase when after n=0.9, indicating a less uniform pattern (Figure 5.13). The optimized ratio between LED intervals and the projecting distance is therefore found near n = 0.9, to achieve the relatively best homogeneous intensity at the target range.

5.4.3. LED IN A MATRIX LAYOUT

The earlier discussions, while focused on 2-dimensional line layout models, offer valuable insights that can be extended to 3-dimensional matrix layout simulations. The layout of these arrays is critical in achieving the desired light distribution, and different layout configurations can lead to different characteristics. Two specific LED matrix layouts are explored in this section for light intensity pattern analysis and compared with their properties: checkerboard layout and equilateral layout

In the first simulated layout proposal, an LED matrix consisting of 16x16 elements arranged in a **checkerboard layout** (Figure 5.14a). In this configuration, both the row and column intervals are set at D=n*H, where H represents the projecting height of the measuring panel above the light sources. To remove the edge effects due to the finite number of LEDs, the areas at the first and last rows or columns are excluded from the calculations of average intensity and standard deviation.

The multiplier n serves to normalize the distance D about the projecting height H. When n is close to zero, the LED chips' light patterns overlap significantly and behave as one large point light source. Whereas at higher values of n (e.g., n=3), the overlap

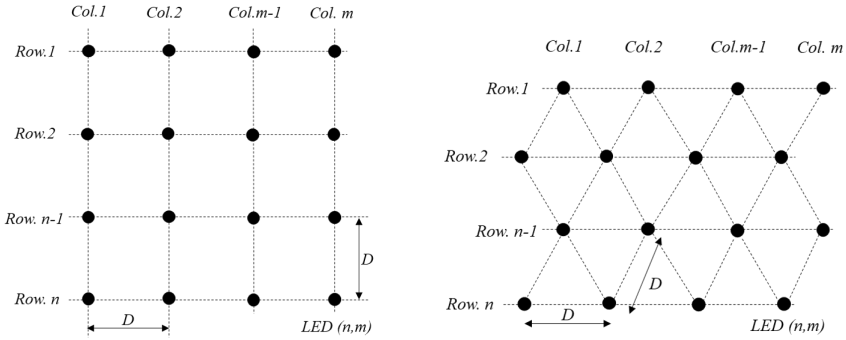

(a) Checkerboard layout (b) Equilateral layout

Figure 5.14: Two layout options for the LED matrix elements

5

decreases, reducing the interference between adjacent LEDs, and behaving as multiple individual light systems.

Simulation results indicate that the uniformity of the light intensity pattern across the LED matrix is strongly determined by the interval distance between each LED chip. The intensity standard deviation (Std), relative standard deviation (Std/Avg), and relative light intensity variation (Max-Min/Avg) are calculated for the overall light intensity, to evaluate the uniformity of the light pattern. The calculated parameters first drop before n=1.1, indicating a more uniform pattern, and increase when after n=1.1, indicating a less uniform pattern. The optimized ratio between LED intervals and the projecting distance is therefore found near n = 1.1, to achieve the relatively best homogeneous intensity at the target plane for the checkerboard layout.

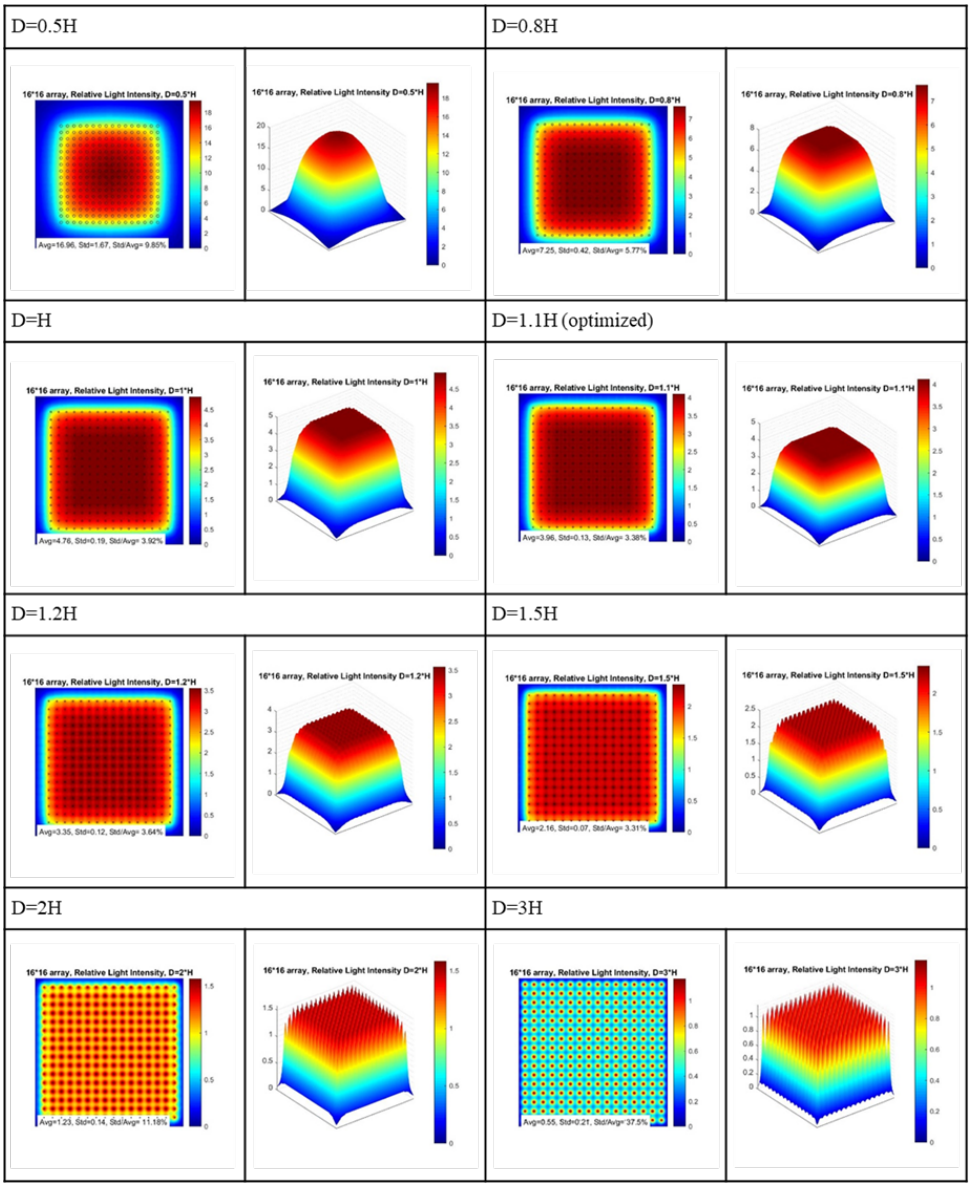

Figure 5.15: Simulation of the actual light intensity pattern of an LED array of 16x16 elements in the **checkerboard layout** with fixed row and column interval of D=n*H, where H is the measuring panel above the light sources

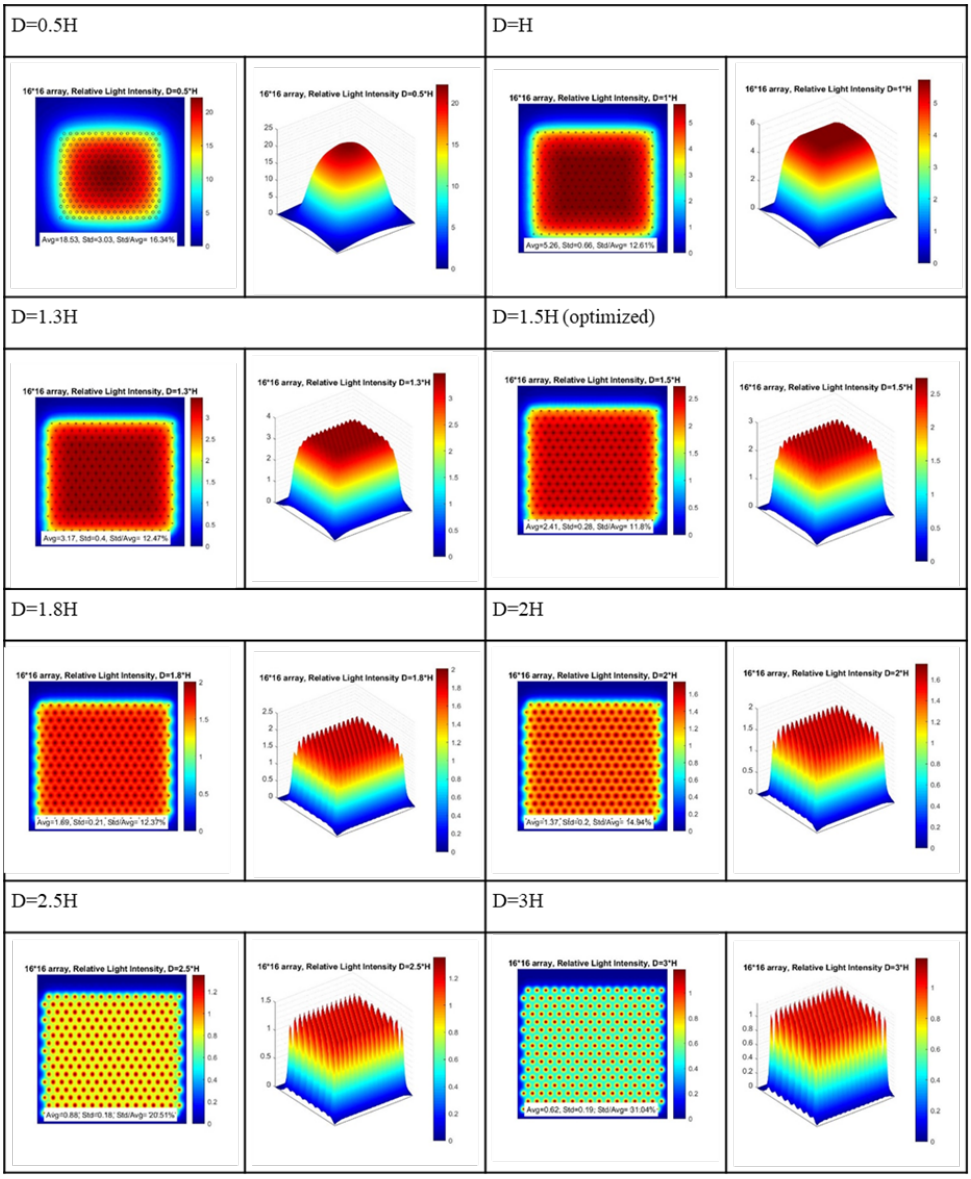

Figure 5.16: Simulation of the actual light intensity pattern of an LED array of 16x16 elements in the **equilateral layout** with fixed row and column interval of D=n*H, where H is the measuring panel above the light sources

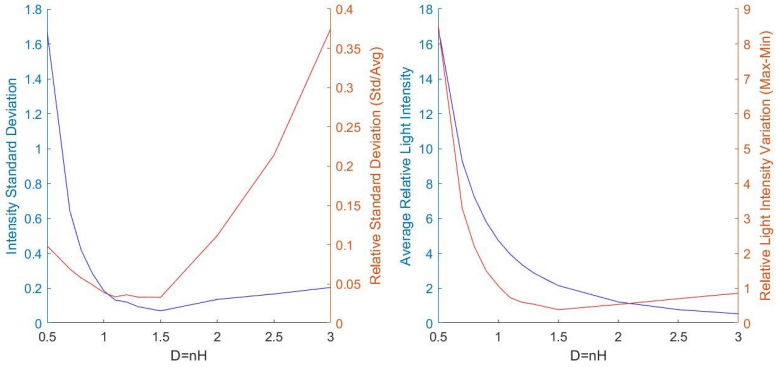

(a) Average intensity (A.U.) and intensity delta (A.U.)

(b) intensity standard deviation and relative standard deviation

Figure 5.17: The parameters to evaluate the light uniformity in simulated 16x16 LEDs in **checkerboard layout** with interval distance of D=nH. The most uniform intensity distribution is found near D=1.1H

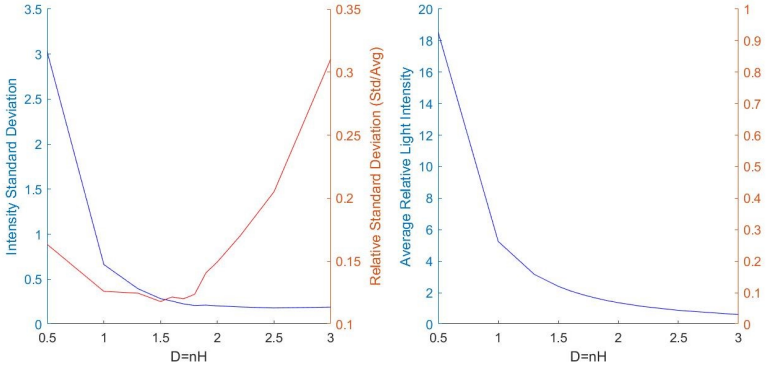

(a) Average intensity (A.U.) and intensity delta (A.U.)

(b) intensity standard deviation and relative standard deviation

Figure 5.18: The parameters to evaluate the light uniformity in simulated 16x16 LEDs in **equilateral layout** with interval distance of D=nH. The most uniform intensity distribution is found near D=1.5H

In the second proposal of matrix layout design, the 16x16 LED elements are positioned in an **equilateral layout** (Figure 5.14b), where each LED is equidistant from its neighboring LEDs, both in rows and columns, with intervals set at D=n*H. H represents the projecting height of the measuring panel above the light sources. The equilateral ar-

rangement typically results in a more symmetric pattern of light distribution compared to the checkerboard arrangement. A similar simulation is applied to the equilateral layout of an LED matrix of 16x16 elements (Figure 5.16).

The calculated parameters first drop before n=1.5, indicating a more uniform pattern, and increase after n=1.5, indicating a less uniform pattern. The optimized ratio between LED intervals and the projecting distance is found near n = 1.5, to achieve the relatively best homogeneous intensity at the target plane for equilateral layout.

The decision is made for the illumination system to be designed for the hiAM AF model experiments that the LED matrix will use an equilateral layout. Choosing an equilateral layout over a checkerboard layout has several advantages, particularly in terms of design simplicity and manufacturing feasibility. When considering the same projection distance, the equilateral layout allows for a (1.5/1.1-1.1 = 36%) larger optimized interval between each LED element to achieve the most uniform illumination. With increased space between the elements in an equilateral layout, the design of the LED matrix becomes less complex. This additional space simplifies the manufacturing process, as it reduces the fabrication constraints and challenges associated with placing components very close to each other, therefore potentially reducing manufacturing costs. More space between LED elements also eases the wire routing, which can be challenging in a dense matrix without causing interference or short circuits. The larger interval between LEDs in an equilateral layout also contributes to better thermal dissipation to increase system stability and reliability.

5.4.4. LED MATRIX DESIGN IN THE ILLUMINATION SYSTEM

Combining all the above calculations and pattern distribution modeling, the expected optical parameters of the proposed LED matrix illumination system with 16x16 LXZ1-PB01 Blue LEDs in an equilateral layout can be discussed.

In the expected experimental setup, the hiAM AF model cell culture is presented at the bottom of each well of a standard 6-well plate (Costar 6-well plate, Corning, USA). According to the provided datasheet, the thickness of the well bottom is specified as 1.27mm. Additionally, there is a need for an extra layer on top of the LED, serving dual purposes of electrical encapsulation and thermal conduction. This layer is anticipated to have a thickness in the range of 0.4 to 0.5mm. Therefore, the projecting distance is determined from the LED to the target surface:

$$H = 1.73mm \tag{5.11}$$

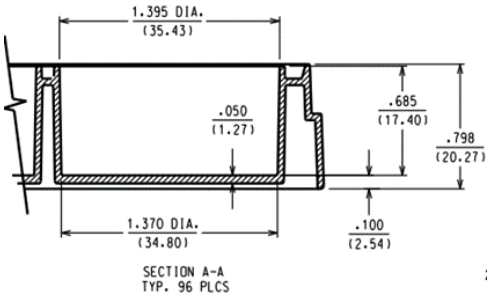

Figure 5.19: Corning Costar 6-well plate datasheet, the thickness of the well bottom wall is 1.27 mm [12]

Following the most critical parameter of the design, other design parameters are calculated based on previous discussions and calculations:

Optimal intervals between each LED element in the equilateral layout for best uniformity:

$$D = 1.5 \times H = 2.60mm \tag{5.12}$$

Diameter of each pixel (the initial requirement of less than 2mm):

$$2r_{px} = 0.7664 \times H = 1.32mm \tag{5.13}$$

With a 16x16 equilateral layout matrix, the effective illumination area:

$$L = 2.60 \times 16 = 41.6mm \tag{5.14}$$

$$W = 2.60 \times 16 \times \frac{\sqrt{3}}{2} = 36.0mm \tag{5.15}$$

$$AREA = L \times W = 1498.7mm^2 \tag{5.16}$$

The irradiance of the device is estimated by the total radiant power characterized in Chapter 3 since the same LED chips are used, and divided by the area of the matrix. The pixel irradiance (only one LED in the matrix is switched on) is calculated by the peak-to-average factors from the optical simulations.

By the row-scanning way of control, only one row out of the total number of rows is emitting radiant power at any given moment. Since not all LEDs in the matrix are on simultaneously, but rather sequentially by row, the total radiant power emitted at any

instant is calculated by a fraction of several rows. Therefore,

Maximum average irradiance of LED matrix area @1000mA:

$$I_{matrix} = \frac{676mW \times 256}{16 \times 41.6 \times 36mm^2} = 7.22mW/mm^2 \tag{5.17}$$

Maximum average irradiance of each pixel @1000mA:

$$I_{pixel} = I_{matrix}/2.41 = 2.99mW/mm^2 \tag{5.18}$$

Reduced average irradiance of LED matrix area @100mA:

$$I_{matrix} = \frac{104mW \times 256}{16 \times 41.6 \times 36mm^2} = 1.11mW/mm^2 \tag{5.19}$$

Reduce the average irradiance of each pixel @100mA:

$$I_{pixel} = I_{matrix}/2.41 = 0.46mW/mm^2 \tag{5.20}$$

Note these theoretical irradiance values of the LED matrix significantly surpass the minimum requirements even with a reduced current output of 100mA. However, this excess in theoretical irradiance offers greater flexibility in adjusting the system's output power, accommodating a broad range of experimental conditions. It also provides a valuable margin to account for operational variations that might lower the actual irradiance. Such variations could include the control logic changes (higher refresh rate). Additionally, the duty cycle of the LEDs, including the on and off time of the chip, can influence the actual irradiance. The higher theoretical values, therefore, ensure that even with these reductions, the system can still deliver the necessary light intensity for effective optogenetic experiments. The system is characterized and measured after implementation

5.5. LED MATRIX SUBSYSTEM FABRICATION AND INTEGRATION

The same high-power LED chip, LUMILEDS LXZ1 PB01 Blue 470nm, is selected for the matrix in this chapter of work as a continuity in the choice of hardware. This consistency can offer several advantages, such as familiarity with the LED's performance characteristics, ease of integration into the existing system, and potential reuse of hardware and software. By using a known and tested component, existing knowledge and experience contribute to a more efficient and effective development process.

Layout design (Figure 5.20) is based on the previously discussed equilateral layout

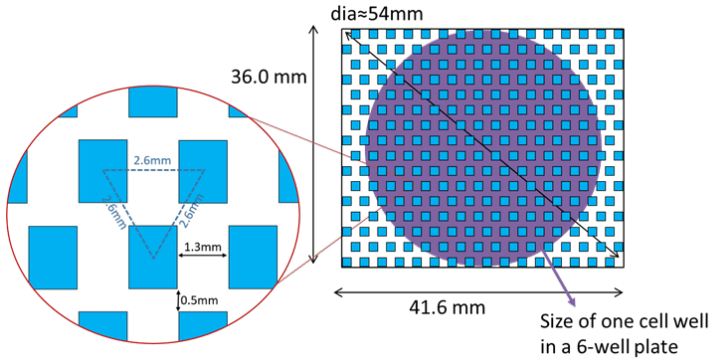

Figure 5.20: Layout of the 16x16 LED matrix with equilateral layout matrix and D=2.6mm interval. The matrix can cover the bottom of one cell well in a 6-well plate

matrix with D=2.6mm interval and implemented to the PCB design on computer-assisted software. Then the design files are sent to the manufacturer and suppliers for fabrication, following the fabricating classifications of the manufacturer which represents the capabilities and limitations.

The device used in this work is outsourced to EuroCircuits (Belgium) with their Standard PCB Pool classification. Main fabrication specifications include:

- Dielectric core material: 1.8mm High Tg FR-4 board
- Copper layer: 2 layers (top and bottom only) with 2oz (70um) thickness
- Minimum trace width: 8 mil (0.2 mm)
- Minimum trace clearance: 8 mil (0.2 mm)
- Minimum clearances between features: 8 mil (0.2 mm)
- Minimum via hole size: 2 mils (0.5 mm)
- Silkscreen color: Green

Other specifications are considered not important in the design of this work and thus not listed. The specifications share the same as LED panels in swine model research in previous chapter.

For each LED chip, interconnects of the cathode and anode are placed with the provided coordinates defined by previous section. The footprint is converted from the chip manufacturer's recommended design. All exposed interconnect pads are finished with

flash gold treatment for better electrical connections. The remaining area without interconnect pads is finished with a green solder mask, to reflect the green/lime light from the LEDs. White silkscreen text is placed at the top side of the panel indicating the numbers of the components for easy diagnostics. A circular mark and a cross mark are labeled on the center of the matrix to help align with the well plate.

Each LED chip measures 1.3mm by 1.7mm in width and length, and it's managed into an equilateral matrix layout with an interval of 2.6mm. This spacing results in a gap of 1.3mm between adjacent LEDs within the same row and 0.5mm between rows. This configuration provides sufficient space for interconnects and wire routing using just two layers of the PCB. Through-hole vias are positioned between the LED chips to allow connections between two layers. The column control signal wires (LED anodes) are placed on the top layer of the PCB, while the row selecting wires (LED cathodes) are located on the bottom layer with the wires running perpendicularly to each other to minimize signal interference. The through holes are covered and filled with solder masks. This not only protects the vias but also contributes to the overall durability of the PCB for later encapsulation processes. The remaining areas without interconnects or routes of the PCB design are finally plated with grounding copper structures on both sides, enhancing the electrical interference stability of the device.

After the PCB is fabricated, LED chips are assembled using surface-mount technology (SMT). Lead-free solder paste (SAC305) is applied to the board where components will be placed. This is typically done using a stencil that ensures paste is applied only to the intended interconnect pads. LED chips are placed on the PCB by automated pick-and-place machines that accurately place the chips on their designated pads with programmed coordinates. The PCB with all LEDs placed is then passed through a reflow oven. The solder paste melts (reflows), solidifying to form solder joints that electrically connect the LED chips to the board. The assembled PCB with LEDs is inspected for any soldering defects, misplaced components, or other issues. This can be done through manual checks, Automated Optical Inspection (AOI), or X-ray inspection by the manufacturer.

The controlling signal routing is managed by directing the row and column signals from the matrix's center to the PCB edges. The PCB is accordingly extended to dimensions of 160mm by 144mm, accommodating experimental setups of a 6-well plate or Petri dish, providing stability and necessary space for wiring and connectors. At the PCB's edge, two flat cable connectors are positioned to link these signals to the system's driver.

The assembled PCB with LED chips requires an additional protective layer on top of

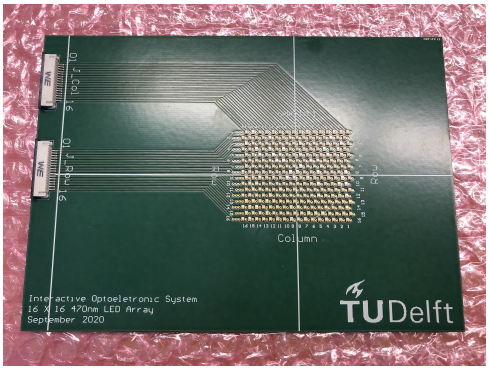

Figure 5.21: Fabricated LED matrix PCB with assembled LED chips

the chips for a few reasons. Firstly, the correct projecting distance to the target surface needs to be maintained as the design value of 1.73mm and the bottom thickness of the well plate at 1.27mm. So a layer approximately 0.5mm thick is necessary to achieve the desired projecting distance. This layer ensures that the light from the LEDs is projected at the correct distance to the cell culture in an optimized and uniform way.

Secondly, high irradiance from the LED chips with high current and consequently high heat generation. If the LED chips are in direct contact with the well plate, there's a risk that this heat could be rapidly transferred to the bottom of the well plate, potentially affecting the temperature of the cell culture in the well. Since maintaining a stable environment at 37°C is significant for the normal biological activity of the cell culture, a layer of thermal barrier is essential. This barrier will help minimize rapid heat transfer, dissipating the heat evenly and reducing the impact of hot spots created by LED chips.

Additionally, during the PCBA process, components are mainly leveled by solder surface tension, which means they might not be perfectly flat. This irregularity can lead to an uneven top surface of the matrix. The protective layer on top of the LEDs will need to be flat to ensure a good interface with the well plate, thereby enabling a level and stable setup for the experiments. A flat and even interface is also beneficial for maintaining a stable temperature throughout the experiments.

Polydimethylsiloxane (PDMS, SYLGARD 184, Dow Chemical Company, USA) has demonstrated its effectiveness as encapsulation material in previous chapters. PDMS has good thermal barrier propertieste , transparency to the specific wavelengths used, and simplicity of fabrication, making it an ideal material for this application.

The projecting distance for the LED illumination is calculated from the top surface of the LED chips. Therefore, it's essential to precisely measure the standing height of

the LEDs after the soldering process. This height can vary depending on factors like the amount of solder used and the soldering technique. The standing height of multiple LEDs in different corners of the matrix is measured by a precise height gauge (Mitutoyo, Japan). The result shows that most LED chips (>80%) have a standing height, measured from the surface of PCB to the top surface of the LED, between 0.65 to 0,75 mm (Figure 5.22). An average value of 0.70mm is then used in the following calculation. This allows for most LED elements less than 5% error in total projecting distance.

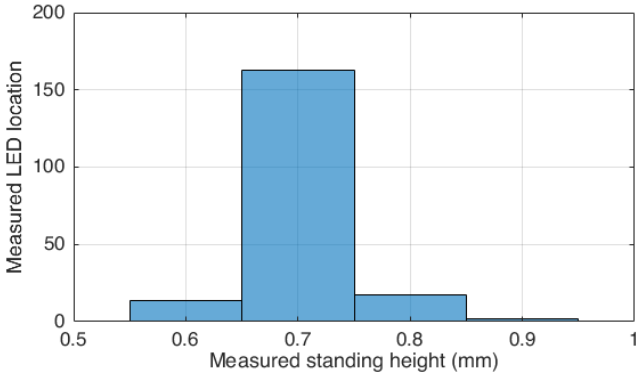

Figure 5.22: Histogram of the standing height measurement at LED locations

The PDMS layer needs to be fabricated with a thickness that matches the designed height requirement, as the designed projecting distance plus the standing height of the LED chips (0.7+1.73=2.43mm), since it is more practical to mold the whole LED matrix with one over-wrapping layer of polymer than add layer just on top of chips. Additionally, the top surface of the PDMS layer must be perfectly flat for a uniform interface with the well plate.

A 3D-printed customized mold made from ABS plastic is designed as a square ring structure with dimensions of 80mm by 100mm and a height of 2.4mm. The height of the mold is particularly significant as it determines the thickness of the PDMS layer. When the PDMS mixture is poured into this mold, it is allowed to flow and spread until it reaches the 2.4mm height and overflows. PDMS has a low shrinking rate of less than 2% at the used curing temperature, this means that the mixture's height before curing will be almost the same as after it is cured, ensuring precision in the final thickness of the layer.

The mold is taped to the PCB board to cover the LED matrix area, and the PCB board is placed on a carrier plate with measured leveling. PDMS elastomer and curing agent liquid are then mixed 10 to 1, the recommended ratio by the supplier to ensure the best

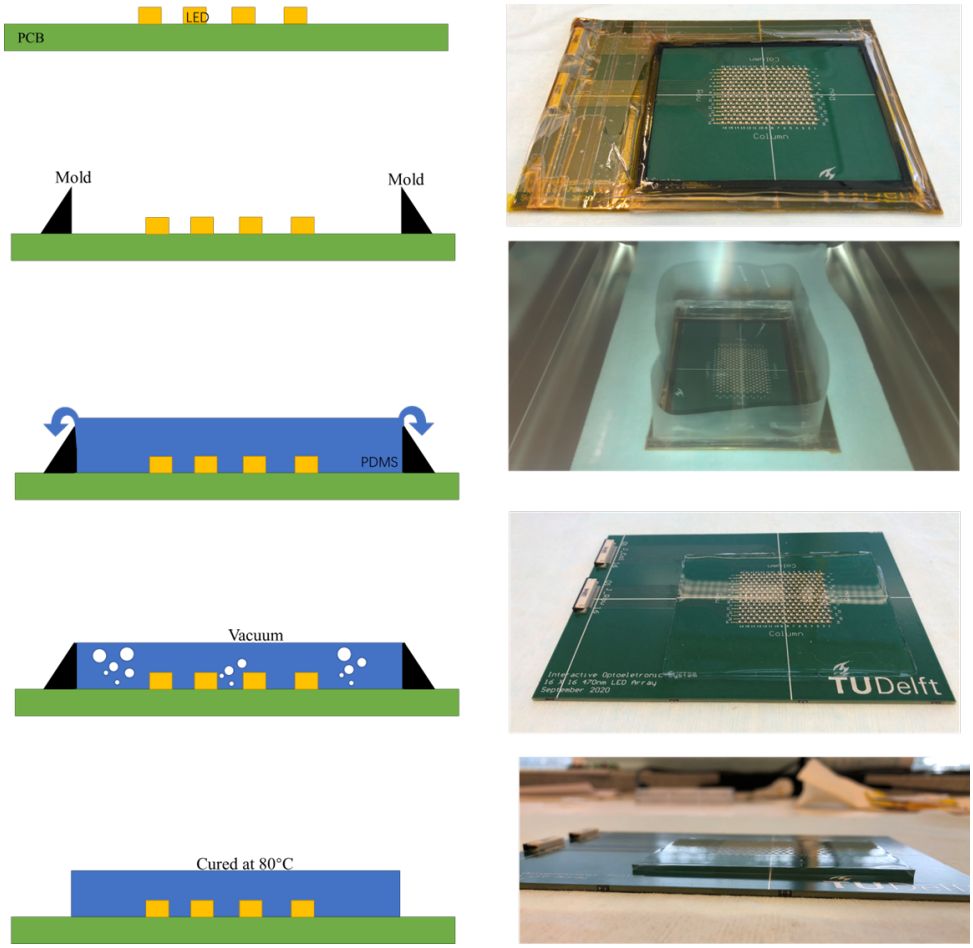

Figure 5.23: LED matrix encapsulation process with PDMS polymer

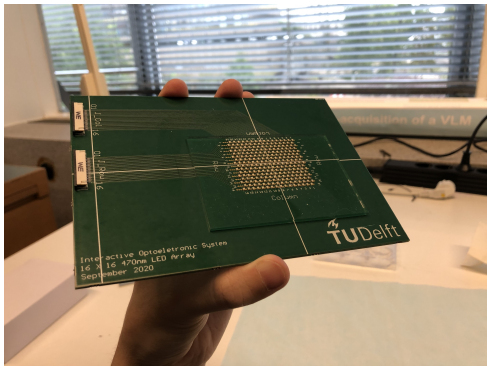

Figure 5.24: Fabricated LED matrix with trimmed PDMS encapsulation

curing quality. The viscous mixture is carefully poured over the prepared mold area until the excess mixture overflows from the edge of the mold. This liquid covers the mold uniformly due to the hydrophobic layer of the PCB solder mask. The setup is then placed in a vacuum oven for 10 minutes without heating to de-gas the PDMS to remove any air bubbles.

Once the initial de-gassing is complete, an additional PDMS mixture is poured into the mold as the escaping gas bubbles reduce the height of the layer. The setup is again placed in a vacuum oven for 10 minutes without heating to de-gas. These adding PDMS mixture and vacuum steps are repeated 3 times to ensure perfect de-gassing in the layer as well as a precise thickness.

After de-gassing, the PDMS starts to cure. The oven is set to 80°C for 1 hour with the vacuum remaining in the chamber. The temperature drops naturally and the assembly is left to cool down to room temperature after the oven set time in about 2 hours with the vacuum disconnected.

After PDMS is cured, excess polymer to the edge of the LED matrix is cut out by a sharp razor with 20 mm clearance to the first and last columns, and the last row of LEDs. Only 3 mm clearance is left to the first row of the matrix to avoid interference with the well plate extending lips. The LED matrix is ready for function verification (Figure 5.24).

5.6. LED MATRIX DRIVER AND CONTROL SUBSYSTEM DESIGN AND IMPLEMENTATION

The development of a sophisticated LED matrix driver system is necessary to effectively operate the 16x16 high-power LED matrix as fabricated in the previous section for the

demonstrative purpose of the hiAM arrhythmia research. The design of this driver system is critical, as it must fulfill specific requirements. Apart from the driver system, a user interface on the PC will be developed to handle image data processing and user interactions.

This section is a result of collaborative work which is presented in detail in the Master Thesis: *Advanced optoelectronics driver system for biomedical applications* by Deng, Shanliang (2021) Delft University of Technology,

5.6.1. DRIVER REQUIREMENTS

The initial step of the development involves determining the appropriate matrix driver topology and communication protocol based on the requirements. These foundational elements are key to ensuring that the driver system can reliably and efficiently control the LED matrix according to the desired specifications. The communication protocol exchanges the pattern data among various components of the system, such as the PC controlling interface, AI algorithm, and the hardware LED drivers. Some aspects of this communication protocol design should be considered such as data format, latency, drivability, and expandability.

First of all, for the proof-of-concept demonstrator, the data format should be tailored to a 16x16 element matrix to align with the LED matrix design. Each element within this data matrix will represent grayscale levels, encoded as 8-bit values. This means each element can represent 0-255 levels of grayscale, providing sufficient granularity for pattern representation.

Secondly, the system needs to be capable of updating the display on the matrix within 60ms from the moment a new frame is received. This rapid refresh rate is determined by the biological characteristics of the light-sensitive ion-channel switching time. The refresh time consists of several key components in the process of data transferring:

- Accessing AI-generated data from PC RAM
- Communication between PC interface and controller
- Processing and configuration in the driver electronics
- Response time of the LED Matrix

In addition to these components, implementing a robust flow control method in the communication protocol is important to ensure complete data delivery, and to prevent data package loss and incomplete data transmission. This is particularly important in a

high-speed, data-intensive environment to maintain the integrity and reliability of the pattern display.

Furthermore, the LED matrix uses high-power LEDs with a maximum operating current of 1A. The driver electronics system must be capable of providing the necessary output capacity to effectively drive the entire matrix at this high level of current. The driver must offer output linearity with an accuracy higher than 95%. This high degree of linearity is essential to ensure the precision of the controlling of the light irradiance. Given that each experiment is designed to last for at least 30 minutes, the driver must maintain a stable output throughout this duration against thermal drift or overheating.

Finally, the protocol needs to be designed with flexibility, allowing it to accommodate different matrix sizes for future development of LED matrix. This expandability is crucial to ensure that the system can be adapted or scaled up in the future without requiring a complete redesign of the communication framework. Potential updates for the LED matrix are the increase of matrix dimensions, an increase or decrease in LED driving current, etc.

5.6.2. DATA COMMUNICATION DESIGN

As the total latency budget of the system is determined as 60ms, the communication time between the PC interface and controller module is taken as a fraction of the budget to stay below 20ms. This constraint is determined to ensure that the cumulative latency of the entire system remains within the desired threshold. Based on this requirement, the communication speed of the system is estimated. The system must achieve a minimum communication speed, according to the calculation in Equation 5.21 of 102.4kbps (kilo-bits-per-second). This speed is calculated by the ideal minimum necessary data size of the 16x16 pattern within the required time limit, ensuring that the system responds and updates in real-time or near-real-time, which is particularly important in dynamic experimental conditions where rapid response is required.

$$MinimumDataSpeed = 16 \times 16 \times 8bits \times \frac{1}{20ms} = 102.4kbps \tag{5.21}$$

To determine the most appropriate communication method for transmitting data from the computer to the controller module, several possible options have been evaluated. These options and their characteristics are detailed in Table 5.2.

Serial Port RS232: The serial port is a widely used method for data transmission between measurement or acquisition equipment for its simplicity and accessibility in implementation. Standard baud rates for serial ports are typically divisors of 921600. Practically, the highest baud rate recommended by IEEE is 115200, which translates to

Table 5.2: Proposed data communication methods and evaluations

Proposals	**Serial port**	**USB port**	**Bluetooth**	**Wi-Fi**
Wired/Wireless	Wired	Wired	Wireless	Wireless
Protocol/Standard	RS232	USB2.0	Bluetooth 4.0	802.11b/g
Theoretical maximum speed	250kpbs	480Mbps	3Mbps	54Mbps
Practical maximum speed	-	++	++	++
Implementation complexity	++	-	+	+

115200 bits per second. Considering the overhead bits for each byte (1 start bit, 8 data bits, and 1 stop bit), the real effective data transfer rate is about 11.520KB/s. This speed fails to meet the requirements for the system as proposed.

USB 2.0: USB 2.0 offers significantly higher speeds than the outdated serial port communication up to 480Mbps theoretically, which is much more than sufficient for the system proposed. However, the challenge with USB 2.0 communication is its complexity in developing compatible drivers for both the PC and the microcontroller in the driver module. This complexity can lead to extended development time and risks.

Bluetooth 4.0: As a wireless method also known as Bluetooth Low Energy (BLE), Bluetooth can achieve speeds up to 3MB/s within a short range (0.5m) theoretically, which is much more than sufficient for the system proposed. Moreover, establishing Bluetooth connections between devices today is simple thanks to the easy availability of user-friendly BLE modules in the market, or even embedded in advanced microcontroller chips. These modules, which are easily integrated into various devices, come with the plug-and-play nature of built-in electronics and antennas, along with accessible documentation and community support, making BLE connectivity easily achievable for developers. While it offers the convenience of wireless communication and high speed, its low-energy feature makes it easily suffer connection issues or instability when there are obstacles between the transmitter and receiver, or when exposed to strong interference signals. Therefore, this method is mainly used for energy-sensitive and low-data applications such as smart home devices or audio devices.

Wi-Fi 802.11b/g: Wi-Fi, operating at 2.4GHz, offers robust wireless connectivity with a much wider range than Bluetooth. 802.11b/g standards can maintain a stable link up to 10m distance. Additionally, Wi-Fi's capability to access local area networks means it can use standard communication protocols like TCP/IP, ensuring reliable and correct

communication of large and continuous data transfer. Similar to Bluetooth connection, establishing Wi-Fi connections between devices today is also simple thanks to the plug-and-play modules embedded in the micro-controller units. This makes it easier for developers to implement Wi-Fi connectivity for data transfer, remote control, or even Internet access.

Given all considerations, Wi-Fi 802.11b/g is chosen for data communication between the PC and the control module. It meets the system's need for high-speed data transfer and offers the benefits of wireless connectivity with low complexities in implementation thanks to available Wi-Fi modules. The stable 802.11b/g communication protocols further ensure the reliability and stability of the link, making it a suitable choice for the design in this chapter.

5.6.3. DRIVER AND CONTROL SYSTEM IMPLEMENTATION

Based on the technical requirements, Wi-Fi communication method, and the design of a 16x16 LED matrix, the driver and control system architecture is designed and presented in Figure 5.25. The driver and control system consists of a few groups based on functions and features of the integrated chips: micro-controller chip, current source and controllers, row-scanning controllers, and power supply. The function groups or chips are inter-communicated with the I2C protocol for effective synchronization. Customized software on the microcontroller and PC interface is developed to support the hardware integration and system functionality.

Micro-controller unit: The micro-controller unit is the brain of the system. It processes the input data from the external PC and translates the information to hardware signals to trigger the low-level drivers of LED scanning and illumination. It is also the main interface for programming the driver system as the developer needs. ESP8266 (Espressif Systems, China) is selected as the main micro-controller unit of the driver and control system. The most important advantage of this chip is the built-in Wi-Fi module, including transceiver electronics and a built-in antenna, allowing data transfer directly to a PC via a Wi-Fi link or through a Wi-Fi router. It has a built-in I2C port for inter-communication with other chips in the system. Programming the ESP8266 is made easy through its APIs via an external PC, and its clock speed of 160MHz is sufficiently fast for this application.

Current source and controllers: PCA9635 (NXP Semiconductors, The Netherlands) is chosen for LED matrix column control with support of I2C inter-communication. A main switch pin is linked to a hardware switch and offers the ability to immediately cut off the illumination. 16 output pins provide PWM signals connected to the Constant Cur-

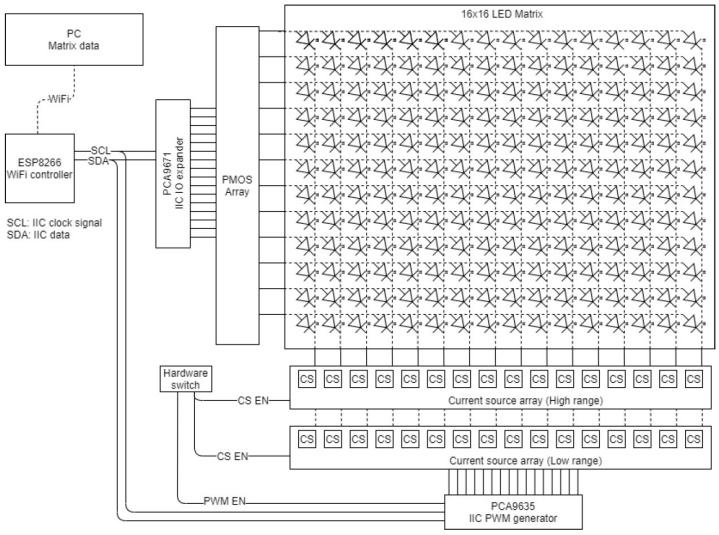

Figure 5.25: System architectural schematics of the LED matrix driver and controlling system

rent Source (CCS) array. STCS2 (STMicroelectronics, Switzerland) chips are selected to build the CCS array, capable of providing up to 2A of output current and compatible with PWM input. This aligns with the system's requirement for a maximum output current of maximum 1A.

An external pin is used for the system to select between high and low current ranges. The CCS array is designed to handle high or low output ranges of 0-1A and 0-100mA respectively, with the current limit set by selective external feedback resistors. The feedback resistors can be calculated to be 1Ω for 1A output and 0.1Ω for 100mA output to give larger flexibility to the system. The CCS is connected to a hardware-enabled switch, ensuring that the current source can be manually disabled immediately if the system is in an abnormal state as an additional safety feature. The current controlling signals are sent to the LED matrix via flat cables of high or low current mode respectively.

Row-scanning controller: PCA9671 (NXP Semiconductors, The Netherlands) is selected for the row-scanning main controller. The row scanning is achieved by the chip controlling the anode of the LED matrix, therefore the rows of the LED matrix, switching each row on and off one at a time with a programmed refresh rate. The control chip cannot directly handle the high current that flows to the LED matrix rows, therefore a PMOS array is used as a switch to directly control the current.

Each PMOS transistor (PMV65XP, NXP Semiconductors, The Netherlands) gate pin

in the array is connected to one of the output-selecting pins of the row selection chip. When a signal is sent from the control chip to a particular PMOS, the transistor channel opens and allows current flow through the selected row, thereby illuminating the corresponding row of LEDs in the matrix. By sequentially switching on the next PMOS in the array while switching off the current one, the system can illuminate the LEDs row by row and therefore the pattern of a matrix. The row-scanning signals are sent to the LED matrix via a flat cable.

Power supply: With each row containing 16 LEDs and each LED requiring up to 1A of current, the total maximum current requirement for a single row is 16A when all elements in that row are switched on. TPS543B20 (Texas Instruments, USA) is selected as an onboard step-down converter chip with a maximum output of 24A. This chip is not just a high power converter, it also includes a power management function, crucial for monitoring and ensuring the stability of the output voltage. The control and driver module is powered by a standalone AC-DC power supply (RPS-400, Mean Well, USA). The power supply is selected by its high power density (maximum 400W, 48V) and high energy efficiency (94%) with minimum footprint. It conforms to international medical regulations and EMC standards, perfectly fitting for various medical system equipment.

The system hardware architecture is implemented to a PCB layout design by computer-assisted software. Then the design files are sent to the manufacturer and suppliers for fabrication, following the fabricating classifications of the manufacturer which represents the capabilities and limitations. The device used in this work is outsourced to EuroCircuits (Belgium) with their Standard PCB Pool classification, similar to previously discussed PCB prototypes. After the PCB is fabricated, LED chips are assembled using surface-mount technology (SMT). Lead-free solder paste (SAC305) is applied to the board where components will be placed. This is typically done using a stencil that ensures paste is applied only to the intended interconnect pads. LED chips are placed on the PCB by automated pick-and-place machines that accurately place the chips on their designated pads with programmed coordinates. The PCB with all LEDs placed is then passed through a reflow oven. The solder paste melts (reflows), solidifying to form solder joints that electrically connect the LED chips to the board. The assembled PCB with LEDs is inspected for any soldering defects, misplaced components, or other issues. This can be done through manual checks, Automated Optical Inspection (AOI), or X-ray inspection by the manufacturer.

The PCB board with driver electronics and power supply is carefully assembled into a custom-made plastic case (Figure 5.26), designed to accommodate the components with a compact and efficient layout. Push buttons and status LED indicators are located

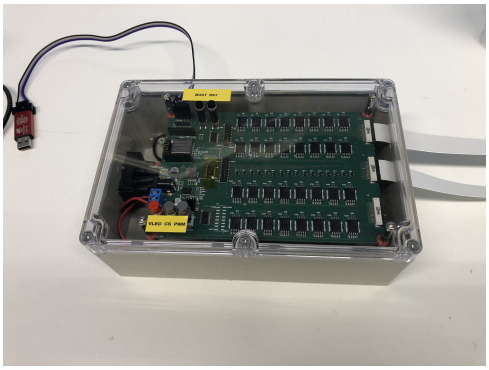

Figure 5.26: The driver and control system assembly

at the top cover of the case as the user interface. Flat cables are fed through the side opening of the case to be connected to the LED matrix.

The complete system operation relies on two software components: the micro-controller program on the ESP8266 which controls the hardware electronics, and the PC software for user interaction and pattern processing. The former program manages tasks like Wi-Fi communication and matrix control, ensuring the LED matrix illumination functions correctly. The latter program processes user inputs, creates display patterns, and sends this data to the driver module via wireless communication.

The micro-controller program is based on C++ programming with an Arduino compiler environment. It uses a system clock-generated ticker for inter-communication and matrix control. Each duty cycle has 50ms to fetch data of the next pattern frame from the wireless communication, and 10ms to verify the completeness of the last pattern frame data in RAM. Incoming data is temporarily stored in a 16x16 byte buffer in RAM, then moved to another buffer for matrix control processing. An unsynchronized matrix control duty cycle has 8ms to send control signals to the column control chip via the IIC port. Then another control signal activates the scanning to the next row and deactivates the previous one. This process repeats 16 times to refresh the entire matrix.

The PC program is based on a Python environment. It processes user inputs and visualizes the system functionality. It also prepares the input matrix data for transmission to the driver system via wireless communication. The PC software operates various tasks concurrently using different threads, eliminating the need for tickers. With PCs typically having GHz-speed CPUs, the processing time is negligible.

The user interface (UI) of the PC program (Figure 5.27), displays the matrix pattern visually, mirroring the actual LED matrix layout. Each element in the UI represents an

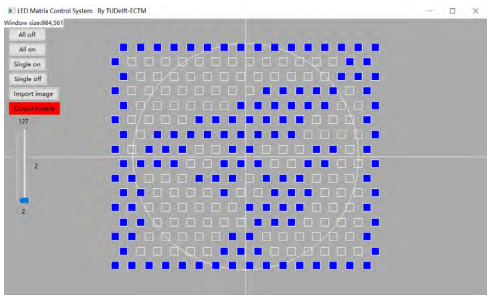

Figure 5.27: User interface (UI) of the PC program

LED element in the matrix, with an empty box indicating an off state and a blue box for an on state. The UI includes widgets such as buttons for turning all LEDs on or off, modifying individual LEDs, importing pre-defined 16x16 pixel images, and adjusting the global output radiant intensity from 0 (off) to 127 (maximum power). An indicator button also shows Wi-Fi connectivity and controls wireless communication. Input made on the UI is instantly processed by a background image processing thread, ensuring that any changes are updated to the LED matrix instantly.

Measurements and tests are done to ensure the implemented system meets the requirements of data transfer latency and refresh speed. Data showed over 85% of tested transmission commands take less than 8ms to be transferred from the PC to the microcontroller unit. In some very rare situations, less than 0.1% of tested commands, it takes more than 60ms to transfer data potentially due to environmental interference. These rare cases are triggered in the UI to be eliminated during the application and experiments. An oscilloscope is used to measure the waveform of the control signals to characterize the actual pattern refresh rate. Data shows the total sweep time by measuring the time of scanning each row of the LED matrix is 6.8ms. The measurements show the driver and control system meet the initial design specifications and are capable of testing with the LED matrix for optogenetics research purposes.

5.7. SYSTEM OPTICAL CHARACTERIZATION AND VERIFICATIOJN

Following the system integration of the driver and control electronics and the LED matrix, optical characterizations are conducted.

The initial system characterization involves a basic functionality test, where the LED matrix is expected to display a pattern corresponding to an input received from a PC. A predefined 16x16 pixel image, specifically a university logo, is chosen as the sample. This image is inputted into the PC program and set to an illumination irradiance level of

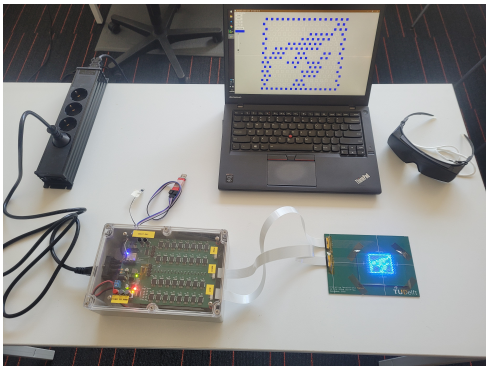

Figure 5.28: System overview during LED matrix function tests

10. The PC software processes the image, adapting it to fit the layout of the LED matrix. Once processed, the image data is transmitted to the driver and controller system using wireless communication. The driver and controller then prepare the received data and control the LED matrix to light up the corresponding elements, recreating the university logo illumination as intended (Figure 5.29a). The logo image is replaced with an image of text: 'TUD LUMC' and the matrix immediately changes the pattern (Figure 5.29b). This test verifies that the system can accurately convert and display a given image pattern on the LED matrix, demonstrating its basic operational capabilities.

The next step in the system characterization involves verifying and calibrating the irradiance settings in the user interface program, which range from 0 to 127, against the actual irradiance emitted by the LED matrix. This process is similar to the calibration setup previously utilized for the LED panel in the swine model treatment project.

A high-power optical sensor (S142C, Thorlabs, USA) is placed at the center of the LED matrix (Figure 5.30). The optical sensor has a 10mm diameter measurement window that covers 10 elements in the matrix. This placement allows for a thorough assessment of the average irradiance at the center of the matrix. The sensor is connected to a readout console (PM100D, Thorlabs, USA), which provides irradiance readings for selected wavelengths. To perform the calibration, all LED elements are switched on with the UI input setting gradually adjusted from 0 to 127, incrementally increasing the driving current to the LEDs. At each step, the sensor measures the irradiance, and the readout console displays and records the value. Each input setting value is measured three times and then averaged to obtain a final, representative value. The same measurements are repeated for the low current range setting and high current range setting.

The collected data from the calibration tests is plotted (Figure 5.31) to evaluate the

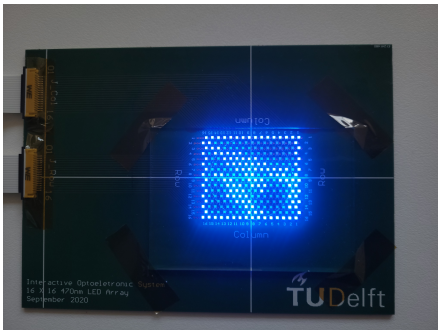

(a) Pattern illumination by an input image

(b) Pattern illumination by another image

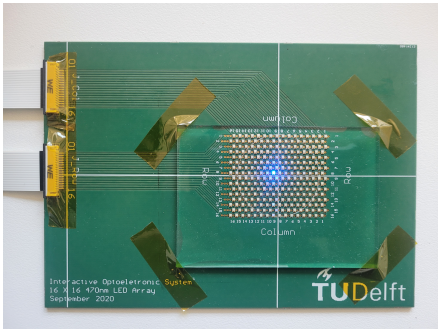

(c) 1 LED with low irradiance (level 10)

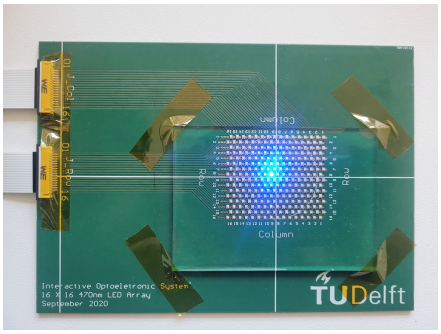

(d) 1 LED with high irradiance (level 127)

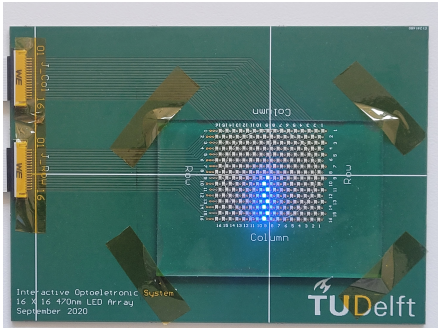

(e) 1 LED line connecting to edge

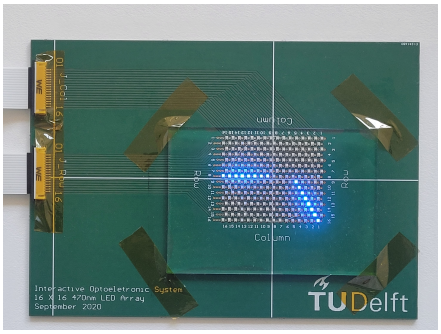

(f) 2 LED lines connecting to edges

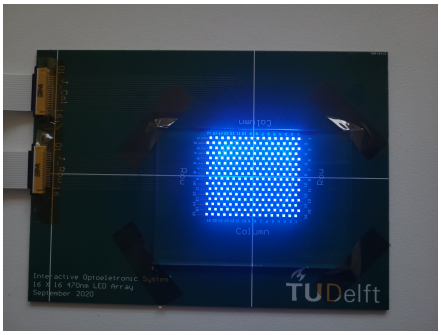

(g) Global illumination with all LEDs

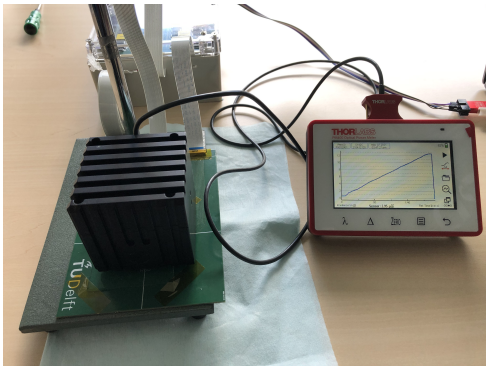

Figure 5.30: Setup for calibrating the irradiance settings in the user interface program

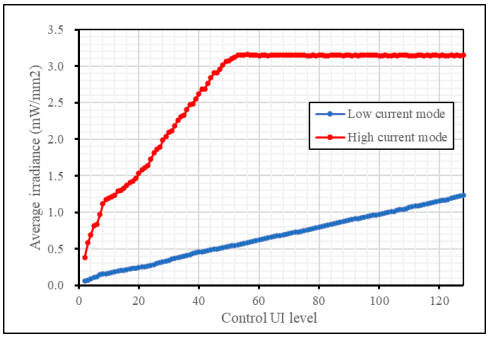

Figure 5.31: calibrating the irradiance settings in the user interface program: low current mode and high current mode

relationship between the LED matrix irradiance and the UI input values. For the low current range setting (up to 100mA) the plot shows a strong linear relationship between the irradiance with the UI input values. This linearity indicates that as the input values on the UI are adjusted, the irradiance from the LED matrix changes proportionally, demonstrating predictable and consistent behavior. However, for the high current range setting, non-linearity is seen for outputs below 1.2mW/mm^2. Despite this non-linearity at lower outputs, it is not a concern for practical applications since this irradiance range overlaps with that of the low current range. Therefore, in actual use, this lower output range under the high current setting will not be used in the application. At the higher output range of the high current setting (above 1.2mW/mm^2), the relationship returns to linearity, up until the point where the irradiance value starts to clip at 3.1mW/mm^2. This clipping is due to the limitations of the measurement setup, which is unable to accurately measure irradiance values beyond this point.

The results from the optical characterization of the system reveal that the implemented LED matrix illumination system can achieve irradiance levels higher than the required reference of 0.3mW/mm^2. It's also observed that the actual irradiance (maximum 1.2mW/mm^2 @100mA) values measured match well with the predicted value by the simulations (maximum 1.11mW/mm^2 @100mA) discussed in the previous section.

Overall, the characterization provides valuable insights into the performance of the LED matrix across different input settings and helps in understanding the limitations and capabilities of the system in various operational scenarios. The implemented illumination system is capable of the hiAM optogenetics research applications.

5.8. SYSTEM VALIDATION: HIAM AF TERMINATION EXPERIMENTS

This section is a result of collaborative research between TU Delft and the Laboratory of Experimental Cardiology, LUMC.

A series of optogenetics experiments are conducted using the LED matrix illumination system as the stimulating light source. This system is implemented as part of the microscopy-based optical voltage mapping setup. figure

In the experimental setup, the LED matrix is taped on a work platform, which includes a hot plate positioned directly above it. This hot plate is programmed to automatically maintain a temperature of 37°C, a critical condition for preserving normal biological activity in cell cultures. A 6-well plate is carefully positioned on top of the PDMS interface layer of the LED matrix. This alignment is helped by the circular and cross marks at the matrix center, ensuring that the center of one of the wells in the plate aligns perfectly with the center of the matrix. At the bottom of this well lies a monolayer of hiAM cell culture.

Above the cell culture, an optical voltage mapping system is installed with a camera to capture and record the cellular optogenetic responses. Adjacent to the LED matrix, the driver and control case are positioned and connected to the matrix via flat cables to avoid additional vibrations or disturbances. The main controlling PC for operating the entire system and processing the data is placed next to the experimental setup. This placement ensures seamless integration and coordination between the various components of the system, allowing for efficient control and wireless data communication during the optogenetics experiments.

The entire setup (Figure 5.32), including the LED matrix, the hot plate with the cell culture, and the optical voltage mapping system, is placed inside a dark room. This specific location choice is crucial to minimize external light interference, which could potentially affect the optogenetic responses of the cell culture or the accuracy of the

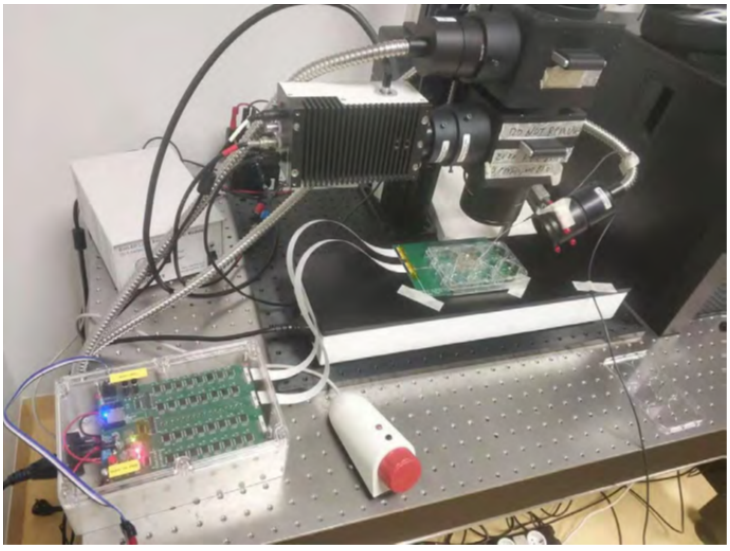

Figure 5.32: Experiment setup for hiAM AF termination with LED matrix illumination system

optical voltage mapping measurements.

The hiAM cell culture, as introduced in the previous section, is prepared and cultured with matured processes. These cells are then genetically modified to present light-sensitive ion channels. A fluorescent dye indicator is added to the cell culture surface to transform the electrical potential of the cells to optical illumination to be captured by the optical voltage mapping setup. To test and verify the optogenetic response of these modified cells, an external light source is used as a reference. This light source emits light at a wavelength of 470nm, which is the optimal wavelength for activating the light-sensitive ion channels in the hiAM cells. The irradiance of this light is kept at a low level, specifically at 0.3mW/mm^2. This verification process is critical to confirm that the genetically modified cells respond as expected to light stimulation. The successful activation of these light-sensitive ion channels by the external light source validates the functionality of the cell modifications and sets the stage for more complex experiments using the LED matrix.

Pacing by single LED element point stimuli

To assess the light response of the ion channels to LED illumination in the hiAM cell culture, an experiment is conducted using a single LED element to provide a low irradiance point stimulus. This is aimed at generating pacing electrical potential waves,

observable through optical voltage mapping images. For this test, the irradiance of the LED is set to 2.5mW/mm^2. Only the central LED is activated for a duration of 500ms and then switched off. However, the observation of pacing potential waves after illumination is hardly found. Only some faint remains of potential waves are noticeable at the edge of the cell culture for a very short duration. This limited observation can be attributed to the large contrast between the intensity of the LED illumination and the high sensitivity of the optical voltage mapping system. When the LED is switched on, even at relatively low irradiance, the optical voltage mapping camera becomes saturated due to its high gain settings, which are intentionally set to capture the fluorescent light emitted by the dye used in the cell culture. As a result, the pacing wave propagates rapidly to the edges of the cell culture before the optical mapping system can refresh and recover from the saturation caused by the LED's high irradiance. Further experiments with reducing LED irradiance to a minimum of 0.5mW/mm^2 or manipulating the illumination duration show similar results.

However, the absence of observable pacing waves is more indicative of the technical limitations of the experimental setup rather than the failure of the LED to stimulate the ion-channel hiAM cells.

Arrhythmia termination by global illumination of LED matrix

The following experiment is to terminate AF potential waves using global illumination from the LED matrix. AF is initially induced in the hiAM cell culture in resting potential using high-frequency electrical stimuli via an electrode pin placed at the edge of the cell culture. For an arrhythmia condition to be considered valid for a termination experiment, a stable rotational AF wave must be observed through optical voltage mapping images for more than 5 seconds (Figure 5.33).

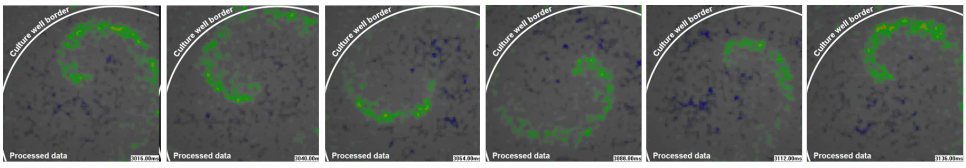

Figure 5.33: Self-sustained rotational AF wave in hiAM cell culture with a cycle time of 120ms

Once a self-sustained AF wave is established, all LEDs in the matrix are activated simultaneously for a duration of 500ms, with the irradiance set at 10mW/mm^2. After the optical voltage mapping camera recovers from the saturation caused by the LED light to

the normal optical voltage mapping levels, the results show an absence of arrhythmic waves in the cell culture. The cell culture returns to an overall resting potential state.

This termination experiment is repeated multiple times, with variations in the LED irradiance. Remarkably, even at the minimum LED irradiance level of 0.5mW/mm^2, the AF wave is effectively terminated by the 500ms period of global illumination. This suggests that the global illumination from the LED matrix effectively 'resets' the electrical potentials of the cell culture by simultaneously polarizing all cells, and thereby stopping the propagation of the arrhythmia rotational wave. This result demonstrates the efficacy of the LED matrix in ontogenetically manipulating cell culture's electrical potential activity, particularly in the context of controlling cardiac arrhythmias.

Arrhythmia termination by selective illumination of LED matrix

Building on the success of terminating AF using global illumination, the following experiments explore the possibility of terminating arrhythmia in hiAM cell culture with selective activation of LED elements. The hypothesis is that illuminating LEDs in a straight line from the center of the AF rotational wave to the nearest edge of the cell culture could create a polarized potential barrier, effectively blocking the AF wave propagation.

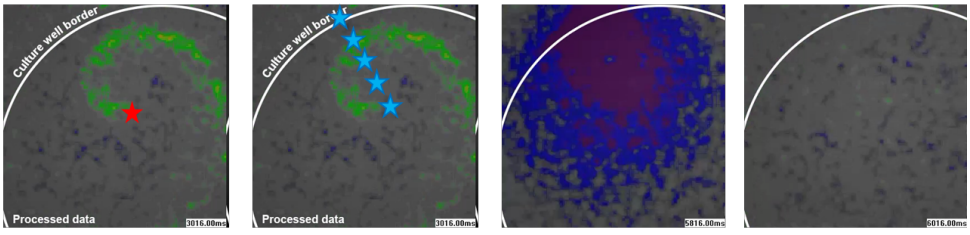

Identify rotation center | Determine LED line | Light pulse 150ms 1.2mW/mm² | AF terminated

Figure 5.34: Arrhythmia termination by selective 'line barrier' illumination of LED matrix

To test this assumption, AF rotational waves are induced to the hiAM cell culture and allowed to stabilize with the same methods as previous experiments. Once a stable rotational center is established typically after a few seconds, it is identified by the operator through optical voltage mapping images (Figure 5.34). The operator then selects the LED element nearest to the rotational center and additional LEDs along a line extending to the nearest edge of the matrix, using the UI program on the controlling PC. These selected LEDs are illuminated for 150ms at an irradiance of 1.2mW/mm^2.

Following the selective illumination, a successful termination of the AF waves is observed. The cell culture returns to an overall resting potential state. This outcome demon-

strates the potential of using localized LED illumination patterns to interrupt and terminate arrhythmia waves, offering a more precise approach than global illumination. This result indicates a significant advancement in optogenetic techniques for controlling cardiac arrhythmias, particularly in terms of precision and efficiency.

These experiments not only test and assess the possibility of optogenetic arrhythmia treatment in hiAM cell cultures but also evaluate the design and functionality of the LED matrix illumination system as designed and implemented in previous sections. The experiments focus on the system's precision in targeting and controlling illumination, effectiveness in stimulating ion-channel behavior, and the usability of the interface and operation. Additionally, the experiments test the system's reliability across multiple long sessions and its integration with optical voltage mapping systems for real-time analysis. This evaluation demonstrates the system's comprehensive functions in cardiac electrophysiology studies.

5.9. CONCLUSION AND LIMITATIONS

This chapter introduces an innovative approach to studying arrhythmia behaviors using a human immortalized atrial myocyte (hiAM) model, emphasizing the design and development of an LED matrix illumination system for proof-of-concept purposes. It details the application of the V-model methodology in developing the high-power LED illumination system, covering the entire development cycle, from requirement analysis to verification. Detailed process is discussed including the fabrication, testing, and implementation of a specialized, modular LED matrix and its control system. The functionality of the LED matrix system is validated through a hiAM AF termination experiment. The positive results from this experiment demonstrate the system's effectiveness in successfully terminating and blocking AF rotational waves, proofing the potential of this LED matrix system in advancing optogenetics cardiovascular research as an experimental platform.

This work also lays a theoretical and practical foundation for advanced cardiovascular research, setting the stage for more sophisticated illumination systems in the following chapter.

The primary limitation of this part of the work is the absence of AI algorithm integration. Initially, the proposed design is a fully autonomous system where an AI algorithm would continuously monitor optical voltage mapping images, identify AF wave patterns, and automatically generate corresponding patterns, such as a line barrier, to trigger the LED matrix. Then the selective illumination of LED elements should effectively terminate the AF wave to complete the cycle. However, during the time of the above experiments, the AI algorithm is not fully developed, leading to the manual identification and

pattern generation by operators. It's important to note that the focus of this chapter is primarily on the design and development of the LED matrix itself, rather than the integration of AI. Despite this limitation, the tests conducted have effectively demonstrated the functionality and potential of the LED matrix in terminating AF waves. Therefore, the future completion and integration of the AI algorithm into the existing setup are expected to be straightforward.

Another limitation of the current LED matrix illumination system is the size of the LED chips and the relatively large interval between each element. The current design has intervals of 2.6mm, which is significantly larger than the estimated optimal pixel size of 500µm for precise stimulation of a group of muscle sarcomeres. This design choice is primarily driven by the decision to minimize development risks and costs for this initial proof-of-concept version, where the system's fundamental capabilities and potential in optogenetic applications are demonstrated. Future developments of the illumination system are proposed to include smaller LED chips (such as mini-LED or micro-LED) and reduced intervals between each element. This will make the system closer to the ideal pixel size, thereby enhancing its precision and effectiveness in controlling the cell culture response.

An additional limitation is its limited overall matrix size. While the current matrix is sufficient to cover one well of a 6-well plate, it does not fully cover a 145mm Petri dish. Petri dishes of this size offer a larger area for growing hiAM cell cultures, which more closely approximate the area of the human atrial wall. Experiments conducted on these larger dishes are likely to yield results that are more representative of real clinical applications. For future development and clinical research, the proposed improvement involves increasing the size of the LED matrix to adequately cover a 145mm Petri dish.

The optical voltage mapping equipment is not able to manage the high contrast between LED illumination and the fluorescence from the indicator dye. This issue leads to missed observations of initial wave activities immediately after the LEDs are switched off, due to the camera's saturation and slow recovery. To overcome this, an upgrade of the optical voltage mapping system should increase the camera's dynamic range and speed up its recovery time after saturation. These improvements would enable more accurate and complete capture of electrical responses during critical moments of the experiments.

BIBLIOGRAPHY

[1] Pim RR Van Gorp et al. “Multicellular in vitro models of cardiac arrhythmias: focus on atrial fibrillation”. In: *Frontiers in Cardiovascular Medicine* 7 (2020), p. 43.

[2] Jia Liu et al. “Generation and primary characterization of iAM-1, a versatile new line of conditionally immortalized atrial myocytes with preserved cardiomyogenic differentiation capacity”. In: *Cardiovascular Research* 114.14 (2018), pp. 1848–1859.

[3] Niels Harlaar et al. “Conditional immortalization of human atrial myocytes for the generation of in vitro models of atrial fibrillation”. In: *Nature Biomedical Engineering* 6.4 (2022), pp. 389–402.

[4] John Y Lin et al. “ReaChR: a red-shifted variant of channelrhodopsin enables deep transcranial optogenetic excitation”. In: *Nature neuroscience* 16.10 (2013), pp. 1499–1508.

[5] Laura Diaz-Maue et al. “Follow the light-from low-energy defibrillation to multisite photostimulation”. In: *2018 40th Annual International Conference of the IEEE Engineering in Medicine and Biology Society (EMBC)*. IEEE. 2018, pp. 4832–4835.

[6] Seiichiro Sakai et al. “Parallel and patterned optogenetic manipulation of neurons in the brain slice using a DMD-based projector”. In: *Neuroscience research* 75.1 (2013), pp. 59–64.

[7] Aanchal Bhatia, Sahil Moza, and Upinder S Bhalla. “Patterned optogenetic stimulation using a DMD projector”. In: *Channelrhodopsin: Methods and Protocols* (2021), pp. 173–188.

[8] ProjectScreen.com. *HOW DOES A DLP PROJECTOR WORK?* 2020. URL: https://www.projectorscreen.com/blog/How-does-a-DLP-projector-work.

[9] Oscar J Abilez. “Optogenetic LED array for perturbing cardiac electrophysiology”. In: *2013 35th Annual International Conference of the IEEE Engineering in Medicine and Biology Society (EMBC)*. IEEE. 2013, pp. 1619–1622.

[10] Brian O Bingen et al. “Light-induced termination of spiral wave arrhythmias by optogenetic engineering of atrial cardiomyocytes”. In: *Cardiovascular research* 104.1 (2014), pp. 194–205.

[11] Marta Lemme et al. “Chronic intermittent tachypacing by an optogenetic approach induces arrhythmia vulnerability in human engineered heart tissue”. In: *Cardiovascular research* 116.8 (2020), pp. 1487–1499.

[12] Corning Inc. *Costar® 6-well Clear TC-treated Multiple Well Plates*. 2020. URL: https://ecatalog.corning.com/life-sciences/b2b/NL/en/Microplates/Assay-Microplates/96-Well-Microplates/Costar%C2%AE-Multiple-Well-Cell-Culture-Plates/p/3516.

6

A MINI-LED MATRIX ILLUMINATION SYSTEM FOR HIAM OPTOGENETICS RESEARCH

6.1. INTRODUCTION

The successful implementation of the first proof-of-concept demonstrative 16x16 LED matrix illumination system for hiAM optogenetics research leads to the proposal of an improved version. This improved system aims to achieve more precise control of the electrical response of hiAM cell culture in advanced optogenetic research. The upgrade includes using mini-LED bare-die chips, which significantly reduce the size of each LED element, allowing for more targeted and refined illumination. Additional improvements include substrate materials used for the LED matrix implementation, enhancing performance, and durability, and creating more possibilities with flexible material. The driver and controller system is also refined to accommodate the demands of the smaller, more precise LED elements, ensuring more accurate, faster, and consistent control over the illumination patterns. This improved illumination system contributes to a new intersection of cardiovascular research and advanced electronics technology and opens a new path for understanding and potentially controlling arrhythmia.

6.1.1. REDUCE MATRIX PIXEL SIZE: PROPOSALS

The proof-of-concept version LED matrix illumination system discussed in the previous chapter has limitations of the too-large size of its LED chips and too large spacing between them. The existing design intervals of 2.6mm between LED elements are much larger than the ideal pixel size of 500µm needed for precise stimulation of muscle sarcomeres. This design is chosen to reduce development risks and costs for the initial proof-of-concept version, focusing on demonstrating the system's basic capabilities. For the improved design, the system is expected to use smaller LED chips, and narrower intervals between each element. This advancement will align the system more closely with the desired pixel size, significantly improving its precision and effectiveness. To accomplish such miniaturization, traditional LED chips with plastic or ceramic packages become less feasible due to additional phosphor layers or footprint limitations. Instead, the focus shifts to other promising solid-state-lighting solutions, such as mini-LEDs, micro-LEDs, LCD, or OLED display technologies, which provide considerably smaller element sizes and are more suitable for the refined requirements of advanced optogenetics applications.

Mini-LED is characterized by its notably smaller size compared to traditional LEDs. Mini-LEDs are regulated in size between 100 to 200um but still provide high brightness and precision control. Despite their minimized size, mini-LEDs maintain the luminous efficacy of conventional LEDs, making them suitable for various applications that demand precise light control and efficiency. The compact size of mini-LEDs allows for a

denser array within a given space, enabling precise manipulation of light intensity and distribution. Additionally, their small form factor aids in more efficient heat dissipation, which is crucial for maintaining performance and extending the lifespan of the products. In consumer electronics, automotive lighting, and display technologies, mini-LEDs are increasingly favored for their ability to offer enhanced brightness, energy efficiency, and improved color representation while being implemented in a small or thin space. Their use in displays has been promoted for providing higher contrast ratios and better color accuracy, contributing to a better viewing experience.

Mini-LED chips are typically provided by the manufacturer as bare dies, rather than in commercial packages or with standard footprints. This requires die-level packaging processes such as die pick-and-place, wire-bonding, and flip-chip bonding techniques, for the integration of systems or products, adding complexity and cost to the implementation process. One of the constraints of mini-LEDs is their limited range in the light spectrum. Unlike conventional LEDs, mini-LEDs often don't include phosphor materials that can modify the spectrum of emitted light. The available wavelengths for mini-LEDs are generally restricted to UV or blue light for productivity reasons. This limitation can be a significant consideration in optogenetic research of ion channels requiring certain wavelengths of light, where additional phosphor materials are needed. The maximum drive current for mini-LEDs is typically lower than that of conventional LEDs due to their smaller size, but this does not necessarily limit the total power effectiveness. The smaller dimensions of mini-LEDs allow for a higher density of elements within the given area. This high-density layout can significantly increase the power density, meaning that a mini-LED matrix can achieve a higher total illumination power despite the lower power per individual chip.

Micro-LED chips are even smaller LED elements, less than 100um in size, typically between 30 to 50um. While sharing the reduced chip size concept with mini-LED, micro-LED chips offer even greater precision in illumination control. Like mini-LEDs, micro-LEDs also typically come without packages, allowing for an extremely high density in the LED matrix with a high power density. However, similar to mini-LEDs, the range of wavelengths available for micro-LEDs is limited due to the absence of phosphor materials. Several researchers have already used micro-LED technology in cardiac[1][2] or neural[3][4] optogenetics studies with promising results.

The integration of micro-LEDs into systems is a significant challenge due to their extremely small size. Traditional methods like pick-and-place or wire-bonding are not efficient or cost-effective for assembling large-scale matrices that could include hundreds of thousands of micro-LED elements. More advanced die-level packaging technologies

are employed, such as self-assembly, panel-transfer, or nano-imprint, particularly in specialized applications like high-end displays or in research and technical demonstrators. These advanced methods enable the effective and efficient assembly of micro-LED matrices, although they often involve more complex and costly manufacturing processes compared to conventional LED or mini-LED implementation techniques.

Displays, commonly found in small portable devices like smartphones or tablets, is an alternative approach to achieving high-resolution control. Small displays can offer HD resolution (1920x1080) within dimensions as compact as 100mm by 50mm. This translates to an incredibly small pixel size of about 50µm, which is even smaller than some micro-LED chips and more than adequate for the precision required in this work of improvement of illumination systems. However, LCDs come with a fundamental limitation as the pixels in an LCD screen do not emit light themselves. Instead, light is provided by a backlight panel situated behind the pixel layer. This backlight is often composed of mini-LED arrays combined with light diffusion materials. As a result, the total irradiance achievable by an LCD screen is limited by the power of these mini-LEDs in the backlight. Small high-resolution displays are typically engineered to consume low power to optimize battery usage for portable devices. This further limits the maximum light power that such displays can provide. For example, a typical maximum brightness of a small LCD is 625nits (iPhone 11, Apple, USA) with a 90.3 cm2 screen size. This is theoretically converted to 555nm irradiance of the order of 0.01mW/mm^2. Although high-brightness smartphone displays have been proven effective in some optogenetics research with specific extra-sensitive ion-channels[5], it is an order too low to activate the ReaCHR[6] ion-channel used in this work (0.5mW/mm^2). Therefore, the application of LCD in optogenetics might be restricted due to the limited light intensity unless the complete redesign of the backlight of a display, with additional risks and effort.

OLED displays use organic compounds that emit light when electricity is applied. These organic layers are located between two thin-film conductor layers and when an electric current is applied, a light is emitted from the organic layers[7]. Each pixel in an OLED display generates its light, eliminating the need for a backlight. This allows for deep blacks and a high contrast ratio. OLED displays can be made much thinner and even more flexible compared to traditional LCDs. OLED technology has been used in some optogenetics research to stimulate neurons[8][9][10]. However, OLEDs typically have an even lower peak light brightness compared to LCDs due to the organic materials used in OLEDs degrading over time, especially under high current loads required for brighter output. Prolonged exposure to high brightness levels can lead to quicker degradation of these materials, reducing the display's lifetime.

Considering the three proposals for the improved version of the illumination system with their limitations. the decision to choose the mini-LED proposal is made. This choice is to find a balance between the need for higher precision in light control and the constraints of material availability and system feasibility. Mini-LEDs, with their smaller size compared to conventional LEDs used in the previous system, offer a significant reduction in pixel dimension. This miniaturization allows for a more densely packed array, enabling finer control over the light output and distribution. At the same time, mini-LEDs can provide sufficient light irradiance for effective optogenetic stimulation. Additionally, the relatively straightforward availability of mini-LEDs and simplified implementation and integration process compared to more advanced options like micro-LEDs or OLEDs makes this choice more practical.

6.1.2. MICRO-LED: ASSEMBLY TECHNOLOGY

Advanced assembly technologies are employed in specialized applications like high-end displays or research and technical demonstrators. These advanced methods enable the effective and efficient assembly of mini-LED or micro-LED matrix, although they often involve more complex and costly manufacturing processes compared to conventional LED implementation techniques.

High-Throughput Pick-and-Place:

Pick-and-place technology is a critical component of semiconductor packaging. The pick-and-place machines are designed to accurately place semiconductor components onto respective packages. These machines are equipped with sophisticated robotic arms and advanced sensors. The special nozzles on the robotic arms are designed to handle different sizes and shapes of components, while the arms are capable of rapid and precise movements. The nozzles pick individual components from various types of feeders using a vacuum or a mechanical gripper and align the components with advanced vision systems. The machine adjusts the rotation of the components, or flips the component in case of flip-chip design components, and places the component at the designated place on the packages or substrates. The machine repeats the actions at an extremely fast speed to meet the high throughput requirements.

Precision and accuracy are the key features of pick-and-place techniques. For use in the assembly of mini-LED or micro-LED chips, the components become increasingly smaller, typically under 100um. The alignment of these components is critical, as even a minor misplacement can lead to functional defects in the final product. Speed and efficiency are also important considerations since the application of mini-LED or micro-

LED chips often comes with a matrix design where thousands or even hundreds of thousands of components are assembled into one product. High throughput placement is consequently essential for mass production and reducing manufacturing costs.

To address these challenges, technological advancements in robotics, vision systems, and software are continuously being developed. An advanced pick-and-place system for small devices has a high throughput to assemble up to 48.000 dies per hour with a roadmap to 60.000 dies per hour (ADAT3 XF DBRE, ITEC, The Netherlands). With customized assembly profiles and calibrations to the feeder and the substrate, this technology is promising to assemble the mini-LED matrix (or micro-LED matrix in future improvements) as required in this work with high yield and reliability.

Mass transfer

Compared to the pick-and-place technique where individual elements are placed on the substrate by mechanical robotics, mass transfer technology has been introduced recently in creating large-area mini- or micro-LED displays for its advantage of transferring a large number of elements at the same time. This technique involves transferring the large part of or full LED chip wafer to a receiver substrate[11].

Manufacturers or researchers have developed various approaches for efficient mass transfer, including direct wafer-to-substrate transferring using external forces such as electrostatic[12][13] or van der Waals force[14][13]. Both methods involve using an electrostatically charged transfer stamp, or van der Waals force enhanced transfer stamp to move the mini- or micro-LED chips from the wafer directly to the substrate. However, the voltage or the external physical force applied during this process can damage the micro components. Therefore, delicate process control on voltage or pressure is critical for those direct transferring techniques.

Another direct transferring technique is the laser-based method, which uses laser beams to detach mini- or micro-LEDs from the carrier substrate and release them to the receiver substrate. This method has demonstrated high transfer speeds and accuracy in various research or applications[15][16][17]. However, keeping high consistency with the laser transfer method can be challenging.

Self-assembly

The self-assembly technique is the method where the transferred method is assembled without the influence of external forces individually on each element, but aligned automatically into the designated location[18][19]. The assembly automation can be based on various physics depending on the properties of the elements or substrate. Fluidic-

based self-assembly uses the physical properties of the components to be transferred and aligned, as well as the liquid or solvent. The driving force of the self-assembly can be liquid surface tension or evaporation, which generates mechanical forces to push or pull the components with designed actions. Also, nano-structures can be created to generate capillary forces that the components can move in the liquid. Usually, the fluidic-based method needs special treatment at the target substrate that either creates special crystal structures or patterns. This method has been popular in much research of nano-materials[20][21][22][23]. Additional external forces, not to individual elements, but a global stimulation method to guide all components to move and align at the substrate are also studied. The forces can be electrical[22][24], magnetic[25], or even temperature difference[26]. The transferred elements are manufactured or post-treated to be active on these external forces.

These assembly techniques are capable of handling large amounts of elements with small-scale component applications. While they deliver effective results, they require specialized expertise and specific tools that are not immediately available and come along with a high risk. Therefore, in the work in this chapter, the assembly of the mini-LED matrix is done by using a semi-automatic pick-and-place tool with manual operations. This approach is chosen because the system is intended for technical demonstration, and the scale of the matrix is relatively small and reasonable for manual operations. Looking ahead to future systems that might involve a larger matrix scale or smaller component sizes, the assembly process could be greatly accelerated by using a fully automated high-throughput pick-and-place machine. This machine would need to be equipped with the appropriate tooling to manage the smaller size and flip-chip design of the mini-LEDs efficiently.

6.2. A 16x16 MINI-LED MATRIX ILLUMINATION SYSTEM DESIGN AND INTEGRATION

The development of a 16x16 mini-LED matrix illumination system is developed with shared methodologies from previous designs while incorporating technical improvements. Using a mini-LED matrix allows for a reduction in the dimension and interval of matrix elements, enhancing the system's precision in controlling light exposure.

Despite these improvements, the scale of the matrix is maintained at 16x16. For the reuse of the control and driver systems from the previous design, facilitating a more rapid development process, as the main purpose of the proposed system is a techni-

Figure 6.1: The mini-LED wafers used in the system, in flip-chip packaging on carrier films

cal demonstrator to test the assembly and integration of the mini-LED matrix. While the system is still compatible with smaller cell culture formats like a 12-well plate, the knowledge, and techniques gained in the development can be applied simply to scale up the matrix for use with larger platforms such as 6-well plates or 145mm Petri dishes with hiAM cell culture, which are more representative of clinical scenarios. This section introduces the design and fabrication of this advanced mini-LED matrix illumination system, with a stress on the integration techniques for the mini-LED matrix assembly

6.2.1. MINI-LED MATRIX SUBSYSTEM DESIGN

The mini-LED chips (BFB0F11C, Aucksun Optoelectronics Technology, China) used in the illumination system are provided in the form of diced wafers (Figure 6.1). These InGaN-based mini-LEDs are produced through 3-inch semiconductor manufacturing processes and are diced onto a dicing foil. The specifications are provided by the manufacturer.

The mini-LED chips are designed in flip-chip packaging (Figure 6.2), where the top side of the mini-LED emits light, and the contact pads and pre-coated solder balls for interconnection are located on the bottom side of the chip. This packaging results in higher matrix illumination efficiency as the entire chip area is dedicated to light emission, unlike other mini-LED chips where bonding pads occupy some of the illuminating surface areas. Additionally, the flip-chip design allows for denser integration of the chips

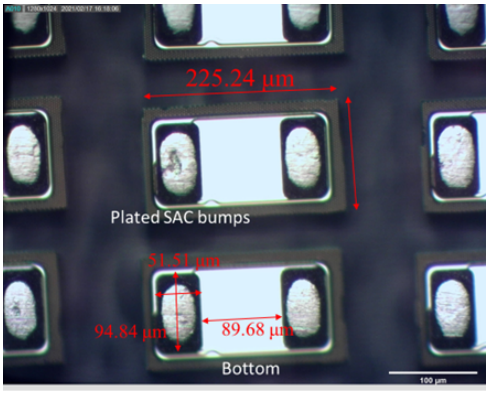

Figure 6.2: Microscopic photo of the mini-LED chips used in the system

on the substrate. Since the footprint of each mini-LED is the same as the chip size and no extra wire bonding pads are needed, it's possible to pack the elements more closely together.

Each mini-LED measures 125 by 250 um in size and has a thickness of 90 um. The radiant power of these mini-LEDs is provided by the manufacturer that at a driving current of 5mA, each mini-LED is rated to deliver 9mW of radiant power at a peak wavelength of 450nm. The mini-LED can be driven with a maximum current of 20mA. This specification suggests that with a well-designed thermal dissipation system and when operated in short pulse modes, each mini-LED is capable of delivering a light power as high as 30mW. This high output potential is significant for optogenetic applications, which is well within the effective range for activating ion channels in cells modified with the ReaChR gene in the hiAM monolayer.

In the new system with mini-LEDs, unlike the previous system where conventional LEDs are arranged in an equilateral layout for better light uniformity, a change in the matrix layout has been made due to the reduced size of the mini-LED elements and the element intervals.

In the equilateral layout of the previous system, the routing between each row has to pass through the narrow triangular spaces between column LEDs. While this is still feasible with larger conventional LED intervals and footprints, the significantly smaller dimensions in the mini-LED system face the challenge of implementing a similar equilateral layout. The much-reduced distance between elements and the smaller footprint of mini-LEDs make the routing between column elements in an equilateral layout exceedingly difficult. The checkerboard layout, on the other hand, offers more space between columns and rows, reducing the challenges of routing within the densely packed

mini-LED matrix. Therefore, for the proposed mini-LED system, the checkerboard layout has been selected. It provides a more practical solution for integrating the smaller, densely-packed mini-LEDs.

Optical simulation is then made to estimate the illumination distribution of the mini-LED matrix in the experimental applications. The methods and calculations are identical to the design progress of the LED matrix system discussed in the previous section.

This mini-LED matrix technical demonstrator is designed for potential future optogenetics research using a 145mm Petri dish, therefore, the optical design is based on its specific dimensions accordingly. The 145mm Petri dish is particularly preferred in advanced hiAM optogenetic research since the area of the cell cultures is closer to the size of the human atrial wall.

Measurement is conducted for the bottom thickness of a standard 145mmx20mm Petri dish with a typical value of 0.4mm. In addition to this protective layer at the top, the mini-LED is necessary as discussed in the previous section. This protective layer serves multiple purposes: it physically protects the mini-LEDs against Petri dish scratching and impacts, provides additional support to ensure mini-LEDs remain fixed in place, and acts as a thermal barrier to manage the heat generated by the mini-LEDs. An additional 0.15mm of the protective layer is added to the projecting distance, making the total projecting distance (H) from the mini-LED to the target cell culture surface 0.55mm.

By optical simulations conducted in previous sections, an optimized matrix layout is based on achieving the best possible uniformity of light at the target surface. For the checkerboard layout, it has been determined that the optimized result is attained when the ratio of the interval (D) between elements to the projecting distance (H) is D:H=1.1. Given the calculated projecting distance (H) of 0.55mm, the optimal interval between the elements in the matrix is determined as 0.55mm * 1.1 = 0.6mm (Figure 6.3).

By considering these physical and optical requirements, the mini-LED matrix system is designed to ensure optimal illumination of the cell cultures. This level of optimized uniformity can be equally beneficial in future advanced system design for ensuring consistent and reliable results in optogenetics research that the larger matrix should cover all cell cultures in the 145mm Petri dish. Once the mini-LED matrix layout is determined, the light irradiance of the matrix is also estimated by calculating the fraction between the total radiant power of all mini-LEDs and the matrix area. Approximation of the projecting area on the hiAM surface as the mini-LED matrix size is used in the calculation since the scale of the system is small. When using the same row-scanning controlling methods, the theoretical average irradiance when driving each mini-LED at a specified 5mA is:

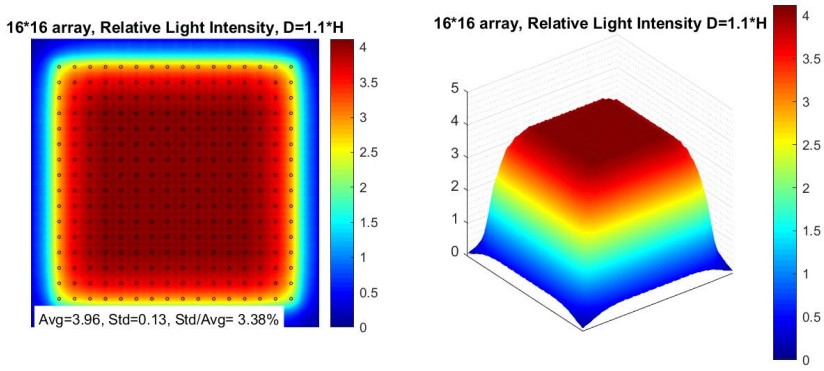

(a) 2D plot

(b) 3D plot

Figure 6.3: Simulated light distribution with matrix interval (D) and projecting distance (H) ratio is D:H = 1.1 to achieve uniform light distribution at the target surface

$$I_{max} = \frac{16 \times 16 \times 9mW}{(0.6 \times 16)^2 mm^2} \times \frac{1}{16} = 1.56mW/mm^2 \tag{6.1}$$

When considering the mini-LED switch on and off latency to reduce the real active duty cycle, a more realistic estimation of the average irradiance is not lower than 0.5mW/mm^2, which is already proven by previous experiments to be sufficient for hiAM potential wave pacing and AF wave global termination.

When driving the mini-LED matrix with a maximum current of 20mA, the maximum estimated average irradiance is not lower than 2.5mW/mm^2, which is proven sufficient for hiAM AF wave blocking and termination.

6.2.2. MINI-LED MATRIX SUBSYSTEM ASSEMBLY AND INTEGRATION

The assembly process is the most critical and challenging part of integrating the mini-LED matrix system, especially considering the minimized size of the mini-LED chips. Standard automated pick-and-place machines, typically used in electronics assembly, require specialized tooling to handle such small components as the mini-LED chips used in this project. For the 16x16 mini-LED matrix as the technical demonstrator with a total of 256 elements, manual assembly of a vacuum pick and place tool is still a feasible option with reasonable time-consuming. Completing the assembly manually is estimated to take around two hours by an experienced operator, which is acceptable for a small number of samples for research purposes.

Additional complexity in the assembly process comes from the flip-chip design of the mini-LEDs used in this system, which requires an additional step where each chip must be picked up from the carrier film, flipped on its side, and placed accurately aligned with the substrate so that its solder balls connect correctly with the designated footprint on the substrate. This step is crucial for guaranteeing a 100% yield with proper electrical connections and functionality of each LED in the matrix. The assembly process could be significantly speeded up with an automated pick-and-place machine equipped with the necessary tooling to handle the small size and flip-chip design of the mini-LEDs. Such high-throughput pick-and-place machines are used in the manufacturing of RFID tags, which is a promising technical solution for future improvements with a much larger-scale mini-LED matrix.

Finding an appropriate substrate for the mini-LED matrix is another significant challenge, again due to the small size of the mini-LEDs. The flip-chip design requests the footprint on the substrate exactly matching the dimensions of the mini-LED chip itself, to ensure the alignment of the contact pads with the solder balls of the chip. This means that the contact pad dimensions and the minimum footprint feature clearances on the substrate need to be manufactured with extremely high precision, in the range of about 100µm. Additionally, the determined interval of 0.6mm between each mini-LED element in the matrix results in a minimal empty spacing of around 400µm between each chip in a row. This tight spacing adds complexity to the substrate design to place electrical routing and vias around each mini-LED footprint.

Traditional FR4 material PCBs as used in previous systems, are not suitable for this application anymore due to the technical limitations in achieving the required minimal feature clearances, via sizes, contact pad dimensions, etc. There is a clear need to explore new substrate materials and manufacturing techniques that are capable of meeting these tight specifications while maintaining relatively low development risks and reasonable effort and cost. Polyimide substrate PCB and corresponding fabrication and assembly techniques are chosen for their unique advantages.

Polyimide substrate PCB is a specialized type of Printed Circuit Board with a polyimide thin film as the intermediate layer between two or more copper layers in the sandwich structure of a PCB. Polyimide PCB supports smaller design features than traditional FR4 PCBs, such as finer lines, smaller vias, and tighter spacing, etc. This is due to the much thinner thickness of the substrate material, commonly 0.1 to 0.5mm, supporting higher resolution in the lithographic and etching process in the manufacturing of the polyimide PCB. The advanced polyimide PCB can support as small as 80um features of interconnects and a minimum diameter of 100um, which meets the design requirements

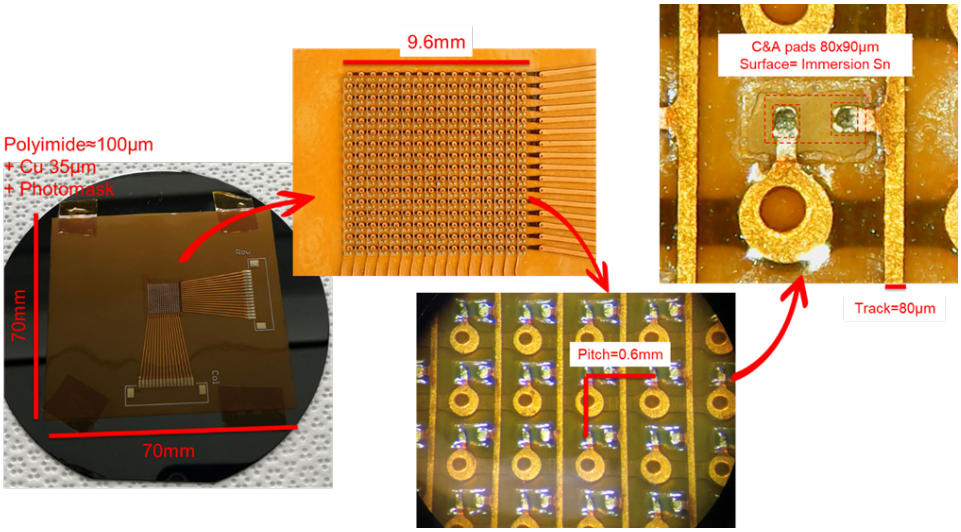

Figure 6.4: The customized polyimide PCB substrate fabricated for the mini-LED matrix system

of this mini-LED system layout. The manufacturing of polyimide PCBs shares most processes and facilities as normal PCBs, therefore the manufacturing process is stable and consistent with reasonable cost.

Polyimide PCB is also known for its flexibility. This feature makes it suitable for applications where the electronics system needs to conform to irregular, narrow spaces or bend, as it is often used in the interconnecting flat cables of consumer electronics and specialized moving devices. This feature can be potentially beneficial for the future development of implantable systems where the illumination matrix might need to conform to the geometry of a heart in real clinical treatments.

Polyimide PCB also has a higher resistance to temperature compared to traditional composite materials. They can withstand significant heat up to 200°C without structural damage, which is essential in applications where the electronics may be exposed to high temperatures. This feature can be beneficial for the high-dense mini-LED matrix where high thermal density might create hot spots on the substrate. Moreover, polyimide substrates offer improved electrical properties, including higher dielectric strength, enhancing the system's overall electrical insulation and performance.

The 16x16 mini-LED matrix layout with determined design values is translated into a physical layout using computer-assisted software. Then the design files are outsourced to manufacturers and suppliers for fabrication, following the fabricating classifications of the manufacturer which meet the capabilities and limitations.

The customized polyimide PCB substrate has a dimension of 70mm by 70mm. The intermediate polyimide layer has a thickness of 100um with 35um thick copper wiring layers on both sides. The active mini-LED matrix is located at the center of the substrate with a size of 9.6mm by 9.6mm according to the 16x16 matrix with 0.6mm interval design.

In each mini-LED footprint, two contact pads with dimensions of 80x90um are printed to align with the flip-chip solder balls. The surface is coated with an immersion Tin layer of 1.0um thickness to enhance the performance of the reflow solder process in the following assembly. The substrate is covered with approximately 20um thickness of transparent solder mask, with square openings at the mini-LED footprints. This design should allow the mini-LED chips to be somewhat fixed within their footprint area during the following assembly processes to further increase the yield.

The column current signal wires are routed vertically at the front side of the substrate, while the row-scanning signal wires are routed horizontally at the backside of the substrate with through-substrate vias connecting the contact pads at the front side. The vias and signal wires are accurately placed at the in-between spacing of mini-LED chips without creating potential short circuits. This design pushes the limit of the substrate fabrication technology. The row-scanning signal wires are designed with extra width for carrying a higher current than the full row of mini-LEDs.

Both column-scanning signal wires and column signal wires are extended from the active matrix area to the side of the substrate and connected to a flat cable connector respectively. These connectors thereby connect the mini-LED matrix with its external control and driving system. The polyimide PCB substrate is temporally taped to a bare silicon wafer for better handling and physical protection for following the assembly process.

A customized assembly process (Figure 6.5) is developed for the integration of a mini-LED matrix on the polyimide PCB substrate with some unique innovations.

1. **Substrate preparation**

   The outsource polyimide PCB substrate is first cleaned with isopropanol liquid and let dry on a hot plate. A plastic masking sheet with a square opening in the center is taped on top of the substrate. The opening has a dimension of 12x12mm to expose the matrix area and to cover the rest part of the substrate. A thin layer of flux (SK10, KONTAKT CHEMIE, The Netherlands) is applied to the front side of the substrate. The spraying is done manually by the operator evenly spraying the aerosol can at a 20cm distance to the front five times, then waiting for 30 minutes for the aerosol solvent to evaporate and leave a dry flux layer. Then the masking

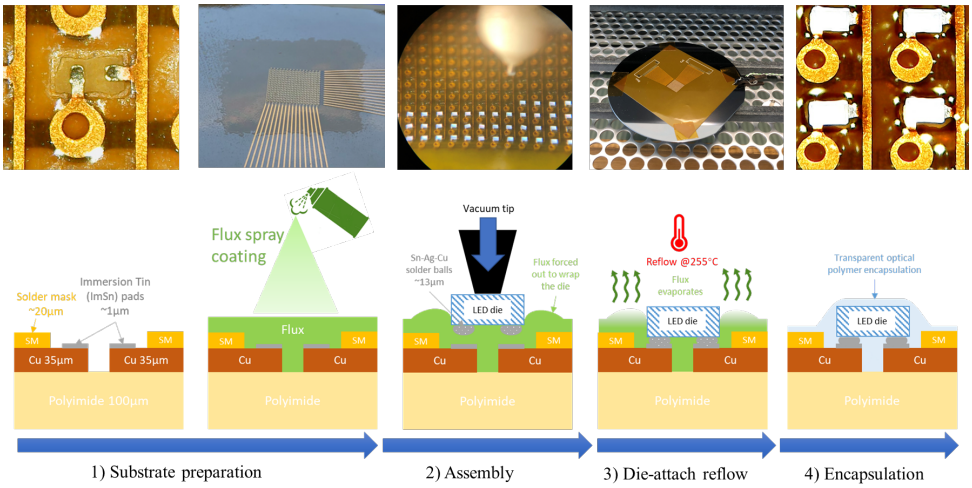

Figure 6.5: Assembly process of mini-LED chips and polyimide PCB substrate

sheet is removed.

Thickness measurement is conducted by a precise height gauge (Mitsutoyo, Japan) at various batches of spray samples at different locations on the masked matrix area, and the dried flux layer is measured between 50 to 100 um thick. The flux layer is even and continuous on top of the matrix footprint area without opening spots or excessive residues.

2. **Assembly pick-and-place**

The mini-LED chips are designed in flip-chip packaging, where the top side of the mini-LED emits light, and the contact pads and pre-coated solder balls for interconnection are located on the bottom side of the chip. The chips are delivered in an upside-down diced wafer format, where individual dies are separated from the wafer and attached to a blue carrier film with the bottom side and solder balls facing outside. In automatic industrial assembly processes, a special machine is used to release the dies from the carrier film and flip them for following pick-and-place to the substrate. However, this is not possible with limited resources in the manual assembly of this demonstrator system. Instead, the whole carrier film with mini-LED dies is placed upside down to a carrier bare wafer, and the dies are released by soaking the setup in acetone for 30 seconds. The carrier film is removed carefully without flipping the released chips. The chips are then let dry for 10 minutes. Most chips remain in the reversed position on the carrier wafer

and are then ready for assembly to the substrate.

One of the purposes of applying a flux layer is to adhere the mini-LED chips to the substrate after the pick-and-place process where a semi-auto vacuum pick-and-place tool is used. This tool is particularly modified for handling the small size of the mini-LED packages by the use of a customized vacuum tip, which is designed with a very thin stainless-steel hollow needle tip at a diameter of 100um. The size of the vacuum tip aligns well with the dimensions of the mini-LED chips to ensure a reliable pick-and-place process.

The tool also features an automated vacuum release valve. The movement and the pressure applied by the vacuum tip are calibrated by an adjustable valve to automatically trigger the vacuum switch for either switched on for pick actions or switched off for place actions. The release pressure is adjusted to 40psi after multiple trial tests. This pressure is at the lower end of typical settings for such tools to avoid applying excessive force on the mini-LED chips, which could potentially damage the illuminating top side or crush their solder balls. Despite the lower pressure, the bonding yield of the chips to the substrate is not compromised because the flux provides adequate adhesion of the components.

Each chip is individually picked up by vacuum tip with the help of an optical microscope (Figure 6.6). After aligning the chip with the footprint on the polyimide substrate, the vacuum tip is carefully lowered and the set pressure is applied to ensure that the chip adheres properly to the flux layer with the help of solder mask windows on the substrate. Once the chip is placed, the vacuum is switched off automatically by the pressure setting, and the operator conducts a visual inspection to verify the alignment and bonding of the chip using the microscope. If a chip is improperly aligned, tilted, or not adequately bonded, it is removed and disposed of to avoid potential damage from multiple vacuum actions. Completing the pick-and-place process of the entire 16x16 mini-LED matrix using this method takes about two hours for an experienced operator.

3. **Die-attach reflow**

The next step in the assembly process is to create electrical bonding between the substrate and the mini-LED chips. This is achieved through a die-attach reflow process. The substrate assembled with the mini-LED chips is carefully transferred to a reflow oven (EC ReflowMate V4, EuroCircuits, Belgium). A carrier bare wafer is used for safe transferring and carrying of the assembly. The flux layer applied earlier secures the position of the chips by adhering them to the substrate, preventing

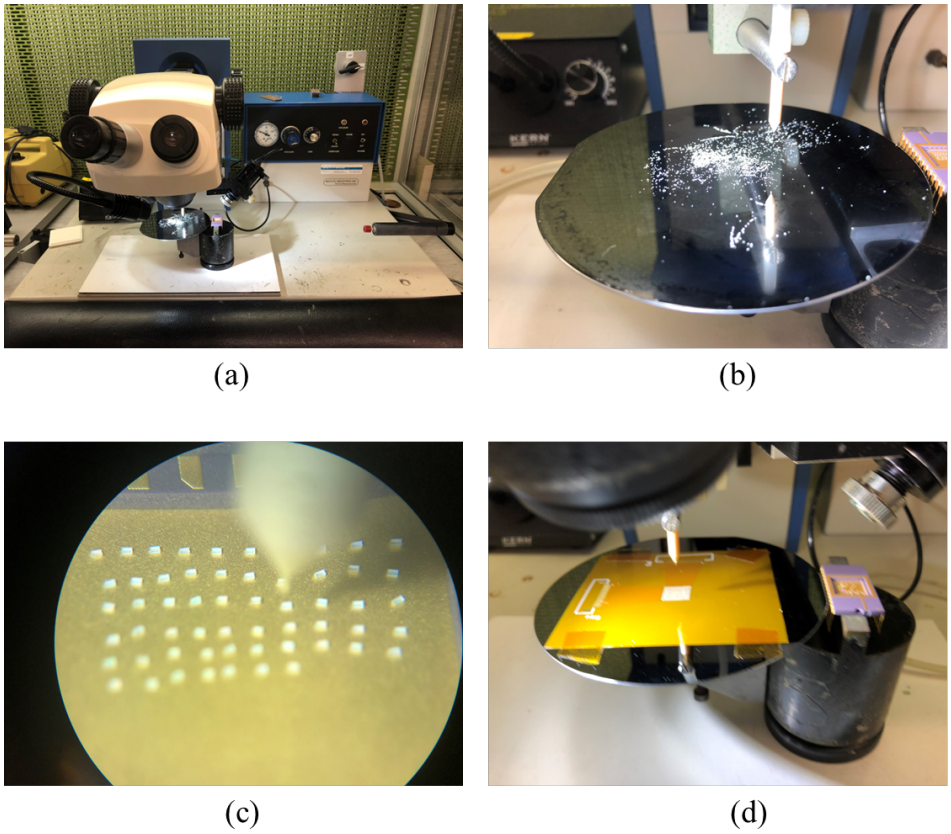

Figure 6.6: Assembly by pick-and-place technique: (a) A semi-automatic pick-and-place tool with a microscope; (b) Mini-LED dies released from the carrier film; (c) Mini-LED dies being picked up by the vacuum tip; (d) Mini-LED dies transferred to the polyimide substrate

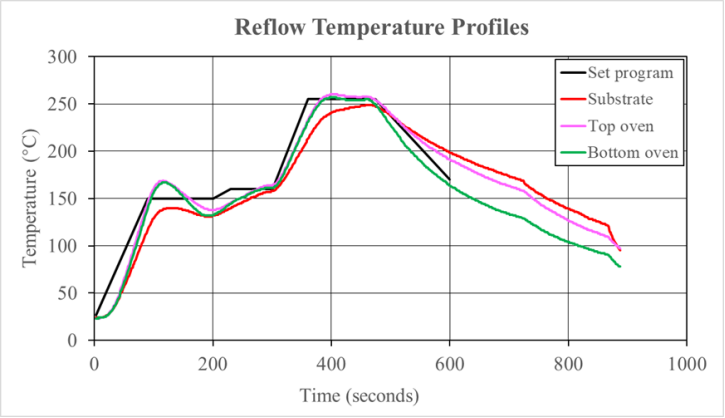

Figure 6.7: Reflow temperature profiles of set program and measured values from the sensor at the substrate surface, top and bottom of the oven tray table

any movement or misalignment during the transfer.

Once the substrate is secured in the reflow oven tray, a controlled reflow program is applied. This program is typically standard for SAC305 (Tin-Silver-Copper) solder, which is the material used for the solder balls of the mini-LED chips. The profile includes a stabilizing heating up to 160‘C in the beginning 5 minutes, followed by a rapid reflow phase of 255°C plateau of 1 minute. After the reflow phase, the temperature is rapidly cooled down in 2 minutes to 170°C by forced convection cooling to solidify the solder joints. After 2 minutes the reflow oven is opened and the assembly is cooled down to room temperature by natural convection. The temperature profile is controlled to ensure that the solder reflows properly, forming robust and reliable electrical connections between the mini-LED chips and the substrate connecting pads. Three temperature sensors are placed at the surface of the substrate, the top, and the bottom of the oven tray table, and measured temperature data shows a reasonable response following the reflow program (Figure 6.7).

In the die-attach reflow process, the flux plays several crucial roles to ensure the successful bonding of the mini-LED chips to the substrate. During the reflow process, the flux heats up and melts, enveloping the solder balls under the mini-LED chips and the tin-coated contact pads on the substrate. The flux acts as a cleaning agent by removing any oxidation from the surface of the solder balls and contact pads. During the high temperatures of the reflow process, the flux serves as a protective layer that prevents the solder from further oxidation, ensuring the

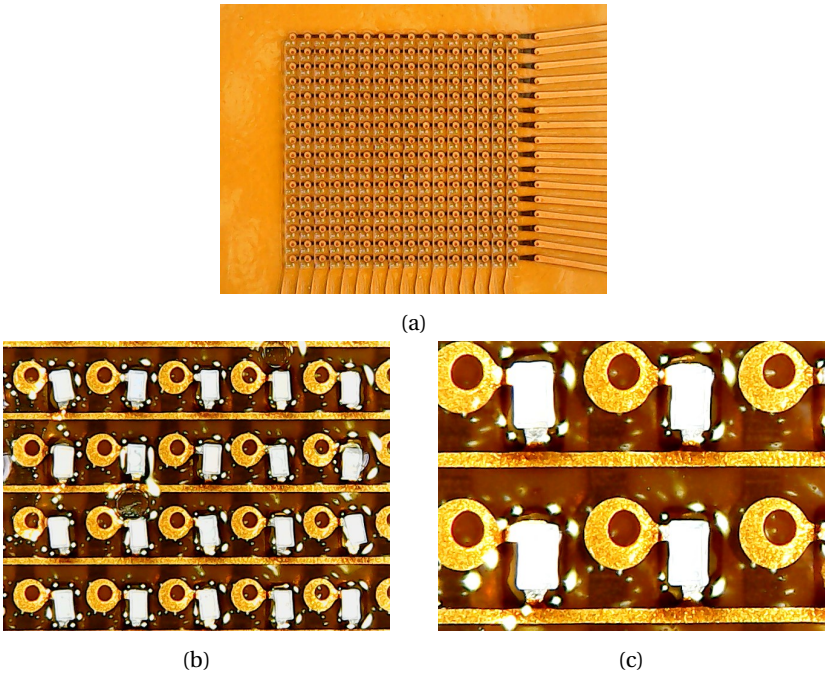

(a) (b) (c)

Figure 6.8: Microscopic photos of a mini-LED matrix with the encapsulation layer

integrity of the finished solder joints. Moreover, the flux reduces the surface tension between the tin coating and the molten solder and allows for better flow of the molten solder. This feature helps the correctly aligning of the mini-LED chip with the footprint, as the surface tension of the molten solder helps to pull the chip into the proper position.

After the reflow process, the majority of the flux decomposes and evaporates, leaving behind a small amount of residue. This residue is cleaned with isopropanol.

4. **Encapsulation**

A protective layer on top of the mini-LEDs is applied in the following step. It should protect the mini-LEDs from potential scratches and impacts that might occur from contact with a Petri dish. Also, it provides structural support to keep the mini-LEDs securely in place in addition to solder joints only. The layer also functions as a thermal barrier for the heat generated by the mini-LEDs during operation.

As the thickness of the protective layer should impact the optical performance of the matrix light projecting, it should be kept at 0.15mm thick precisely. In previous illumination systems, the protective and encapsulation layers are made with

PDMS polymer for their great thermal isolating characteristics and bio-compatibility. However, the viscosity of the PDMS mixture is high and it makes it challenging to form the requested very thin layer evenly without bumps or residues. Instead, the transparent UV-curable optical adhesive (NOA63, Norland Products Inc. USA) is used. A thin, transparent layer of the UV-curable optical adhesive, with a thickness of approximately 0.15mm at the illumination side of the mini-LED is then applied by a drop pipette and a fine brush. The adhesive is then cured at room temperature under four 15W ultraviolet lamps (CLEO Compact, Philips) for 10 minutes.

After the mini-LED matrix is assembled and processed, two flat cable connectors are soldered manually at the edge of the substrate. The whole setup is finally cleaned with isopropanol to remove remaining flux excess or grease and is ready for characterization.

6.2.3. DRIVER AND CONTROL SUBSYSTEM DESIGN AND IMPLEMENTATION

The control and driver system for the 16x16 mini-LED illumination system shares a similar design architecture with the previous system with conventional LEDs (Figure 6.9). In this system, the electronics have much fewer design constraints or limitations because the mini-LED matrix is now driven by a 10 times lower current of 100mA compared to 1A in the previous system. Available open-source projects for small-scale display can be adopted together with highly integrated hardware solutions.

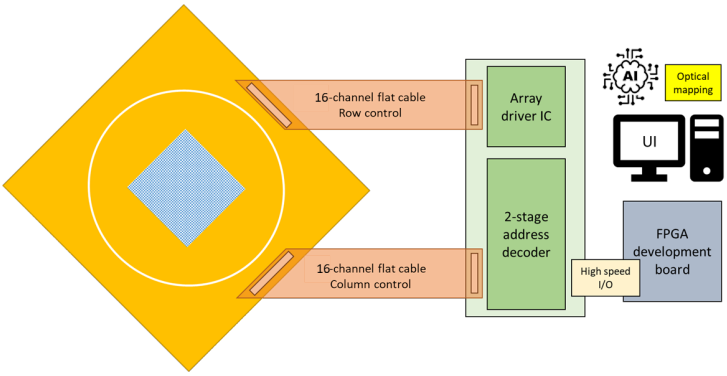

Figure 6.9: The architectural schematic of the mini-LED matrix illumination system

The control logic for the mini-LED matrix follows a similar approach to what is discussed in previous chapters (Figure 6.10). The mini-LED matrix also operates using a row-scanning method that sequentially activates each row of the matrix at a set refresh rate. This method has been tested and proven to be able to manage the complex pattern of an LED matrix effectively. An array of PMOS transistors switch from each row

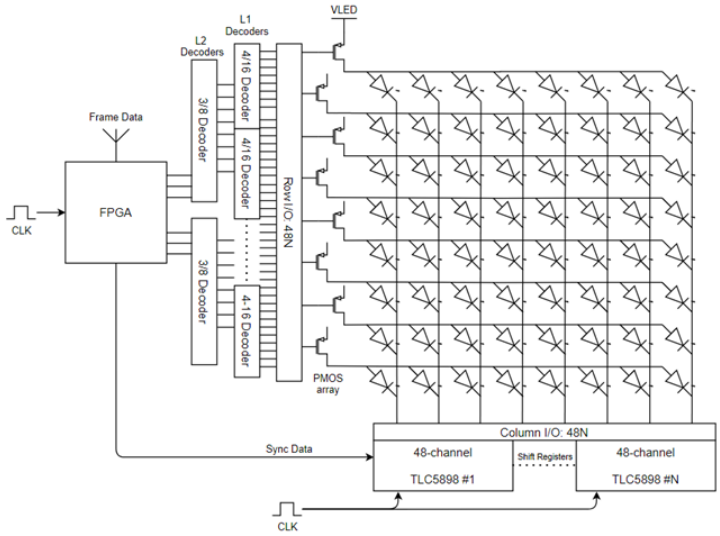

Figure 6.10: The architectural schematic of the driver and control system for the mini-LED matrix

of the matrix, and the transistor array is controlled and synchronized by two levels of the address finding 3-bit and 4-bit decoder chips (SN74HC138 and CD74HC154, Texas Instruments, USA). The scanning is operated with a specific refresh rate through all the rows in the matrix, which can affect both the final irradiance and the consistency of the projected patterns.

At the other end of the mini-LED matrix interconnects against the row-scanning component, current sources are connected to the columns of the matrix. These current sources are responsible for controlling the amount of current flowing through each mini-LED and therefore, control the irradiance output. Advanced LED control chips (TLC59581, Texas Instruments, USA) are used. The highly integrated chip is powerful with embedded digital regulation functions to automatically translate the high-speed digital signals to analog current signals, and drive the external up to 48 channels through the embedded current sources. This chip is perfect for small-scale, high-speed LED display or matrix applications with minimized circuit design.

Both the row-scanning and column-driving chips are controlled via series protocol by an external Field Programmable Gate Arrays (FPGA) development system. An FPGA has integrated circuits that can be programmed after manufacturing. They consist of a matrix of configurable logic blocks and programmable I/O interconnects, allowing highly customizable hardware tailored to specific applications. They are generally more

complex and expensive to program and develop compared to MCUs. The FPGA sends synchronizing clock signals to all the chips that directly control the mini-LED matrix and it communicates with the overhead PC with pattern recognition and advanced algorithms. The communications are operated via the high-speed Wi-Fi function built-in in the FPGA development system.

The driver and control electronics and the FPGA development system are connected via two customized flat cables made of polyimide. The flexible flat cable offers high freedom of the system positioning while still being capable of handling the power of a mini-LED matrix. All electronics in the illumination system are powered by an external 5V power supply.

The driver and control system in this system has significant improvements primarily in flexibility and scalability. The electronics and architecture as developed are capable of supporting larger matrices up to a size of 96x96. This improved flexibility and scalability is largely due to the introduction of two-level decoders and 48-channel current source chips. These components enable a modular design of controlling the mini-LED matrix. To expand the matrix, additional decoder chips and current source chips can be integrated directly into the system without the need to alter its fundamental architecture. This modular design not only eases the expansion process for future development of large-scale mini-LED matrix for Petri dish full coverage but also ensures that the system remains adaptable for various research and application requirements.

6.2.4. SYSTEM CHARACTERIZATION AND VERIFICATION

After integrating the whole illumination system with the mini-LED matrix and the driver/control system, characterizations are performed to assess the system's functionality and performance. The characterization procedures are similar to the LED matrix system as discussed in the previous chapter.

Note that the characterization is done with the driver system of the LED matrix in the previous chapter due to the FPGA system not being developed with stability. The maximum current is set to 20mA to align with the mini-LED design. There is no main difference between the MCU-based control electronics and with FPGA-base system since the major improvement of the FPGA-base system is the extendibility of the matrix scale. Therefore, the characterization results are in general valid for the mini-LED matrix.

The characterization involves testing the system's ability to accurately display a pattern based on PC input. A university logo, represented as a 16x16 pixel gray-level image, is input into the PC software, which is set to an illumination irradiance level of 10. The software processes and adapts the image to the mini-LED matrix layout and wirelessly

transmits it to the driver and controller system, which changes the LED matrix to illuminate the corresponding mini-LED elements and display the image (Figure 6.11).

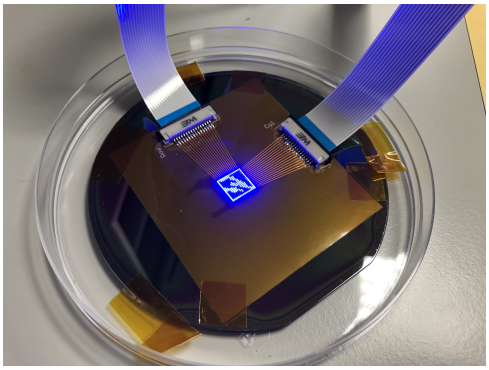

Figure 6.11: Mini-LED functional tests with illumination of an input image

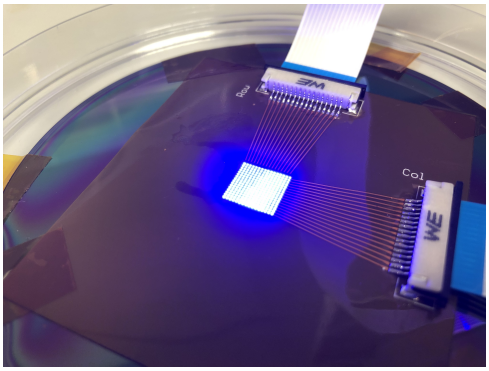

Figure 6.12: Mini-LED functional tests with global illumination of all elements

The second characterization involves calibrating the user interface program's irradiance settings, ranging from 0 to 127, to match the actual irradiance emitted by the mini-LED matrix (Figure 6.12). This process is operated as the same calibration method used previously a high-power optical sensor is positioned at the center of the matrix, covering a 10mm diameter circular area to measure the average irradiance. The measured area just covers the full mini-LED matrix active area. As the UI input setting increases from 0 to 127, the sensor reads the irradiance at each step, with each reading taken three times and averaged for accuracy.

Data from the irradiance characterization is plotted (Figure 6.13) to reveal the linear relationship between the UI input values and the mini-LED matrix irradiance. The specific irradiance is measured as 0.75mW/mm^2 at 5mA (UI input = 31) and the maximum

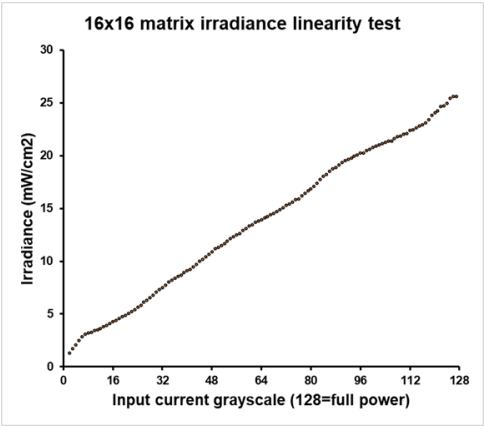

Figure 6.13: Optical characterization of mini-LED matrix irradiance versus UI input current setting

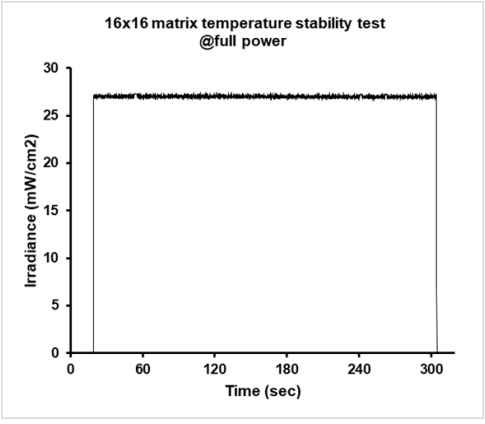

Figure 6.14: Thermal stability characterization of mini-LED matrix irradiance versus operation time

irradiance is measured as 2.5mW/mm^2 at 20mA (UI input = 127). It is observed that the actual measured irradiance values are lower than those predicted in simulations due to the mini-LED having relatively long rise and fall times during switching, which are not counted in the simulations. However, the measured specific irradiance is still sufficient for hiAM potential AF wave global termination, and the maximum estimated average irradiance is sufficient for hiAM AF pacing, wave blocking, and termination.

Additional characterization is conducted to assess the irradiance long-term stability of the mini-LED matrix, particularly considering its increased thermal density due to the reduced size of the matrix. There is a concern about the potential for hot spots,

which could affect the optical performance of the mini-LEDs. To evaluate this, the mini-LED matrix is fully operating with all elements switched on and powered at maximum capacity using a current of 100mA. The matrix is placed on a plastic board, simulating the conditions in an optical voltage mapping setup. This arrangement aims to closely mimic the actual environment in which the matrix would be used. An optical sensor is positioned directly above the matrix to measure the irradiance continuously over 5 minutes. The data collected during this test (Figure 6.14) demonstrates that the irradiance output remained stable, showing no significant decrease over the extended duration of the test.

6.3. CONCLUSIONS AND LIMITATIONS

The development of the 16x16 mini-LED illumination system for hiAM optogenetics research is discussed and presented in this chapter.

Based on previous experience, this system improves its capability of more precise control of illumination by adopting mini-LED chips. The polyimide substrate material enables the implementation of the mini-LEDs with their small size and flip-chip design, with the help of a customized assembly process including pick-and-place with unique flux layer treatment. The improved controller and driver design with advanced integrated chips and FPGA enable easy expansion of the matrix for future scaling up of the system without extensive redesigns, making the system versatile and adaptable to various research needs.

Looking forward, this development lays the groundwork for further advancements as a technical demonstrator for the main challenges in high-density mini-LED matrix design and integration, such as chip assembly technique and control systems. It opens possibilities for incorporating illumination systems with larger matrix scales or even smaller LED components and exploring high-resolution display technologies for finer control over light patterns for future advanced research in hiAM optogenetics.

One of the primary limitations currently faced in the development of the mini-LED illumination system is related to the driver and control system, specifically the integration and testing with an FPGA-based system. This challenge stems from the technical complexities associated with developing and implementing FPGA-based solutions, which require specialized expertise in FPGA programming and embedded systems.

Another notable limitation in the current phase of the mini-LED illumination system is the lack of testing with hiAM cell cultures in biomedical experiments. This testing phase is crucial for evaluating the system's effectiveness and practicality in real-world research applications. The current dimensions of the mini-LED matrix prevent it from

covering the entire bottom of a well in a 6-well plate. One potential workaround for this limitation is to conduct tests with hiAM cell cultures in smaller wells, such as those found in 12-well plates, with the corresponding risk of missing bioelectrical response information due to the limitation of surface area. A more long-term proposal is in the future development of the system, specifically scaling up the size of the mini-LED matrix to cover the entire area of a standard 145mm Petri dish. Since the irradiance parameters of the current system are already tested sufficiently, this expansion would not compromise the system's functionality but rather extend its capability in larger-scale experiments.

BIBLIOGRAPHY

[1] Sebastian Junge et al. “A micro-LED array based platform for spatio-temporal optogenetic control of various cardiac models”. In: *Scientific Reports* 13.1 (2023), p. 19490.

[2] Sofian N Obaid et al. “Multifunctional flexible electro-optical arrays for simultaneous spatiotemporal cardiac mapping and modulation”. In: *bioRxiv* (2022), pp. 2022–05.

[3] Nir Grossman et al. “Multi-site optical excitation using ChR2 and micro-LED array”. In: *Journal of neural engineering* 7.1 (2010), p. 016004.

[4] Robert Scharf et al. “Depth-specific optogenetic control in vivo with a scalable, high-density μLED neural probe”. In: *Scientific reports* 6.1 (2016), p. 28381.

[5] Kimmo Lehtinen, Miriam S Nokia, and Heikki Takala. “Red light optogenetics in neuroscience”. In: *Frontiers in Cellular Neuroscience* 15 (2022), p. 778900.

[6] John Y Lin et al. “ReaChR: a red-shifted variant of channelrhodopsin enables deep transcranial optogenetic excitation”. In: *Nature neuroscience* 16.10 (2013), pp. 1499–1508.

[7] Yuge Huang et al. “Mini-LED, Micro-LED and OLED displays: present status and future perspectives”. In: *Light: Science & Applications* 9.1 (2020), p. 105.

[8] Anja Steude et al. “Arrays of microscopic organic LEDs for high-resolution optogenetics”. In: *Science advances* 2.5 (2016), e1600061.

[9] Andrew Morton et al. “High-brightness organic light-emitting diodes for optogenetic control of Drosophila locomotor behaviour”. In: *Scientific reports* 6.1 (2016), p. 31117.

[10] Dongmin Kim et al. “Ultraflexible organic light-emitting diodes for optogenetic nerve stimulation”. In: *Proceedings of the National Academy of Sciences* 117.35 (2020), pp. 21138–21146.

[11] Abdur Rehman Anwar et al. “Recent progress in micro-LED-based display technologies”. In: *Laser & Photonics Reviews* 16.6 (2022), p. 2100427.

[12] Xue Feng et al. “Competing fracture in kinetically controlled transfer printing”. In: *Langmuir* 23.25 (2007), pp. 12555–12560.

[13] E Menard et al. “A printable form of silicon for high performance thin film transistors on plastic substrates”. In: *Applied Physics Letters* 84.26 (2004), pp. 5398–5400.

[14] Hoon-sik Kim et al. “Unusual strategies for using indium gallium nitride grown on silicon (111) for solid-state lighting”. In: *Proceedings of the National Academy of Sciences* 108.25 (2011), pp. 10072–10077.

[15] Andrew S Holmes and Sabri M Saidam. “Sacrificial layer process with laser-driven release for batch assembly operations”. In: *Journal of Microelectromechanical Systems* 7.4 (1998), pp. 416–422.

[16] Val Marinov et al. “Laser-enabled advanced packaging of ultrathin bare dice in flexible substrates”. In: *IEEE Transactions on Components, Packaging and Manufacturing Technology* 2.4 (2011), pp. 569–577.

[17] Val R Marinov. “52-4: Laser-Enabled Extremely-High Rate Technology for μLED Assembly”. In: *SID Symposium Digest of Technical Papers*. Vol. 49. 1. Wiley Online Library. 2018, pp. 692–695.

[18] George M Whitesides and Bartosz Grzybowski. “Self-assembly at all scales”. In: *Science* 295.5564 (2002), pp. 2418–2421.

[19] Ryan van Dommelen, Paola Fanzio, and Luigi Sasso. “Surface self-assembly of colloidal crystals for micro-and nano-patterning”. In: *Advances in colloid and interface science* 251 (2018), pp. 97–114.

[20] Hwa Seng Khoo et al. “Self-assembly in micro-and nanofluidic devices: A review of recent efforts”. In: *Micromachines* 2.1 (2011), pp. 17–48.

[21] Valeria Lotito and Tomaso Zambelli. “Self-assembly of single-sized and binary colloidal particles at air/water interface by surface confinement and water discharge”. In: *Langmuir* 32.37 (2016), pp. 9582–9590.

[22] Stéphane Reculusa and Serge Ravaine. “Synthesis of colloidal crystals of controllable thickness through the Langmuir- Blodgett technique”. In: *Chemistry of materials* 15.2 (2003), pp. 598–605.

[23] Junhu Zhang, Zhiqiang Sun, and Bai Yang. “Self-assembly of photonic crystals from polymer colloids”. In: *Current Opinion in Colloid & Interface Science* 14.2 (2009), pp. 103–114.

[24] Fuduo Ma, David T Wu, and Ning Wu. “Formation of colloidal molecules induced by alternating-current electric fields”. In: *Journal of the American Chemical Society* 135.21 (2013), pp. 7839–7842.

[25] Ahmet F Demirörs et al. “Colloidal assembly directed by virtual magnetic moulds”. In: *Nature* 503.7474 (2013), pp. 99–103.

[26] Xue Li, Olivia Niitsoo, and Alexander Couzis. “Electrostatically driven adsorption of silica nanoparticles on functionalized surfaces”. In: *Journal of colloid and interface science* 394 (2013), pp. 26–35.

7

CONCLUSION

The innovation of health care and biomedical research through the integration of advanced technology plays a significant role in enhancing clinical outcomes and pioneering new frontiers in medical science. This work finds itself at an intersection of advanced optoelectronics technology and the innovative field of cardiac optogenetics.

Development methodology

A significant part of the dissertation is dedicated to the development of advanced illumination systems for optogenetics in cardiac applications. Employing the V-model system engineering methodology significantly benefits the efficiency and effectiveness of the design and development cycle. The methodology begins with a thorough analysis of system requirements, informed by the specific needs of cardiac optogenetics research. This phase is critical for ensuring that the final product aligns with the intended biomedical applications. The following step is system architecture design, breaking down the complex illumination system into subsystems. Each subsystem is designed with precision, considering its unique functionalities and requirements, and implemented with the components assembled according to the design specifications. Verification processes for both individual subsystems and the integrated system are done by thorough testing and simulations to ensure that each component functions as intended and that the overall system meets the defined specifications. The dissertation underscores the importance of these steps in developing a reliable and effective illumination system.

The culmination of the development process is the system validation phase, where the illumination system is deployed in optogenetics experiments for arrhythmia study. This phase is critical for assessing the system's performance in real-world applications and for making necessary adjustments to optimize its functionality.

Development of illumination systems for cardiac optogenetics This work presents the design and development processes of four specialized optoelectronic illumination systems following the guiding development methodology, each uniquely engineered for optogenetic cardiac applications.

A fully customized, implantable, high-power LED light source system for both in-vivo and ex-vivo VF treatment experiments in rats has been developed. The design of the 'apex-cup' shaped device offers a tailored fit to the rat's ventricular apex. This minimized and thin structure is crucial for avoiding interference with other organs in in-vivo experiments. The cup geometry is particularly designed with 3 high-power LED chips at the 3 arm structures respectively, as well as a center LED chip at the middle of the apex. The design focuses on light distribution to enhance the activation of local ion channels that require high irradiance stimulation.

The wavelengths of the LEDs are selected as 567nm (lime) and 617nm (red-orange), based on optical simulations, where it concluded that those wavelengths can not only produce essential membrane potential responses but also larger peak photocurrents with superior tissue penetration than 470nm (blue) light. The electrical and optical characteristics are calibrated by measurements with a customized setup.

Original fabrication processes are used to create a bio-compatible packaging of the LED apex-cup device for both in-vivo and ex-vivo experiments, with the use of polymers and assembly techniques. The thermal impact of the high-power device is assessed by temperature measurements and finite element simulations, which both conclude that the LED chips will create 'hot spots' and 'thermal shock' to the target area, however, the maximum temperature and expected damage are limited due to thermal barrier material used in the design as well as short operation cycle of the LEDs.

The apex-cup LED system is validated by intensive in-vivo and ex-vivo in rad heart models. The device is validated to deliver more than 25mW/mm^2 irradiance to sufficiently activate the light-sensitive ion channels and shows successful termination of VF with high consistency.

Additional transthoracic illumination device is shortly introduced as an exploration of new possibility of treating AF in rat models without open-chest operations.

A similar approach is used in the development of a high-power LED panel system for optogenetics AF treatment of in-vivo and ex-vivo swine models. The 50mm diameter panel is designed with 100 high-power LED elements, which have a layout of 10 individual illumination zones. This design focuses on finding the balance between uniform light pattern and high irradiance for deep penetration of ion channel activation, which is supported and verified by optical modeling.

Original assembly processes are introduced in the LED panel device integration to ensure bio-comparability as well as durability during the expected intensive animal tests. Advanced material, such as PDMS polymer, is used for encapsulation and thermal barrier layer, fabricated with customized spacers and release layers.

Thermal simulation of the device and the application is carried out via finite element modeling. The simulation results show the nature of the device creating thermal 'hot spots' on the subject surface, and the thickness of the polymer thermal barrier is fine-tuned to optimize the heat dissipation to avoid physical damage.

A customized driver and control subsystem is developed as the interface of device manipulation, with flexibility and operation safety as the main considerations. The system verification tests show sufficient irradiance values, >50mW/mm^2 for a 470nm LED device and >17mW/mm^2 for a 567nm LED device. Although the system is not validated for both in-vivo and ex-vivo experiments due to the limitation of the technical issues in optogenetic swine models, it still proves the technical potential of integrating an implantable high-power illumination system.

The development of an LED matrix illumination system for proof-of-concept purposes of an innovative approach to studying arrhythmia behaviors using a human immortalized atrial myocyte (hiAM) model is then discussed. The detailed process is presented including the fabrication, testing, and implementation of a specialized, modular LED matrix and its control system.

The optogenetics test platform has changed from animal models to cell cultures along with unique requirements, especially for the illumination system's capability of providing precise and fine patterns. A 16x16 matrix with 256 LED elements design is presented as a demonstrator of the proof-of-concept test platform. The equilateral matrix layout is particularly analyzed via optical simulation to achieve better light uniformity, where the optimized element interval-projecting distance factor is found as 1.5. The design is translated to practical device manufacturing with an original encapsulation process to cover the matrix with PDMS polymer with high precision. The polymer acts as a good thermal barrier between the high-power LED chips and the delicate mono-layer of cell

culture.

The system is verified with a customized control and driver system as the main user interface electronics to support a fully functional illumination pattern design. The optical characterization proves the system has sufficient irradiance (>3.0mW/mm^2) over the 46mm by 36mm matrix area to activate the genetically modified hiAM cell cultures. Further validation experiments show good consistency of terminating rotation AF waves with full matrix global illumination of 0.5mW/mm^2 as well as innovative selective illumination of a 'blocking line' of 1.2mW/mm^2.

This work lays a theoretical and practical foundation for in-vitro optogenetics research with advanced illumination systems and sets the technical stage for more sophisticated illumination systems.

Finally, following the success of the previous prototype systems, the feasibility of a 16x16 mini-LED matrix illumination system is proposed as the more advanced solution. This upgraded system is designed for more precise control in hiAM cell culture experiments. Several design proposals with advanced light technologies are made and eventually, the mini-LED matrix solution is chosen as a thoughtful balance between system performance and manufacturing complexity.

Original assembly processes of the mini-LED matrix are developed with a combination of semi-auto pick-and-place of mini-LED bare-die chips and advanced polyimide substrates. A more refined illumination is achieved with a 16x16 matrix of 0.6mm pixel intervals over a 9mm by 9mm area. An advanced driver and controller system for more effective management of the smaller mini-LED components is designed and proposed.

The mini-LED matrix is verified with optical characterization that demonstrates the fast pattern display function as well as sufficient irradiance (>2.5mW/mm^2) that is required for the optogenetics experiments. This development lays the fundamentals for further advancements as a technical demonstrator for the main challenges in high-density mini-LED matrix design and integration for the special application in cardiac hiAM optogenetics.

The research not only provides a technical methodology for developing advanced illumination systems but also offers insights into the potential clinical applications of optogenetics in cardiology. The work is poised to have a significant impact on the field, offering developing tools for the exploring of novel, patient-friendly approaches to treating cardiac arrhythmias.

List of Publications

3. Nyns, Emile CA, **Tianyi Jin**, Magda S Fontes, Titus van den Heuvel, Vincent Portero, Catilin Ramsey, Cindy I Bart, Katja Zeppenfeld, Martin J Schalij, Thomas J van Brakel, Arti A Ramkisoensing, Guoqi Zhang, Rene H Poelma, Balazs Ördög, Antoine AF de Vries, Daniel A Pijnappels, *Optical ventricular cardioversion by local optogenetic targeting and LED implantation in a cardiomyopathic rat model*, Cardiovascular research, 118, no. 10 (2022): 2293-2303.

2. Nyns, Emile CA, **Tianyi Jin**, Cindy I. Bart, Wilhelmina H. Bax, Guoqi Zhang, René H. Poelma, Antoine AF de Vries, and Daniël A. Pijnappels, *Ultrasound-Guided Optogenetic Gene Delivery for Shock-Free Ventricular Rhythm Restoration.*, Circulation: Arrhythmia and Electrophysiology, 15, no. 1 (2022): e009886.

1. Nyns, Emile CA, Vincent Portero, Shanliang Deng, **Tianyi Jin**, Niels Harlaar, Cindy I Bart, Thomas J van Brakel, Meindert Palmen, Jesper Hjortnaes, Arti A Ramkisoensing, Guo Qi Zhang, René H Poelma, Balázs Ördög, Antoine AF de Vries, Daniël A Pijnappels, *Light transmittance in human atrial tissue and transthoracic illumination in rats support translatability of optogenetic cardioversion of atrial fibrillation.*, Journal of Internal Medicine, (2023).

CURRICULUM VITÆ

18-05-1993 Born in Zhejiang, China.

EDUCATION

2011–2015 Bachelor in Microelectronics
Shanghai Jiao Tong University
Shanghai, China

2015–2017 Master of Science in Electrical Engineering
Delft University of Technology
Delft, The Netherlands

2017–2024 Doctoral Candidate in Electrical Engineering
Delft University of Technology
Delft, The Netherlands
Promotors: Prof. dr. G.Q. Zhang
Prof. dr. D.A. Pijnappels
Copromotor: Dr. ir. R.H. Poelma

ACKNOWLEDGEMENTS

Completing this doctoral thesis has been an immensely challenging yet rewarding journey, marked by periods of intense dedication and hard work. I would like to express my profound gratitude to many individuals who have been significantly important in the realization of this dissertation, which has extended over a longer period than anticipated.

First and the most, I would like to express my deepest gratitude to my promoter, Prof.Dr.Guo-Qi (Kouchi) Zhang, for his invaluable guidance, support, and mentorship throughout the course of my research. His expertise and insightful feedback have been instrumental in shaping both the direction and success of my work. Also, his commitment to academic excellence and dedication to guiding my growth as a researcher has been truly inspiring. I am deeply thankful for the encouragement, patience, and understanding he has shown me, even during the most challenging phases of my research. Prof.Zhang's unwavering belief in my abilities and potential has been a constant source of motivation and confidence. This accomplishment would not have been possible without his mentorship.

I would like to express my heartfelt thanks to my promotor Prof.Dr.Daniel A. Pijnappels from the Laboratory of Experimental Cardiology, Leiden University Medical Center, for coordinating the collaboration, support, and assistance during the multi-discipline research. I also want to express my appreciation to the colleagues and research partners from his laboratory: Niels, Emile, Twan, Tim, Sven, Vincent, Balazs, Titus, Minka, Cindy, and others, for their expertise and contributions which are invaluable to the completion of this project.

I extend my deepest gratitude to my co-promotor and daily supervisor, Dr.Rene H. Poelma, for his unwavering guidance, invaluable advice, and continuous support throughout my research journey. His expertise, patience, and encouragement were instrumental in shaping both this work and my professional development.

I am profoundly grateful to my thesis committee members, for their insightful feedback and constructive critiques during this work. Their expertise and perspectives have been immensely beneficial in refining my research.

I wish to express my sincere gratitude to my Delft colleagues who worked together on this research project: Shanliang, Catlin, and Romina. Working together has significantly

contributed to the success of our work and my personal development. Thank you for the collaboration and the shared commitment to our goals.

I am also thankful to my colleagues and alumni in the Electronic Components, Technology, and Materials (ECTM): Lina, Willem, Sten, Max, Amir, Baoyun, Brahim, Boyao, Daniel, Dong, Fengze, Hande, Hongyu, Jian, Jianlin, Jiarui, Jiajie, Joost van Ginkel, Joost Romijn, Leiming, Leandro, Leo, Luke, Manju, Paul, Romina, Shinnosuke, Shuhan, Xiao, Xinrui, Xinyun, Yaqian, Zichuan, Zhen and others. Your kindness and support made this challenging journey more manageable and memorable.

Special appreciation goes to the faculty of Electrical Engineering, Mathematics, and Computer Science (EEMCS) in Delft University of Technology, for coordinating the financial support for this research. Their support was crucial in facilitating the resources and opportunities needed to conduct this study.

To my family, thank you for your endless love, patience, and encouragement. Your unwavering faith in me and constant support have been the pillars of strength throughout my academic pursuits.

Lastly, I extend my gratitude to all others who directly or indirectly contributed to this research. Your insights and assistance have been a significant part of this journey.